Design of Coatings Embedded with Tolerant, Tailored and Responsive Underwater Oil Wettability and Oil Adhesion

A Thesis Submitted by

Angana Borbora

Roll No: 176122115

to

Indian Institute of Technology Guwahati

for the award of the degree of

Doctor of Philosophy

Department of Chemistry,

Indian Institute of Technology Guwahati

North Guwahati-781039

Assam, India

01/09/2023

Indian Institute of Technology Guwahati

Department of Chemistry

STATEMENT

I hereby declare that the work incorporated in the thesis entitled "**Design of Coatings Embedded with Tolerant, Tailored and Responsive Underwater Oil Wettability and Oil Adhesion**" is the result of investigations of research work carried out by me in the Department of Chemistry, under the supervision of Dr. Uttam Manna, Associate Professor, Department of Chemistry, Indian Institute of Technology Guwahati, Assam, India.

Research materials used in this thesis from any other source has been fully cited and acknowledged. This work is original and has not been submitted elsewhere for the award of any degree.

01/09/2023

IIT Guwahati

Angana Barbora

Indian Institute of Technology Guwahati

Department of Chemistry

CERTIFICATE

This is to certify that the work presented in this thesis entitled **"Design of Coatings Embedded with Tolerant, Tailored and Responsive Underwater Oil Wettability and Oil Adhesion"** by **Angana Borbora**, a Ph.D. student of Department of Chemistry, Indian Institute of Technology Guwahati, for the award of degree of Doctor of Philosophy has been carried out under my supervision and this work has not been submitted elsewhere for the award of any degree.

01/09/2023

Dr. Uttam Manna

Thesis Supervisor

Department of Chemistry

Indian Institute of Technology Guwahati

North Guwahati–781039, Assam, India.

Dedicated to My Maa and Deti

I would like to offer my sincere gratitude to the many extraordinary people who have accompanied me on my half-a-decade wonderful PhD journey at IITG; without whom, my journey wouldn't be what it is, and this thesis wouldn't be possible.

First and foremost, I would like to express my heartfelt gratitude to my supervisor, Dr. Uttam Manna. I feel fortunate to carry out my PhD work under his supervision, and I couldn't imagine a better mentor with constant efforts to bring the best out of his students. I am forever grateful for your constant motivation, guidance, and support and for providing the best possible opportunities. I thank you for always believing in me while providing difficult tasks, which helped me grow and uplift my research grasp.

I would like to extend my gratitude to my doctoral committee members, Prof. Mohammad Qureshi, Prof. Debapratim Das, and Dr. Manabendra Sarma, for their valuable suggestions, guidance, and periodic evaluation of my thesis work. I convey my gratitude to Dr. Xiaoguang Wang for his advice and expertise in performing collaborative works. I thank Prof. Biman B. Mondal for his assistance in collaborative work. I thank the staff members of the Department of Chemistry and the central instrumentation facility (CIF) for their help in instrumentation facilities. I would like to acknowledge my collaborators, Souradeep Dey, Dr. Yang Xu, and Robert L. Dupont, for their much-needed assistance in performing experiments and preparing manuscripts.

I would like to extend my gratitude to all my teachers/faculties and friends from my academic career, whose direct and indirect support and motivation have guided me to reach this milestone. A particular person to mention is Avnash Kumar from IICT; I am always indebted for his selfless help that I needed the most. I am thankful to Dr. Tridip Goswami sir, for his motivation and guidance in pursuing a PhD.

My deepest appreciation cum gratitude goes to all the members of CHEL-302 who were around me in the last five years, creating a friendly work environment and fun-filled moments that I will cherish for a lifetime. I am grateful to my seniors Dr. Adil M. Rathar, Dr. Dibyanagana Parbat, Dr. Avijit Das, Dr. Kousik Maji, Mr. Nirban Jana, Dr. Arpita Shome, Dr. Supriya Das, Dr. Upama Baruah, Dr. Deepsikha Hazarika, Dr. Subhankar Mandal, Dr. Haydar Ali and my juniors Manideepa Dhar, Sourav Kumar, Debasmita Sarkar, Nishanta Barman, Jaysri Das, Hrishikesh Sarma, Chittaranjan Mishra for creating cooperative lab environment, and for their help and insights, without which this journey wouldn't have been so memorable. Thanks should also go to Dr. Kousik Maji for being my mentor in my initial PhD days, guiding me, and being

a friend more than a mentor. I would be remiss in not mentioning project students Pritam Giri, Anushree Mondal, Chetna Mohanty, Priyam Mondal, Karan Jain, and Swaraj Roy for their help in various experiments. My sincere appreciation goes to everyone, who was part of the lab, whether for a short or long period, during my PhD duration and helped me to create so many beautiful memories. I will treasure the wonderful time spent with Mrs. Tumpa Manna Jana and little Irsia Manna.

I am so grateful to all my dear friends at IITG for their love and support and for creating cherishable moments. My heartfelt gratitude to Sourav Bhowmick, Monikha Chetia, Shilpa Bhuyan, Rakesh Mazumdar, Manoj Kumar Mohanta, Manideepa Dhar, Nikita Chakraborty, Chandrakanta Parida, Partha Pratim Nath, and Himangshu Bhattacharyya for giving me the unforgettable memories; I am thankful for all the happy times we have spent together. I feel so blessed to have two amazing friends and badminton partners, Dr. Sourav Bhowmick and Ashish Singh, who not only teach me badminton but also inspire me every day with their positivity, kindness, and selflessness. I am grateful to my dear friend Chandan Jyoti Choudhury, for his unceasing support and comfort in my highs and lows over a decade.

Finally, I thank my pillar of strength, without whom this endeavour would not have been possible, “my family”; who actuated and accelerated the journey through their countless sacrifice and unconditional love. I lack words to describe the struggle and affection they put forth in building my career. My mother, Mrs. Basanti Borbora, who taught me to be independent, courageous, and carefree and supported me in every decision. My father, Mr. Dilip Kumar Borbora, who taught me to fly high and dream big; and be positive and strong even during the worst days. Last but not least, I would like to mention my primary source of inspiration and passion, Dr. Ankita Borbora, my dear elder sister, whose footsteps and life lessons have been my guiding principles since childhood to date.

Angana Borbora

Table of Contents

Abstract

The anti-oil wettability of various naturally existing underwater creatures has inspired researchers to develop artificial super oil repellent interfaces for multiple applications in engineering, healthcare, and environmental remediation. In the past, several approaches were adopted to artificially fabricate underwater oil-repellent surfaces, formally known as underwater superoleophobicity, by co-optimizing hydrophilic chemical composition and rough micro/nano-structures on their surface. However, the earlier reported approaches in deriving underwater superoleophobicity were unable to associate some other essential properties, such as, physical and chemical durability, adaptive tuning of oil adhesion, and transparency in the prepared surfaces. Here, a facile 1, 4-conjugate addition reaction is exploited to derive covalently crosslinked chemically reactive coatings on various surfaces loaded with residual chemical functionalities that provide the opportunity to embed underwater superoleophobicity through appropriate post-covalent modifications. While the covalent crosslinking tailored mechanical property, the adequate chemical post-modification customized oil adhesion and optical transparency. The synopsis report entitled "**Design of Coatings Embedded with Tolerant, Tailored and Responsive Underwater Oil Wettability and Oil Adhesion**" is presented in six chapters. **Chapter 1** introduces bio-mimicked underwater superoleophobic surfaces, the existing challenges associated with conventional artificial fabrication approaches, and the objectives of the thesis work. **Chapter 2** demonstrates the fabrication of a dually reactive multilayer coating following the 1, 4-conjugate addition reaction and the post-covalent modification of the multilayer coating to immobilize highly sensitive bare micro-meter sized nematic liquid crystal (LC) droplets underwater for single LC droplet based repetitive sensing application. **Chapter 3** accounts for the utilization of the dually reactive multilayer coating to develop various responsive underwater superoleophobic surfaces via post-modifications and their adaptive oil adhesion for sensing different amphiphilic (cationic, anionic and facial) molecules. **Chapter 4** demonstrates the rational functionalization of the dual reactive multilayer coating to depict the highly selective raising of the oil contact angle (OCA) and rolling of a beaded oil droplet underwater in the presence of targeted and relevant toxic chemicals. **Chapter 5** introduces a covalently crosslinked and chemically reactive sol-gel conversion process through the 1, 4-conjugate addition reaction to achieve a substrate-independent, mechanically durable, and optical transparent coating embedded with underwater superoleophobicity. Moreover, this approach allows to modulate mechanical property of highly

deformable objects. **Chapter 6** provides a brief summary and the future outlook of the work presented here.

Chapter 1: Introduction

Several creatures in nature possess surfaces with diversified special wettabilities that allow them to survive and adapt to harsh environmental conditions. For instance, the underwater anti-oil wettability (formally recognized as underwater superoleophobicity) of various aquatic organisms, such as fish scales, shark skin, clam's shell, seaweed, filefish, etc., helps them to survive in oil-contaminated water without their surface being stained with oil. Bio-mimicking such surfaces enables us to design and prepare bionic interfaces with underwater superoleophobicity, which greatly contributes to potential applications such as oil/water separation, oil-droplet manipulation, production of marine infrastructures, etc. Detailed investigations on the natural underwater superoleophobic interfaces revealed the existence of

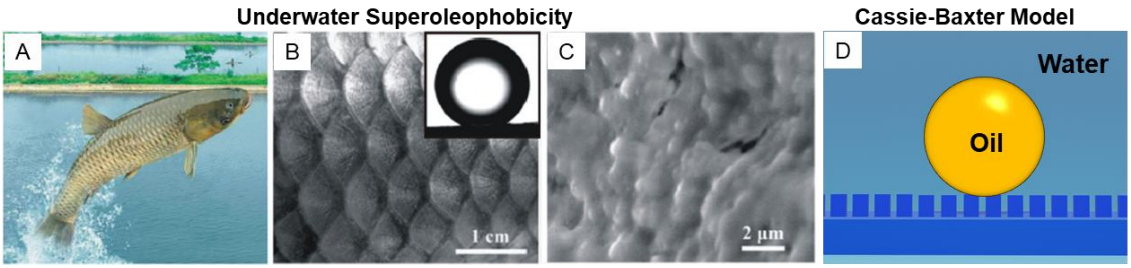

Figure 1. (A) Photographs and (B, C) scanning electron microscope (SEM) images of fish scales. (D) Schematic depiction of Cassie-Baxter model. (A-C) Reproduced with permission from *Adv. Mater*., 2009, **21**, 665. Copyright 2009, Wiley.

hydrophilic chemical compositions and hierarchical rough (micro and nano) topography (Figure 1A−C) attributed to the underwater superoleophobicity. Theoretically, such an anti-wetting phenomenon can be explained with the Cassie-Baxter model (Figure 1D), where water can wet the surface due to its hydrophilic nature and be trapped in the rough microstructures of fish scales, creating an oil-repelling water cushion. In this case, the beaded oil droplet experiences heterogeneous wettability on the composite interface of solid and water and results in high OCA (> 150º) and low roll-off angle (<10º). Based on this principle, two biomimetic principles have to be fulfilled to fabricate artificial underwater superoleophobic surfaces: (i) micro and nanoscale hierarchical structures on the surface, (ii) incorporation of hydrophilic (high surface energy) chemical composition on it. Drawing inspiration from nature, researchers have adopted several approaches to fabricate numerous artificial underwater superoleophobic surfaces for diverse applications; however, earlier approaches remained inappropriate to

associate other essential properties besides underwater superoleophobicity. Firstly, chemical and physical/mechanical durability of the artificial underwater superoleophobic surfaces is vital for their long-term performance in harsh underwater conditions; however, the commonly employed coating approaches involved the integration of hydrogel, metal-oxide, and electrostatic multilayer, etc., suffer from durability issues underwater. Secondly, a few recent reports demonstrate the tailoring of oil adhesion on the superoleophobic surface by switching between ground and stimulated oil adhesion state, while demonstrations of the gradual tuning of oil adhesion while retaining the oil-repellence property for various potential applications is

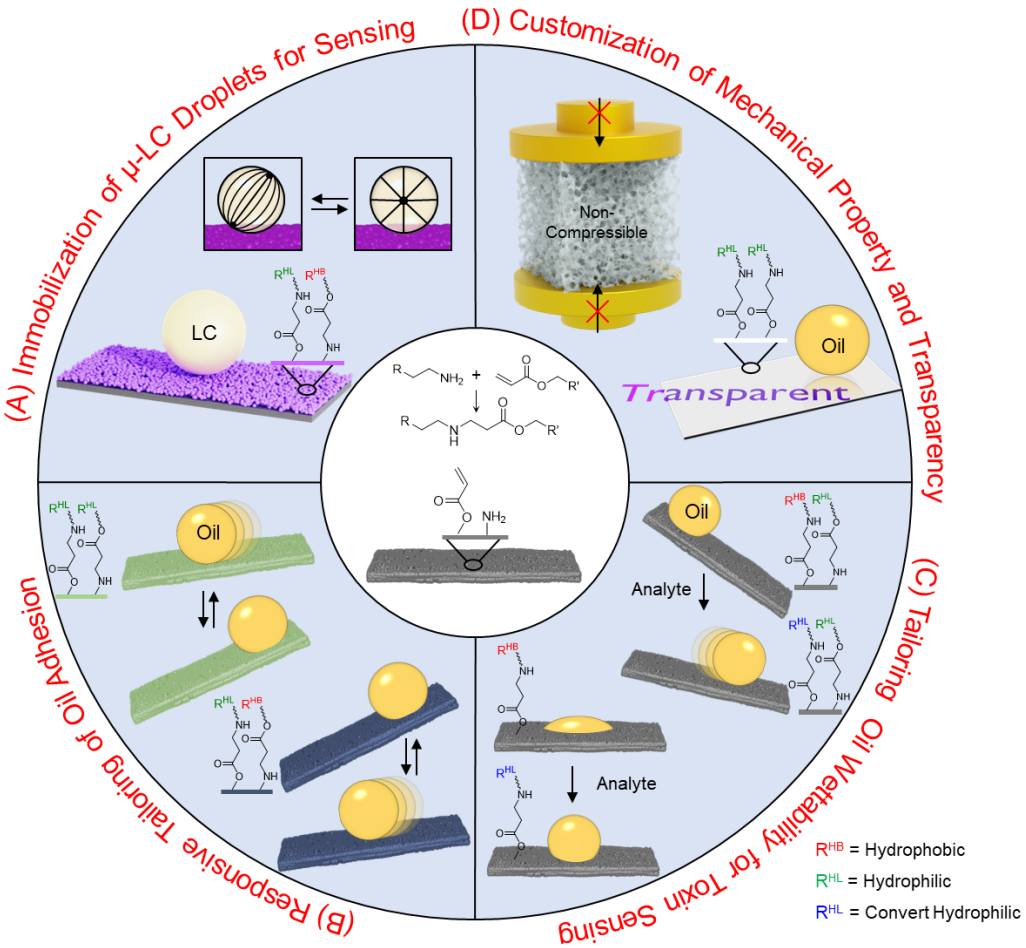

Figure 2. Schematic depiction of 1, 4-conjugate addition reaction for generating a reactive coating with residual functional moieties. The derivation of various desired underwater anti-oil wetting surfaces via the post-covalent modifications of residual reactivities with selected chemical functionalities: (A) underwater liquid crystal (LC) repellent surface for the immobilization of the µ-LC droplet for sensing application, (B) underwater superoleophobic surfaces with reversible amphiphile-responsive tuning of oil adhesion, (C) chemically customized surface for the selective tailoring of oil wettability (oil contact angle (OCA) and oil adhesion) in the presence of toxins, (D) induction of mechanical property and transparency in underwater superoleophobic coating.

rare in literature. Moreover, transparency is another essential property for underwater superoleophobic surfaces in various relevant applications; however, the requirement of rough microstructure on the substrate surface makes achieving transparency on the surface challenging.

To address the existing challenges, I have utilized facile and readily reactive covalent chemistry, i.e., 1, 4-conjugate addition reaction between amine and acrylate for constructing reactive coatings loaded with residual chemically reactive moieties that provides the essential topography and chemical composition via post-modification to embed underwater superoleophobicity. Moreover, the appropriate post-covalent modifications of the residual reactivities with desired chemicals allowed to achieve underwater oil adhesive superoleophobicity for the immobilization of ultra-sensitive LC microdroplets for its sensing application (Figure 2A). Furthermore, the reactive multilayer coating was rationally post-modified to demonstrate the reversible tailoring of oil adhesion on underwater superoleophobic surfaces in the presence of selected amphiphiles (Figure 2B). Besides, the rational chemical modulation of the same surface allowed to depict the raising of the OCA and rolling of a beaded oil droplet underwater, indicating the presence of targeted toxic chemicals (Figure 2C). Moreover, a separate chemically reactive covalently crosslinked sol-gel conversion chemistry is introduced to tailor the mechanical properties of deformable objects. This approach was explored to achieve optically transparent underwater superoleophobic coating for their relevant underwater applications (Figure 2D).

Chapter 2: Bio-mimicked Liquid Crystal Repellent Coating for Immobilizing Liquid Crystal µ-Droplets—Without Affecting Their Sensitivity

In this chapter, a 1, 4-conjugate addition reaction is utilized to develop a multilayer coating of reactive nanocomplex that displayed extreme repellence to a nematic LC phase with tailored adhesion after association of adequate chemical modifications. In the past, the nematic micrometer-sized LC droplets (denoted as µ-LC) of 4-cyano-4′-pentylbiphenyl (5CB) were strategically used for monitoring different biological events, sensing various analytes, etc. The triggered and reversible ordering transition of µ-LC droplets from bipolar to radial configurations due to the preferential surface anchoring of appropriate amphiphilic molecules resulted in a distinct optical appearance of LC droplets under a cross-polar microscope. However, the optical characterization of ordering transition in a single micrometer-sized, bare, and free-floating LC droplet in the aqueous phase is an extremely challenging task due to

unavoidable Brownian motion, which limits its scope for practical applications. In this chapter, an extremely LC-repellent (dented as super-LC-phobic) interface was designed through the appropriate co-optimization of surface topography and chemistry. In this context, a dually reactive multilayer coating (Figure 3A) comprised of two types of residual functional groups, acrylate and amine, was fabricated following a layer-by-layer (LbL) assembly of branched polyethylenimine (BPEI) and chemically reactive nanocomplexes (CRNC, obtained by mixing BPEI and dipentaerythritolpenta-acrylate (5Acl)) through 1, 4-conjugate addition reaction. The adequate chemical modifications of the reactive multilayer coating with glucamine and selected alkyl acrylates provided an interface with an extreme repellence to beaded LC droplets with tailored adhesive force (Figure 3B). Such interfaces enabled immobilizing the μ-LC droplets on it after sedimentation without altering their shape and sensitivity. Moreover, the reactive multilayer coating was spatially selectively and orthogonally modified to associate an underwater adhesive super-LC-phobic pattern confined by a hydrophobic boundary for selective sedimentation of μ-LC droplets, where the surrounding hydrophobicity prevented the arbitrary spreading of both the beaded aqueous dispersion of μ-LC droplets and the aqueous solution of analytes (Figure 3C). Eventually, such a simple principle allowed effortless and repetitive characterization of triggered ordering transition in a single and bare μ-LC droplet (Figure 3D).

The underwater super-LC-phobicity was achieved only through successful co-optimization of surface chemistry and hierarchical surface topography in a 15-bilayer coating after glucamine modification (with LC contact angle 170°, Figure 3E), where settled LC droplets were found with “bipolar” orientation (Figure 3F). Next, the transition in the orientational ordering from bipolar to radial was observed upon the addition of 1 mM of an amphiphilic molecule, i.e., sodium dodecyl sulfate (SDS, Figure 3G). In contrast, the bare μ-LC droplet that directly sedimented on a bare glass surface was found with a bias orientation in the absence of amphiphiles, where mostly a pole defect remained adhered to the surface (Figure 3H). Furthermore, to immobilize the bare LC droplet on the super-LC-phobic surface with controlled adhesive interaction for monitoring repetitive and reversible configurational changes in a single sedimented bare μ-LC droplet, the residual amines of the glucamine-modified coating was post-modified with selected hydrophobic alkyl acrylates through 1, 4-conjugate addition reaction (Figure 3I). The glucamine/butyl acrylate-modified interface provided an underwater super-LC-phobic coating with optimum adhesion force to immobilize LC droplets with a “bipolar-like” appearance (Figure 3J). Next, the SDS exposure resulted in

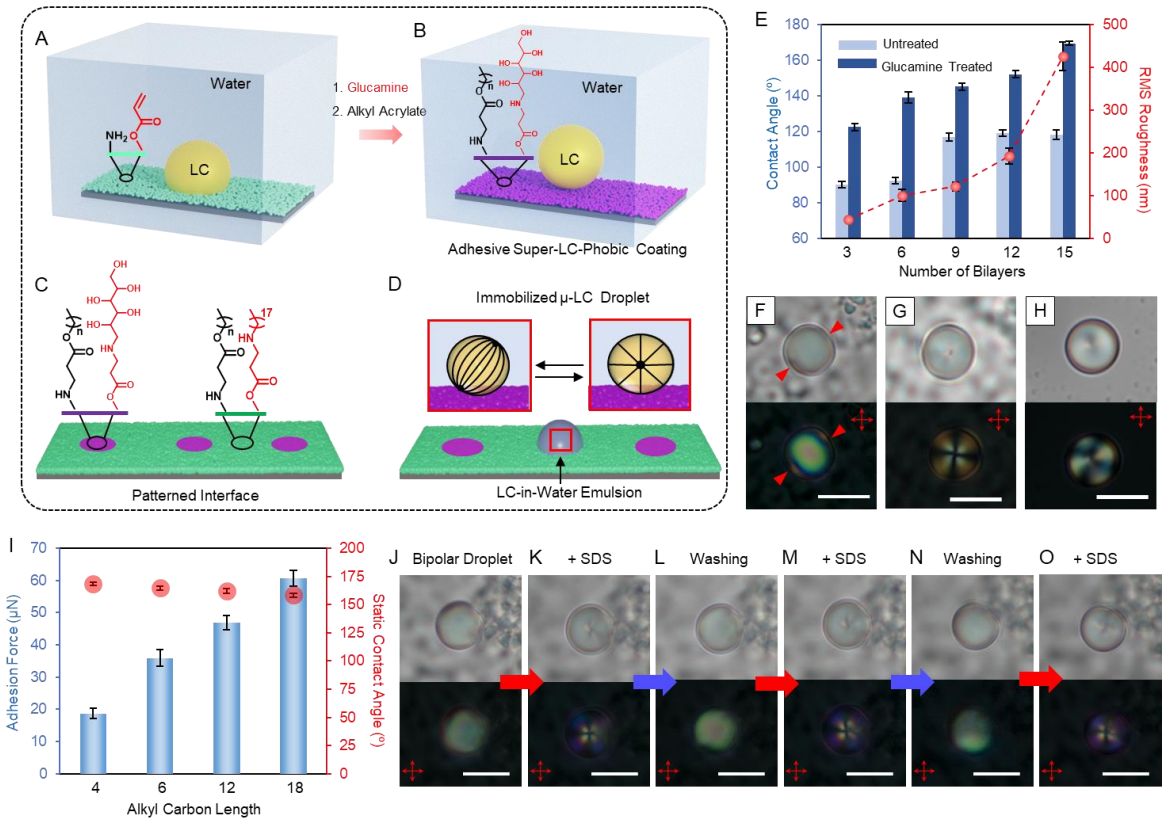

Figure 3. Depicting the post-covalent modification of (A) reactive multilayer coating with glucamine and alkyl acrylate to obtain (B) adhesive super-LC-phobicity underwater. (C, D) patterned interface with superhydrophilic spots on a hydrophobic background created through the spatial covalent modification of the residual functionalities on the coating with appropriate molecules for the confinement of the LC-in-water emulsion solution in the superhydrophilic regions (E) Depicting the effect of number of bilayers on RMS roughness of the coating and underwater LC contact angle. (F-H) Bright-field and polarized optical micrographs of a sedimented µ-LC droplet on (H) uncoated and (F, G) coated (super-LC-phobic) glass surfaces (F, H) before and (G) after exposing to sodium dodecyl sulfate (SDS, 1 mM). (I) Effect of alkyl carbon chain length on the adhesion force and static contact angle of a beaded LC droplet underwater. (J-O) Bright-field and polarized optical micrographs demonstrate the repetitive and reversible ordering transition on a single immobilized µ-LC droplet. Scale bars, 5 µm. Adapted with permission from *Langmuir*, 2022, **38**, 9221. Copyright 2022, The American Chemical Society.

a radial configuration, and subsequent washing with deionized water allowed to achieve a reversible transition from radial to bipolar configuration. Eventually, such a simple principle allowed effortless and repetitive characterization of triggered ordering transition in a single and bare µ-LC droplet (Figure 3J-O).

Chapter 3: Dually Reactive Multilayer Coatings Enable Orthogonal Manipulation of Underwater Superoleophobicity and Oil Adhesion via Post-Functionalization

Chapter 3 demonstrates the independent tuning of underwater superoleophobicity and oil adhesion through the orthogonal functionalization of two types of reactive moieties at ambient conditions, which cannot be achieved in conventional underwater superoleophobic surfaces. Although some rare previous attempts show the tunable/switchable oil adhesion properties by using responsive molecules or polymers, such as thermo-responsive polymers (*e.g.*, poly(*N*-isopropylacrylamide) (PNIPAM)) and pH-responsive polymer (*e.g.*, poly(acrylic acid) (PAA)), these surfaces are only able to switch between ground and stimulated oil adhesion state and lack the ability to tune the contact angle hysteresis (CAH) and the consequent oil droplet mobility precisely. Here, I extended the dual reactive multilayer coating (demonstrated in Chapter 1) to orthogonally modify with a rich palette of chemicals to independently tune the OCA and CAH of oil droplets underwater. Further, the non-covalent, cooperative assembly of amphiphiles (*e.g.*, ionic or facial surfactants) on the appropriate chemically modified underwater superoleophobic coatings gives rise to a switchable underwater oil-adhesion with a precisely tunable CAH ranging from ~ 5° to ~ 30° (Figure 4A−C). Notably, the synergistic effect between the chemical modification, the pH of the aqueous phase, and the cooperative assembly of amphiphiles on the oil adhesion of the coatings enables the detection of synthetic surfactants with different charges and physiologically important metabolites (*i.e.*, bile acids) with the naked eye (Figure 4C).

Here, non-adhesive underwater superoleophobic coatings: (1) mono-functionalized (modified with 3-(dimethylamino)-1-propylamine (DMAPA), Figure 4A) coating, and (2) dual-functionalized coating (modified with β-alanine and 2-carboxyethyl acrylate (CEA), Figure 4B) were rationally selected to reversibly switch oil adhesion through the cooperative assembly of surfactants on the modified interfaces. Specifically, the DMAPA-modified surface exhibited an oil adhesive behaviour while keeping the superoleophobicity selectively to anionic surfactants, e.g., SDS, in an acidic solution (pH = 5; Figure 4D), and the CAH of a beaded oil droplet (5 μL) adopted a linear increase from 4.2 ± 0.2° to 29.6 ± 0.8° with an increase in the concentration of SDS from 0 μM to 600 μM. This can be attributed to the electrostatic attraction between the anionic head groups of SDS and the protonated amine moieties in the surface at acidic pH, which resulted in an enhancement of the physical contact between the beaded oil droplet and the exposed hydrocarbon tail of the assembled SDS on the coating (Figure 4A, D). Similarly, the dissociation of the carboxylic acid groups of the β-alanine/CEA-modified surface in alkaline conditions can trigger a cooperative assembly of cationic surfactants (dodecyltrimethylammonium bromide (DTAB)) at the surface, resulting in decrease in the

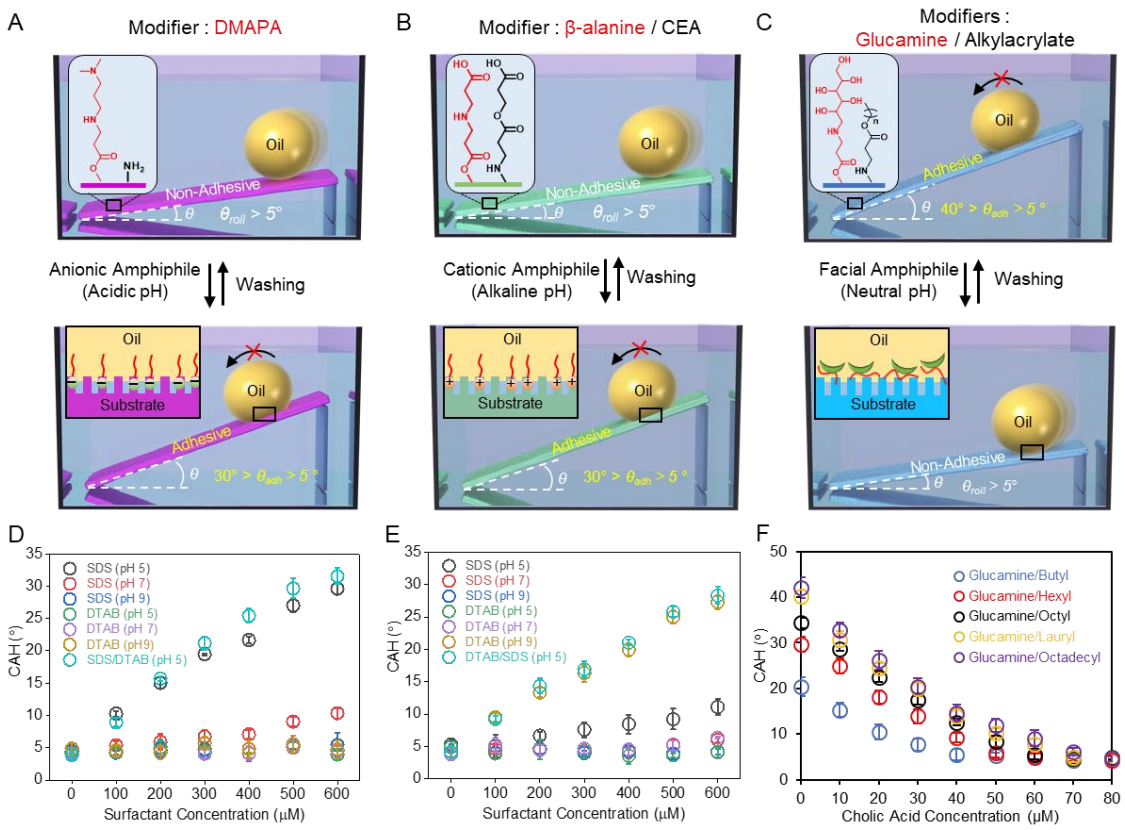

Figure 4. (A−C) Schematic illustration of the non-covalent, cooperative assembly of (A) anionic surfactants on DMAPA-modified coatings in an acidic solution, (B) cationic surfactants on β-alanine/CEA-modified surfaces in an alkaline solution, and (C) facial amphiphiles on glucamine/alkyl amine-modified coatings at a neutral pH, to reversible switch the oil adhesion. (D and E) Effect of surfactant type and concentration on the CAH of oil droplets on (D) DMAPA-modified and (E) β-alanine/CEA-modified superoleophobic coatings at different pH values. (F) The effect of cholic acid concentration and the aliphatic tail length of acrylates on the CAH of oil droplets on the glucamine/alkyl acrylate-modified superoleophobic coating. Adapted with permission from *Mater. Horiz*., 2022, **9**, 991. Copyright 2022, The Royal Society of Chemistry.

CAH of the surface (Figure 4B, E). Moreover, a patterned interface of two distinctly modified portions was prepared to display a contrast in the underwater oil adhesion depending on the ionic type (cationic or anionic) of the surfactants in acidic and alkaline conditions that can be utilized to determine the molecular structure of ionic surfactants. Furthermore, another oil adhesive interface was developed by modifying with glucamine and alkyl acrylates (Figure 4C). Upon exposure to one of the primary bile acids, *i.e.*, cholic acid, the interface exhibited a cholic acid concentration-dependent decrease in oil adhesion through the interaction between the hydrocarbon tail of the coating and the cholic acid (Figure 4F). This approach provides a highly sensitive and reusable platform for cholic acid sensing.

Chapter 4: Chemically Selective Underwater Raising and Rolling of Oil-Droplet Enabled Sensing of Toxic Chemicals

Sensing toxic chemicals is essential to manage pollution timely and efficiently. In the past, various sophisticated equipment-dependent sensing approaches—i.e., electrochemistry, surface-enhanced Raman spectroscopy (SERS), colorimetry, fluorometry, chromatography etc., were successfully introduced for sensing different toxic chemicals. This chapter introduces an equipment-free and naked-eye detection of harmful chemicals with high selectivity and sensitivity, where a dual chemically reactive multilayer coating is rationally subjected to mono- and dual-functionalization at ambient conditions to depict the raising of the OCA and rolling of a beaded oil-droplet underwater, respectively, only in the presence of targeted toxic chemicals (e.g., nitrite (NO_2^-) ion and hydrazine (N_2H_4)). Specifically, the dual chemically reactive multilayer coating of CRNC (as prepared in Chapters 2 and 3) was rationally modified with specifically selected hydrophobic and hydrophilic moieties to achieve mono and dual-functionalization through 1, 4-conjugate addition reaction, as shown in Figures 5A and B. The covalently embedded hydrophobic moiety in mono and dual-functionalized coating can selectively convert into hydrophilic moiety after treating with specific toxic chemicals. Such converted hydrophilic moiety in the coatings attributed to the raising in the OCA (in the mono-functionalized coating, Figure 5A) and rolling of beaded oil droplets (in the dual-functionalized coating, Figure 5B) underwater, indicating the presence of a toxic chemical.

For instance, the dual chemically reactive multilayer coating was modified with hydrophobic phenyl of N-phenylethylenediamine (PEDA) and hydrophilic carboxylic acid of CEA to achieve mono and dual-functionalization in the coating, where the hydrophobic phenyl moiety is capable of conversion into hydrophilic sulfonamide moiety in the presence of nitrite ion, through a modified Griess reaction (Figure 5C). Thus, when the mono (PEDA)-functionalized coating was exposed to a mixture of the sulfanilamide and nitrite ions at acidic conditions, it resulted in the elevation of underwater OCA depending on the concentration of nitrite ions in the aqueous phase due to gradual conversion of hydrophobic phenyl groups to hydrophilic sulfonamide moiety (Figure 5D). Further, the dual-functionalized (PEDA/CEA) coating that displayed an adhesive underwater superoleophobicity was explored to demonstrate the sensing of nitrite ions just by observing the rolling of a beaded oil droplet at a certain tilting angle of the surface, where the elevated concentration of nitrite ion reduced the oil-adhesion property as indicated by the decrease in roll-off angle of the beaded oil droplet (Figure 5E). Furthermore, the current design extended to sense another relevant toxic chemical, i.e., hydrazine (N_2H_4), by

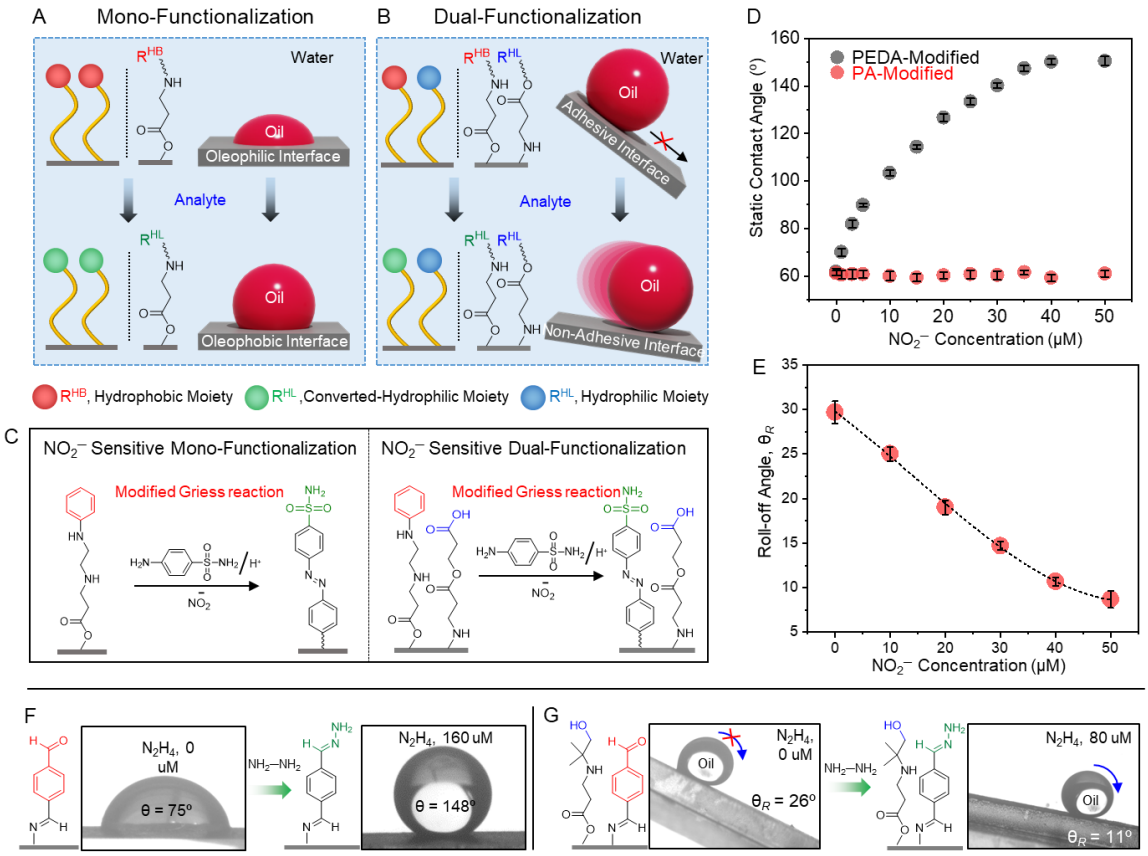

Figure 5. (A, B) Schematic representation of (A) mono and (B) dual-functionalization, where the selected hydrophobic aromatic moiety converts into a hydrophilic moiety on exposure to selected analytes, resulting in the raising of the OCA and rolling of beaded oil droplets underwater, respectively. (C) Nitrite ion sensitive functionalization, where the hydrophobic phenyl moiety converts into a hydrophilic moiety in the presence of nitrite ions, following a modified Griess reaction. (D) The nitrite ion concentration dependent alteration of OCA. (E) Roll-off angle (θ_R) as a function of nitrite ion concentration on dual-functionalized surface. (F−G) Contact angle goniometer images depicting (F) mono (TPA)-functionalized multilayer coating and its conversion into oleophobicity, and (G) dual (TPA/AMP)-functionalized multilayer coating and its conversion into non-adhesive superoleophobicity, after treatment with hydrazine. Adapted with permission from *Chem. Commun.*, 2023, **59**, 7915. Copyright 2023, The Royal Society of Chemistry.

strategic modification with terephthalaldehyde (TPA) and 2-amino-2-methyl-1-propanol (AMP) to develop another set of mono and dual-functionalized coatings (Figure 5F and G). In the case of the mono (TPA)-functionalized coating, the residual aldehyde group present in it allowed to demonstrate the raise in underwater OCA through Schiff base reaction with hydrazine (Figure 5F), whereas a gradual depletion of oil adhesion property was observed for dual (TPA/AMP)-modified coating after hydrazine treatment (Figure 5G).

Chapter 5: Chemically Customizing Mechanical Properties and Optical Transparency in Underwater Superoleophobic Coating

The co-association of mechanical durability and optical transparency with underwater superoleophobicity is essential for the realistic performance of marine infrastructures and other applications. While the design of mechanically durable and absolutely optically transparent underwater superoleophobic coating remains challenging, in this chapter, a covalently crosslinked and chemically reactive sol-gel conversion process is introduced through 1, 4-conjugate addition reaction to achieve a substrate-independent and tolerant coating for orthogonally modulating the underwater oil wettability, optical transparency, and even mechanical properties of highly deformable porous and fibrous substrates.

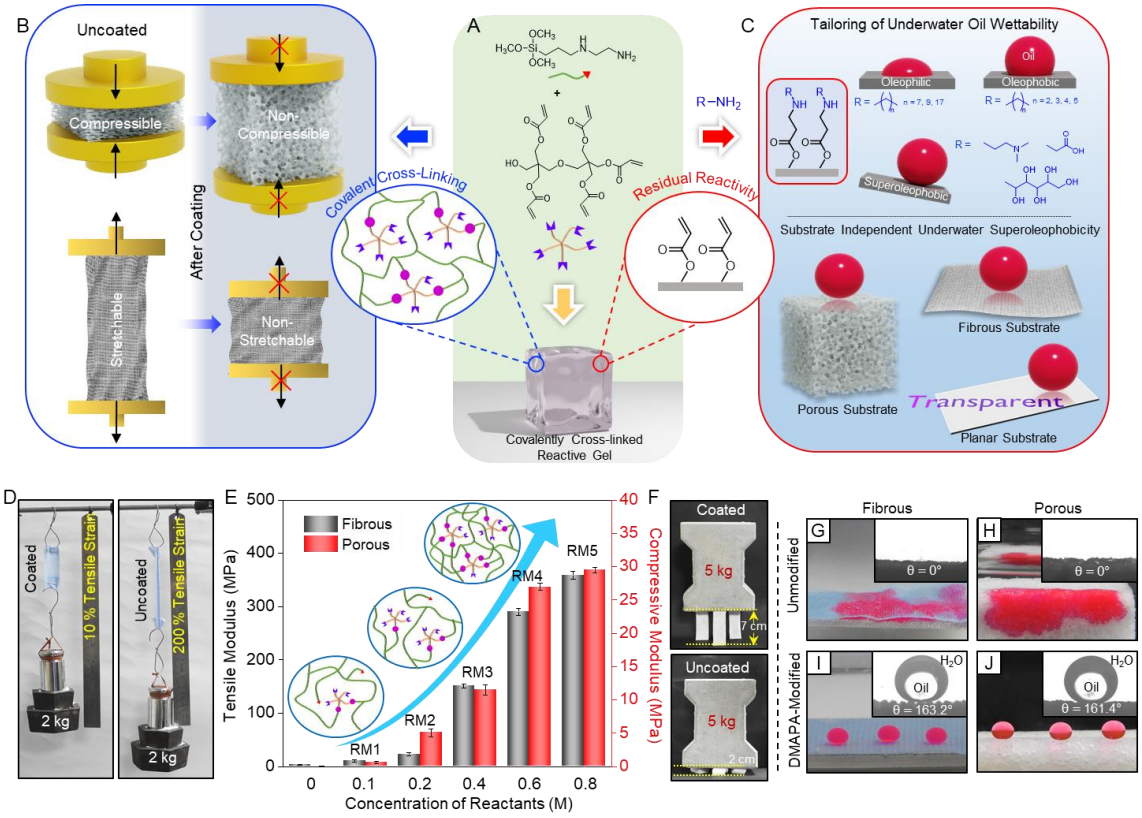

Figure 6. (A) Mutual reaction between AEAPTMS and 5Acl yields a covalently cross-linked reactive gel comprising of residual acrylate moieties. (B) Schematic represents the customization of the mechanical properties (compressive and tensile) of the highly deformable porous and fibrous substrates after coating with the covalently cross-linked reactive gel. (C) Schematic depicting the customization of underwater oil wettability on various substrates following the post modification. (D) Digital images showing tensile deformation of coated and bare fabric under an applied load of 2 kg. E) Graph illustrates the impact of different reaction mixture coatings on the tensile modulus and compressive modulus of fabric (grey) and sponge (red), respectively. F) Photographs of compressive deformation of coated and bare sponges under an applied load of 5 kg. (G-J) Photographs and contact angle goniometer images (inset) showing the underwater oil wettability of the coated (G, I) fabric and (H, J) sponge, (G, H) before and (I, J) after DMAPA modification. Adapted with permission from *Adv. Funct. Mater*., 2023, **33**, 2302569. Copyright 2023, Wiley.

The 1, 4-conjugate addition reaction between a self-polymerizable monomer, i.e., 3-(2-aminoethylamino)propyl-trimethoxysilane (AEAPTMS) and a cross-linker, i.e., 5Acl, in ethanol yielded a covalently crosslinked, optically transparent, and chemically reactive gel within 10 min, at ambient conditions (Figure 6A). Taking advantage of such facile sol-gel conversion of the reaction mixture of the small molecule and cross-linker, two distinct geometrically complex (fibrous and porous), and highly deformable (tensile and compressive) substrates were coated with the reactive gel, following the dip-coating approach. The tensile and compressive modulus of the highly deformable substrates was significantly improved after

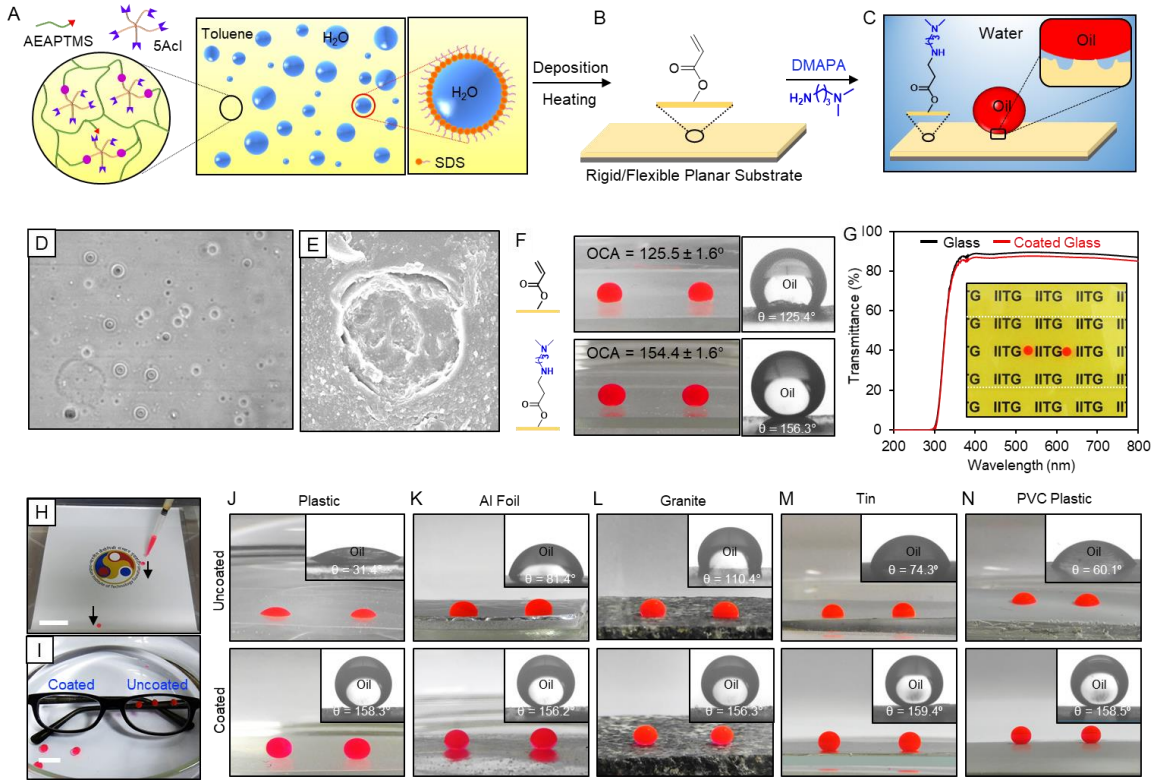

Figure 7. (A) Schematic depicting the dispersed micrometer-sized droplets of DI water in the reaction mixture of AEAPTMS and 5Acl in toluene. (B) The deposition of the reaction mixture on a planar substrate and sequential heating gives a transparent coating with residual acrylates. C) The post-modification of residual acrylates with DMAPA conferred underwater superoleophobicity. (D) Optical microscopic image and (E) FESEM image of the coating show depleted hemispherical domains. Scale bars, 10 µm (D), 2 µm (E). (F) Digital images and contact angle goniometer images of underwater oil wettability of the coating on a glass substrate before and after modification with DMAPA. G) Comparison of optical transparency of bare glass and coated glass. (H, I) Photographs showing the rolling of beaded oil droplets on a coated (H) large glass object, and (I) spectacle. (J-N) Digital and contact angle goniometer images (inset) showing the underwater oil wetting on (J) plastic film, (K) Al foil, (L) granite slab, (M) tin plate and (N) PVC plastic, before and after depositing DMAPA modified coating. Adapted with permission from *Adv. Funct. Mater.*, 2023, **33**, 2302569. Copyright 2023, Wiley.

the deposition of reactive gel, followed by its gelation (Figure 6B and D−F). Thereafter, the residual chemical reactivity of the coating deposited on the fabric and sponge was explored to achieve underwater superoleophobicity, following the post-modification with DMAPA through the 1, 4-conjugate addition reaction at ambient conditions (Figure 6C and G−J). Moreover, the selection of various hydrophilic and hydrophobic primary amine-containing small molecules as modifiers provided a facile basis to tailor other intermediate underwater oil-wettability. Further, the association of the oil repellence property did not compromise the mechanical property of the coated substrates, and coated substrates displayed tolerance to various practically relevant severe physical and chemical durability tests.

Next, I sought to achieve such bio-inspired transparent coating on a featureless planar substrate following a simple doctor blade method, where AEAPTMS and 5Acl were dissolved in a water-immiscible organic solvent, i.e., toluene and the inverse emulsion of water was generated in the presence of a stabilizer, i.e., SDS (Figure 7A). The planar substrate was coated with the as-obtained reaction mixture and kept for gelation, and the evaporation of dispersed water droplets on elevated temperature left behind depleted hierarchical topography in the coating (Figure 7B, D and E). The post-functionalization of the reactive coating with DMAPA resulted in underwater superoleophobicity (Figure 7C, F) with high transparency, similar to bare glass (Figure 7G). This method is extended to coat various objects, large glass surfaces, spectacles, flexible (plastic film, aluminium foil), and rigid planar (granite slab, tin plate, and PVC plastic) substrates (Figure 7H−N). Thus, such a facile and scalable chemical approach for developing optically transparent, substrate-independent, and physically/chemically tolerant underwater superoleophobicity would be useful in a wide range of relevant indoor and outdoor applications.

Chapter 6: Conclusion and Future Directions

In conclusion, this synopsis report introduces rapid and facile synthetic approaches for preparing artificial underwater superoleophobic surfaces by co-optimizing essential topography and chemistry, following LbL deposition and sol-gel conversion process adopting readily reactive covalent chemistry, i.e., 1, 4-conjugate addition reaction. The mutual reaction between amine and acrylates of the strategically selected precursors through the 1, 4-conjugate addition reaction allowed the construction of coatings with residual reactivities, which provides the opportunity to post-modification with desired small molecules to derive tolerant, tailorable, and responsive underwater oil wettability and oil adhesion. The strategic post-modifications of

the residual reactivities with selected chemicals provided underwater oil adhesive superoleophobicity for the immobilization of ultra-sensitive LC microdroplets for its sensing application. Moreover, the reactive coating enables the design of reversibly responsive underwater superoleophobic coating with tailored oil adhesion in the presence of selected amphiphiles in specified pH conditions after the appropriate post-covalent modifications. Further, the reactive coatings were extended for toxic chemical sensing by monitoring the raising of the OCA and rolling of a beaded oil droplet underwater in the presence of targeted toxic chemicals. Moreover, the same covalent chemistry allowed to tailor mechanical properties of deformable objects and transparency in the underwater superoleophobic coating.

In this synopsis report, underwater superoleophobicity derived from dually reactive multilayer coatings is unprecedently utilized for the naked-eye sensing of relevant toxic chemicals. In this context, such principles provide the basis for monitoring other different toxic chemicals, and biological events, such as protein-lipid interaction and enzymatic activity in underwater superoleophobic surfaces through modulation of oil wettability and adhesion, which will be explored in the near future. Furthermore, past studies reported that underwater superoleophobicity has a significant role in exhibiting anti-platelet adhesion. The platelet activation/adhesion is affected by many factors, such as chemical composition, surface morphology, charge, and wettability. In this context, the chemically reactive coatings reported in this synopsis appeared as an ideal candidate for the investigations on platelet activation/adhesion, as it provides a wide window to tailor chemical composition, charge, and wettability of the surface through desired chemical modifications. Future efforts will seek a detailed investigation in this particular direction.

Moreover, the underwater superoleophobic surfaces also become superaerophobic after water immersion, inhibiting the air bubble adhesion on its surface. This special anti-bubble adhesion property has been used for various relevant underwater applications. In this context, the underwater superoleophobic coatings prepared in the synopsis report would efficiently perform underwater superaerophobic properties with tailored adhesion which will be explored in the field of controlled transport of gas bubbles, gas phase micro reactions, etc. Moreover, the deposition of such coating on electrochemical electrodes could able to perform enhanced H_2 gas production through water splitting due to the early detachment of the generated gas bubble from the electrolyte surface.

1. Introduction

1.1 Biomimicry: Innovation Inspired by Nature

Biomimicry is a practice of taking inspiration from the strategies found in nature and translating the principles to human engineering to solve different challenges.[1] For hundreds of years, nature has been proven to have solutions to humans' most significant challenges. There are numerous examples of biomimicry in action; a few of them has been highlighted here. Leonardo da Vinci pioneered taking inspiration from nature's creation when he intended to design human "wings", taking inspiration from birds' anatomy. His idea was one of humankind's greatest inspirations from nature, leading the Wright brothers to design and fly the first airplane in 1903.[2] The bullet train is another example, inspired by Kingfisher's pointed beak.[3] The designers noticed that kingfishers can dive into the water to catch prey, making minimum splash due to the pointed shape of their beaks. Mimicking this shape into the front of the train reduced the air pressure when travelling through tunnels, thus reducing the noise pollution at the tunnel's exit. The fins of humpback whales inspired to design of efficient wind turbine blades, fans, etc.[4] The designers discovered that humpback whales can move underwater with surprising speed and efficiency due to the bumps in their fin, which generate lift, reduce drag and delay stall. The adaptation of such designs in the wind turbine blades made them more stable, quiet, and durable than conventional blades. Another famous example of biomimicry is Velcro. George de Mestral, a Swiss engineer, invented Velcro, taking inspiration from a particular seed with tiny hooks that fastened to soft fur or fabric.[5] There are many more examples where biomimicry gave us astounding innovations, such as antimicrobial film mimicking sharkskin[6], harvesting water like the Stenocara beetle[7], absorbing shock like a woodpecker[8], ventilation systems inspired by termites[9] etc.

Every creature in nature has its own survival skills that allow them to thrive. To survive and adapt to the complex environment on earth, they have evolved exceptional capabilities to cope with all kinds of harsh living conditions. Superwetting or anti-wetting surfaces widely found in nature's creatures bestow their survival under harsh environmental conditions.[10] For instance, superhydrophobicity of the lotus leaf[11,12] makes it clean in dirt and dust, underwater superoleophobicity of fish scales[13,14] keeps themselves clean in oily water, slippery property of pitcher plants[15,16] helps capture insects readily, patterned wettability in Stenocara beetle[7] enables it to collect water in drought condition. Bio-mimicking such superwetting behavior of naturally existing creatures has paved the way for developing superwetting functional materials

for a wide range of applications in engineering, healthcare, and environmental remediation.[17-20] This chapter outlines an extensive discussion in bio-inspired liquid wettability, theoretical explanation, the development of artificial liquid wetting surfaces, its applications, and challenges.

1.2. Creatures in Nature with Superwettability

There are many organisms in animals and plants kingdom possessing surfaces with diversified special wettabilities. Imitating such examples from nature enables us to design and prepare bionic interfaces with superwettability, which greatly contributes to the research and development of materials. For instance, Barthlott studied the self-cleaning effect and superhydrophobic phenomenon on a lotus leaf surface[11] (Figure 1.1A), which opened up a new horizon for developing biomimetic superwetting materials. Beaded water droplets remained perfectly spherical on the lotus leaf and readily rolled off on the surface, carrying the dust and dirt deposited on it. Although this self-cleaning effect of the lotus leaf surface was observed early, the mechanism behind this phenomenon was known after the careful investigation of the surface topography of the lotus leaf surface through scanning electron microscope (SEM) imaging. Over the past decades, research on lotus leaves revealed that the surface of lotus leaf is composed of micro and nanostructures (Figure 1.1A), topped with hydrophobic epicuticular wax crystalloids, which is the key to its superhydrophobicity.[21-23] Since then, various water-repelling surfaces in nature with diversified wetting behaviors have been discovered, such as high-adhesive superhydrophobic surfaces of rose petals[24] (Figure 1.1B), the anisotropic wettability of the rice leaf[25] (Figure 1.1C), the directional adhesion of a butterfly wing[26] (Figure 1.1D), the anti-fogging ability of a mosquito eye[27] (Figure 1.1E), water-collection of a desert beetle[7] (Figure 1.1F), underwater long-termair retentions of Salvinia plants[27] (Figure 1.1G), the ability of a water strider to walk and jump on the surface of water[29] (Figure 1.1H), etc. The detailed investigations led the researchers to conclude that both hierarchical surface topography and chemical composition on the surface confer special wettabilities in the creatures mentioned above.

Most of these above-mentioned special liquid wettability is performed in air. In recent years, many creatures were also found to display another important super liquid wettability that performs underwater, where beaded oil droplet is extremely repelled by naturally existing surfaces of some creatures. Such extreme oil repellence underwater is termed underwater

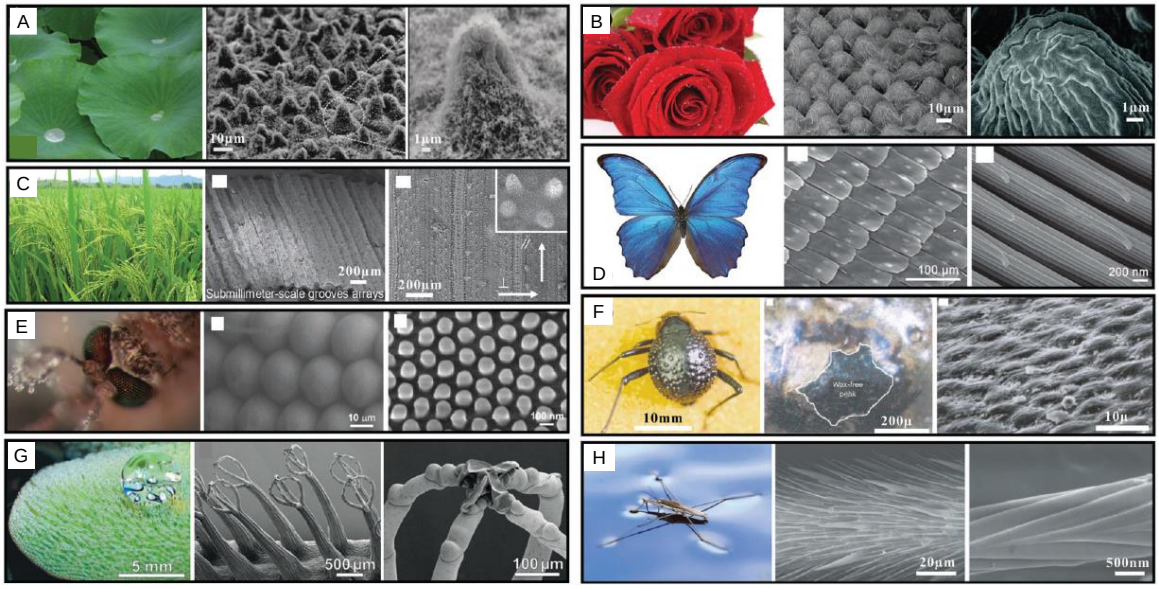

Figure 1.1. Photographs and scanning electron microscope (SEM) images of various animals and plants exhibiting special wettability: (A) lotus leaf, showing superhydrophobicity, (B) rose petal with adhesive superhydrophobicity, (C) rice leaf exhibiting anisotropic superhydrophobicity, (D) butterfly wing with directional adhesive superhydrophobicity, (E) mosquito eye with anti-fogging ability, (F) desert beetle with patterned wettability, (G) salvinia plant exhibiting superhydrophobicity, and (G) leg of a water strider with superhydrophobicity. (A) Reproduced from ref. 12 with permission from Wiley, copyright 2008. (B) Reproduced from ref. 24 with permission from American Chemical Society, copyright 2008. (C) Reproduced from ref. 25 with permission from Wiley, copyright 2011. (D) Reproduced from ref. 26 with permission from Royal Society of Chemistry, copyright 2007. (E) Reproduced from ref. 27 with permission from Wiley, copyright 2007. (F) Reproduced from ref. 7 with permission from NPG, copyright 2001. (G) Reproduced from ref. 28 with permission from Wiley, copyright 2010. (H) Reproduced from ref. 29 with permission from NPG, copyright 2004.

superoleophobicity. A detailed description of a few such creatures and the origin of such special wettability on their surface is provided below.

a) Fish Scale

Jiang *et al.* reported the underwater superoleophobic property of fish scale (Figure 1.2A−B), which helps the fishes to survive even in oil-contaminated water without their skin being stained.[13] Fish scales comprise a hydrophilic calcium phosphate ($Ca_3(PO_4)_2$) skeleton and protein coated with a thin layer of mucus. SEM images revealed that the scale's surface is distributed with many oriented micropapillae with length of 100–300 μm and width of 30–40 μm (Figure 1.2C). Even the micropapillae are not smooth and instead possess fine-scale roughness (Figure 1.2D). Water can wet the surface due to its hydrophilic nature and be trapped in the rough microstructures of fish scales, creating an oil-repelling water cushion. Thus, the

co-association of hydrophilic chemical composition and rough microstructures in the fish scales enabled to exhibit underwater superoleophobicity.

b) Shark skin

Shark skin is fascinating to researchers due to its exceptional swimming speed and extreme oil-repellent property in water. The shark skin is covered with many small single tooth-like scales, which have ribbed structures oriented parallel to the local direction of water flow (Figure 1.2E−F).[30] These structures can reduce drag or resistance and help sharks to swim quickly and efficiently in water. Furthermore, these scales are hydrophilic in composition, and there is a thin layer of mucus on the top of the ribbed structures (Figure 1.2F), which confer underwater superoleophobic property to the shark skin to prevent marine fouling and bio-adhesion, thus exhibiting a self-cleaning property.

c) Clam's Shell

The internal surface of a clam's shell can be divided into two areas: the relatively smooth edge region (region-1) and the coarse central region (region-2), as shown in (Figure 1.2G).[31] Although the chemical compositions of these two regions are almost similar, the surface topographies have significant dissimilarity. Region-1 is covered with micrometer-scale leaf-like slices, while region-2 is featured with rough micrometer-scale chunks heaped in an irregular pattern, which are further decorated by several nanometer-scaled blocks (Figure 1.2H). When the clam's shell was exposed to the oil/oily phase, region-1 was fouled by the oil phase, whereas region-2 remained cleaned. This exceptional anti-oil property of region-2 is due to the existence of the hydrophilic $CaCO_3$ surface having rough hierarchical microstructures.

d) Lower Side of the Lotus Leaf

The superhydrophobic property and the self-cleaning effect of the upper surface of lotus leaf are described in the previous section. However, Cheng *et al.* discovered that the lower surface of the lotus leaf gets completely wet with water in air, and it exhibits superoleophobic property underwater (Figure 1.2I).[32] The reason behind this inverse wettability exhibited by the upper and lower surfaces of lotus lead can be attributed to the differences in chemical composition and surface microtopography. Studies reveal that there is no wax crystals layer on the lower surface of the lotus leaf, and the surface microstructures are different from the upper surface, with tabular and slightly convex lumps covered with nanogroove structures (Figure 1.2J). The

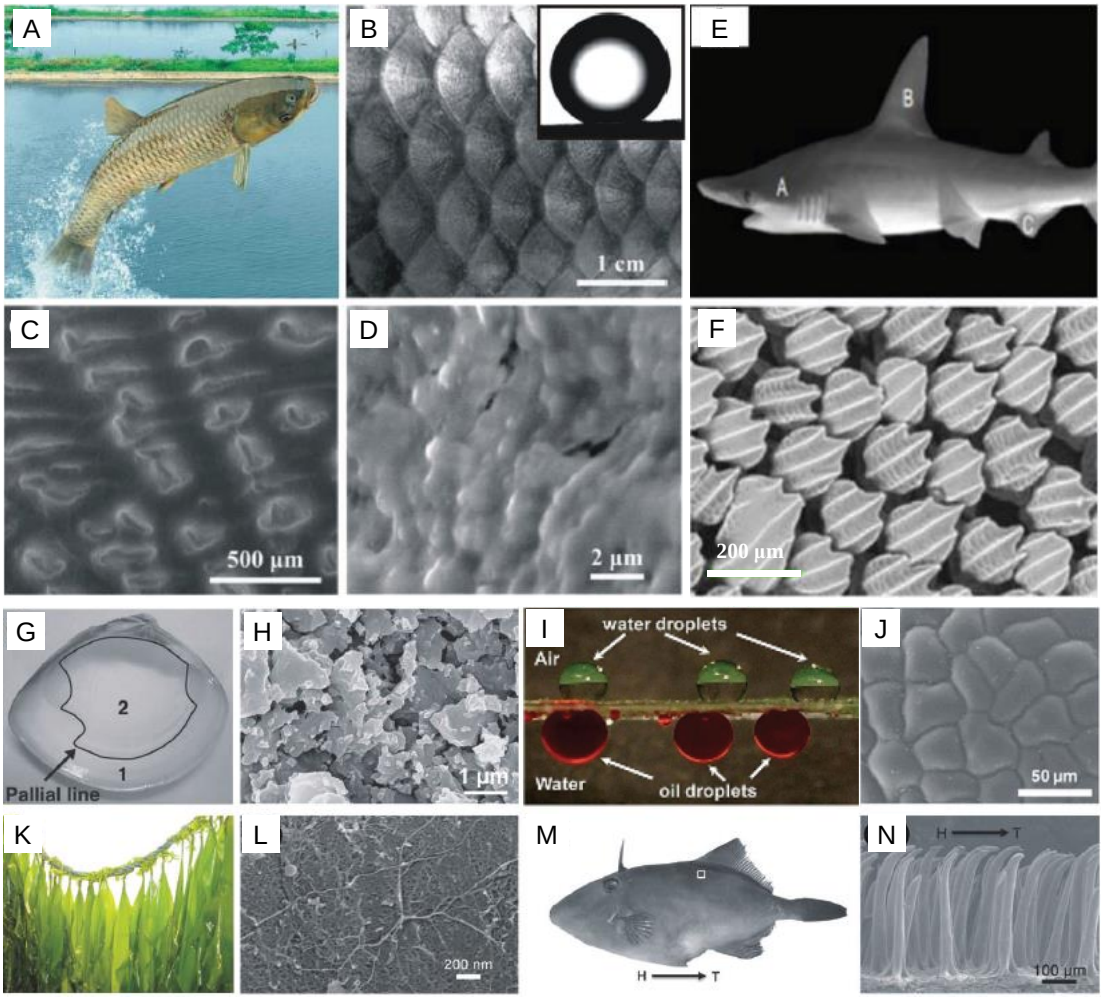

Figure 1.2. Photographs and SEM images of natural creatures with underwater superoleophobicity: (A−D) fish scale, (E, F) shark skin, (G, H) clam's shell, (I, J) lower surface of lotus leaf, (K, L) seaweed, (M, N) filefish. (A−D) Reproduced from ref. 13 with permission from Wiley, copyright 2009. (E, F) Reproduced from ref. 30 with permission from Company of Biologists, copyright 2014. (G, H) Reproduced from ref. 31 with permission from Wiley, copyright 2012. (I, J) Reproduced from ref. 32 with permission from Royal Society of Chemistry. Copyright 2011. (K, L) Reproduced from ref. 33 with permission from Wiley, copyright 2015. (M, N) Reproduced from ref. 34 with permission from Wiley, copyright 2014.

combination of hydrophilic chemistry and hierarchical surface roughness makes the lower surface hydrophilic in air and superoleophobic in water.

e) Seaweed

Seaweed surfaces possess highly porous structures, as shown in Figure 1.2K−L, and are composed of several natural polysaccharides, such as alginate, carrageenan, and agar, which makes them exhibit durable underwater superoleophobicity.[33] Moreover, the uninterrupted underwater superoleophobicity is observed even in high salinity since the polysaccharide molecule can quickly bond to water molecules in the high salinity solution as well. The

combination of porous microstructures and salt-tolerant polysaccharides confer salt-insensitive underwater superoleophobicity.

f) Filefish

Filefish exhibits a unique anti-oil wetting property, i.e., anisotropic underwater superoleophobicity, where the oil droplets tend to directionally roll-off its skin from head to tail, keeping it clean, while fouled by the oil droplet in the opposite direction. This remarkable wetting behavior prevented the oil phase getting accumulated at the filefish's head. The filefish skin (Figure 1.2M) is comprised of plenty of hydrophilic organics such as collagen, and it is decorated by oriented hook-like spines providing a high degree of surface roughness (Figure 1.2N).[34] Both the hydrophilic chemistry and rough topography are essential to confer underwater superoleophobicity, and simultaneously the curved tips of the spines endow the unidirectional movement of oil droplets.

1.3. Theoretical Basis to Understand Underwater Superoleophobicity

Wetting of liquid on a solid surface is conventionally characterized by the contact angle (Figure 1.3A). It represents the angle formed by a liquid at the three-phase boundary where a liquid, gas and solid intersect. Over the period, various theories have evolved for a better understanding of the liquid wetting phenomenon, which are discussed below in detail.

a) Young's Model

In 1805, the pioneer of wettability research, Thomas Young, proposed an equation to define the contact angle of a liquid on an ideally flat surface.[35] According to Young's model, when a liquid droplet contacts a surface in air, it will have an inevitable tendency to reach an equilibrium state with the lowest energy; thus, the contact angle (θ_Y) can be determined by the balance of three interfacial energy/surface tension between the liquid–vapor (γ_{LV}), liquid–solid (γ_{LV}), and vapor–solid (γ_{LV}) interfaces (Figure 1.3A), as follows,

$$cos\ \theta_Y = \frac{\gamma_{SV} - \gamma_{SL}}{\gamma_{LV}} \quad (1)$$

b) Wenzel Model

Young's equation only applies to ideal surfaces with homogenous surface chemistry and smooth topography. However, real surfaces do possess surface roughness and chemical inhomogeneity. In 1936, Wenzel defined the relationship between surface roughness and wettability by introducing the concept of surface roughness, r, which refers to the ratio of the

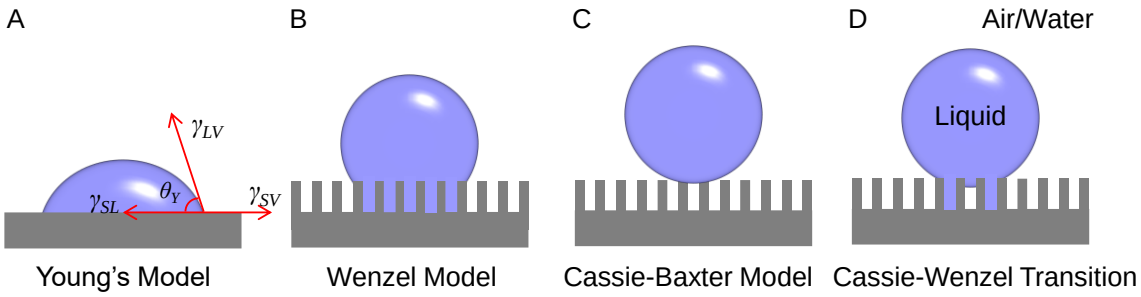

Figure 1.3. Wetting models to describe liquid droplet wettability on different surfaces: (A) Young's model, (B) Wenzel model, (C) Cassie-Baxter Model, (D) Cassie-Wenzel transitional Model.

actual area to the apparent surface area (Figure 1.3B).[36] The modified Young's equation is as follows,

$$cos\ \theta^* = \frac{r(\gamma_{SV}-\gamma_{SL})}{\gamma_{LV}} = r\cos\theta_Y \qquad (2)$$

θ is the intrinsic contact angle of the liquid droplet on a flat substrate. In Wenzel state, the liquid completely fills the voids in the rough surface, as shown in Figure 1.3B. According to this equation, as r is greater than 1 for rough surfaces, the surface roughness leads to the amplification of the intrinsic wettability of a surface. This implies that a hydrophilic substrate becomes more hydrophilic and a hydrophobic substrate becomes more hydrophobic on the association of surface roughness in air.

c) Cassie-Baxter Model

Wenzel's equation assumes that the liquid penetrates the rough grooves of the surface, and thus Wenzel's equation cannot be applied where the liquids do not penetrate the grooves. Cassie–Baxter model describes the wetting of a droplet suspended over the rough structure, resulting in a composite interface, as shown in Figure 1.3C.[37] The voids on the surface are filled with air, forming a trapped air cushion. In this case, the liquid sits on the composite interface of solid and air, and the resultant contact angle derived by Cassie and Baxter in 1944 can be expressed as:

$$cos\ \theta_{CB} = f_s\, cos\ \theta_s + f_v\, cos\ \theta_v \qquad (3)$$

where, cos θ_{CB} defines the apparent contact angle, f_s and f_v represents geometrical fractional contact area for solid-liquid and vapor-liquid interfaces, respectively. θ_s and θ_v are the intrinsic contact angle of a liquid droplet on those two interfaces, solid-liquid and vapor-liquid,

respectively. Here, $f_s + f_v = 1$, and $\theta_s = \theta_Y$, and the contact angle in the air is almost equal to 180°, i.e., $\theta_v = 180°$; thus, the Equation (3) can be simplified into:

$$cos\ \theta_{CB} = f_s\,(cos\ \theta_Y + 1) - 1 \quad (4)$$

In the case of underwater superoleophobic interfaces, the voids on the rough surface are filled with trapped water, forming a water cushion. In this case, the oil droplet sits on the composite interface of solid and water, and the apparent oil contact angle ($cos\ \theta_{CB}^{oil}$) can be described as:

$$cos\ \theta_{CB}^{oil} = f_s\, cos\ \theta_s + f_w\, cos\ \theta_w \quad (5)$$

Where f_s *and* f_w represent fractional contact area for solid-oil and water-oil interfaces, respectively. θ_s and θ_w are the contact angles of the oil droplet in the solid-oil and water-oil interface, respectively, in underwater conditions.

d) Cassie-Wenzel Transitional Model

In addition, a transition state between the Cassie and Wenzel state is also observed when the liquid droplet partly fills the voids in the rough structure of the surface, resulting in a Cassie-Wenzel transition state, as shown in Figure 1.3D.[38,39] The adhesion of the liquid droplet to the surface can differ from low to high depending on the extent of the liquid penetration in the voids.

1.3.1. Classification of Liquid Wettability

According to young's equation, the contact angle limit, θ = 90°, determines the lyophilicity or lyophobicity of a surface. Thus, in everyday practice, surfaces with a water contact angle < 90° are considered hydrophilic, and those that have contact angles > 90° are hydrophobic (Figures 1.4A and B).[35] Berg *et al*. introduced a new limit of 65° between hydrophilicity and hydrophobicity by considering the actual chemical and structural state of the water droplet,[40] though most researchers still consider the limit of hydrophilicity and hydrophobicity to be 90°. There have not been efforts to revalidate the limit to determine oleophilic and oleophobic surfaces, possibly due to the diversity and complexity of the oil phase. Thus, solid surfaces with oil contact angles θ < 90° are considered to be oleophilic, and those with oil contact angles θ > 90° are oleophobic.

When the water completely wets a surface (and its voids) is considered superhydrophilic, with an apparent contact angle of less than 10° (Figure 1.4C).[41] Notably, superhydrophilic surfaces

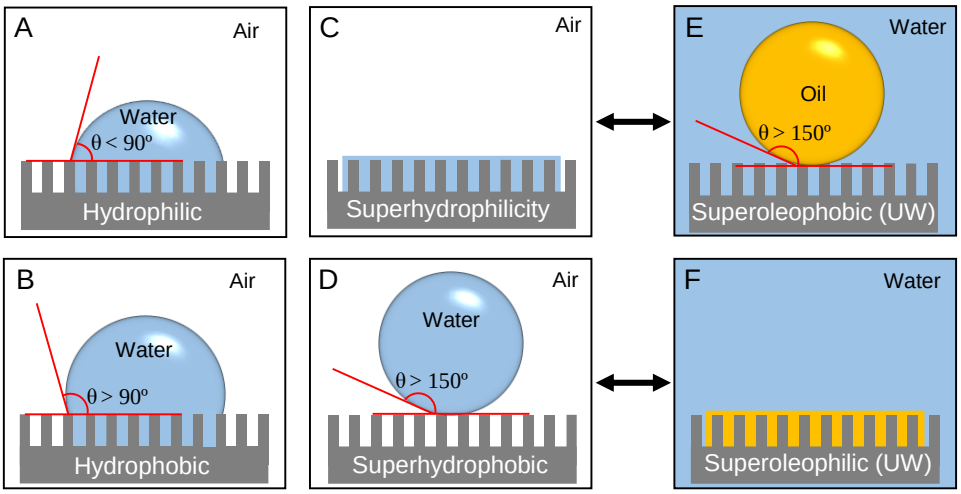

Figure 1.4. Different wetting states: (A) hydrophilicity, (B) hydrophobicity, (C) superhydrophilicity, (D) superhydrophobicity, (E) underwater superoleophobicity and (F) underwater superoleophilicity on rough solid surfaces.

give rise to superoleophobicity (oil contact angle $\theta > 150°$) when immersed underwater due to the entrapment of a water layer within grooves of the rough surface to repel the oil phase (Figure 1.4E).[13] Whereas when the water droplet cannot wet the surface due to the presence of trapped air in the voids, it can be considered a superhydrophobic surface, with a contact angle $\theta > 150°$ (Figure 1.4D).[42] When immersed underwater, the superhydrophobic surface gives rise to superoleophilicity with oil contact angle below 10° (Figure 1.4F).

Besides contact angle, contact angle hysteresis (CAH) and roll-off angle (θ_R) are also measured in wettability studies to acquire information about the liquid-surface adhesion. CAH is defined as the difference between advancing contact angle (θ_{Adv}) and receding contact angle (θ_{Adv}). When a dispensed liquid droplet volume is gradually increased on a solid surface, the maximum contact angle is considered as θ_{Adv} (Figure 1.5A); whereas when the droplet is slowly removed

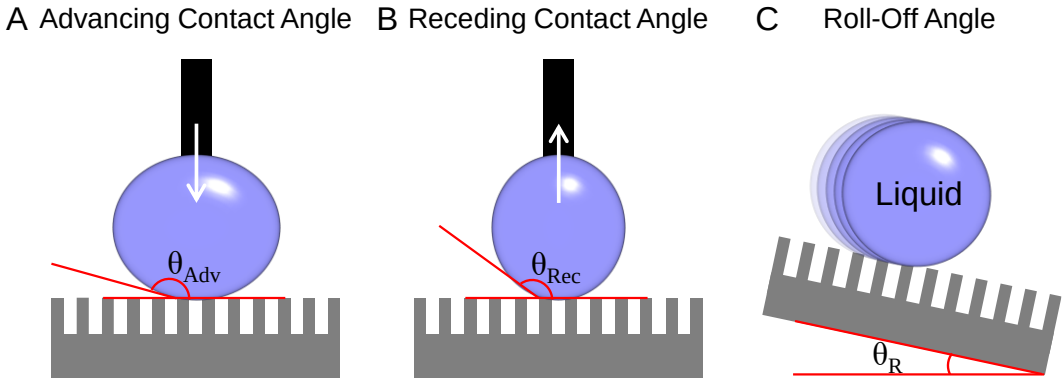

Figure 1.5. Schematic depiction of (A) advancing contact angle, (B) receding contact angle and (C) roll-off angle.

from the surface, the minimum contact angle is defined as θ_{Rec} (Figure 1.5B).[43] The CAH can also be reflected by roll-off angle or tilt angle, i.e., the critical angle of tilting a horizontal surface to allow rolling off a liquid droplet on the solid surface (Figure 1.5C).[23] The solid surfaces with smaller CAH or roll-off angles have smaller adhesion between the beaded liquid droplet and the solid surface, whereas higher CAH or roll-off angles indicate high adhesion between the liquid and solid. When the CAH or roll-off angles are less than 10º, surfaces can be considered non-adhesive, which contributes to self-cleaning performance.

1.4. Design Principles for Artificial Underwater Superoleophobicity

Studies on nature's creatures paved the way to design and fabricate superwettable interfaces artificially in the most effective way. Nature's creatures reveal that co-optimization of both hierarchically rough (micro/nanoscale) topography and the intrinsic chemical composition on the surface is essential to confer superwettability.[10,14,21-23] Figure 1.6 summarizes the importance of both the essential criteria to exhibit bio-mimicked superwettability, where it demonstrates how the chemical composition determines the lyophilicity or lyophobicity of an ideally smooth surface, as described by Young's model. Furthermore, the association of roughness on the surface amplifies the intrinsic wettability of the surface to exhibit superwettability. Thus, fish-scale inspired superhydrophilicity (underwater superolephobicity) can be achieved on artificially prepared micro and nanoscale hierarchical surfaces after the incorporation of hydrophilic (high surface energy) surface coating. This principle was validated in an experiment where the removal of the mucus layer of the fish scale led to a decrease in the oil contact angle dramatically to around 150°, compromising the oil repellence. The degree of such oleophobicity in the fish scale can be attributed to its inherent hierarchical structures in the absence of the mucus layer.[14] Conversely, a rough hierarchical surface can provide lotus leaf-inspired superhydrophobicity (underwater superoleophilicity) after combining the hydrophobic (low surface energy) surface coating.

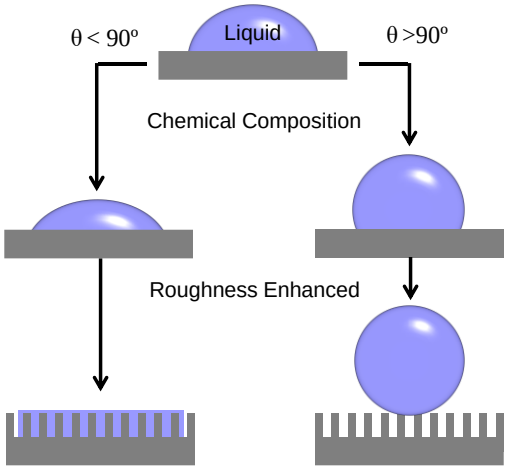

Figure 1.6. Schematic depiction the effect of chemical composition and enhanced roughness on an ideally smooth surface. Adapted from ref. 10 with permission from Springer Nature, copyright 2017.

1.5 Fabrication Methods for Adopting Underwater Superoleophobicity

Based on the inspiration from nature, researchers have adopted several approaches to fabricate numerous artificial underwater superoleophobic surfaces for diverse applications. The main focus is to meet the essential requirement of co-optimizing adequate surface topography and chemical composition through different methods. The following section provides an overview of various physical and chemical methods to fabricate underwater superoleophobic surfaces.

1.5.1 Template Method

In the templating method, surface roughness, which is essential to exhibit underwater superoleophobicity, is achieved by employing either natural or artificial templates with patterns.[13,32,34,44] The method involves the creation of templates with featured structures, pouring the reactants into the mold, and finally, removing the template. For example, Huang *et al.* used a porous anodic aluminum oxide (AAO) template to fabricate hierarchical films consisting of poly(pentafluorophenyl acrylate) free-standing micropillars grafted with poly(methacrylic acid) nanobrushes by in situ polymerization inside the porous AAO template, and subsequent post-polymerization modification allowed to achieve underwater superoleophobicity (Figure 1.7).[44] The method provides simplified fabrication steps and high efficiency; however, it suffers from repeatability and scalability issue since the template removal step, even of a relatively smaller scale, can damage the sample or even the template.

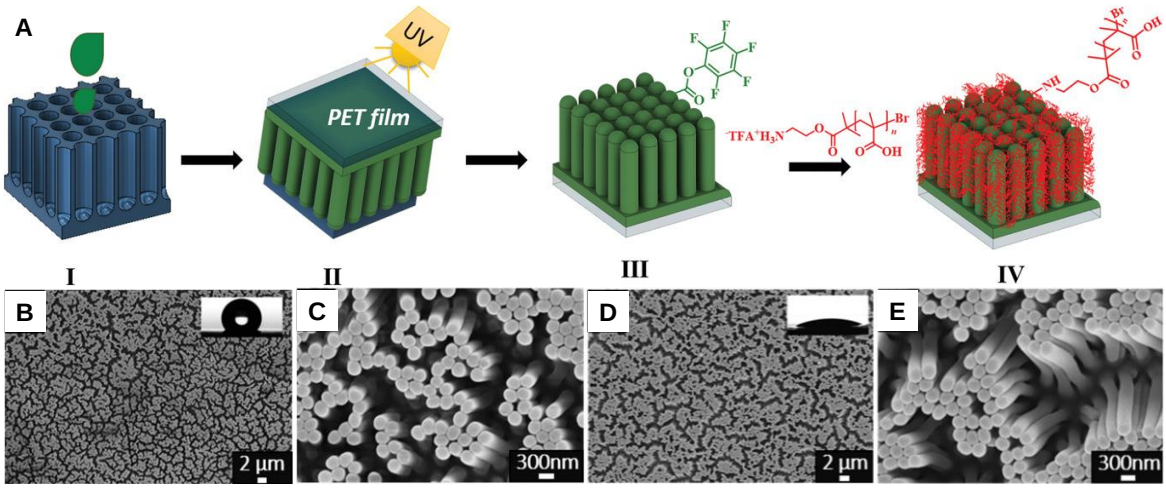

Figure 1.7. (A) Schematic illustration of template method: I) Drop casting the precursor liquid onto the template, II) UV irradiated polymerization in the template, III) removal of the template, and IV) post-polymerization modification. (B−E) Field emission scanning electron microscopy (FESEM) images (at low and high magnifications) of micropillars (B, C) before and (D, E) after post modification. Reproduced from ref. 44 with permission from Wiley, copyright 2020.

1.5.2. Electrospinning Method

Electrospinning is a widely employed method to fabricate micro-/nanostructured fibers exhibiting superwettability.[45-49] In this process, a high voltage is applied between the solution and a counter electrode to generate a repulsive force within the solution forcing the solution to pass through the tip of a needle/spinneret generating hierarchical structured nanofibers. Lim *et al.* adopted this method to fabricate a nanofibrous cellulosic membrane with uniform porous structures to achieve underwater superoleophobicity (Figure 1.8).[45] Ding *et al.* developed an underwater superoleophobic hierarchical nanofibrous membrane by combining electrospinning of polyacrylonitrile as substrate and then electrospraying of silica nanoparticles.[46]

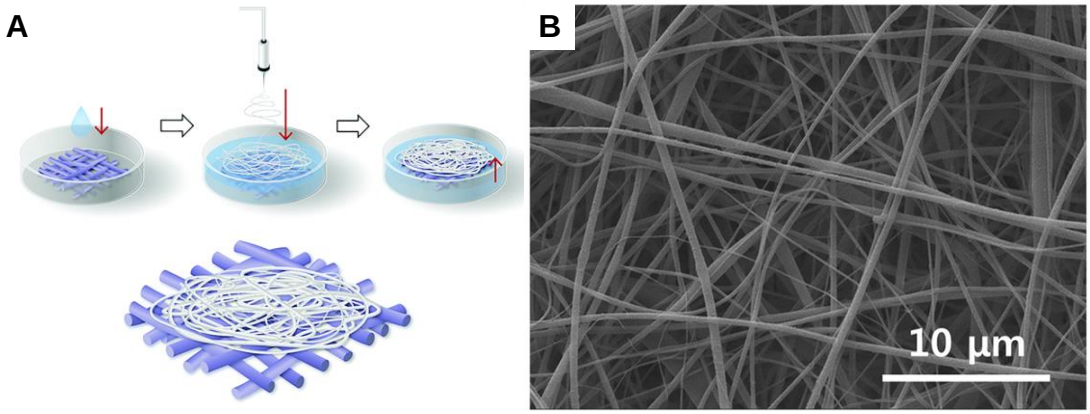

Figure 1.8. (A) Fabrication process of the nanofibrous cellulosic membrane through the deposition of the electrospun cellulose acetate on clean paper. (B) SEM image of the surface of the electrospun membrane. Reproduced from ref. 45 with permission from Royal Society of Chemistry, copyright 2018.

1.5.3. Dip/Spray/Spin Coating Method

The dip-coating is a straightforward approach for developing coating with rough topography on various substrates.[50-53] Specifically, in this approach, the substrate is dipped in the depositing solution to coat the surface with micro/nanoparticles, followed by surface modification. Liu *et al.* prepared polyvinylidene fluoride (PVDF) and stainless steel meshes (SSMs) membranes with superhydrophilicity and underwater superoleophobicity by dip-coating polyaniline (PANI) onto them.[50] Another simple and cost-effective method to create a rough structured coating on surfaces is spray coating, by spraying and subsequently solidifying the depositing solutions onto the substrates.[54-56] The simplicity and versatility of these approaches make them suitable for large-scale production of such interfaces.

Recently, another coating approach, spin coating, has been developed to prepare a coating with uniform and desired thickness where the solution or suspension is dispensed on the substrates

and then spun to achieve the coating.[57,58] Shang *et al.* spin-coated thermoplastic acrylic resin/poly(ethylene-vinyl acetate)-70% mixture solution (TPA/EVA-70%) to obtain TPA/EVA-70% film, where raspberry-like SiO_2@polydopamine@Ag particles were drop cast to achieve a healable underwater superoleophobic coating.[57] Spin coating method shows advantages in easy preparation and low cost but is merely suitable for flat substrates, which limits its further application on geometrically complex objects.

1.5.4. Femtosecond Laser Ablation Method

Laser ablation technique was applied to generate different micro and nano features on surfaces, where ultrashort pulse width and extremely high peak intensity are used to modulate topography.[59] This technique can be applied to a wide range of transparent or opaque surfaces, including silicon, glass, metals, and polymer, to achieve underwater superoleophobic surfaces, though the surfaces have to be flat and rigid.[60-64] Thus, the femtosecond laser approach can directly generate various micro/nanoscale hierarchical structures on the surfaces of a wide range of materials by a simple one-step ablation manner.

1.5.5 Hydrothermal Method

This fabrication method is performed in a hydrothermal reactor (mostly a Teflon autoclave), where the reactants are dissolved and crystallized at high temperatures and pressures to create hierarchal topography.[65-66] For example, Wang *et al.* prepared an underwater superoleophobic coating of TiO_2, where the morphology of hierarchical rutile TiO_2 flowers developed through a simple one-step hydrothermal method.[65] Hydrothermal method can be considered an efficient approach to generate products with high purity and uniform roughness; however, large-scale production of such coating through this method is challenging to achieve as it involves high pressure and temperature.

1.5.6. In-situ Polymerization Method

In-situ polymerization method involves the formation of a cross-linked polymeric coating on a substrate via the polymerization of the selected monomers while sturdily binding selected functional nanoparticles (e.g., SiO_2) in it.[67-69] It is noteworthy that the incorporated nanoparticles create nanoscale roughness, which is essential to exhibit underwater superoleophobicity, whereas the introduction of the functional polymer provides the desired chemistry and enhanced mechanical and thermal stability on the surfaces of selected substrates owing to the cross-linked chemistry. Yang *et al.* prepared an underwater superoleophobic

membrane, where an aldehyde benzoxazine, 3-phenyl-3,4-dihydro-2*H*-benzooxazine-6-carbaldehyde (BA-CHO), was used as a monomer, and additionally, SiO_2 nanoparticles were incorporated to generate nanoscale roughness into a silica nanofibrous membrane, that is previously fabricated by electrospinning method.[67] Notably, *in-situ* polymerization has appeared as a more efficient technique for fabricating durable underwater superoleophobic membranes capable of performing in harsh aqueous conditions when combined with other methods, such as electrospinning and coating methods.[68]

1.5.7. Layer-by-Layer (LbL) Deposition Method

This is a versatile and facile approach for constructing multilayer coatings by alternatively depositing various polyelectrolytes, inorganic nanoparticles, biomolecules, polymers etc., on a selected substrate through different interactions and bondings such as electrostatic, hydrogen bond, coordinate bond, covalent bonds, etc (Figure1.9).[70-76] Notably, this method provides control over coating thickness, generation of micro/nanostructure, and roughness in the coating by simply adjusting the deposition cycles and depositing ingredients. This method was first introduced by Hong and Decher in 1991 in a seminal report.[70] Later, this approach gained immense applicability in biomimicked wettability owing to its fabrication simplicity, ability to

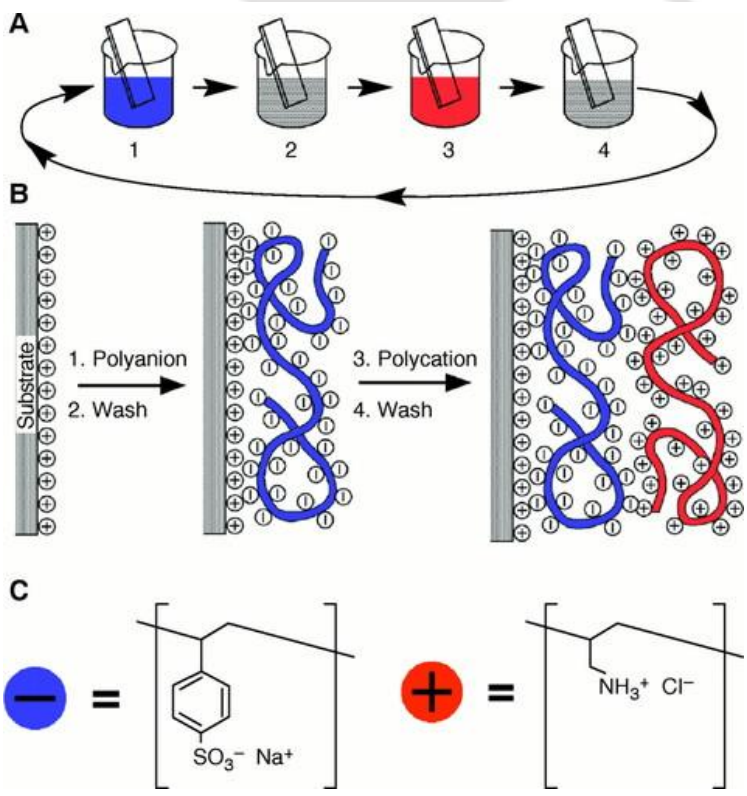

Figure 1.9. (A−C) Schematic depiction of a layer-by-layer (LbL) deposition process. Reproduced from ref. 71 with permission from Science, copyright 1997.

modulate both topography and chemical composition and substrate independency (as it can be applied to various substrates ranging from glass to plastic to fabrics). Jin *et al*. reported the construction of ultrathin Cu^{2+}/alginate hydrogel multilayer with controllable thickness via LbL method. Owing to the inherent water-absorbing ability of the deposited hydrogel layer, the modified membrane displayed superhydrophilicity, underwater superoleophobicity, and antifouling ability for crude oil.[75] Manna *et al.* reported the LbL deposition of two mutually reacting polymers, branched poly(ethyleneimine) and poly(vinyl-4,4-dimethylazlactone), where an azlactone ring-opening reaction between selected reactants allowed to form covalently crosslinked porous multilayer coating with residual azlactone groups. Next, the chemically reactive porous multilayer coating was modified with a small hydrophilic molecule (glucamine) to acquire underwater superoleophobicity.[76]

1.5.8. Sol-Gel Conversion Method

This method involves the immersion of a substrate in a precursor solution (sol), followed by a gelation process by hydrolysis and polycondensation reaction to form a gel network on the surface, which allows to tailor the roughness and chemical composition of the coating.[77-81] For instance, Jin *et al.* reported a sol-gel conversion approach to fabricate a superhydrophilic/underwater superoleophobic coating of TiO_2 nanoparticles on the single-walled carbon nanotube (SWCNT) after UV-light irradiation.[77] Huang *et al*. prepared a non-laminated graphene oxide (GO) membrane via a sol-gel conversion process using polyethyleneimine as the crosslinker. In the non-laminated GO membrane, the GO nanosheets are assembled randomly, forming a micro/nanoscale hierarchical structure on the membrane surface to confer superhydrophilicity/underwater superoleophobicity (Figure 1.10). [78] The advantage of the sol-gel process is that it can be performed at mild conditions and low

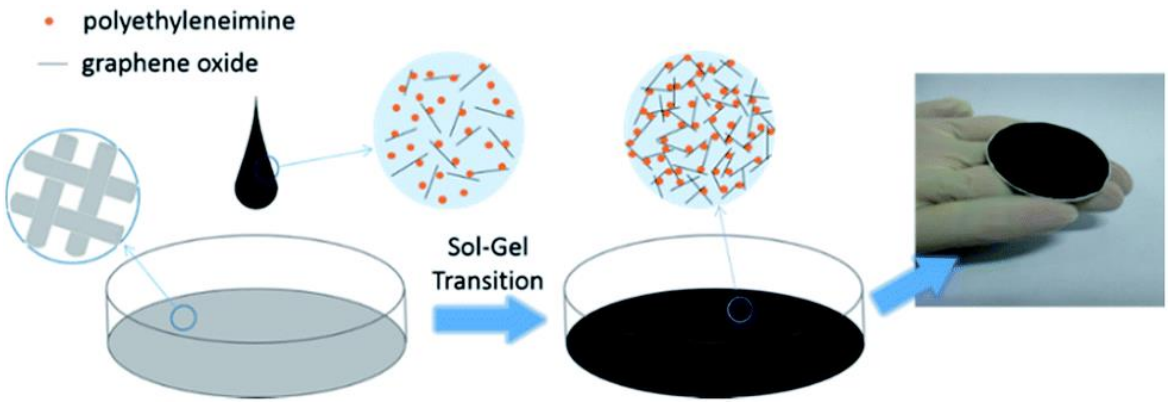

Figure 1.10. Schematic depiction of the formation of an underwater superoleophobic membrane via the sol-gel conversion process. Reproduced from ref. 78 with permission from Royal Society of Chemistry, copyright

temperatures; however, the prolonged and uncontrolled gelation process makes the process complicated.

1.6. Applications of Underwater Superoleophobicity

This section mainly focuses on the various potential applications of underwater superoleophobicty. In the past, underwater superoleophobic coatings were used to demonstrate various potential applications, which are discussed below.

1.6.1 Anti-Oil Fouling and Self-Cleaning

The underwater creatures discussed in section 1.2 show great anti-oil fouling in the water. The biomimicked artificial underwater superoleophobic surfaces have also displayed such anti-oil fouling properties, keeping the interface free from oil contamination.[82-84] For example, Yong *et al.* investigated the anti-oil fouling performance of an underwater superoleophobic glass surface having extremely low oil adhesion prepared through femtosecond laser microfabrication.[82] The rough glass slide was first immersed in the water phase, and then red-

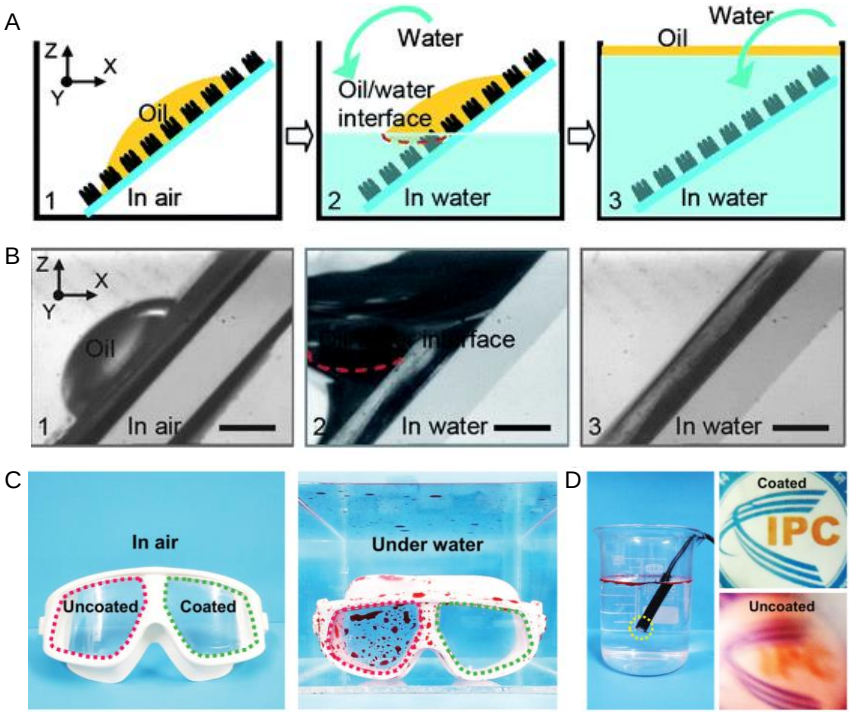

Figure 1.11. (A) Schematic describing the self-cleaning process during immersion of a superoleophobic film into water. (B) Optical microscopic images demonstrating self-cleaning phenomenon. Reproduced from ref. 85 with permission from Royal Society of Chemistry, copyright 2011. (C) Photographs show nacre-inspired mineralized (NIM) film coated goggles before and after immersion in an oil and water mixture. (D) photographs taken with NIM coated/uncoated underwater cameras in an oil and water mixture. Reproduced from ref. 86 with permission from Wiley, copyright 2020.

dyed contaminated oil was intentionally dripped on the surface. No red imprint on the glass slide was observed under an optical microscope, suggesting the existence of an inherent ability to keep the interface oil contamination-free in water.

Thus, the underwater superoleophobic surfaces with extremely low oil adhesion exhibit a self-cleaning phenomenon. When an oil-fouled superhydrophilic surface in air is immersed underwater, the water phase is impregnated into the rough microstructures, pushing the oil out and clearing the oil impurity (Figure 1.11A).[85-90] Wu *et al*. prepared hierarchical microstructures made of polydimethylsiloxane (PDMS) exhibiting extreme underwater superoleophobicity, with an oil contact angle > 170º and roll-off angle <1º. The rough surface was wetted with soyabean oil in the air, and subsequent immersion of the oil-fouled surface into a water phase completely removed the spilled oil phase from the solid/water interface (Figure 1.11B).[85] However, a control experiment on an untreated flat surface could not wash away the oil phase. Chen *et al*. reported underwater superoleophobic nacre-inspired mineralized (NIM) coating composed of aragonite platelets and chitosan modified with methacrylic anhydride (CSMA).[86-87] The highly transparent coating can be applied on various transparent objects. For instance, they applied the NIM coating on swimming goggles and immersed into an oil-polluted water tank. The coated side of the glass remained transparent and clean, while the uncoated side was stained with oil (red-dyed), indicating the self-cleaning ability of the prepared coating (Figure 1.11C). Moreover, the NIM film can also be applied to the underwater camera lens without compromising the transparency and clarity of the lens in the oil-contaminated water, whereas the uncoated camera lens fouled with oil, severely affecting underwater observation (Figure 1.11D).

1.6.2. Oil/Water Separation

The oil spill accidents and the increasing amount of oily sewage industrial discharges continue to contaminate open water resources, severely affecting the ecological system.[91-93] In this context, the oil/water separation approach exploiting the superwetting materials has become a recently grown field to save the ecosystem and minimize economic loss. Both the superhydrophobic/superoleophilic and superhydrophilic/underwater superoleophobic materials have been successfully applied in oil/water separation technology.[94-100] However, in most cases, the water content is large compared to the oil phase in the contaminated oil/water mixture, where selective filtration of the water phase is required. In this context, superhydrophilic/underwater superoleophobic materials, especially membranes and meshes are

used, where such materials allow the selective passage of the water phase while restricting the oil phase (Figure 1.12A).[45,101-103] For instance, Hong *et al.* reported the separation of oil/water mixtures through a porous nanofibrous cellulosic membrane exhibiting underwater superoleophobicity. The membrane showed continuous high-flux separation with efficiencies of more than 99% (Figure 1.12B and C).[45] Bai *et al.* reported underwater superoleophobic 'hydrogel paint' derived from hydrogen bond cross-linking between polyvinyl alcohol (PVA) and tannic acid (TA), which can be applied on porous substrates by different one-step coating approaches, e.g., dip, spray or brush coating., etc. The hydrogel-coated membrane exhibits excellent oil-water separation efficiency (> 99%) with long-term cyclic stability.[103]

Besides oil and water separation, the oil-in-water emulsion separation is more challenging with conventional approaches owing to the complex phase state and relatively small size of the dispersed oil droplets (< 10 μm) in the bulk water phase. Recently, the separation of oil-in-water emulsion with the help of superhydrophilic/underwater superoleophobic membranes has

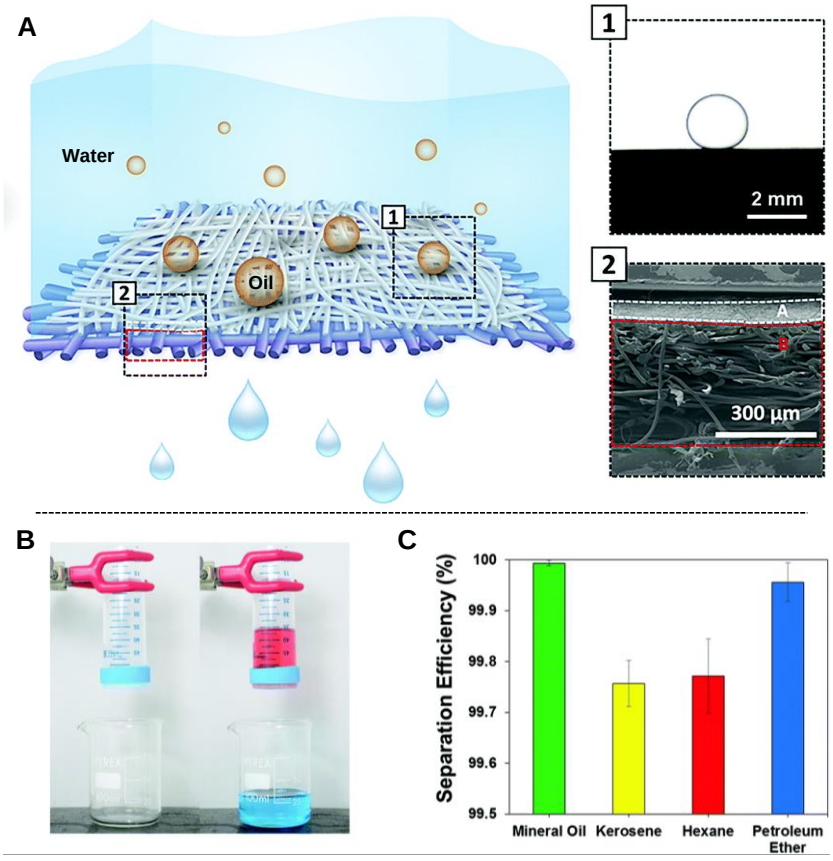

Figure 1.12. (A) Schematic depicting oil/water separation technique with underwater superoleophobic membrane. (B) Experimental set-up for the oil/water separation process. (C) Separation efficiency for various oils separated using nanofibrous cellulosic membrane. Reproduced from ref. 45 with permission from Royal Society of Chemistry, copyright 2018.

appeared as an advanced approach with high efficiency and low operational cost.[46,100,104-106] Ge *et al.* reported a superhydrophilic and underwater superoleophobic polyacrylonitrile nanofibrous membrane fabricated via an electrospinning method, which remained effective in separating micro-scaled oil-in-water emulsions an ultrahigh permeation flux and excellent separation accuracy.[46]

1.6.3. Underwater Oil-Droplet Manipulation

Underwater oil-droplet manipulation is another potential application where underwater superoleophobicity was explored extensively to demonstrate controlled and no-loss liquid transportation, underwater droplet-based micro reactions, labs-on-chips, etc.[82,107-110] Huo *et al.* showed underwater oil droplet manipulation with the help of an underwater superoleophobic miniature "mechanical hand" based on tunable oil adhesion of patterned glass substrates created through femtosecond laser (Figure 1.13).[107] The patterned areas exhibited underwater superoleophobicity with controllable oil adhesion based on the extent of the laser ablation, which enabled patterned surfaces to demonstrate a miniature "mechanical hand" in the no-loss transportation, fusion, and capture of oil droplets.

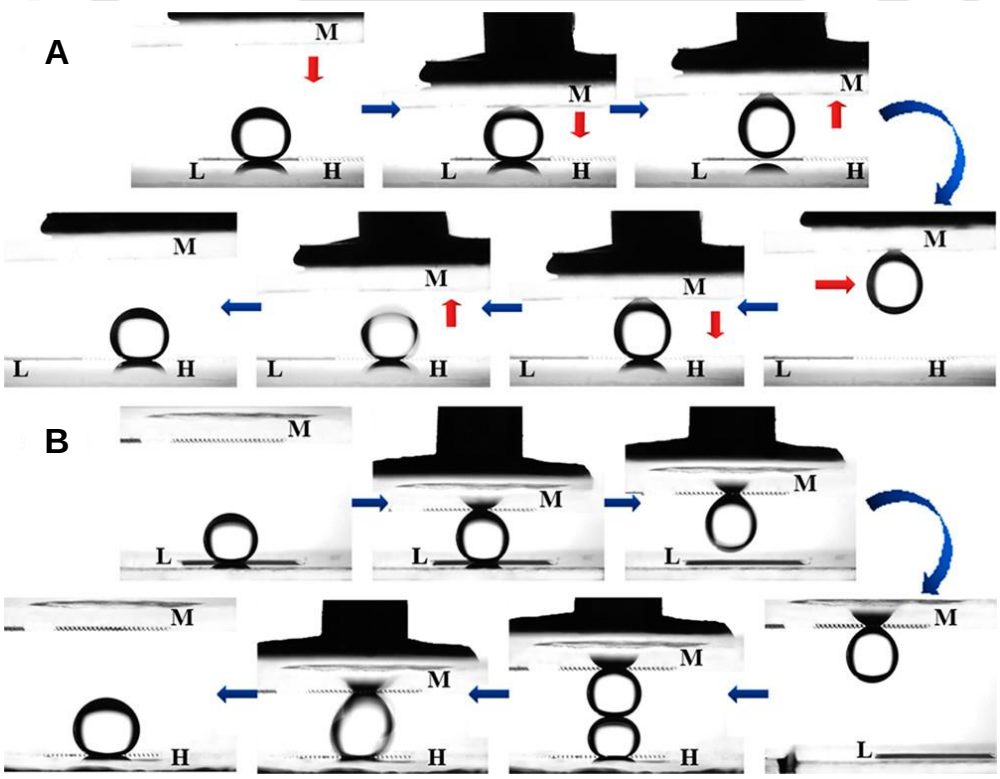

Figure 1.13. (A) Underwater oil droplet manipulation using oil adhesive surface (M-surface) as a "mechanical hand", ultralow oil adhesive surface (L-surface), and ultrahigh oil adhesive surface (H-surface). Reproduced from ref. 107 with permission from American Chemical Society, copyright 2017.

1.6.4. Bio-Adhesion

Biomedical devices and implants in the human or animal body easily absorb blood proteins and cause platelet activation and adhesion, resulting in blood coagulation and thrombosis. The platelet activation/adhesion is affected by many factors, such as chemical composition, surface morphology, charge, and wettability.[111-112] Recent studies revealed that underwater superoleophobicity has a significant role in exhibiting anti-platelet adhesion.[113-115] Chen *et al.* reported the platelet adhesion behavior on poly(N-isopropylacrylamide) (PNIPAAm)-modified silicon nanowire array (SiNWAs) surfaces in vitro, where the modified surface had shown a strong inhibition towards the platelet adhesion both below and above the lower critical solution temperature (LCST) of PNIPAAm (~ 32 °C).[113] Such inhibition effect was not observed on other surfaces, including smooth silicon wafer, non-grafted bare SiNWA, and PNIPAAm-grafted smooth silicon wafer (Figure 1.14A). The SiNWA-PNIPAAm sample exhibited underwater-superoleophobicity with ultralow oil adhesion, regardless of the temperature above or below the LCST, forming a hydration layer of the polymer outer chains, thus preventing the platelets' adhesion (Figure 1.14B).

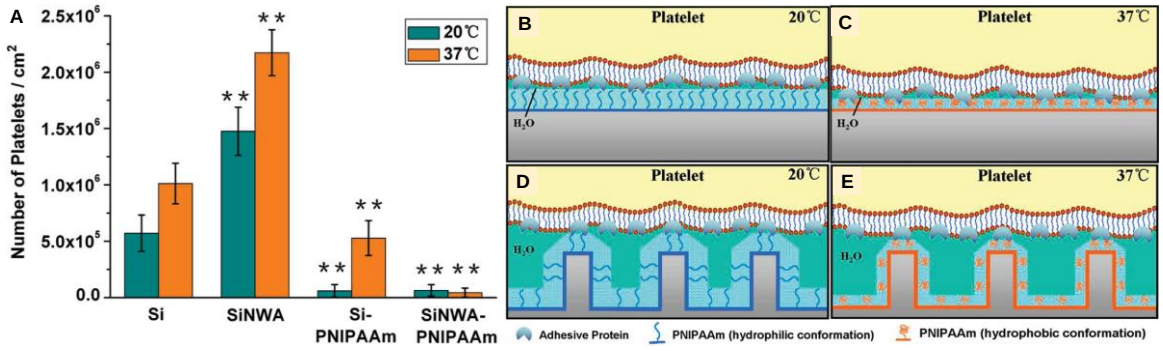

Figure 1.14. (A) Quantification of the number of adhered platelets on different surfaces at 20 °C (blue bars) and 37 °C (orange bars). (B−E) Hypothetical platelet adhesion mechanisms for different surfaces. Reproduced from ref. 113 with permission from American Chemical Society, copyright 2009.

1.6.5. Microfluidics

Microfluidic systems have attained great interest in the recent past due to their increasing demand in chemical, material, and biological science. Often microfluidic closed channels suffer from blockage due to adhesion and deposition of the oil droplet on the wall of the closed channel. Owing to the great oil repellence of the underwater superoleophobic interfaces, they are also applied in microfluidic channels.[85,87] Chen *et al.* utilized a transparent NIM film with underwater superoleophobicity in a microfluidic device to subside the challenge of deposition

of oil/oily phase on the wall of the microchannel. The transparency of the coating enabled the clear visualization of the microdroplets during the transportation process.[87]

1.6.6. Other Applications

Superhydrophilic coating can exhibit anti-fogging performance on transparent surfaces due to its strong affinity to water molecules.[116,117] When water vapor hits a cold superhydrophilic surface, condensed water drops spread out to form a thin film, resulting in anti-fogging properties. Underwater superoleophobicity can also be applied in pipelines due to its anti-blocking ability.[60] Pipe blockages are often seen in household kitchens and industries caused by the discharge of oil-contaminated water, where the oil-impurity droplets stick to the inside wall of the pipe, hindering the water flow through the pipe and reducing the efficiency of the drainage system (Figure 1.15A). On the contrary, the use of an underwater superoleophobic pipe can solve such an issue and provide a highly effective drainage pipe (Figur 1.15B).

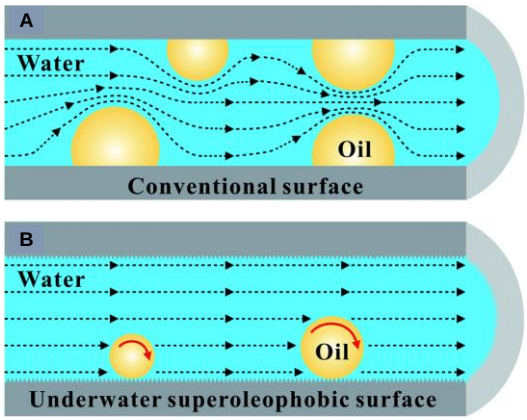

Figure 1.15. (A, B) Schematic shows flowing of water with oil impurity in (A) conventional water pipe and (B) water pipe with underwater superoleophobic inner wall. Reproduced from ref. 60 with permission from Royal Society of Chemistry, copyright 2014.

1.7. Tailoring of Oil Adhesion in Underwater Superoleophobic Surfaces

Fish-scale-inspired underwater superoleophobic surfaces exhibit ultralow oil adhesion of beaded oil droplet, and the oil droplet can be rolled off in slight tilting (below 10º) of such surfaces. On the other hand, when the beaded oil droplets stick to a substrate and do not roll off at a relatively high (above 10º) tilted angle, the surface can be termed as adhesive superoleophobic surface. In the past, the tuning of oil adhesion (from low to high) on underwater superoleophobic interfaces was explored to demonstrate various potential applications, such as oil droplet manipulation, no loss transfer of oil droplets, etc. [82,107-110] The oil adhesion phenomenon on a surface can be explained with the help of Cassie-Wenzel transitional states.[36,37] In the Wenzel state, the oil droplet can completely fill the voids of the rough surface underwater, leading to a homogeneous wetting of oil on a solid surface. In contrast, in the Cassie-Baxter state, the oil droplet just sits on the surface due to water pockets

filling the voids of the rough surface, resulting in heterogeneous wetting of oil on a solid surface. The minimum contact between the beaded oil droplet and the solid surface ensures the association of non-adhesive underwater superoleophobicity. Moreover, the increased contact between the beaded oil droplet and solid surface leads to the formation of Cassie-Wenzel transitional states and allows to modulate of the oil adhesion behaviour.

Previously, the different high/low oil adhesion states on underwater superoleophobic surfaces were fabricated by controlling the surface topography, i.e., tuning the micro/nanostructures with different sizes.[82,107-108,118-123] Yong *et al.* reported underwater superoleophobic surfaces with controlled oil adhesion, prepared by the femtosecond laser method on glass at different laser scanning speeds and the shift of scanning lines, as shown in Figure 1.16.[82] Adopting this method, they developed three different micro/nanostructured surfaces: i) surface comprised of periodic micro islands with numerous nanoscale porous structures and protrusions, giving rise to ultralow oil adhesion (Cassie state, Figure 1.16A−D), ii) wave-like micro craters structures uniformly covered with a layer of nanoparticles, showing oil adhesive underwater

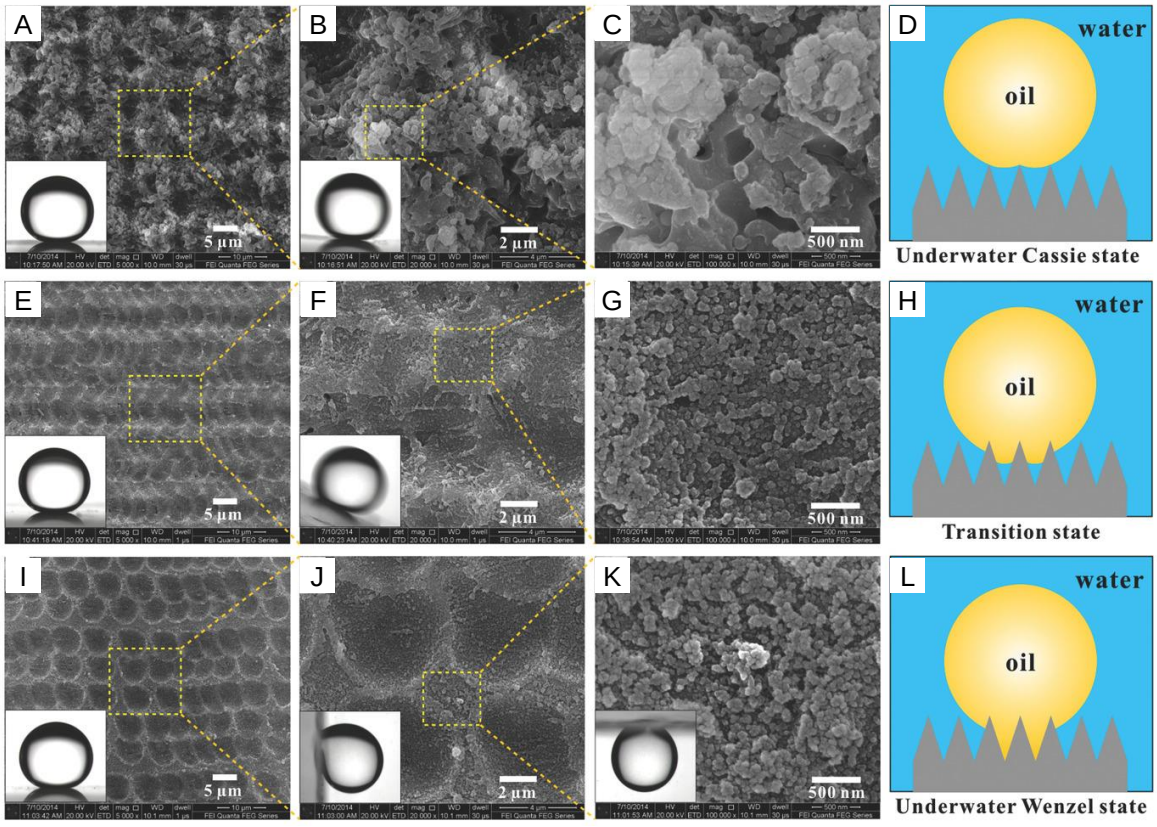

Figure 1.16. (A−L) FESEM images demonstrating surface microstructures of underwater superoleophobic surfaces prepared through femtosecond laser method, and contact angle images and schematic representations show corresponding wetting states. Reproduced from ref. 82 with permission from Springer 2015.

superoleophobicity with a roll-off angle of 25.5°, giving rise to Cassie-Wenzel transition state (Figure 1.16E−H), iii) surfaces with complete micro craters, further decorated with irregular nanoscale particles, resulting in underwater superoleophobicity ultrahigh adhesion (Wenzel state, Figure 1.16I−L).[82] Huang *et al.* prepared three typical underwater superoleophobic films with controlled oil adhesion derived from assembled colloidal latex particles (with spherical, cauliflower-like, and single-cavity structures). The underwater oil adhesion of the superoleophobic film can be tuned from high to moderate to low adhesion with adhesive forces > 69.6 μN, 43.1 μN, and 9.8 μN by varying the latex structures from spherical to cauliflower-like to single cavity.[119] Zhang *et al.* prepared three different microstructured Ni/NiO surfaces derived by electro-deposition and annealing to varying temperatures. The prepared porous surfaces exhibited underwater superoleophobicity with controlled oil adhesion, e.g., from extremely low (< 1 μN) to high (~ 60 μN) adhesion forces.[108] Huo *et al.* introduced another approach for fabricating underwater superoleophobic surfaces with controllable oil adhesion using a femtosecond laser, where the adjustment in the ratio of the untreated flat glass area to the laser-ablated rough area in a selected surface allowed to achieve ultralow to ultrahigh oil adhesion, which has been applied in oil droplet manipulation.[107] While controlling topography provided a basis to modulate oil adhesion property, the large-scale fabrication of such interfaces is challenging.

Instead of adjusting the surface topography, the modulation of surface chemical composition has recently appeared as a more simple and practical approach to achieve controllable oil adhesion in underwater superoleophobic surfaces.[124-131] For instance, Cheng *et al.* fabricated controlled oil adhesive superoleophobic interfaces by the self-assembly of different n-alkanoic acids monolayers on a nanostructured copper substrate. By adjusting the chain length of the n-alkanoic acids from 1 to 12, the oil adhesion can be tuned from ultralow (< 1 μN) to ultrahigh (> 58 μN) adhesive force.[126]

1.7.1. Responsive Underwater Oil Adhesion

Design of underwater superoleophobic interfaces that display responsive oil adhesive behaviour is important for developing functional adaptive interfaces. In this context, Chen *et al.* achieved the reversibly switchable oil adhesion between Wenzel and Cassie state in an underwater superoleophobic surface derived from thermal-responsive poly(N-isopropylacrylamide) (PNIPAm) hydrogel.[127] The PNIPAm hydrogel exhibits ultralow oil adhesion below the LCST ~ 32 °C and becomes oleophobic with high adhesion above the

LCST, owing to the thermal-responsive, reversible swelling/deswelling behavior below and above LCST. Du *et al.* designed a hierarchical structure composed of poly(acrylic acid) (PAA) micro-brushes decorated with stimuli-responsive polymer (PNIPAm) nano-brushes. The micro/nano-brush dual structural surfaces can switch the underwater oil adhesion between low and high while keeping the superoleophobicity at 20 °C and 60 °C, respectively (Figure 1.17).[128] Shang *et al.* developed a photothermal responsive coating by casting thermal responsive poly(styrene-co-n-isopropylacrylamide) (P(St-NIPAm) colloidal spheres and Fe_3O_4 nanoparticles on selected substrates. The near-infrared irradiation of such coatings can locally and remotely tune the oil adhesion from a low-adhesive rolling state to a high-adhesive pinning state with a fixed magnitude of change in oil adhesion underwater.[129] Ding *et al.* prepared an underwater superoleophobic film of aligned PANI nanowires by an electrochemical polymerization technique, which shows reversible oil adhesion switching from the rolling state to the pinned state in water by tuning an applied electrochemical potential.[130] Chen *et al.* demonstrated pH-responsive reversible switching of oil adhesion on a nanostructured PAA surface, where the intramolecular hydrogen bonding of PAA at low pH gives rise to high oil

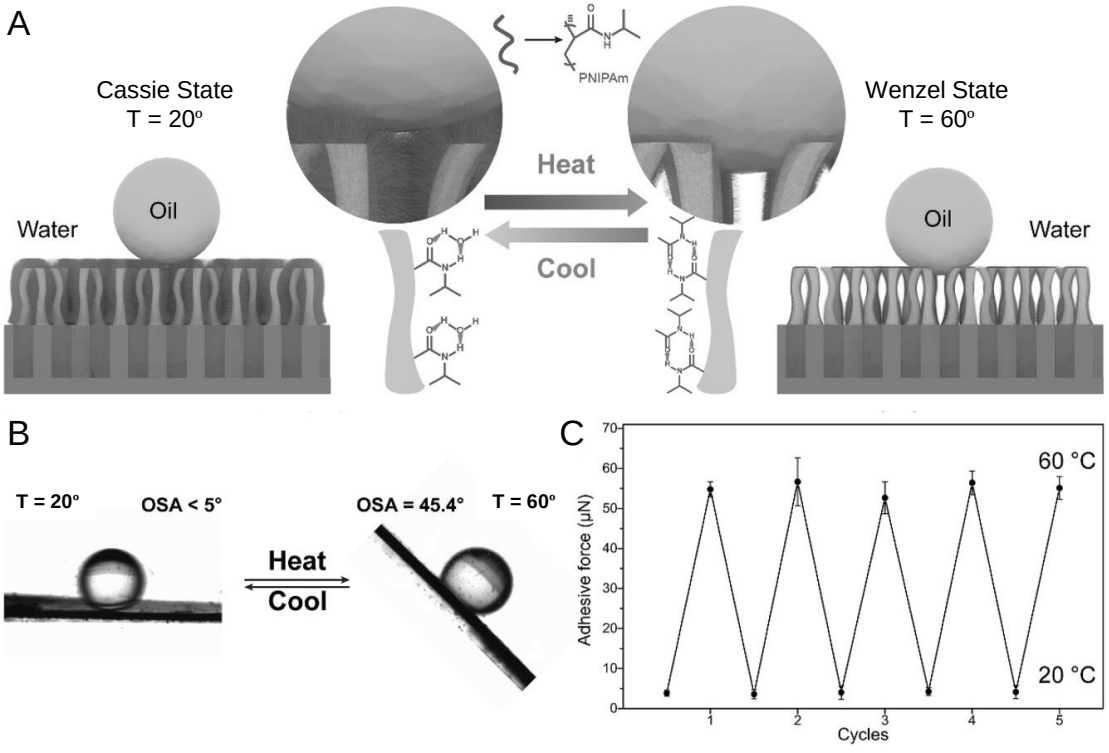

Figure 1.17. (A) Schematic showing poly(N-isopropylacrylamide) (PNIPAm) brushes formed intermolecular hydrogen bonding interactions and adopted Cassie state at 20 ºC, while intramolecular hydrogen bonding to collapse resulting in Wenzel state at 20 ºC. (B) Underwater oil droplet mobility at the two states. (C) Underwater oil adhesion forces of the interface reversibly switched between low and high adhesion for five cycles. Reproduced from ref. 128 with permission from Royal Society of Chemistry, copyright 2010.

adhesion, whereas intermolecular hydrogen bonding between PAA at high pH results in rolling off the beaded oil droplet due to low oil adhesion.[131] The above-mentioned approaches in achieving controlled oil adhesion are only able to switch between ground and stimulated oil adhesion state with a fixed change in oil adhesion of beaded oil droplet; however, these approaches do not allow to tune the oil adhesion property in a range and the consequent oil droplet mobility. Thus, there is a scope for designing underwater superoleophobic surfaces that would be capable of providing tailored and responsive oil adhesion property.

1.8. Underwater Superoleophobicity in Sensing Application

In the recent past, various superwetting surfaces, such as superhydrophobic, patterned liquid wettability, and slippery surfaces, have been strategically used in sensing applications by integrating with different analytic techniques, e.g., colorimetry, fluorescence, surface-enhanced Raman spectroscopy (SERS), electrochemical analysis etc.[132-140] For example, microchips with patterned superhydrophilicity-superhydrophobicity are used as a biosensing platform for the detection of routine physiological markers.[132] Gao *et al.* introduced a simple approach for the naked eye detection of important analytes such as urea and glucose just by naked eye.[133] They fabricated a pH-responsive superwettable surface by modifying silica nanoparticles with organosilanes that provided superhydrophobicity and superhydrophilicity as a function of the pH. The alteration of pH during glucose oxidase (GOx)-catalyzed reaction and urease-catalyzed reaction shows switchability between superhydrophilicity and superhydrophobicity, which can provide quantitative sensing information simply by monitoring contact angle variation with the naked eye.[133] Recently, slippery surfaces providing controllable sliding speed have been utilized for bio-sensing applications.[134] For instance, a liquid crystal (LC)-infused slippery surface was introduced for sensing amphiphiles such as lipids, lipopolysaccharides, and lipoproteins with the naked eye by measuring the sliding speed of the analyte-containing water droplets on the surface, where the interaction of the amphiphile tails with the LC phase slows down the velocity of the droplet.[135]

Previously, the underwater superoleophobic surface has barely been explored in sensing applications, though it specifically performs underwater conditions. In this context, the responsive tailorable oil adhesion and oil wettability variation upon the interaction of a strategically and chemically modulated superoleophobic surface after exposure to selected analytes or toxins (present in water) could be an efficient and economical approach for the naked eye sensing of various relevant toxic chemicals.

1.9. Transparent Underwater Superoleophobic Coating

Transparency is an essential property for superhydrophilic/underwater superoleophobic surfaces for its prospective application in developing anti-fogging glasses, diving goggles, oil-proof windows for underwater cameras, submarines, imageable substrates for biologically active cells, etc. However, the requirement of rough microstructure on the substrate surface for underwater superoleophobicity makes it challenging to achieve transparency on the surface. The rough microstructure causes a strong light scattering, making the surface completely opaque. The petals of *Diphylleia grayi*, found in nature, inspired the achievement of transparency in underwater superoleophobic surfaces.[62] The petals of *Diphylleia grayi* are white on sunny days (Figure 1.18A), but they become transparent on rainy days (Figure 1.18B). The petals are composed of many lacunae and intercellular spaces filled with air on sunny days, causing diffuse reflection in the interface between the colorless cytolymphs and the trapped air. Water can impregnate the intercellular spaces, replacing the trapped air in the rain, causing a reduction in the diffuse reflection and scattering as the refractive indices of cytolymph and water are nearly the same, making the petals transparent.

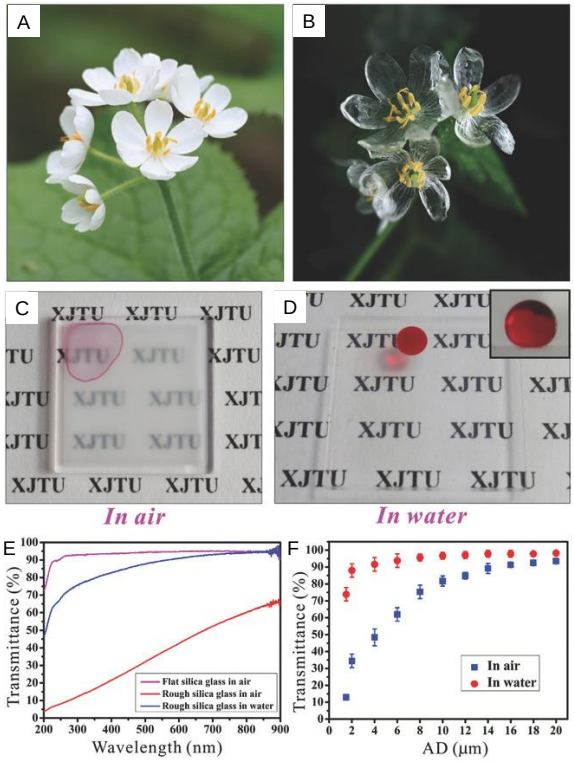

Figure 1.18. (A, B) Petals of *Diphylleia grayi* (A) on sunny days and (B) in the rain. (C, D) Laser-ablated silica glass (C) in air and (D) in water. (E) UV-vis spectra of the silica glasses in air and water. (F) The transmittance of the silica glass after being ablated at different average distance (AD) parameters. Reproduced from ref. 62 with permission from Royal Society of Chemistry, copyright 2015.

Inspired by this simple phenomenon, Yong *et al.* prepared an underwater superoleophobic surface on a silica glass surface using the femtosecond laser ablation method to achieve rough surface topography.[62] The glass surface remained opaque in the air; however, it became superoleophobic and transparent with transmittance very close to the bare flat glass once immersed underwater (Figure 1.18C−F). The excellent transparency resulted from the

existence of the surrounding water environment. The reflectance, R_{12}, at the interface of two different media (1 and 2) can be expressed as follows[141]:

$$R_{12} = \left(\frac{n_1 - n_2}{n_1 + n_2}\right)^2 \quad (6)$$

where n_1 and n_2 are the refractive indexes of medium-1 and medium-2, respectively. According to equation (6), the smaller the difference in the refractive indexes of both media, the smaller the reflectance generated at the interface. Although this femtosecond laser ablation approach is highly effective in achieving underwater superoleophobicity, the technique is substrate-selective and not feasible to apply in large objects for practical applications. Manabe *et al.* fabricated a robust and transparent hydrophilic surface with anti-fogging and anti-reflective properties, following an LbL deposition approach.[142] A polyelectrolyte multilayer was

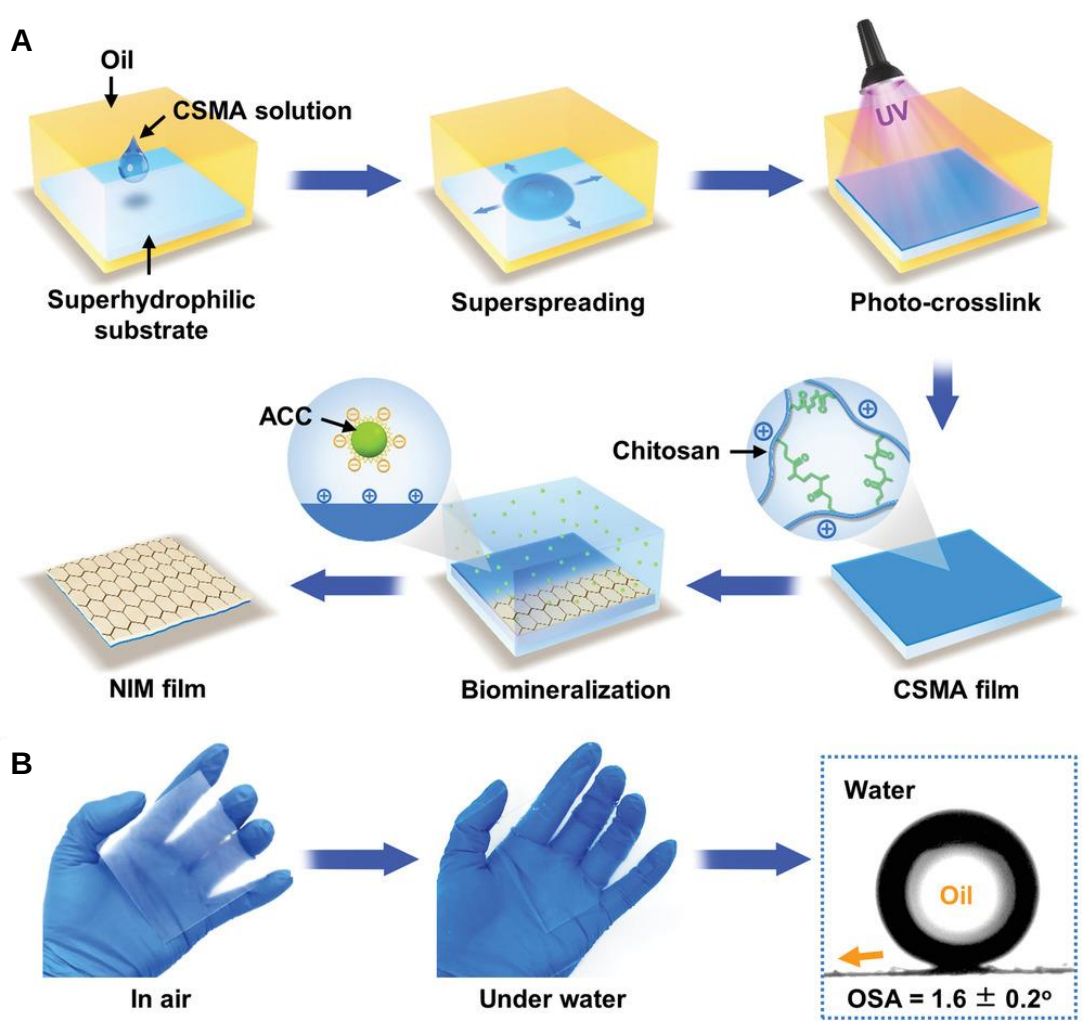

Figure 1.19. (A) Schematic depiction of the fabrication procedure of NIM film based on superspreading and biomineralization. (B) The NIM film shows high transparency underwater, and exhibit extremely low oil sliding angle. Reproduced from ref. 86 with permission from Wiley, copyright 2020.

prepared from poly(allylamine hydrochloride) (PAH)–PVA–PAA blends (as the cationic solution) alternately deposited with PVA–PAA blends (as the anionic solution), resulting in the formation of coatings with hierarchical surface. The anti-fogging ability was derived from hydrophilicity combined with PVA's strong hydrogen bonding ability in the coating. There have been several efforts to make transparent underwater superoleophobic coatings; however, developing a substrate-independent and mechanically and chemically durable transparent underwater superoleophobic coating remained a substantial challenge.[143-150]

Cheng *et al.* introduced a NIM film to achieve underwater superoleophobicity with high transparency and mechanical durability.[86] They adopted the superspreading method to prepare CSMA films with well-defined thicknesses and then biomineralization of the CSMA films by depositing amorphous calcium carbonate (ACC) (Figure 1.19A). The prepared film comprised crystalline aragonite platelets, which resulted in mechanically robust underwater superoleophobicity with ultralow oil adhesion and high transparency (Figure 1.19B). Moreover, such films can be applied to various surfaces, such as glass, polystyrene, poly(ethylene terephthalate), and polypropylene, with the association of highly transparent and mechanically durable underwater superoleophobicity.[86,87] Such nacre-inspired derivation of well-ordered crystalline films provided high transparency upon coating various planar substrates; however, developing such well-ordered structures on geometrically complex fibrous and porous substrates would be challenging. Moreover, the inherent instability of such earlier reported mechanically durable coating at relevant harsh settings (i.e., in acidic environments, presence of chelating agents, etc.) would impact the uninterrupted performance of the embedded bio-inspired wettability at diverse aquatic conditions. Therefore, further design is essential to address the existing challenges related to transparency, substrate independency, and coating durability following a single and scalable fabrication process.

1.10. Durability of Underwater Superoleophobic Coatings

Chemical and physical/mechanical durability for the artificial underwater superoleophobic surfaces is essential for their potential practical applications in harsh environments with long-term performance. In the past, numerous efforts have been made to prepare underwater superoleophobic surfaces with improved durability. However, the commonly employed approaches to achieve underwater superoleophobicity, such as hydrogel coatings, metal-oxide coatings, and electrostatic multilayer coatings, suffer from durability issues.

Hydrogels are delicate in nature and tend to absorb a large amount of water and swell when exposed to water, thus unable to withstand mechanical stress. Thus, hydrogel-coated surfaces have remained unsuitable for long-term underwater stability, and even the water swelling can destroy the surface microstructures.[97,151-155] Recently, composite hydrogels have been prepared to overcome stability issues by bonding with rigid structures, such as clay, inorganic material, and metals, to improve mechanical stability.[115,156-162] For instance, Lin *et al.* fabricated hierarchical composite hydrogel by incorporating spherical cuprous oxide-tannic acid submicron particles into PVA hydrogels, exhibiting underwater superoleophobicity with improved mechanical strength and moduli.[157] Although the composite hydrogels showed enhanced mechanical durability, the chemical stability under prolonged harsh aqueous exposures still remains a challenge.

Metal oxides are rigid in nature, and thus underwater superoleophobic surfaces derived from metal oxides show high mechanical stability.[31,66,108,163-170] However, owing to the brittle and reactive nature of the metal oxides, it is unstable in long-term exposures to aqueous corrosive solution (e.g., acidic, alkaline, and high salinity). Thus, metal oxide-based underwater superoleophobic materials are still far from 'real world' practical application because of the mentioned challenges.

Another commonly used approach for preparing underwater superoleophobicity is multilayer coating assembled through weak electrostatic interaction between oppositely charged polyelectrolytes.[75,171-175] However, the multilayer coatings of the polyelectrolytes are labile to disintegrate in harsh aqueous solutions (e.g., high salinity and low and high pH), and likely to compromise the oil repellence property in such harsh conditions.

Conventional underwater superoleophobic materials exhibiting excellent anti-oil wettability suffer physical and chemical instability towards long-term practical applications. Thus, there is an immense need to develop a common synthetic approach to achieve underwater superoleophobicity that can survive all hash physical and chemical exposures for its potential applications.

1.11. Motivation and Objectives

In the last decade, remarkable advancements have been made in the development of artificial underwater superoleophobic surfaces to fulfill its enormous practical applications. Various approaches and chemical components have been adopted to improve the performance of such underwater oil-repellent surfaces, which are already discussed in sections 1.5 and 1.6.

However, there is still a need for the improvement of the existing systems as they suffer from various challenges, as described in sections 1.7, 1.8, 1.9 and 1.10. Firstly, a simply achievable underwater superoleophobic system is on demand for the controlled tuning of oil adhesion for its relevant applications, such as sensing, droplet manipulation, etc. Secondly, most existing underwater superoleophobic materials derived from hydrogel, metal oxide, and electrostatic multilayer coatings suffer from physical and chemical instability towards long-term practical applications. Thus, there is an immense need to develop a facile synthetic approach to achieve underwater superoleophobicity for its unperturbed practical applications. Thirdly, the installation of mechanical properties and transparency in the underwater superoleophobic coating following a single and scalable approach is of utmost importance for its diverse aquatic applications.

To address the aforementioned challenges, the utilization of a facile and readily reactive covalent chemistry would be a rational approach for constructing essential topography and chemical composition to embed underwater superoleophobicity. In this context, recently, a 1,

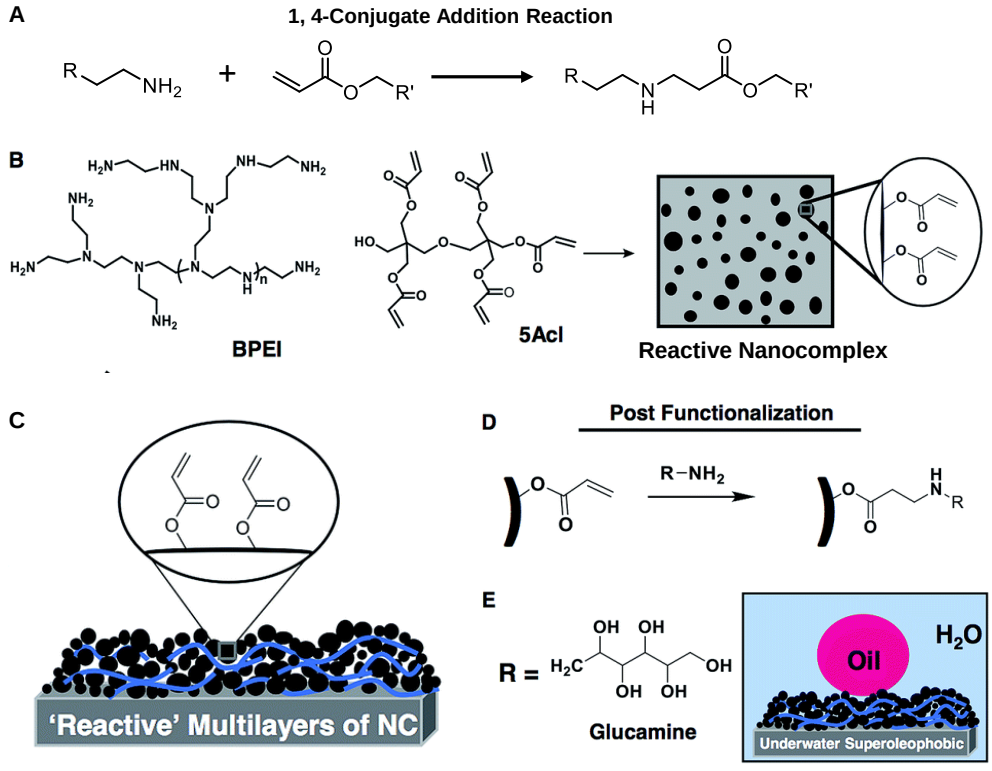

Figure 1.20. (A, B) Schematic depiction of (A) 1, 4-conjugate addition reaction for generating (B) reactive nanocomplexes with residual acrylate. (C) Reactive multilayer coating loaded with residual acrylate derived from reactive nanocomplexe. (C−E) Post-functionalization of the multilayer coating with amine containing glucamine to achieve underwater superoleophobicity. Adapted from ref. 149 with permission from Royal Society of Chemistry, copyright 2017.

4-conjugate addition reaction between amine and acrylate functionalities of a branched polymer and a crosslinker, respectively, was exploited to develop nanocomplexes with residual reactivity, which allowed to derive rough microstructures and chemistry (through post-modification of the residual reactivity with the desired functionality) for achieving super wetting surfaces (Figure 1.20A, B).[149,176-180] For instance, the sol-gel conversion of the reactive nanocomplexes led to the formation of a free-standing porous monolith with superhydrophobicity after the post-covalent modification with hydrophobic octadecyl amine,

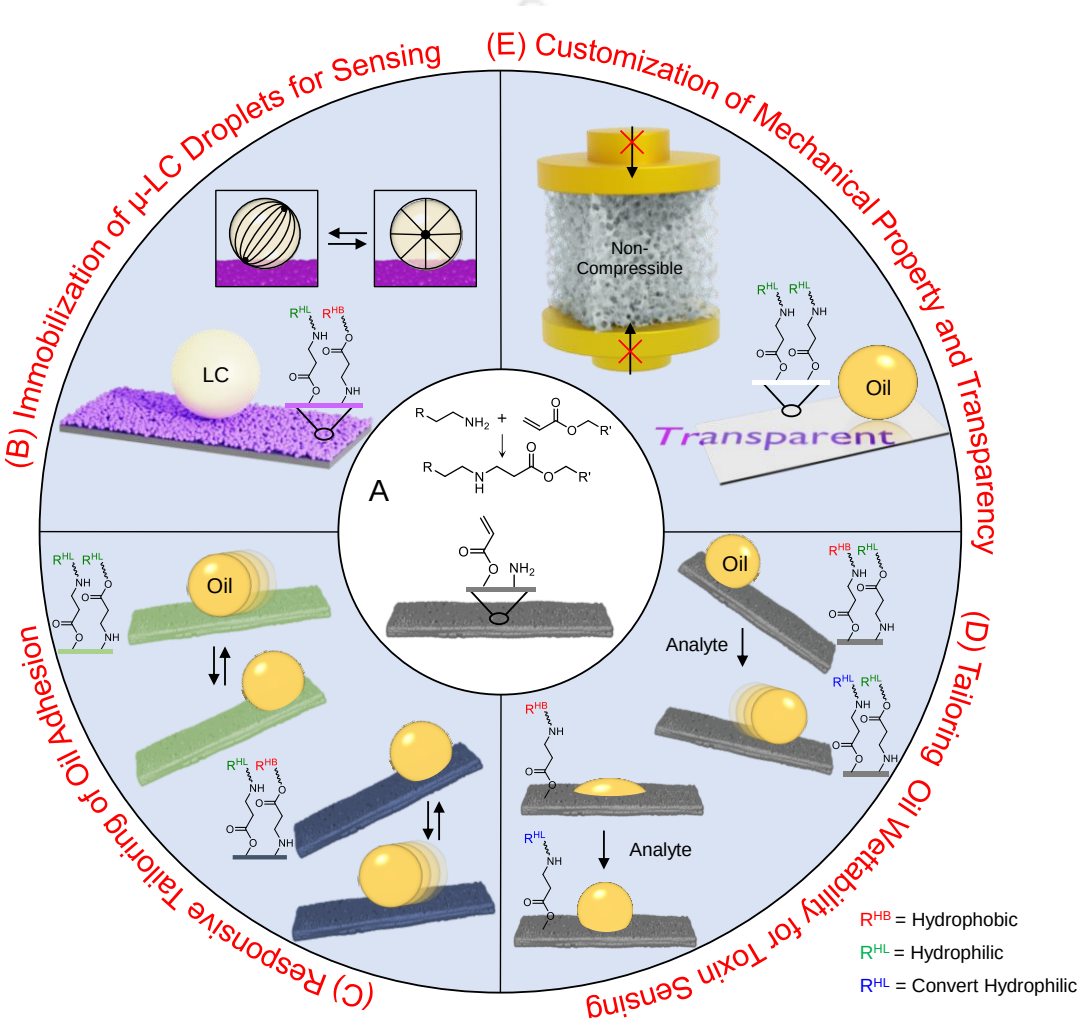

Figure 1.21. (A) Schematic depiction of 1, 4-conjugate addition reaction for generating a reactive coating with residual functional moieties. (B−E) The derivation of various desired underwater anti-oil wetting surfaces via the simple post-covalent modifications of reactive reactivities with selected chemical functionalities: (B) underwater liquid crystal (LC) repellent surface for the immobilization of the LC droplet for sensing application, (C) underwater superoleophobic surface enabled reversible amphiphile-responsive tuning of oil adhesion, (D) chemically customized surface for the selective tailoring of oil wettability (oil contact angle and oil adhesion) in the presence of toxins, and (E) induction of mechanical property and transparency in underwater superoleophobic coating.

whereas the LbL assembly of the nanocomplexes allowed to achieve underwater superoleophobicity after modifying with hydrophilic glucamine molecule (Figure 1.20C−E).[149]

Inspired by the previous reports, I have exploited the facile 1, 4-conjugate addition reaction in my thesis work to develop reactive coatings for tailoring various underwater oil-repellent surfaces through the post-modification approach that addresses the existing challenges in the literature. The objectives of my thesis work are summarized in Figure 1.21. Briefly, a 1,4-conjugate addition reaction derived reactive multilayer coating (Figure 1.21A) will be unprecedently explored for the immobilization of ultra-sensitive LC microdroplets by conferring the anti-LC wettability through post-modification for its sensing application (Figure 1.21B). Next, the reactive multilayer coating will be rationally post-modified to demonstrate the stimuli-responsive (pH) reversible and controlled tailoring of oil adhesion on underwater superoleophobic surfaces in the presence of selected amphiphiles (Figure 1.21C). Further, the multilayer reactive coating will be extended for sensing toxins by rational chemical modulation, where the variation in oil contact angle and oil droplet mobility on the modified surface can act as a naked eye sensor (Figure 1.21D). Moreover, the 1, 4-conjugate addition derived sol-gel conversion approach will be adopted to induce mechanical properties on deformable objects and transparency in the underwater superoleophobic coating for their relevant underwater applications (Figure 1.21E).

1.12. References

1 J. F.V. Vincent, O. A. Bogatyreva, N. R. Bogatyrev, A. Bowyer and A.-K. Pahl, *J. R. Soc. Interface*, 2006, **3**, 471.

2 W. Wright and O. Wright, *U. S. Patent*, 1906, **821**, 393.

3 S. Linic, V. Lucanin, S. Zivkovic, M. Rakovic and M. Puharic, *Experimental and Computational Investigations in Engineering*, 2020, **153**, 65.

4 F. Fish, P. Weber, M. Murray and L. Howle, *Integrative and Comparative Biology*, 2011, **51**, 203.

5 G. D. Mestral, *U. S. Patent 2*, 1955, **717**, 437.

6 A. Kesel and R. Liedert, *Comp. Biochem. Physiol. Mol. Integr. Physiol*., 2007, **146**.

7 A. R. Parker and C. R. Lawrence, *Nature*, 2001, **414**, 33.

8 S. V. Wassenbergh, E. J. Ortlieb, M. Mielke, C. Böhmer, R. E. Shadwick, and A. Abourachid, *Current Biology*, 2022, **32**, 3189.

9 V. Dhokia, W. P. Essink and J. M. Flynn, *CIRP Annals*, 2017, **66**, 153.

10 M. Liu, S. Wang, and L. Jiang, *Nat. Rev. Mater.*, 2017, **2**, 17036.

11 W. Barthlott and C. Neinhuis, *Planta*, 1997, **202**, 1.

12 V. Zorba, E. Stratakis, M. Barberoglou, E. Spanakis, P. Tzanetakis, S. H. Anastasiadis and C. Fotakis, *Adv. Mater*., 2008, **20**, 4049.

13 M. Liu, S. Wang, Z. Wei, Y. Song and L. Jiang, *Adv. Mater*., 2009, **21**, 665.

14 P. R. Waghmare, N. S. K. Gunda and S. K. Mitra, *Sci. Rep.*, 2014, **4**, 7454.

15 M. Nosonovsky, *Nature*, 2011, **477**, 412.

16 T.-S. Wong, S. H. Kang, S. K. Y. Tang, E. J. Smythe, B. D. Hatton, A. Grinthal and J. Aizenberg, *Nature*, 2011, **477**, 443.

17 S. Zhang, J. Huang, Z. Chen, S. Yang and Y. Lai, *J. Mater. Chem. A*, 2019, **7**, 38.

18 B. Xiang, Q. Sun, Q. Zhong, P. Mua and J. Li, *J. Mater. Chem. A*, 2022, **10**, 20190.

19 R. J. Archer, B. Becher-Nienhaus, G. J. Dunderdale and A. Hozumi, *Adv. Funct. Mater*., 2020, **30**, 1907772.

20 H. Yan, Q. Wu, C. Yu, T. Zhao and M. Liu, *Adv. Mater. Interfaces*, 2020, **7**, 2000966.

21 R. Nishimura, K. Hyodo, H. Sawaguchi, Y. Yamamoto, Y. Nonomura, H. Mayama, S. Yokojima, S. Nakamura and K. Uchida, *J. Am. Chem. Soc*., 2016, **138**, 10299.

22 K. Koch, B. Bhushan, Y. C. Jung and W. Barthlott, *Soft Matter*, 2009, **5**, 1386.

23 L. Feng, S. Li, Y. Li, H. Li, L. Zhang, J. Zhai, Y. Song, B. Liu, L. Jiang and D. Zhu, *Adv. Mater*., 2002, **14**, 1857.

24 L. Feng, Y. Zhang, J. Xi, Y. Zhu, N. Wang, F. Xia and L. Jiang, *Langmuir*, 2008, **24**, 4114.

25 D. Wu, J.-N. Wang, S.-Z. Wu, Q.-D. Chen, S. Zhao, H. Zhang, H.-B. Sun and L. Jiang, *Adv. Funct. Mater*., 2011, **21**, 2927.

26 Y. Zheng, X. Gao and L. Jiang, *Soft Matter*, 2007, **3**, 178.

27 X. Gao, X. Yan, X. Yao, L. Xu, K. Zhang, J. Zhang, B. Yang and L. Jiang, *Adv. Mater*., 2007, **19**, 2213.

28 W. Barthlott, T. Schimmel, S. Wiersch, K. Koch, M. Brede, M. Barczewski, S. Walheim, A. Weis, A. Kaltenmaier, A. Leder and H. F. Bohn, *Adv. Mater*., 2010, **22**, 2325.

29 X. Gao and L. Jiang, *Nature*, 2004, **432**, 36.

30 L. Wen, J. C. Weaver and G. V. Lauder, *J. Exp. Biol.*, 2014, **217**. 1656.

31 X. Liu, J. Zhou, Z. Xue, J. Gao, J. Meng, S. Wang and L. Jiang, *Adv. Mater*., 2012, **24**, 3401.

32 Q. Cheng, M. Li, Y. Zheng, B. Su, S. Wang and L. Jiang, *Soft Matter*, 2011, **7**, 5948.

33 Y. Cai, Q. Lu, X. Guo, S. Wang, J. Qiao and L. Jiang, *Adv. Mater*., 2015, **27**, 4162.

34 Y. Cai, L. Lin, Z. Xue, M. Liu, S. Wang and L. Jiang, *Adv. Funct. Mater*., 2014, **24**, 809.

35 T. Young, *Philos. Trans. R. Soc. London*, 1805, **95**, 65.

36 R. N. Wenzel, *Ind. Eng. Chem.*, 1936, **28**, 988.

37 A. B. D. Cassie and S. Baxter, *Trans. Faraday Soc.*, 1944, **40**, 546.

38 E. Bormashenko, *Colloids Surf. A*, 2009, **345**, 163.

39 H. Y. Erbil and C. E. Cansoy, *Langmuir*, 2009, **25**, 14135.

40 J. M. Berg, L. G. T. Eriksson, P. M. Claesson and K. G. N. Borve, *Langmuir*, 1994, **10**, 1225.

41 J. Drelich and E. Chibowski, *Langmuir*, 2010, **26**, 18621.

42 S. Wang and L. Jiang, *Adv. Mater.*, 2007, **19**, 3423.

43 R. J. Good, *J. Adhes. Sci. Technol.*, 1992, **6**, 1269.

44 X. Huang, H. Mutlu and P. Theato, *Adv. Mater. Interfaces*, 2020, **7**, 2000101.

45 S. K. Hong, S. Bae, H. Jeon, M. Kim, S. J. Cho and G. Lim, *Nanoscale*, 2018, **10**, 3037.

46 J. Ge, J. Zhang, F. Wang, Z. Li, J. Yu and B. Ding, *J. Mater. Chem. A*, 2017, **5**, 497.

47 D. Shu, P. Xi, B. Cheng, Y. Wang, L. Yang, X. Wang and X. Yan, *Int. J. Biol. Macromol.*, 2020, **162**, 1536.

48 J.-J. Li, L.-T. Zhu and Z.-H. Luo, *Chem. Eng. J.*, 2016, **287**, 474.

49 J. Ge, D. Zong, Q. Jin, J. Yu and B. Ding, *Adv. Funct. Mater.*, 2018, **28**, 1705051.

50 M. M. Liu, J. Li and Z. G. Guo, *J. Colloid Interface Sci.*, 2016, **467**, 261.

51 Y. Sawai, S. Nishimoto, Y. Kameshima, E. Fujii and M. Miyake, *Langmuir*, 2013, **29**, 6784.

52 W. Zhou, X. Hu, B. Zhan, S. Li, Z. Chen and Y. Liu, *Colloids Surf. A Physicochem. Eng. Asp.*, 2022, **652**, 129805.

53 X. Chen, Y. Zhai, X. Han, H. Liu, Y. Hu, *Appl. Surf. Sci.*, 2019, **483**, 399.

54 J. Li, D. Li, Y. Yang, J. Li, F. Zha and Z. Lei, *Green Chem.*, 2016, **18**, 541.

55 J. Li, L, Yan, H. Li, W. Li, F. Zha and Z. Lei, *J. Mater. Chem. A*, 2015, **3**, 14696.

56 S. Zhao, Y. Liang, Y. Yang, J. Huang, Z. Guo and W. Liu, *Nanoscale*, 2021, **13**, 15334.

57 B. Shang, Y. Zhan, M. Chen and L. Wu, *Appl. Surf. Sci.*, 2020, **528**, 146805.

58 W. Liang, L. Zhu, W. Li, X. Yang, C. Xu and H. Liu, *Langmuir*, 2015, **31**, 11058.

59 J. Yong, F. Chen, Q. Yang, Z. Jiang and X. Hou, *Adv. Mater. Interfaces*, 2018, **5**, 1701370.

60 J. L. Yong, F. Chen, Q. Yang, D. Zhang, U. Farooq, G. Du and X. Hou, *J. Mater. Chem. A*, 2014, **2**, 8790.

61 J. L. Yong, F. Chen, Q. Yang, U. Farooq and X. Hou, *J. Mater. Chem. A*, 2015, **3**, 10703.

62 J. Yong, F. Che, Q. Yang, G. Du, C. Shan, H. Bian, U. Farooq and X. Hou, *J. Mater. Chem. A*, 2015, **3**, 9379.

63 K. Sugioka and Y. Cheng, *Appl. Phys. Rev*., 2014, **1**, 041303.

64 J. L. Yong, F. Chen, M. Li, Q. Yang, Y. Fang, J. Huo and X. Hou, *J. Mater. Chem. A*, 2017, **5**, 25249.

65 H. Wang and Z. Guo, *Appl. Phys. Lett*., 2014, **104**, 183703.

66 Z. Li, H. He, Y. Liang, L. Ouyang, T. C. Zhang and S. Yuan, *Ind. Eng. Chem. Res*., 2020, **59**, 16450.

67 S. Yang, Y. Si, Q. X. Fu, F. F. Hong, J. Y. Yu, S. S. Al-Deyab, M. El-Newehy and B. Ding, *Nanoscale*, 2014, **6**, 12445.

68 A. Raza, B. Ding, G. Zainab, M. El-Newehy, S. Al-Deyab and J. Y. Yu, *J. Mater. Chem. A*, 2014, **2**, 10137.

69 Y. Deng, G. Zhang, R. Bai, S. Shen, X. Zhou and I. Wyman, *J. Membr. Sci*., 2019, **569**, 60.

70 G. Decher and J. D. Hong, *Makromol. Chem., Macromol. Symp*. 1991, **46**, 321.

71 G. Decher, *Science*, 1997, **277**, 1232.

72 W. Ma, H. Xu and A. Takahara, *Adv. Mater. Interfaces*, 2014, **1**, 1300092.

73 K. Hou, Y. Zeng, C. Zhou, J. Chen, X. Wen, S. Xu, J. Cheng, Y. Lin and P. Pi, *Appl. Surf. Sci*., 2017, **416**, 344.

74 J. Dai, L. Wang, Y. Wang, S. Tian, X. Tian, A. Xie, R. Zhang, Y. Yan and J. Pan, *ACS Appl. Mater. Interfaces*, 2020, **12**, 4482.

75 S. Gao, Y. Zhu, J. Wang, F. Zhang, J. Li and J. Jin, *Adv. Funct. Mater*., 2018, **28**, 1801944.

76 U. Manna and D. M. Lynn, *Adv. Funct. Mater*., 2015, **25**, 1672.

77 S. J. Gao, Z. Shi, W. B. Zhang, F. Zhang and J. Jin, *ACS Nano*, 2014, **8**, 6344.

78 T. Huang, L. Zhang, H. Chena and C. Gao, *J. Mater. Chem. A*, 2015, **3**, 19517.

79 J. Chen, Y. Zhou, C. Zhou, X. Wen, S. Xu, J. Cheng and P. Pi, *Chem. Eng. J*., 2019, **370**, 1218.

80 Y. Liu, J. Yin, Y. Fu, P. Zhao, Y. Zhang, B. He and P. He, *Chem. Eng. J*., 2020, **382**, 122925.

81 Y. Chen, N. Liu, Y. Cao, X. Lin, L. Xu, W. Zhang, Y. Wei and L. Feng, *Sci. Rep*., 2016, **6**, 32540.

82 J. L. Yong, F. Chen, Q. Yang, U. Farooq, H. Bian, G. Du and X. Hou, *Appl. Phys. A: Mater. Sci. Process*., 2015, **119**, 837.

83 Y. Ge, W. Wang, K. Li, F. Xiao, Z. Yu, J. Gong, H. Jin and A. Li, *Langmuir*, 2023, **39**, 411.

84 Y. Chen, J. Meng, Z. Zhu, F. Zhang, L. Wang, Z. Gu and S, Wang, *Langmuir*, 2018, **34**, 6063.

85 D. Wu, S. Z. Wu, Q. D. Chen, S. Zhao, H. Zhang, J. Jiao, J. A. Piersol, J. N. Wang, H. B. Sun and L. Jiang, *Lab Chip*, 2011, **11**, 3873.

86 W. Chen, P. Zhang, R. Zang, J. Fan, S. Wang, B. Wang and J. Meng, *Adv. Mater*., 2020, **32**, 1907413.

87 W. Chen, P. Zhang, S. Yu, R. Zang, L. Xu, S. Wang, B. Wang and J. Meng, *Nat. Protoc*., 2022, **17**, 2647.

88 L. Tang, Z. Zeng, G. Wang, L. Shen, L. Zhu, Y. Zhang and Q. Xue, *ACS Appl. Mater. Interfaces*, 2019, **11**, 18865.

89 C. Wang, F. Zhang, C. Yu and S. Wang, *ACS Appl. Mater. Interfaces*, 2020, **12**, 42430.

90 S. Gao, J. Sun, P. Liu, F. Zhang, W. Zhang, S. Yuan, J. Li and J. Jin, *Adv. Mater*., 2016, **28**, 5307.

91 W. Cornwall, *Science*, 2015, **348**, 22.

92 I. Helle, J. Mäkinen, M. Nevalainen, M. Afenyo and J. Vanhatalo, *Environ. Sci. Technol*., 2020, **54**, 2112.

93 C. P. D. Brussaard, L. Peperzak, S. Beggah, L. Y. Wick, B. Wuerz, J. Weber, J. S. Arey, B. van der Burg, A. Jonas, J. Huisman and J. R. van der Meer, *Nat. Commun*., 2016, **7**, 11206.

94 X. Jiang, F. Yang and Z. Guo, *J. Mater. Chem. A*, 2022, **10**, 14273.

95 T. Huang, Z. Su, K. Hou, J. Zeng, H. Zhou, L. Zhang and S. P. Nunes, *Chem. Soc. Rev*., 2023, **52**, 4173.

96 L. Qiu, Y. Sun and Z. Guo, *J. Mater. Chem. A*, 2020, **8**, 16831.

97 Y. Lv, X. Xi, L. Dai, S. Tong and Z. Chen, *Adv. Mater. Interfaces*, 2021, **8**, 2002030.

98 J. Yu, C. Cao and Y. Pan, *Adv. Mater. Interfaces*, 2021, **8**, 2100061.

99 W. Zhang, N. Liu, Y. Cao, X. Lin, Y. Liu and L. Feng, *Adv. Mater. Interfaces*, 2017, **4**, 1700029.

100 Y. Cai, S. Q. Shi, Z. Fang and J. Li, *Adv. Mater. Interfaces*, 2021, **8**, 2100799.

101 F. Zhang, W. B. Zhang, Z. Shi, D. Wang, J. Jin and L. Jiang, *Adv. Mater*., 2013, **25**, 4192.

102 X. Gao, L.-P. Xu, Z. Xue, L. Feng, J. Peng, Y. Wen, S. Wang and X. Zhang, *Adv. Mater*., 2014, **26**, 1771.

103 Z. Bai, K. Jia, C. Liu, L. Wang, G. Lin, Y. Huang, S. Liu and X. Liu, *Adv. Funct. Mater*. 2021, **31**, 2104701.

104 W. Zhang, Y. Zhu, X. Liu, D. Wang, J. Li, L. Jiang and J. Jin, *Angew. Chem. Int. Ed*., 2014, **53**, 856.

105 M. S. Shalaby, G. Sołowski and W. Abbas, *Adv. Mater. Interfaces*, 2021, **8**, 2100448.

106 Z. Wang, S. Ji, F. H. M. Cao, S. Peng and Y. Li, *J. Mater. Chem. A*, 2018, **6**, 3391.

107 J. Huo, Q. Yang, F. Chen, J. Yong, Y. Fang, J. Zhang, L. Liu and X. Hou, *Langmuir*, 2017, **33**, 3659.

108 E. Zhang, Z. Cheng, T. Lv, L. Li and Y. Liu, *Nanoscale*, 2015, **7**, 19293.

109 X. Yao, J. Gao, Y. Song and L. Jiang, *Adv. Funct. Mater*., 2011, **21**, 4270.

110 J. L. Yong, Q. Yang, F. Chen, H. Bian, G. Du, U. Farooq and X. Hou, *Adv. Mater. Interfaces*, 2015, **2**, 1400388.

111 A. Ranella, M. Barberoglou, S. Bakogianni, C. Fotakis and E. Stratakis, *Acta Biomater*., 2010, **6**, 2711.

112 E. Stratakis, A. Ranella and C. Fotakis, *Biomicrofluidics*, 2011, **5**, 13411.

113 L. Chen, M. Liu, H. Bai, P. Chen, F. Xia, D. Han and L. Jiang, *J. Am. Chem. Soc*., 2009, **131**, 10467.

114 D. Parbat, B. K. Bhunia, B. B. Mandal and U. Manna, *Chem. Asian J.*, 2021, **16**, 1081.

115 D. Zang, H. Yi, Z. Gu, L. Chen, D. Han, X. Guo, S. Wang, M. Liu and L. Jiang, *Adv. Mater*., 2017, **29**, 1602869.

116 W, Deng, Y. Su, C. Zhang, W. Wang, L. Xu, P. Liu, J. Wang, X. Yu and Y. Zhang, *J. Colloid Interface Sci*., 2023, **642**, 255.

117 M. Choi, L. Xiangde, J. Park, D. Choi, J. Heo, M. Chang, C. Lee and J. Hong, *Chem. Eng. J*., 2017, **309**, 463.

118 W. Liu, S. Xiang, X. Liu and B. Yang, *ACS Nano*, 2020, **14**, 9166.

119 Y. Huang, M. Liu, J. Wang, J. Zhou, L. Wang, Y. Song and L. Jiang, *Adv. Funct. Mater*., 2011, **21**, 4436.

120 H. Feng, X. Xu, W. Hao, Y. Du, D. Tian and L. Jiang, *Phys. Chem. Chem. Phys*., 2016, **18**, 16202.

121 G. Li, Y. Lu, P. Wu, Z. Zhang, J. Li, W. Zhu, Y. Hu, D. Wu and J. Chu, *J. Mater. Chem. A*, 2015, **3**, 18675.

122 D. Tian, Z. Guo, Y. Wang, W. Li, X. Zhang, J. Zhai and L. Jiang, *Adv. Funct. Mater*., 2014, **24**, 536.

123 Y.-K. Lai, Y.-X. Tang, J.-Y. Huang, F. Pan, Z. Chen, K.-Q. Zhang, H. Fuchs and L.-F. Chi, *Sci. Rep*., 2013, **3**, 3009.

124 L. Tie, Z. Guo and W. Liu, *ACS Appl. Mater. Interfaces*, 2015, **7**, 10641.

125 H. Liu, X. Zhang, S. Wang and L. Jiang, *Small*, 2015, **11**, 3338.

126 Z. Cheng, H. Liu, H. Lai, Y. Du, K. Fu, C. Li, J. Yu, N. Zhang and K Sun, *ACS Appl. Mater. Interfaces*, 2015, **7**, 20410.

127 L. Chen, M. Liu, L. Lin, T. Zhang, J. Ma, Y. Songa and L. Jiang, *Soft Matter*, 2010, **6**, 2708.

128 T. Du, S. Ma, X. Pei, S. Wang and F. Zhou, *Small*, 2017, **13**, 1602020.

129 B. Shang, M. Chen and L. Wu, *Small*, 2019, **31**, 1901888.

130 C. Ding, Y. Zhu, M. Liu, L. Feng, M. Wan and L. Jiang, *Soft Matter*, 2012, **8**, 9064.

131 Q. Cheng, M. Li, F. Yang, M. Liu, L. Li, S. Wang and L. Jiang, *Soft Matter*, 2012, **8**, 6740.

132 T. Xu, W. Shi, J. Huang, Y. Song, F. Zhang, L. P. Xu, X. Zhang and S.Wang, *ACS Nano*, 2017, **11**, 621.

133 Z. F. Gao, E. E. Sann, X. Lou, R. Liu, J. Dai, X. Zuo, F. Xia and L. Jiang, *NPG Asia Materials*, 2018, **10**, 177.

134 Z. F. Gao, R. Liu, J. H. Wang, J. Dai, W. H. Huang, M. J. Liu, S. T. Wang, F. Xia and L. Jiang, *Chem*. 2018, **4**, 2929.

135 Y. Yao, R. K. A. Bennett, Y. Xu, A. M. Rather, S. Li, T. C. Cheung, A. Bhanji, M. J. Kreder, D. Daniel, S. Adera, J. Aizenberg and X. Wang, *Proc. Natl. Acad. Sci. U. S. A*., 2022, **119**, e2211042119.

136 E. Ueda and P. A. Levkin, *Adv. Mater*., 2013, **25**, 1234.

137 T. L. Xu, L. P. Xu, X. J. Zhang and S. T. Wang, *Chem. Soc. Rev.*, 2019, **48**, 3153.

138 J. Hou, H. Zhang, Q. Yang, M. Li, L. Jiang and Y. Song, *Small*, 2015, **11**, 2738.

139 H. Z. Li, Q. Yang, J. Hou, Y. N. Li, M. Z. Li and Y. Song, *Adv. Funct. Mater*., 2018, **28**, 1800448.

140 F. J. Huang, Y. Chen, Y. Q. Wang and F. Xia, *Anal. Bioanal. Chem*., 2019, **411**, 4721.

141 S. Nishioka, M. Tenjimbayashi, K. Manabe, T. Matsubayashi, K. Suwabe, K. Tsukada and S. Shiratori, *RSC Adv*., 2016, **6**, 47579.

142 K. Manabe, M. Matsuda, C. Nakamura, K. Takahashi, K.-H. Kyung and S. Shiratori, *Chem. Mater*. 2017, **29**, 4745.

143 M. W. England, T. Sato, C. Urata, L. Wang and A. Hozumi, *J. Colloid Interface Sci*., 2017, **505**, 566.

144 Y. Gu, J. Yang and S. Zhou, *J. Mater. Chem. A*, 2017, **5**, 10866.

145 Q. Wang, P. Wang, L. Kou, H. Wei and J. Zhou, *J. Appl. Polym. Sci*., 2022, **139**, e52205.

146 A. Owais, T. Smith- Palmer, A. Gentle and C. Neto, *Soft Matter*, 2018, **14**, 6627.

147 K. Chen, S. Zhou, and L. Wu, *ACS Nano*, 2016, **10**, 1386.

148 Q. Wang, Y. Fu, X. Yan, Y. Chang, L. Ren and J. Zhou, *Appl. Surf. Sci*., 2017, **412**, 10.

149 D. Parbat and U. Manna, *Chem. Sci*., 2017, **8**, 6092.

150 L. Li, G. Zhang and Z. Su, *Angew. Chem. Int. Ed*., 2016, **55**, 9093.

151 Y. Wang, V. Kozlovskaya. I. G. Arcibal, D. M. Cropek and E. Kharlampieva, *Soft Matter*, 2013, **9**, 9420.

152 Z. Xue, S. Wang, L. Lin, L. Chen, M. Liu, L. Feng and L. Jiang, *Adv. Mater*., 2011, **3**, 4270.

153 T. Matsubayashi, M. Tenjimbayashi, M. Komine, K. Manabe and S. Shiratori, *Ind. Eng. Chem. Res*., 2017, **56**, 7080.

154 X. Xie, L. Liu, L. Zhang and A. Lu, *Carbohydr. Polym.*, 2020, **229**, 115467.

155 B. Chen, G. Ju, E. Sakai and J. Qiu, *RSC Adv*., 2015, **5**, 87055.

156 L. Lin, M. Liu, L. Chen, P. Chen, J. Ma, D. Han and L. Jiang, *Adv. Mater.*, 2010, **22**, 4826.

157 X. Lin, X. Huang, C. Zeng, W. Wang, C. Ding, J. Xu, Q. He and B. Guo, *J. Colloid Interface Sci.*, 2019, **535**, 491.

158 C. Teng, D. Xie, J, Wang, Y. Zhu and L. Jiang, *J. Mater. Chem. A*, 2016, **4**, 12884.

159 F. Li, G. Zhang, Z. Wang, H. Jiang, X. Feng, S. Yan, L. Zhang, H. Li, T. Zhao and M. Liu, *Chem. Eng. J*., 2019, **375**, 122047.

160 J. Lu, Z. Gao, T. Xu, X. Zhu, X. Miao, Y. Song, G. Ren and X. Li, *ACS Appl. Mater. Interfaces*, 2020, **12**, 49138.

161 W. Xiao, H. Li, H. Yang, Y. Shu, T. Tu, B. Li and X. Liao, *Adv. Eng. Mater*., 2013, **25**, 2201258.

162 C. Wang, G. He, J. Cao, L. Fan, W. Cai and Y. Yin, *ACS Appl. Polym. Mater*., 2020, **2**, 1124.

163 M. A. Gondal, M. S. Sadullah, M. A. Dastageer, G. H. McKinley, D. Panchanathan and K. K. Varanasi, *ACS Appl. Mater. Interfaces*, 2014, **6**, 13422.

164 J. Li, L. Yan, W. Li, J. P. Li, F. Zha and Z. Lei, *Mater. Lett.*, 2015, **153**, 62.

165 Z. Cheng, H. Lai, Y. Du, K. Fu, R. Hou, C. Li, N. Zhang and K. Sun, *ACS Appl. Mater. Interfaces*, 2014, **6**, 636

166 Q. Wen, J. Di, L. Jiang, J. Yu and R. Xu, *Chem. Sci.*, 2013, **4**, 591.

167 J. Li, L. Yan, H. Li, W. Li, F. Zha and Z. Lei, *J. Mater. Chem. A*, 2015, **3**, 14696.

168 S. Yuan, C. Chen, A. Raza, R. Song, T.-J. Zhang, S. O. Pehkonen and B. Liang, *Chem. Eng. J*., 2017, **328**, 497.

169 T. Meng, J. Zhang, H. Wang, N. Fu, M. Wang, W. Li, R. Shi, B. Peng, P. Li and Z. Deng, *Adv. Mater. Interfaces*, 2021, **8**, 2101179.

170 J. Ji, H. He, C. Chen, W. Jiang, A. Raza, T.-J. Zhang and S. Yuan, *ACS Sustainable Chem. Eng*., 2019, **7**, 2569.

171 L.-P. Xu, J. Zhao, B. Su, X. Liu, J. Peng, Y. Liu, H. Liu, G. Yang, L. Jiang, Y. Wen, X. Zhang and S. Wang, *Adv. Mater*., 2013, **25**, 606.

172 Y. Wang, Y. He, H. Li, J. Yu, L. Zhang, L. Chen and Y. Bai, *J. Membr. Sci.*, 2021, **639**, 119776.

173 T. Guo, L. Heng, M. Wang, J. Wang and L. Jiang, *Adv. Mater*., 2016, **28**, 8505.

174 H. Cao and Y. Liu, *J. Colloid Interface Sci*., 2021, **598**, 483.

175 A. Prasannan, J. Udomsin, H.-C. Tsai, C.-F. Wang and J.-Y. Lai, *Chem. Eng. J*., 2020, **391**, 123585.

176 S. L. Bechler and D. M. Lynn, *Biomacromolecules*, 2012, **13**, 1523.

177 J. Yang, H. Wang, Z. Tao, X. Liu, Z. Wang, R. Yue and Z. Cui, *Chem. Eng. J*., 2019, **359**, 149.

178 A. M. Rather and U. Manna, *Chem. Mater*., 2016, **28**, 8689.

179 D. Parbat, S. Gaffar, A. M. Rather, A. Gupta and U. Manna, *Chem. Sci*., 2017, **8**, 6542.

180 M. E. Buck, J. Zhang and D. M. Lynn, *Adv. Mater*., 2007, **19**, 3951.

Bio-mimicked Liquid Crystal Repellent Coating for Immobilizing Liquid Crystal µ-Droplets—Without Affecting Their Sensitivity*

The aqueous interface of nematic liquid crystal (LC) that undergoes a triggered change in ordering transition of mesogens under an appropriate stimulus has emerged as an important tool for various relevant applications. Further, the confinement of LC into a micrometer dimension appeared to be a facile approach for improving their relevant features and performance. However, the optical characterization of ordering transition in a single micrometer-sized, bare, and free-floating LC droplet in the aqueous phase is an extremely challenging task due to unavoidable Brownian motion, which limits its scope for practical applications. The 1, 4-conjugate addition reaction is exploited to fabricate a multilayer coating of reactive nanocomplex that displayed an extreme repellence to beaded LC droplets with tailored adhesive force through the association of adequate orthogonal chemical modifications with glucamine and selected alkyl acrylates. Further, a spatially selective underwater adhesive super-LC-phobic pattern on a hydrophobic background was developed for immobilizing bare and micrometer-sized LC droplets from their aqueous dispersion without having any arbitrary spillage of the aqueous medium. The settled micrometer-sized LC droplets remained efficient for the triggered change in ordering transition from bipolar (having boojum defects at poles) to radial (with a single defect in the center) configuration. Eventually, a simple and fundamentally distinct chemical strategy of immobilizing a soft and functional material by associating bio-inspired wettability allowed to demonstrate the repetitive triggered LC ordering transition in a single and bare LC droplet.

*A. Borbora, and U. Manna, *Langmuir*, 2022, **38**, 9221.

2.1. Introduction

The ordering transition of thermotropic liquid crystals (LC) appeared as an emerging tool for developing various functional and responsive soft materials.[1-10] In this context, the strategic use of highly sensitive micrometer-sized droplets of nematic LC (4-cyano-4′-pentylbiphenyl, 5CB) and their ordering transition from bipolar to radial configurations (Figure 2.1A−C) provided an elegant basis for monitoring different biological events, sensing various analytes, and modulating arrangement of nanoparticles.[5-12] The triggered and reversible ordering transition of nematic micrometer-sized LC (denoted as μ-LC) droplets due to the preferential surface anchoring of appropriate amphiphilic molecules resulted in a distinct optical appearance of LC droplets under a cross-polar microscope.[5-12] In the past, the microscopic characterizations of such ordering transition in optical appearance were often performed with randomly and freely translated/rotated μ-LC droplets in the aqueous phase before their sedimentation (Figure 2.1D) to avoid the unfavorable influences of the droplet/solid surface interactions on their configuration.[13-15] However, the random translation of the μ-LC droplets in the aqueous phase with a speed higher than 1 μm s^{-1}, together with their rotation, makes the image acquiring process highly tedious and challenging as the dispersed μ-LC droplets hardly

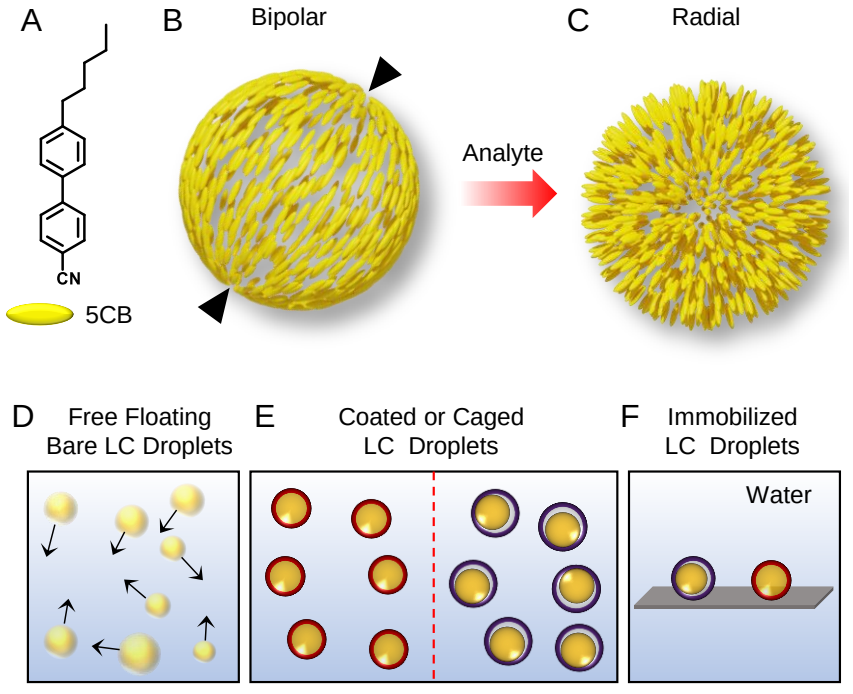

Figure 2.1. (A) Chemical structure of 4′-pentyl-4-biphenylcarbonitrile (5CB). (B, C) Depicting the director configurations in (B) bipolar μ-LC droplet with boojum defects at the poles and (C) radial μ-LC droplet with a single defect at the center. (D–F) Illustrating the earlier microscopic characterization approaches with (D) free-floating bare LC droplets, (E) coated or caged LC droplets, and (F) covalently immobilized coated LC droplets.

stay in the same plane of focus of the microscope during the analysis.[16] In addition, tracking the ordering transition in a single LC droplet is nearly impossible to achieve with such continuously moving LC droplets under cross-polar microscope; eventually, a large number of LC droplets need to be characterized and analyzed to interpret an unambiguous result. Hence, the analysis of a large number of freely moving LC droplets makes the entire process very tedious.

Recently, to overcome the challenges mentioned above, μ-LC droplets are either decorated with various polymeric coatings and matrixes or confined in a polymeric cages prior to immobilizing on a solid interface to restrict their continuous translational movement, as shown in Figure 2.1E, F.[16-24] Although these strategies remained successful in immobilizing the μ-LC droplets, keeping their size and shape intact, the association of the external polymeric coating or matrix around the droplets' surface is likely to (a) influence the LC/aqueous interface and (b) restrict the anchoring of different bulky external agents. Hence, the design of a facile approach for immobilizing a bare μ-LC droplet on a solid surface without compromising their shape and sensitivity is of utmost importance for (1) convenient and unambiguous optical characterization of ordering transition in the LC droplets and (2) decorating the same LC/water interface multiple times with distinct and desired chemicals for realistic applications of such prospective soft materials. However, the report on such a design is yet to be introduced in the literature.

In the recent past, bio-inspired artificial interfaces that possessed hierarchical surface topography and high water affinity (water contact angle (WCA) ~ 0°) and exhibited extreme oil repellence underwater were rationally exploited for protecting various substrates from oil/oily contaminations, anti-biofouling, antiplatelet adhesion, oil/water separation, etc.[25-29] Various prospective applications of such interfaces were mostly demonstrated by using mainly different water-immiscible isotropic organic solvents (e.g., dichloromethane, dichloroethane) and oils.[25-29] Taking inspiration from the bio-inspired underwater superoleophobicity and considering the fact that the anisotropic nematic LC phase exhibits similar immiscibility to the aqueous phase like an oil/oily phase, in this chapter, an extremely LC repellent (dented as super-LC-phobic) interface was designed through the appropriate co-optimization of surface topography and chemistry. Then, the super-LC-phobic interface was unprecedentedly extended to sediment μ-LC droplets on it and to restrict their translational movement without altering their shape and sensitivity. Moreover, the chemically modulated adequate adhesion property on such a super-LC-phobic interface aided in immobilizing the μ-

LC droplet without associating any additional coating or matrix around the droplets' surface. Moreover, the reactive multilayer coating was spatially selectively and orthogonally modified to associate an underwater adhesive super-LC-phobic pattern confined by a hydrophobic boundary for selective sedimentation of μ-LC droplets, where the surrounding hydrophobicity prevented the arbitrary spreading the carrier aqueous solution having the dispersion of μ-LC droplets and the aqueous solution of analytes. Eventually, such a simple principle allowed effortless and repetitive characterization of triggered ordering transition in a single and bare μ-LC droplet.

2.2. Experimental Section

2.2.1. Materials Required

Branched polyethyleneimine (BPEI; molecular weight: 25,000 Da), dipentaerythritol pentaacrylate (5Acl; molecular weight: 524.21 g mol^{-1}), 4′-pentyl-4-biphenylcarbonitrile (5CB), octadecyl amine (ODA), fluorescein isothiocyanate (FITC), 3-(dimethylamino)-1-propylamine (DMAPA), butyl acrylate, hexyl acrylate, lauryl acrylate, octadecyl acrylate, and sodium dodecyl sulfate (SDS) were purchased from Sigma Aldrich, Bangalore, India. D-glucamine was acquired from TCI chemicals (India) Pvt. Ltd. Tetramethylrhodamine cadaverine (TMRC) was purchased from ThermoFisher Scientific, Invitrogen. Ethanol was purchased from TEDIA Company (USA). Tetrahydrofuran (THF) was obtained from RANKEM, Maharashtra, India. Microscopic cover glass was obtained from blue star company. Deionized (DI) water was used for all experiments.

2.2.2. Characterization:

The WCA (in air) and LC contact angles (underwater) were measured at five different positions for each sample using a KRUSS Drop Shape Analyzer-DSA25 instrument at ambient temperature. The surface topography of the fabricated multilayer was visualized using field emission scanning electron microscopy (FFESEM, Sigma Carl Zeiss), where all samples were first subjected to gold sputtering to form a thin gold layer prior to imaging. The surface roughness of the multilayers was acquired by an OXFORD Cypher atomic force microscopy (AFM). The Attenuated total reflectance-Fourier transform infrared (ATR-FTIR) spectra were recorded using a PerkinElmer UATR Two under ambient conditions. Digital photographs were captured using a Canon powershot SX540HS digital camera. The adhesive forces of the LC droplets on the multilayer coatings were measured using a highly sensitive microelectromechanical balance system (Kruss force tensiometer, Germany). The bright-field

and cross-polar microscopy images were obtained using a ZEISS Axio Vert.A1 inverted microscope.

2.2.3. Preparation of Reactive Multilayer Coatings

BPEI (50 mg mL^{-1}) and 5Acl (132.5 mg mL^{-1}) solutions were prepared in ethanol separately, and then the two solutions were mixed in a 1:10 ratio of BPEI:5Acl. After 15 min, the reaction mixture resulted in formation of growing chemically reactive nanocomplex (CRNC). Then, the multilayer coatings were prepared on a microscopic glass cover through the layer-by-layer (LbL) deposition of BPEI and growing CRNC. First, the glass substrate was dipped in the BPEI solution for 10 s. Next, the substrate was removed and washed with an ethanol bath for 10 s followed by a second ethanol bath for another 10 s to remove the unabsorbed or loosely absorbed polymers. Subsequently, the substrate was dipped in the dispersion of CRNC solution for 10 s and then washed using two ethanol baths (10 s each). This one cycle of deposition of BPEI and CRNC is denoted as one bilayer formation. The cycle was repeated for the required times to obtain the polymeric multilayer coatings with desired bilayers, viz., 3, 6, 9, 12, and 15 bilayers.

2.2.4. Post-Modification of Reactive Multilayer Coatings

The post-modification of the residual acrylates on the multilayer coatings was performed via the 1, 4-conjugate addition reaction by treating the prepared multilayers with the selected amine-containing molecule separately. All the multilayers (3, 6, 9, 12, and 15 bilayers) coated on the glass substrate were treated with aqueous glucamine solution (2.5 mg mL^{-1} in water) overnight under ambient conditions and then washed thoroughly with DI water and air-dried. Separately, the 15-bilayer coating was exposed to ODA solution (5 mg mL^{-1} in THF) overnight under ambient conditions, then washed with THF solvent and air-dried.

The multilayer coatings were also treated with acrylate-containing molecules to post-modify the residual amines present in the multilayer coatings. In this case, the 15-bilayer coating was separately treated with different ethanolic solutions (25 µL mL^{-1}) of hydrophobic acrylate molecules, i.e., butyl acrylate, hexyl acrylate, lauryl acrylate, and octadecyl acrylate overnight under ambient conditions. After treatment, the coatings were washed with ethanol solvent and air-dried. For dual functionalization, the 15-bilayer coatings were first treated separately with all the mentioned hydrophobic acrylates similarly and sequentially exposed to glucamine solution (2.5 mg mL^{-1} in water) overnight under ambient conditions.

2.2.5. Fabrication of the Patterned Superhydrophilic (Underwater Super-LC-phobic)/Hydrophobic Interface

To prepare a pattern interface where the underwater super-LC-phobic spots covered by hydrophobic area, the 15-bilayer coatings prepared on the microscopy glass cover were spatially selectively modified in some circular spots (~ 3 mm diameter) by dispensing 20 μL of glucamine solution (2.5 mg mL^{-1} in water) through a pipette. Then, the air-dried coatings with glucamine patterns were exposed to ODA solution (5 mg mL^{-1} in THF) to create the hydrophobic boundary on the background of the superhydrophilic (underwater super-LC-phobic) patterns.

Underwater super-LC-phobic patterns with tailorable adhesive properties were fabricated by first separately exposing the 15-bilayer coatings with the solution of different hydrophobic acrylates, *viz.*, butyl acrylate, hexyl acrylate, lauryl acrylate, and octadecyl acrylate in ethanol solvent (25 μL mL^{-1}) and sequentially modifying the coatings with glucamine patterns as mentioned above. Further, the coatings were treated with ODA solution (5 mg mL^{-1} in THF) to create underwater adhesive super-LC-phobic (superhydrophilic) patterns enclosed by hydrophobic surroundings.

2.2.6. Characterization of Sedimented μ-LC Droplets on the Underwater Super-LC-Phobic Interface

To characterize the μ-LC droplets dispersed in water, an LC-in-water emulsion was first prepared by sonicating and vortex mixing of 3 μL of 5CB in 10 mL of DI water. Then, 10 μL of LC-in-water emulsion solution was dispensed on the superhydrophilic regions of the patterned superhydrophilic/hydrophobic interface and waited for 30 min to sediment the dispersed μ-LC droplets. Then, the focal plane of the microscope was adjusted just above the surface of the coated glass cover to monitor the orientational transition of the sedimented μ-LC droplets before and after the addition of analyte solution in the same region.

To monitor the orientational transition of bipolar LC droplets upon interaction with the SDS surfactant, aqueous SDS solutions (10 μL), that were prepared by varying the SDS concentration, separately added to the LC-containing solution to alter the final concentration of the SDS in the solution as 0.2, 0.4, 0.6, 08, and 1 mM. The repetitive and reversible LC ordering transition with a single LC droplet sedimented on an adhesive underwater super-LC-phobic (butyl acrylate/glucamine-modified) surface was performed by exposing the LC droplet with SDS solution (1 mM) to obtain radial configuration. Thereafter, washing of the droplet

with DI water was performed by adding and removing 10 µL of water several times until the bipolar orientation was regained. This cycle was repeated for several cycles for the repetitive monitoring of the ordering transition in a single LC droplet.

2.3. Results and Discussion

2.3.1. Design of Dually Reactive Multilayer Coatings

In this chapter, a simple chemical approach was introduced to prepare a multilayer coating comprised of two types of residual functional groups, acrylate and amine, following a LbL deposition process. Specifically, a 1, 4-conjugate addition reaction between BPEI and 5Acl in an ethanol medium was exploited to prepare CRNC comprised of residual acrylate group (Figure 2.2A, B). Next, 15 bilayers of a CRNC and BPEI were prepared on a glass substrate through a covalent LbL deposition process to construct a dual reactive multilayer coating loaded with residual amine and acrylate functionalities, as shown in Figure 2.2C.

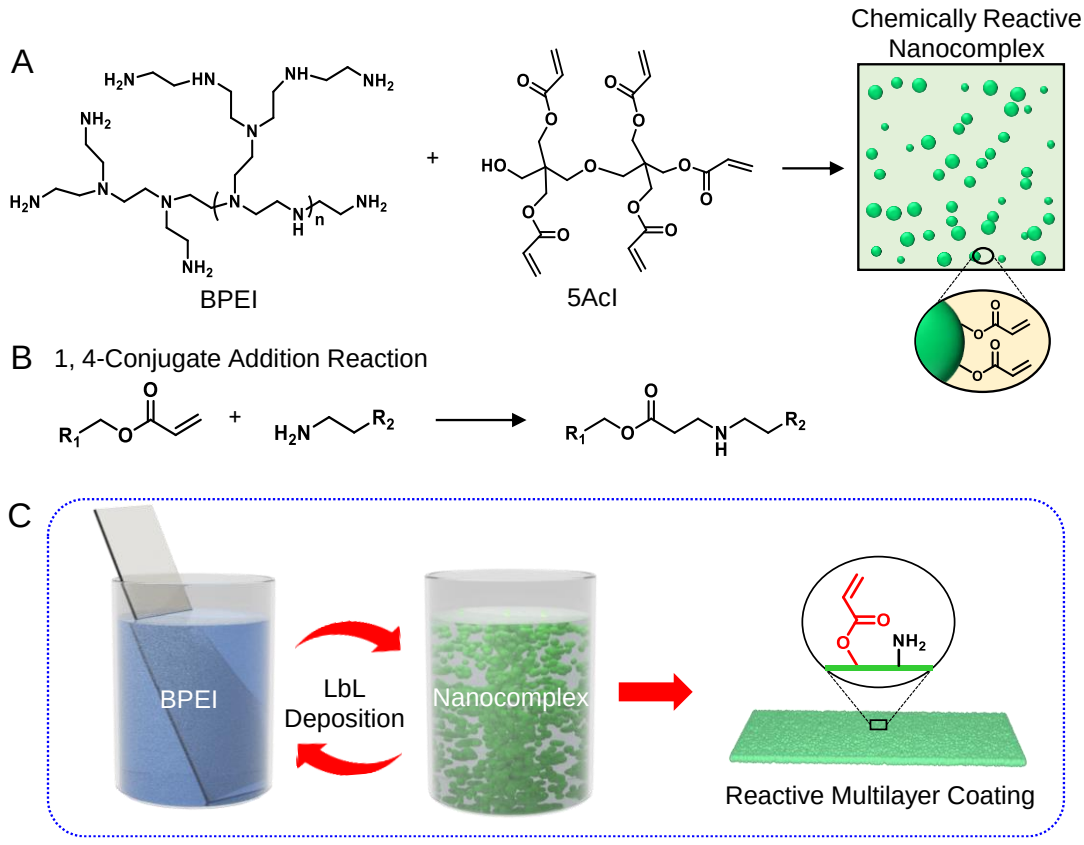

Figure 2.2. (A) Schematic representing the formation of the chemically reactive nanocomplex (CRNC) after mixing of branched polyethyleneimine (BPEI) and dipentaerythritol pentaacrylate (5Acl) in ethanol, where available amine and acrylate spontaneously reacted through (B) 1, 4-conjugate addition reaction. (C) The covalent layer-by-layer (LbL) deposition of BPEI and CRNC on the glass substrate yielded the dual reactive multilayer coating comprised of residual acrylate and amine reactivity.

Next, I sought to validate the existence of the two distinct residual reactive groups in the multilayer coating and the possibility of their independent functionalization with small molecules. The prominent existence of characteristic ATR-FTIR signatures for the C–H deformation of vinyl moiety and carbonyl (C═O) stretching at 1409 cm^{-1} and 1730 cm^{-1}, respectively, confirm the presence of residual acrylate groups in the prepared polymeric coatings (Figure 2.3G (black)). After chemical modification using TMRC, a depletion of the IR signature at 1409 cm^{-1} was observed when compared to the carbonyl stretching at 1730 cm^{-1}, which was expected to remain unaffected during the 1, 4-conjugate addition reaction (Figure 2.3G (red)). The subsequent chemical modification with FITC led to a new characteristic IR signature for the –N–C═S band at 1570 cm^{-1}, confirming the reaction of the residual amines with isothiocyanates (Figure 2.3G, (green)).[30] In addition, TMRC/FITC-

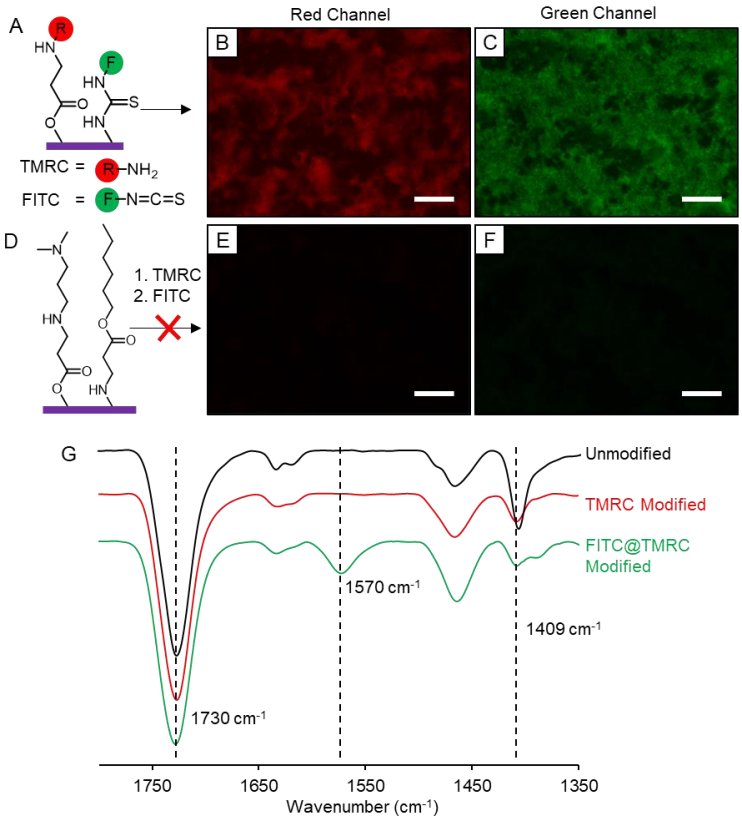

Figure 2.3. (A) Schematic illustration and (B, C) corresponding fluorescence micrographs of the dual reactive multilayer coatings after sequential treatments with tetramethylrhodamine cadaverine (TMRC) and fluorescein isothiocyanate (FITC). (D) Schematic illustration and (E, F) corresponding fluorescence micrographs of 3-dimethylamino-1-propylamine (DMAPA)/hexyl acrylate−modified multilayer coatings after sequential modification using TMRC and FITC. The excitation and emission wavelength of TMRC and FITC are 544 − 571 nm and 495 − 519 nm, respectively. Scale bars, 50 µm. G) Attenuated total reflectance-Fourier transform infrared (ATR−FTIR) spectra before (black) and after TMRC modification (red) and TMRC/FITC modification (green) of the multilayer coating.

functionalized multilayer coatings exhibited both red and green signals in fluorescence microscopy imaging, as shown in Figure 2.3A−C. As a control experiment, the chemical modifications of the acrylate and amine groups of the multilayer coating with two non-fluorescent small molecules (*i.e.*, DMAPA and hexyl acrylate) were attempted to perform, but I failed to achieve it due to lack of covalent bonding with fluorescent dyes TMRC and FITC, resulting in the absence of fluorescent signals, as shown in Figure 2.3D−F. The above observations support the hypothesis that the acrylate and amine groups of the multilayer coatings can be orthogonally functionalized with selective small molecules through the 1, 4-conjugate addition reaction.

2.3.2. Modulation of Liquid Crystal Wettability on Multilayer Coatings

Previous reports demonstrated the appropriate chemical modulations of the monoreactive coating having hierarchal surface topography following the 1, 4-conjugate addition reaction conferred underwater extremes of oil wettability, i.e., superoleophilicity and

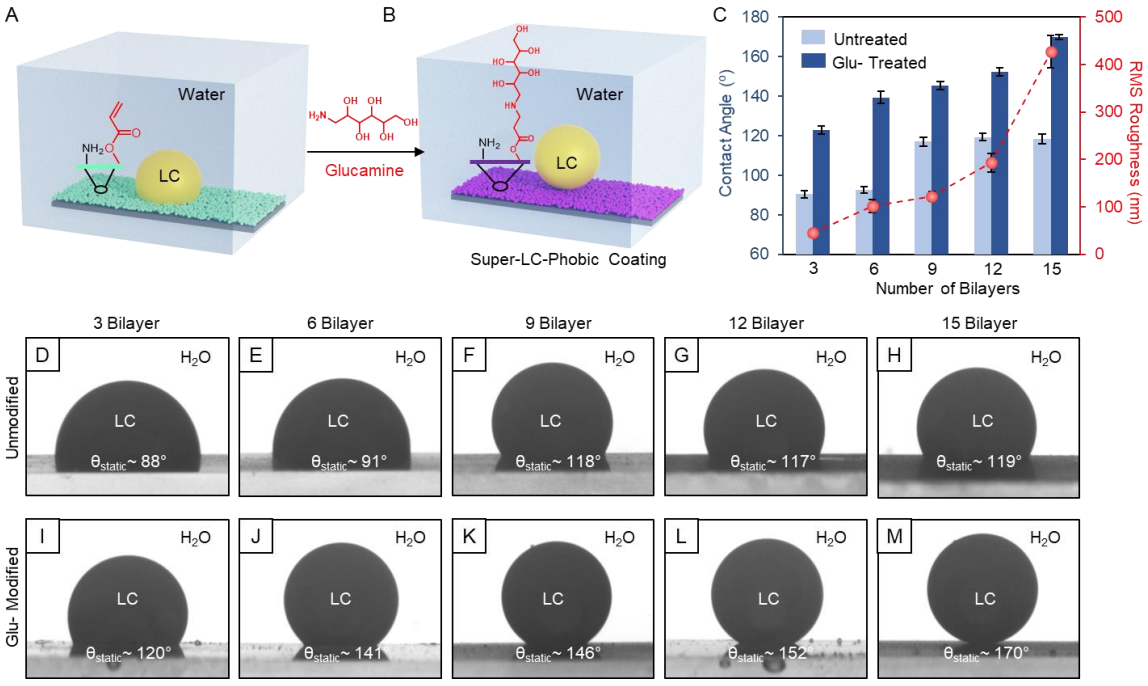

Figure 2.4. (A, B) Schematic depicting the post-covalent modification of (A) reactive multilayer coating with glucamine to achieve (B) super-LC-phobic coating underwater. C) Depicting the effect of the increase in the number of bilayers on RMS roughness of the coating and underwater LC contact angle before and after modification with glucamine. (D−M) Representative contact angle goniometer images of LC droplet on multilayer coatings underwater with the increasing number of bilayers- (D, I) 3 bilayers, (E, J) 6 bilayers, (F, K) 9 bilayers, (G, L) 12 bilayers and (H, M) 15 bilayers, before and after modification with glucamine. The volume of the LC droplet was 5 µL.

superoleophobicity.[31,32] Inspired by the earlier results, in this chapter, a dually reactive multilayer coating was extended to develop (a) underwater super-LC-phobic interfaces with the ability to tailor adhesive properties and (b) pattern interfaces of two distinct wettabilities (i.e., hydrophobicity and underwater super-LC-phobicity) through the association of spatially selective, adequate, and orthogonal post-covalent modifications.

In this chapter, I attempted to optimize the desired LC wettability of the dual reactive multilayer coatings through the post-covalent modification of the residual acrylate moieties with an amine-containing hydrophilic (high surface energy) small molecule, i.e., glucamine, as shown in Figure 2.4A, B. The impacts of both the number of deposition cycles during the LbL process and subsequent post-covalent modulations of prepared multilayer coatings on the underwater LC wettability were thoroughly investigated. The contact angle of beaded LC droplets on the prepared multilayer coatings with the increasing number of bilayers was observed to be enhanced gradually, as shown in Figure 2.4C (light blue) and D−H. This gradual increase in LC contact angle underwater could be attributed to the increase in the roughness of multilayers (RMS roughness from 44.7 ± 4.9 to 426.7 ± 33.8 nm, as calculated from atomic force microscopy analysis (Figure 2.5A−E) with the increase in the number of bilayers from 3 to 15. Further, the association of appropriate high surface energy through the glucamine modification process provided a significant increment in the LC wettability (Figure 2.4C (dark blue) and I-M). Eventually, the moderately hydrophilic (WCA of ~ 65° in air, Figure 2.6A) multilayer (15-bilayer), that displayed moderate LC-phobicity with LC contact angle of ~ 120° underwater (Figure 2.6B, C), became an extremely LC-repellent interface with a contact angle of 170°, (Figure 2.6E, F), after the modification with glucamine, where it also became superhydrophilic with WCA of 0° (Figure 2.6D). This extreme LC repellence property of the prepared coating

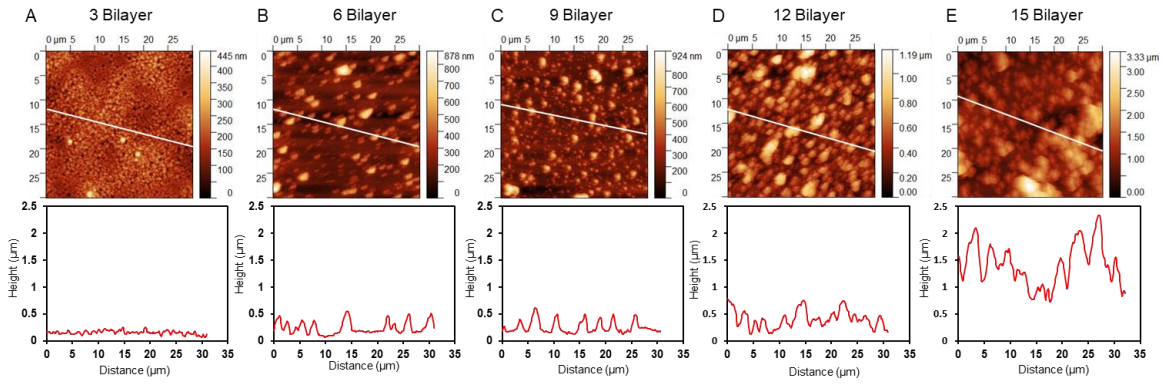

Figure 2.5. (A−E) Atomic force microscope (AFM) images and height profiles of (A) 3 bilayers, (B) 6 bilayers, (C) 9 bilayers, (D) 12 bilayers, and (E) 15 bilayers coating.

underwater is termed as super-LC-phobicity. Such an extreme underwater LC repellence underwater was only achievable due to the successful co-optimization of surface chemistry and hierarchical surface topography in the 15-bilayer coating. The random association of the CRNC as confirmed by the FESEM images (Figure 2.6G, H). The chemical reactivity of the residual acrylate and its ability to react with the selected small molecule (glucamine) were characterized by ATR-FTIR spectral analysis (Figure 2.6I). The appearances of prominent IR signatures at 1730 cm^{-1} and 1409 cm^{-1} for the carbonyl (C═O) stretching and C–H deformation of β-carbon of the vinyl group, respectively, indicated the presence of residual acrylates on the multilayer coating (Figure 2.6I, black spectrum). As expected, selective and significant depletion of the

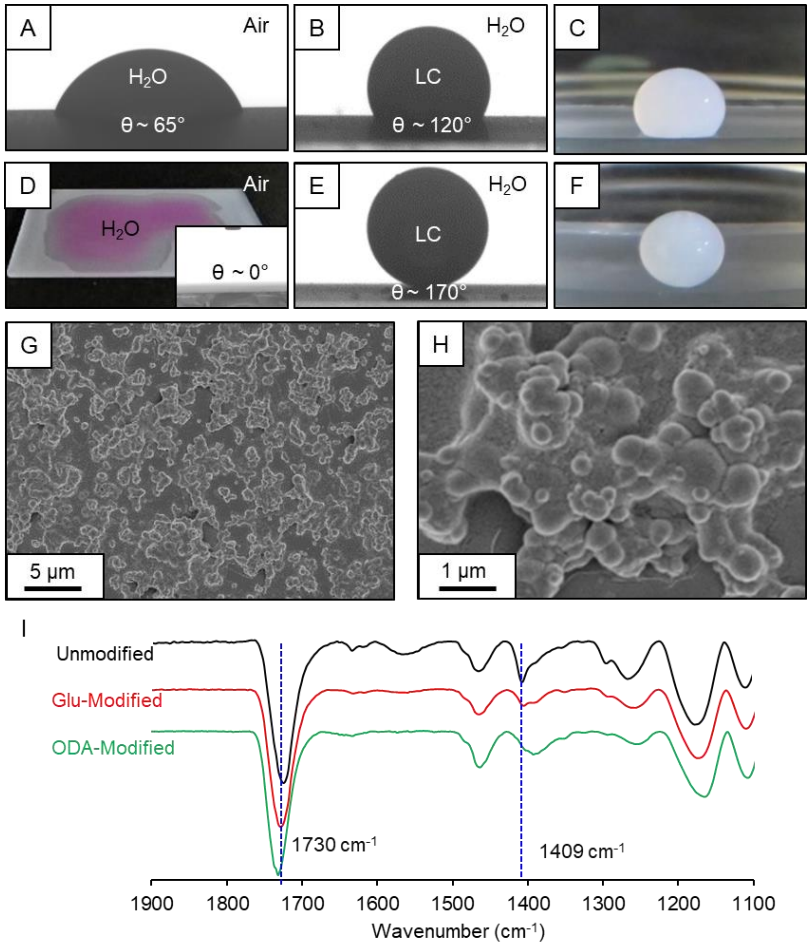

Figure 2.6. (A−C) Contact angle goniometer images and snapshots of (A) water droplet (in air) and (B, C) LC droplet (underwater) on the unmodified multilayer coating. (D) Snapshot and contact angle goniometer image (inset) show the arbitrary spillage of a beaded aqueous phase (red-dyed) on a glucamine-modified coating with a water contact angle (WCA) of 0°. (E) Contact angle goniometer images and (F) snapshots of LC droplet (underwater) on the glucamine-modified multilayer coating. (G, H) Field emission scanning electron microscopy (FESEM) micrographs of 15-bilayer coating in (G) low and (H) high magnifications. (I) ATR-FTIR spectra of the multilayer coatings before (black) and after chemical modifications with glucamine (red) and octadecylamine (ODA, green).

IR peak for C–H deformation of β-carbon of the vinyl group was noted at 1409 cm^{-1} with respect to the IR signature of the carbonyl group after glucamine treatment, indicating the successful post-covalent modification of the multilayer coating (Figure 2.6I, red spectrum). The glucamine-modified underwater super-LC-phobic interface would be useful in minimizing the interaction of sedimented μ-LC droplets and a solid surface. However, the inherent super affinity of such an interface for a water phase leads to the arbitrary and spontaneous spreading of a beaded water phase (Figure 2.6D). Such instant spreading of aqueous droplets made it unfeasible to perform further characterization of a settled μ-LC droplet and its triggered phase transition on a super-LC-phobic coating with a tiny amount (< 50 μL) of analytes and aqueous dispersion of LC droplets. To overcome the instant spreading of aqueous droplets on a glucamine-modified multilayer coating, a spatially selective pattern interface was introduced, where some confined underwater super-LC-phobic spots were created in a hydrophobic background, as shown in Figure 2.7A−C. The hydrophobic background with a WCA of ~ 130º (Figure 2.7D) was created by the post-modification of the multilayer coating with a hydrophobic molecule, i.e., ODA. As expected, ODA modification of the multilayer coating caused the depletion of the characteristic IR peak at 1409 cm^{-1} with respect to the peak at 1730 cm^{-1}, validating the successful post-covalent modification (Figure 2.6I, green). Thus, to achieve such a patterned interface, the residual acrylate group of the multilayer coating was spatially selectively modified with droplets of glucamine solution prior to the treatment of the

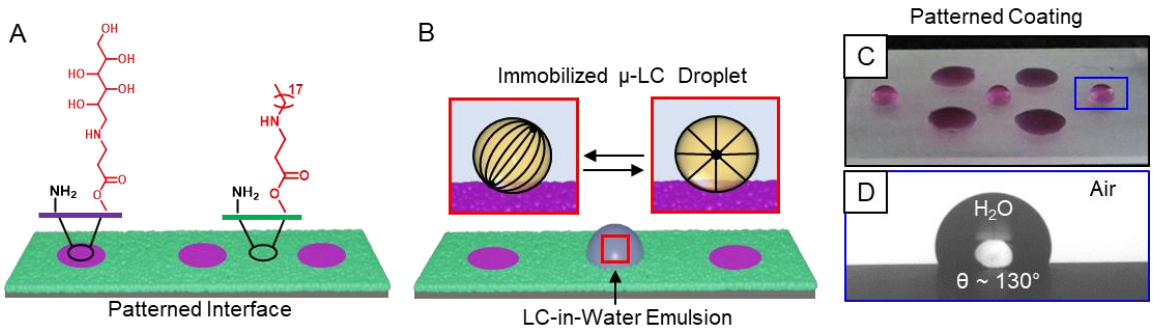

Figure 2.7. (A, B) Schematic depicting (A) patterned interface with superhydrophilic spots on a hydrophobic background created through the spatial covalent modification of the residual functionalities on the coating with appropriate molecules for the (B) confinement of the LC-in-water emulsion solution in the superhydrophilic regions. The immobilization of the sedimented bare μ-LC droplet in the superhydrophilic/super-LC-phobic interface allowed switchable changes of LC ordering. (C) Depicting the wetting behavior of water droplets (red-dyed) on a patterned interface with superhydrophilic glucamine spots on a hydrophobic ODA modified background. (D) Contact angle goniometer image of ODA-modified hydrophobic background (WCA ~ 130°) in air.

entire interface with the solution of ODA. The hydrophobic surroundings restricted the spreading of even a tiny amount (10 µL) of the beaded aqueous phase (Figure 2.7B, C).

2.3.3. Characterization of the Sedimented LC µ-Droplets on the Super-LC-Phobic Interface

The patterned superhydrophilic (underwater super-LC-phobic)/hydrophobic interface was strategically extended to sediment the bare µ-LC droplet without altering its orientational ordering. The LC-in-water emulsion was prepared by sonicating and vortex mixing the selected LC (5CB) in DI water. Afterward, a drop (10 µL) of LC-in-water emulsion was placed on the glucamine-modified spot (exhibiting underwater super-LC-phobicity) and the µ-LC droplets were allowed to settle on the surface for a few minutes. The settled µ-LC droplets were found with "bipolar" orientation (Figure 2.8A, B), where the boojum defects at two poles of the droplets kept rotating, which can be distinctly characterized under a cross-polar microscope, as

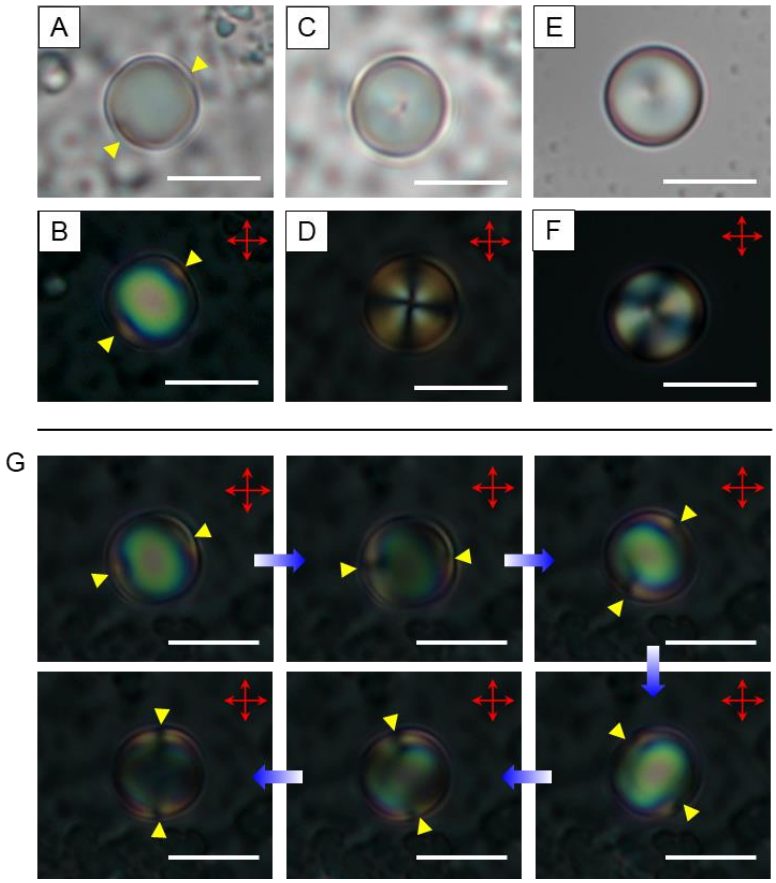

Figure 2.8. (A, C, E) Bright-field and (B, D, F) polarized optical micrographs of a sedimented µ-LC droplet on (E, F) uncoated and (A–D) coated (super-LC-phobic) glass surfaces (A, B, E, F) before and (C, D) after exposing to sodium dodecyl sulfate (SDS, 1 mM). (G) Polarized optical micrograph of sedimented µ-LC droplet on a super-LC-phobic coating with bipolar orientation, where the boojum defects at two poles were continuously rotating. Scale bars, 5 µm.

shown in Figure 2.8G, whereas no significant translation of the sedimented LC droplets was noted. Next, the amphiphile-triggered alteration in the orientational ordering of the sedimented bipolar droplet on the super-LC-phobic interface was investigated. Upon exposing an amphiphilic molecule, i.e., SDS of concentration 1 mM, the interdigitation of hydrocarbon tails of SDS resulted in a radial configuration, wherein the point defect has traveled to the center of the droplet (Figure 2.8C, D). In contrast, the bare μ-LC droplet that directly sedimented on a bare glass surface was found with a bias orientation in the absence of amphiphiles, where mostly a pole defect remained adhered to the surface, and no rotation of defect was noted, which resulted in an ambiguous appearance of the μ-LC droplet under a cross-polar microscope (Figure 2.8E, F). To understand the cause of such distinct appearance of the settled droplet on bare glass and underwater super-LC-phobic interface, the underwater adhesion force of a beaded LC droplet on the respective surfaces was measured. The adhesion force for the beaded LC droplet (5 μL) was significantly high (~ 130 μN) on bare glass (with a contact angle of 110°, Figure 2.9A, B) in comparison to the super-LC-phobic coating (9 μN), as shown in Figure 2.9C, which indicated strong interaction of sedimented LC with bare glass and led to the distinct appearance of beaded μ-LC droplets on bare and coated glass. Furthermore, the impact of a gradual increase in the SDS concentration on the orientational ordering of the settled μ-LC droplets on the super-LC-phobic coating was analyzed; and different orientational configurations were observed, such as axial, escaped radial, and pre-radial in the settled μ-LC droplet (a size of ~ 5 μm) with increasing the SDS concentration in the solution, as shown in Figure 2.10A−D. The different configurational changes in the sedimented droplet were very

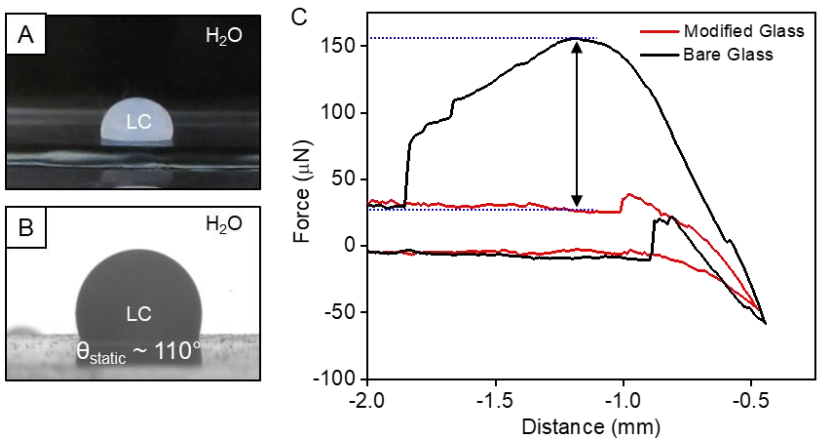

Figure 2.9. Representative (A) digital image and (B) contact angle goniometer image of beaded LC droplet on a bare glass surface underwater. The volume of the droplet was 10 μL for (A) and 5 μL for (B). (C) Underwater LC droplet (5 μL) adhesive force measurements on super-LC-phobic (red) and bare glass (black) interfaces.

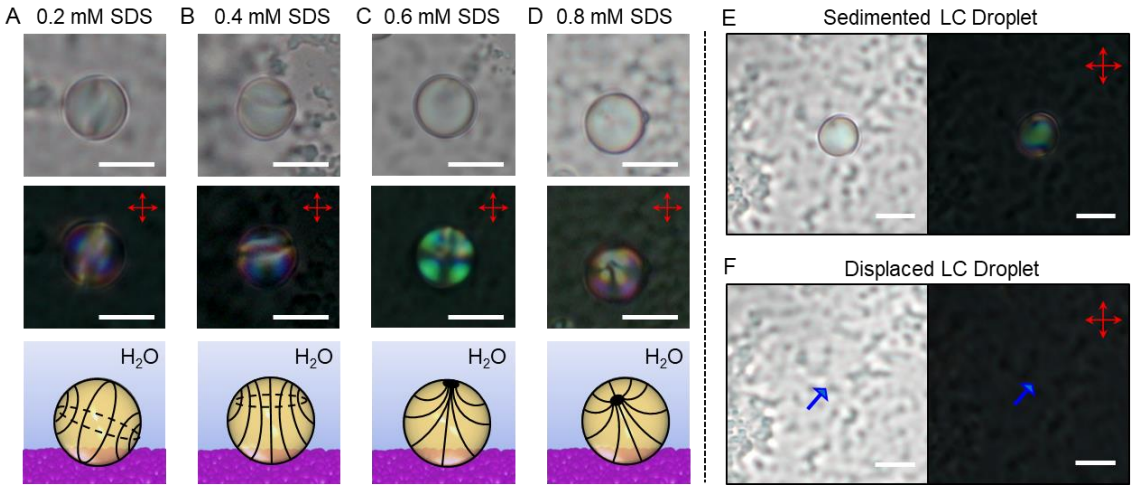

Figure 2.10. (A−D) Bright-field micrograph (top row), polarized optical micrograph (middle row), and schematic representation (bottom row) of sedimented μ-LC droplets on the super-LC-phobic interface with a different orientational ordering achieved by gradually increasing the SDS concentration: (A, B) saturn ring (0.2 and 0.4 mM SDS), (C) escaped radial (0.6 mM SDS), and (D) pre-radial (0.8 mM SDS). (E, F) Bright-field and polarized optical microscopic snapshots showing (E) a sedimented μ-LC droplet on a super-LC-phobic coating and (F) its displacement from the particular region upon addition of a 10 μL volume of analyte (SDS, 1 mM) solution. The blue arrows indicate the initial position of the sedimented μ-LC droplet. Scale bars, 5 μm.

similar to the free-floating droplets reported in the previous literature,[33] which suggested that sedimentation does not cause any impact on the sensitivity of the μ-LC droplets. Although this non-adhesive super-LC-phobic interface allowed the μ-LC droplet to sediment with bipolar configuration with freely rotating boojum defects, it utterly failed to restrict the translation movement of the sedimented μ-LC droplet on imparting the mild turbulence caused during the addition of aqueous analytes or washing of the μ-LC droplet to remove the interdigitated analytes, as shown in Figure 2.10E, F. Hence, the monitoring of reversible ordering transition in a single μ-LC droplet after interaction with an analyte and the repetitive sensing with a single sedimented μ-LC droplet are not feasible to be performed on such non-adhesive super-LC-phobic interfaces. Therefore, a separate design is further required to immobilize the bare μ-LC droplet with controlled adhesive interaction for monitoring repetitive and reversible configurational changes in a single sedimented bare μ-LC droplet.

2.3.4. Underwater Adhesive Super-LC-Phobic Interface to Immobilize the Bare μ-LC Droplet

In the past, the adhesiveness of the beaded liquid droplet on superhydrophobic or underwater superoleophobic interfaces was customized through controlled tailoring of surface roughness.[34,35] However, in this current demonstration, the adhesiveness of the beaded LC

droplet on the multilayer coating was mainly tuned through the strategic association of dual chemical modifications, as shown in Figure 2.11A, B. To control the adhesive interaction between a beaded LC droplet and underwater super-LC-phobic coating, the glucamine-modified multilayer was further post-modified with selected hydrophobic alkyl acrylates through a 1, 4-conjugate addition reaction between residual amine of the multilayer coating and the acrylate group of selected alkyl acrylate (Figure 2.11A, B). While the only modification of the multilayer coating with selected alkyl acrylates having different hydrocarbon tails provided underwater LC-philic coatings (Figure 2.11C−F), the association of the same chemistry on the glucamine-modified multilayer coating allowed to modulate the underwater LC adhesion, keeping the underwater super-LC-phobicity intact in the coating, as shown in Figure 2.11G−J and 2.12A. The adhesion force of the beaded LC droplet (5 μL) on the glucamine/alkyl acrylate-modified multilayer coatings was gradually enhanced underwater with increasing the carbon tail length (C = 4, 6, 12, and 18) of the alkyl group from 18.8 ± 1.6 to 60.7 ± 2.6 μN, as shown in Figure 2.12A. Further, such a change in hydrocarbon tail length resulted in the reduction of the receding contact angle from 159 to 120°, as shown in Figure

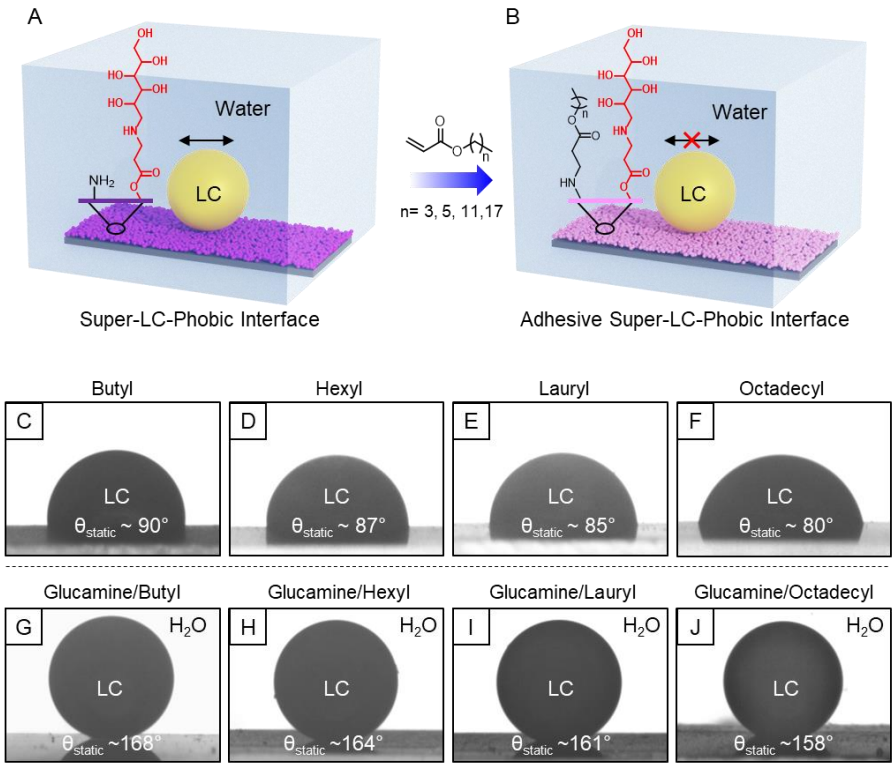

Figure 2.11. (A, B) Schematic depicting the modification of the residual amines in the (A) underwear super-LC-phobic surface with alkyl acrylates to achieve (B) adhesive underwater super-LC-phobicity, underwater. (C−J) Representative underwater static contact angle of beaded LC droplets on different multilayer coatings that were modified with (C−F) alkyl acrylates, and (G-J) both glucamine and alkyl acrylates.

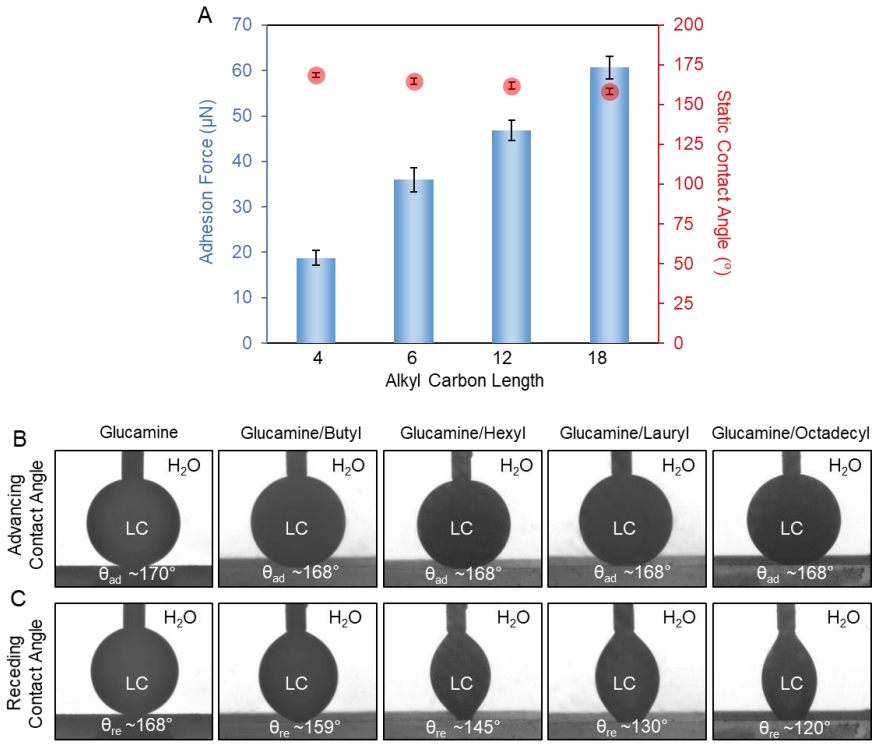

Figure 2.12. (A) Graph representing the effect of alkyl carbon chain length in the super-LC-phobic interface on the adhesion force and static contact angle of a beaded μ-LC droplet (5 μL) underwater. (B, C) Representative underwater (B) advancing and (C) receding LC contact angle on different mono (glucamine) and dual-functionalized (glucamine and alkyl acrylate) multilayer coatings. The volume of the LC droplet was 5 μL.

2.12C. This results independently revalidating the existence of tailored LC adhesion property. The longer hydrocarbon tail in the selected alkyl acrylates (C = 6, 12, and 18) not only enhanced the adhesive force but also affected the appearance of LC droplets under a cross-polar microscope (Figure 2.13A−D), likely due to the interdigitation of longer hydrocarbon tails with LC mesogens. Interestingly, the butyl acrylate (C=4)/glucamine-modified interface provided an underwater super-LC-phobic coating with optimum adhesion force to immobilize LC droplets with a "bipolar-like" appearance (Figure 2.13A). The sedimented LC μ-droplet on such an interface readily transformed to a "radial-like" configuration on the addition of SDS (Figure 2.14A, B), and as expected, the washing of the same droplet with DI water multiple times resulted in a reversible transition from radial to bipolar configuration (Figure 2.14C). During these processes, no translation of the sedimented droplet was noted, which allowed to demonstrate repetitive and reversible LC ordering transition with a single sedimented μ-LC droplet. As a proof of concept demonstration, the same sedimented μ-LC droplet, which was exposed to SDS for achieving radial configuration, was washed thoroughly with DI water for

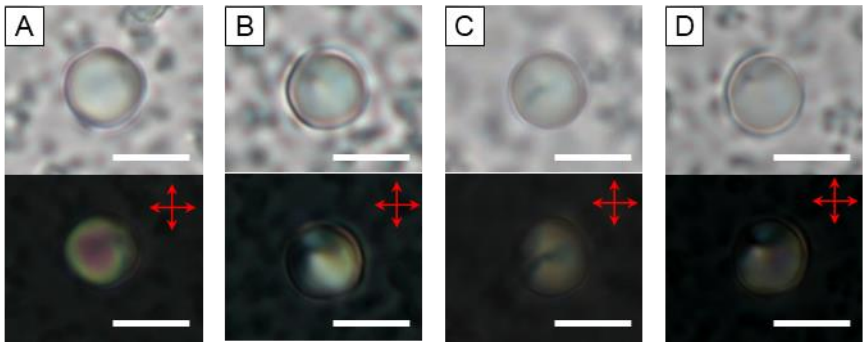

Figure 2.13. (A−D) Bright-field and polarized optical micrographs of sedimented µ-LC droplets on (A) glucamine/butyl acrylate, (B) glucamine/hexyl acrylate, (C) glucamine/lauryl acrylate, and (D) glucamine/octadecyl acrylate-modified underwater adhesive super-LC-phobic coatings having tailored LC adhesion property.

the switching of LC ordering to the initial "bipolar-like" appearance, and this process was successfully repeated for four cycles, as shown Figure 2.14A−H. Hence, this principle would allow to demonstrate sensing of multiple relevant analytes with a single and bare sedimented µ-LC droplet. Apart from improving the sensing ability, the confinement of the LC phase into micrometer-sized droplets provided an elegant basis for achieving topological defect-governed self-assembly of molecules and nanoparticles; it has also allowed to achieve prospective mechano-optical metamaterials.[36-39] The current approach of designing adhesive─but LC repellent─interfaces would allow investigating such complex and smart LC interfaces unambiguously and effortlessly. Moreover, such an interface could be applied to develop underwater responsive photonic materials similar to LC marbles in air.[40]

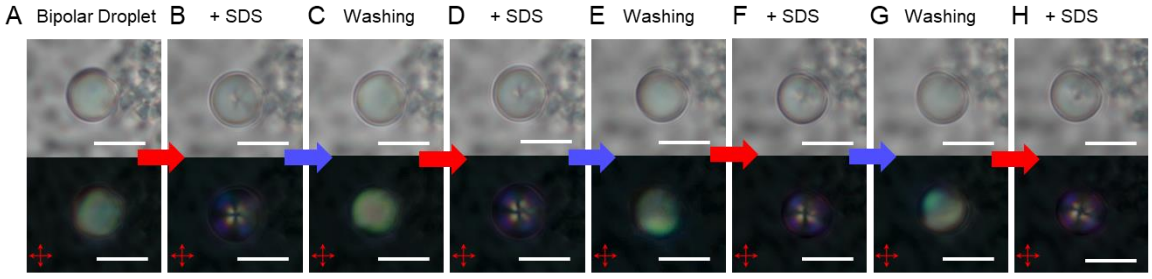

Figure 2.14. Bright-field and polarized optical micrographs demonstrate the repetitive and reversible ordering transition on a single immobilized µ-LC droplet on a adhesive super-LC-phobic interface by sequential exposure to an analyte (SDS, 1mM) and washing with DI water. The red arrow indicated the SDS addition steps and the blue arrow indicated the washing steps with DI water. Scale bars, 5 µm.

2.4. Conclusions

This chapter introduces a simple chemical approach to develop a patterned interface of super-LC-phobicity, where the µ-LC droplets can sediment on the interface without altering their

shape and sensitivity. Further, the association of super-LC-phobicity with an optimum adhesion force between the LC droplet and the interface through the appropriate post-chemical modification enabled to immobilize bare μ-LC droplet─with bipolar configuration. Thus, the association of a simple chemical approach, bio-inspired wettability, and triggered phase transition of immobilized μ-LC droplets provided a simple basis for unambiguous, rapid, and repetitive sensing of various relevant analytes with a single, bare, and sedimented μ-LC droplet.

2.5. References

1 H. Eimura, D. S. Miller, X. Wang, N. L. Abbott and T. Kato, *Chem. Mater.*, 2016, **28**, 1170.

2 N. Bao, J. I. Gold, T. Szilvási, H. Yu, R. J. Twieg, M. Mavrikakis and N. L. Abbott, *J. Mater. Chem.* C, 2021, **9**, 6507.

3 K. Nayani, A. A. Evans, S. E. Spagnolie and N. L. Abbott, *Proc. Natl. Acad. Sci. U. S. A.*, 2020, **117**, 26083.

4 Y. Xu, A. M. Rather, Y. Yao, J.-C. Fang, R. S. Mamtani, R. K. A. Bennett, R. G. Atta, S. Adera, U. Tkalec and X. Wang, *Sci. Adv.*, 2021, **7**, eabi7607.

5 A. Concellón, D. Fong and T. M. Swager, *J. Am. Chem. Soc.*, 2021, **143**, 9177.

6 M. Khan, W. Li, S. Mao, S. N. A. Shah and J.-M. Lin, *Adv. Sci.*, 2019, **6**, 1900778.

7 I. Verma, I. Pani, D. Sharma, S. Maity and S. K. Pal, *Phys. Chem. C*, 2019, **123**, 13642.

8 P. Bao, D. A. Paterson, P. L. Harrison, K. Miller, S. Peyman, J. C. Jones, J. Sandoe, S. D. Evans, R. J. Bushby and H. F. Gleeson, *Lab Chip*, 2019, **19**, 1082.

9 B. J. Ortiz, M. E. Boursier, K. L. Barrett, D. E. Manson, D. Amador-Noguez, N. L. Abbott, H. E. Blackwell and D. M. Lynn, *ACS Appl. Mater. Interfaces*, 2020, **12**, 29056.

10 I. Pani, K. M. F. Nazreen, M. Sharma and S. K. Pal, *Nano Lett.*, 2021, **21**, 4546.

11 X. Yang and Z. Yang, *Langmuir*, 2022, **38**, 282.

12 P. M. Naveenkumar, S. Mann and K. P. Sharma, *Adv. Mater. Interfaces*, 2018, **6**, 1801593.

13 I. H. Lin, D. S. Miller, P. J. Bertics, C. J. Murphy, J. J. de Pablo and N. L. Abbott, *Science*, 2011, **332**, 1297.

14 D. S. Miller, X. Wang, J. Buchen, O. D. Lavrentovich and N. L. Abbott, *Anal. Chem.*, 2013, **85**, 10296.

15 C. D. Ma, L. Adamiak, D. S. Miller, X. Wang, N.C. Gianneschi and N. L. Abbott, *Small*, 2015, **11**, 5747.

16 M. I. Kinsinger, M. E. Buck, N. L. Abbott and D. M. Lynn, *Langmuir*, 2010, **26**, 10234.

17 D. A. Paterson, P. Bao, R. H. Abou-Saleh, S. A. Peyman, J. C. Jones, J. A. T. Sandoe, S. D. Evans, H. F. Gleeson and R. J. Bushby, *Langmuir*, 2020, **36**, 6436.

18 C.-Y. Chang and C.-H. Chen, *Chem. Commun*., 2014, **50**, 12162.

19 A. Dan, S. Aery, S. Zhang, D. L. Baker, H. F. Gleeson and A. Sarkar, *Langmuir*, 2020, **36**, 10091.

20 X. Guo, U. Manna, N. L. Abbott and D. M. Lynn, *ACS Appl. Mater. Interfaces*, 2015, **7**, 26892.

21 J. Deng, W. Liang and J. Fang, *ACS Appl. Mater. Interfaces*, 2016, **8**, 3928.

22 U. Manna, Y. M. Zavala, N. L. Abbott and D. M. Lynn, *ACS Appl. Mater. Interfaces*, 2021, **13**, 42502.

23 K. Mukai, M. Hara, H. Yabu, S. Nagano and T. Seki, *Adv. Mater. Interfaces*, 2021, **8**, 2100891.

24 J. R. Carlton, Y. M. Zayas-Gonzalez, U. Manna, D. M. Lynn and N. L. Abbott, *Langmuir*, 2014, **30**, 14944.

25 M. Liu, S. Wang, Z. Wei, Y. Song and L. Jiang, *Adv. Mater*., 2009, **21**, 665.

26 J. Yong, F. Chen, Q. Yang, J. Huo and X. Hou, *Chem. Soc. Rev*., 2017, **46**, 4168.

27 K. Chen, S. Zhou and L. Wu, *ACS Nano*, 2016, **10**, 1386.

28 Y. Peng, Y. Ning, X. Ma, Y. Zhu, S. Yang, B. Su, K. Liu and L. Jiang, *Adv. Funct. Mater*., 2018, **28**, 1800712.

29 W. Chen, P. Zhang, R. Zang, J. Fan, S. Wang, B. Wang and J. Meng, *Adv. Mater*., 2020, **32**, 1907413.

30 C. N. R. Rao and R. Venkataraghavan, *Spectrochim. Acta*, 1962, **18**, 541.

31 D. Parbat and U. Manna, *Chem. Sci*., 2017, **8**, 6092.

32 D. Parbat and U. Manna, Chem. Sci., 2017, **8**, 6542.

33 J. K. Gupta, J. S. Zimmerman, J. J. de Pablo, F. Caruso and N. L. Abbott, *Langmuir*, 2009, **25**, 9016.

34 J. Huo, Q. Yang, F. Chen, J. Yong, Y. Fang, J. Zhang, L. Liu and X. Hou, *Langmuir*, 2017, **33**, 3659.

35 W. Weng, M. Tenjimbayashi, W. H. Hu and M. Naito, *Small*, 2022, **18**, 2200349.

36 M. Rahimia, T. F. Robertsa, J. C. Armas-Péreza, X. Wang, E. Bukusoglu, N. L. Abbott and J. J. de Pablo, *Proc. Natl. Acad. Sci. U. S. A*., 2015, **112**, 5297.

37 X. Wang, D. S. Miller, E. Bukusoglu, J. J. de Pablo and N. L. Abbott, *Nat. Mater*., 2016, **15**, 106.

38 M. Sadati, J. A. Martinez-Gonzalez, Y. Zhou, N. T. Qazvini, K. Kurtenbach, X. Li, E. Bukusoglu, R. Zhang, N. L. Abbott, J. P. Hernandez-Ortiz and J. J. de Pablo, *Sci. Adv*., 2020, **6**, eaba6728.

39 A. Concellon, C. A. Zentner and T. M. Swager, *J. Am. Chem. Soc*., 2019, **141**,18246.

40 M. Anyfantakis, V. S. R. Jampani, R. Kizhakidathazhath, B. P. Binks and J. P. F. Lagerwall, *Angew. Chem., Int. Ed.*, 2020, **59**, 19260.

Dually Reactive Multilayer Coatings Enable Orthogonal Manipulation of Underwater Superoleophobicity and Oil Adhesion *via* Post-Functionalization*

In this chapter I have demonstrated the design of a dual reactive multilayer coating, whose underwater superoleophobicity and oil adhesion can be independently tuned through the orthogonal functionalization of two types of reactive moieties at ambient conditions. Moreover, the cooperative assembly of amphiphiles on the modified underwater superoleophobic coating gives rise to a switchable oil adhesion while retaining the extreme oil-repellency (advancing oil contact angle >165°). Interestingly, the reversible change in the oil adhesion of the underwater superoleophobic coatings depends on the interplay between the molecular structure and concentration of the amphiphiles and the pH of the aqueous solution. Building on these findings, the superoleophobic chemical sensors were developed, which enabled the real-time and naked eye identification of (1) the charge of synthetic ionic surfactants and (2) the concentration of bile acids. Overall, the findings of this work provide design principles by which molecular self-assembly and oil adhesion can be coupled at underwater superoleophobic surfaces, which allows to rapidly sensed physiologically important amphiphiles and metabolites with the naked eye using the superoleophobic surfaces.

*A. Borbora, R. L. Dupont, Y. Xu, X. Wang and U. Manna, *Mater. Horiz.*, 2022, **9**, 991.

3.1. Introduction

Pioneering work done by Jiang *et al.*[1] has detailed the design of fish scale-mimicking hierarchical surface topography using water compatible polymeric hydrogels that achieved artificial, underwater non-adhesive superoleophobicity. Building on this work, several such artificial interfaces have been developed, primarily using polymeric hydrogels, electrostatic multilayers, and metal oxides.[2–14] Although these conventional underwater superoleophobic surfaces have found potential use in oil separation, the real-time monitoring of human respiration, and as anti-biofouling interfaces and efficient microfluidic devices,[15–23] their oil adhesion, and the consequent oil droplet mobility on these underwater superoleophobic surfaces (reflected as a change in the contact angle hysteresis (CAH) or the roll-off angle), cannot be tuned while retaining their underwater superoleophobicity (oil contact angle (OCA) > 150°).

To achieve tunable/switchable oil adhesion properties, responsive molecules or polymers, such as thermo-responsive polymers (*e.g.*, poly(*N*-isopropylacrylamide) (PNIPAM)), saline-responsive polymers (*e.g.*, poly(2-(succinyloxy)propyl methacrylate) (PSPMA)), and pH-responsive small molecules (*e.g.*, 11-mercaptoundecanoic acid), have been used to create or decorate nano/microscale topographical features (*e.g.*, nanowire arrays, micro-brushes, and micropillars).[24–28] While promising, these surfaces are only able to switch between a ground and stimulated oil adhesion state and lack the ability to finely tune the CAH and the consequent oil droplet mobility. Studies from the recent past demonstrated the design of multilayer coatings with a single type of reactive residual group and its further functionalization through a 1, 4-conjugate addition reaction to yield two extremes of underwater oil wettability: superoleophilicity (OCA ~ 0°) and non-adhesive superoleophobicity (OCA > 150° and CAH < 10°).[29] An independent control over the underwater superoleophobicity and oil adhesion through the functionalization of these mono-reactive multilayer coatings, however, cannot be achieved.

In this chapter, I designed a dual chemically reactive multilayer coating containing two reactive moieties, acrylate and amine, which can be orthogonally modified with a rich palette of chemicals to independently tune the OCA and CAH of oil droplets on an underwater surface (Figure 3.1A, B). Specifically, acrylate moieties can be modified with primary amines containing hydrophilic molecules through a 1, 4-conjugate addition reaction to achieve underwater superoleophobicity (OCA > 150°). The functionalization of the other residual

moiety, amine, with small, hydrophobic acrylates with different hydrocarbon tail lengths allowed for control over the oil adhesion, with a CAH ranging from ~ 20° to ~ 40°, without affecting the underwater superoleophobicity (OCA > 150°), whereas the functionalization with small, hydrophilic acrylates resulted in an unperturbed oil-wettability (Scheme 3.1B). Furthermore, the non-covalent, cooperative assembly of amphiphiles (*e.g.*, ionic or facial surfactants) on the appropriate chemically modified underwater superoleophobic coatings

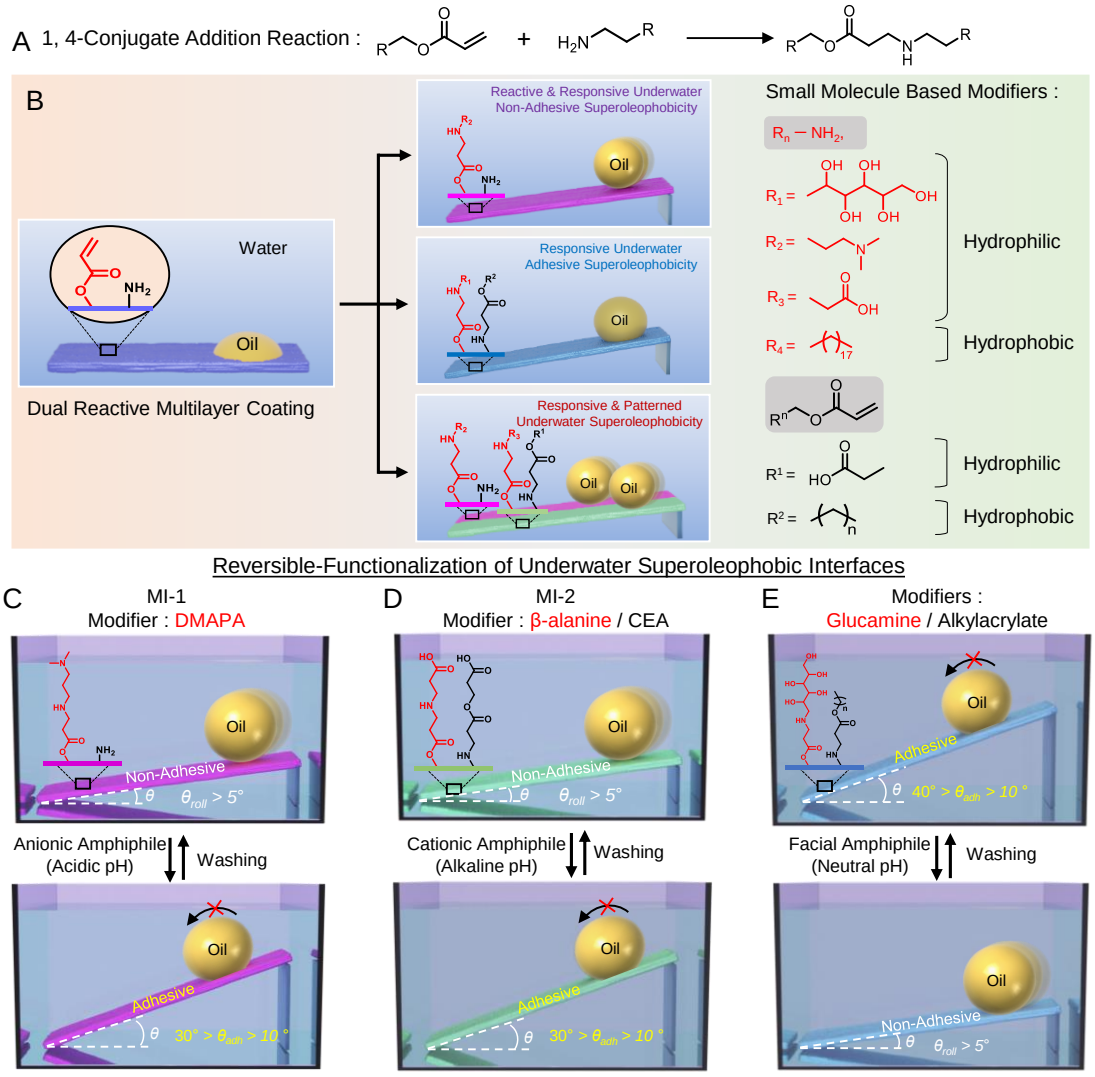

Figure 3.1. (A) The 1, 4-conjugate addition reaction between amine and acrylate. (B) Schematic depiction of a dually reactive multilayer coating, composed of residual acrylate and amine moieties that allow for an orthogonal functionalization to develop reactive, responsive, and patterned adhesive/non-adhesive underwater superoleophobicity underwater. The chemical structures of selected small-molecule based modifiers are provided in the right. (C−E) Schematic illustration of the non-covalent, cooperative assembly of (C) anionic surfactants modified interface-1 (MI-1) in an acidic solution, (D) cationic surfactants on modified interface-2 (MI-2) in an alkaline solution, and (E) facial amphiphiles on glucamine/alkyl amine-modified coatings at a neutral pH, to reversible switch the oil adhesion.

gives rise to a switchable underwater oil-adhesion with a precisely tunable CAH ranging from ~ 5° to ~ 30° (Scheme 3.1C–E). Importantly, the synergistic effect between the chemical modification, the pH of the aqueous phase, and the cooperative assembly of amphiphiles on the oil adhesion of the coatings enables the detection of synthetic surfactants with different charges and physiologically important metabolites (*i.e.*, bile acids) with the naked eye. Overall, these results demonstrate that the dually reactive multilayer coatings provide new principles for designing remarkably responsive superoleophobic surfaces for chemical sensing, catalysis, and no-loss liquid transport.

3.2. Experimental Section

3.2.1. Materials Required

2-carboxyethyl acrylate (CEA), octyl acrylate, decyl acrylate, 2-(dimethylamino)ethyl acrylate (DMAEA), 2-hydroxyethyl acrylate (HEA), hexylamine, sodium tetradecyl sulfate (STS), decyltrimethylammonium bromide (C_{10}TAB), dodecyltrimethylammonium bromide (DTAB), hexadecyltrimethylammonium bromide (C_{16}TAB), cholic acid, L-ascorbic acid and bovine serum albumin (BSA) were purchased from Sigma Aldrich, Bangalore, India. Nile red, β-alanine, sodium decyl sulfate (SDeS), and uric acid were acquired from TCI chemicals (India) Pvt. Ltd. Dichloroethane (DCE) was acquired from Loba Chemie Pvt. Ltd., India. Dichloromethane, chloroform, ethyl acetate, and toluene were purchased from FINAR. n-Heptane were purchased from Alfa-Aesar. Sodium chloride (NaCl), magnesium chloride ($MgCl_2$), calcium chloride ($CaCl_2$), magnesium sulphate ($MgSO_4$), sodium hydroxide (NaOH), di-sodium hydrogen phosphate dihydrate ($Na_2HPO_4{\cdot}2H_2O$), sodium phosphate monobasic monohydrate ($NaH_2PO_4.H_2O$), and dimethyl sulfoxide (DMSO) were obtained from Merck Life Science Pvt. Ltd, Mumbai. Hydrochloric acid (HCl) was purchased from Fischer Scientific, India. PBS buffer was prepared by mixing $Na_2HPO_4{\cdot}2H_2O$ and $NaH_2PO_4{\cdot}H_2O$ following the standard sodium phosphate buffer preparation protocol. Microscopic glass slide was purchased from Jain Scientific Glass Works, India. River water was arranged from the Brahmaputra River, Guwahati, Assam, India. The details of all other materials and chemicals used in this work were discussed previously in section 2.2.1 of chapter 2.

3.2.2. Characterization

The instruments used in this chapter for characterization of synthesized materials were same as discussed previously in section 2.2.2 of chapter 2.

3.2.3. Preparation of Dual-Reactive Multilayer Coating

A dual reactive multilayer coating of branched polyethyleneimine (BPEI) and chemically reactive nanocomplex (CRNC) were prepared on microscopic glass slides (7.5 cm × 1.0 cm) following a layer-by-layer (LbL) deposition process discussed in the section 2.2.3 of chapter 2. The deposition cycle was repeated 20 times to fabricate a porous polymeric coating of 20 BPEI/CRNC bilayers. To form a smooth multilayer coating, a similar LbL deposition process was adopted to prepare 5 bilayers of BPEI/dipentaerythritol pentaacrylate (5Acl).

3.2.4. Post-Modification of Multilayer Coatings Using Amine and Acrylate

The residual acrylates of the multilayers were post-modified with hydrophilic amines, including, 3-(dimethylamino)-1-propylamine (DMAPA, 25 μL mL^{-1} in ethanol), β-alanine (5 mg mL^{-1} in water), and glucamine (2.5 mg mL^{-1} in DMSO) by exposing the multilayer coatings in the respective solutions overnight at ambient conditions, and then washed with ethanol and dryed in air. For further modification of the residual amine groups of the mono-functionalized multilayers, the multilayer coating was exposed to an ethanol solution consisting of a hydrophilic acrylate, CEA (25 μL mL^{-1}), or hydrophobic alkyl acrylates, butyl acrylate (25 μL mL^{-1}), hexyl acrylate (25 μL mL^{-1}), octyl acrylate (25 μL mL^{-1}), decyl acrylate (25 μL mL^{-1}), lauryl acrylate (25 μL mL^{-1}) or octadecyl acrylate (25 μL mL^{-1}), overnight at ambient conditions and then washed with ethanol and dried in air.

3.2.5. Fabrication of Patterned Underwater Superoleophobic Surfaces

To prepare the patterned underwater superoleophobic surfaces, half of the multilayer on the glass substrate (7.5 cm × 2.5 cm) was treated with an ethanol solution of DMAPA (25 μL mL^{-1}) using a paintbrush, followed by rinsing with ethanol and air drying. Next, the other half of the multilayer coating was modified with β-alanine (5 mg mL^{-1} in water) and CEA (25 μL mL^{-1} in ethanol), followed by washing with ethanol drying in air.

3.2.6. Non-covalent, Reversible Modifications of Multilayer Coatings with Ionic Surfactants and Bile Acid

The superoleophobic interfaces modified with DMAPA and with β-alanine/CEA were immersed in aqueous solutions of ionic surfactants (either cationic or anionic). The oil adhesion behaviors were measured by monitoring the change in the CAH of a beaded oil (DCE, 5 μL) droplet, underwater. The concentration of the ionic surfactants was varied between 0 μM and 600 μM, and the pH of the prepared solutions was adjusted using either HCl or NaOH. To

detect cholic acid, the glucamine/alkyl acrylate-modified multilayer coatings were immersed in the cholic acid solution prepared in sodium phosphate buffer solution with a pH of 7. The change in the roll-off angle and the CAH of a beaded oil (DCE, 5 μL) droplet on the coatings was measured as a function of cholic acid concentration.

3.2.7. Chemical, Thermal, and Physical Stability of the Underwater Superoleophobic Properties

The durability of underwater oil wettability in the functionalized multilayer coatings was tested using various forms of physical abrasions, extreme temperatures, and chemically contaminated aqueous phases. Details on the stability studies have been described in the section below.

3.2.7.1. Chemical and Thermal Stability:

The multilayer coatings, which were post-functionalized with appropriate molecules, were immersed in different harsh and chemically complex conditions, including alkaline solution (0.1M NH_3; pH 11), acidic solution (0.1M HCl; pH 1), sodium dodecyl sulfate (SDS, 1mM) solution, DTAB solution (1mM), 5% BSA solution, and artificial seawater for a prolonged 10 days. The artificial seawater was prepared by mixing $MgCl_2$ (0.226 g), $MgSO_4$ (0.325 g), NaCl (2.673 g) and $CaCl_2$ (0.112 g) in 100 ml of deionized water. The underwater oil wettability in the respective materials was examined visually, and the contact angle was measured after exposure to one of the mentioned chemically harsh media for 10 days. To investigate the thermal stability of the modified coatings, the coatings were subjected to -5 °C and 90 °C for 10 days, and the underwater oil wettability was examined with contact angle measurements.

3.2.7.2. Physical Durability:

a. Sand Drop Test: The modified interfaces were placed on a ~ 45° tilted surface using an adhesive tape in air, and a continuous stream of sand grains (50 g) was poured from a height of 20 cm using a funnel. The underwater anti-oil-wetting properties of the material were examined by taking contact angle measurements and digital images before and after performing the sand drop test.

b. Adhesive Tape Peeling Test: One adhesive surface of a double-sided adhesive tape was adhered to the multilayer coating on glass microscope slides. A 100 g load was placed on the system to further facilitate a uniform contact of the polymeric coating against the adhesive surface. After 15 minutes, the adhesive tape was manually peeled off from the polymeric

multilayer coated glass slides, and the underwater oil wetting properties of the coatings were investigated in detail.

c. Finger Rubbing Test: The modified interfaces were rubbed with a finger back and forth 20 times, and then underwater oil wettability was investigated in detail.

3.3. Results and Discussion

3.3.1. Design of Dually Reactive Multilayer Coatings

In this chapter, a simple chemical approach is introduced, where a multilayer coating consisting of two types of residual functional groups─ acrylate and amine, can be selectively functionalized to independently tune the oil wettability (OCA) and oil adhesion (CAH) of the multilayer coating. Specifically, 20 bilayers coating of CRNC and BPEI were prepared on a glass substrate by adopting a covalent LbL deposition process following the method described in the previous chapter.[29,30] Both field emission scanning electron microscope (FESEM) and atomic force microscope (AFM) imaging confirmed that a porous surface topography of randomly aggregated granular domains with a root mean square roughness of ~389 nm was created (Figure 3.2A and B). Notably, this high surface roughness and porous topography are essential to firmly confine the aqueous phase for conferring underwater super-oil-wettability.

3.3.2. Covalent Modification of Dually Reactive Multilayer Coatings

In the next set of experiments, I sought to explore the possibility of tuning the underwater oleophobicity (*i.e.*, OCA and CAH) *via* an orthogonal modification of the residual acrylate and

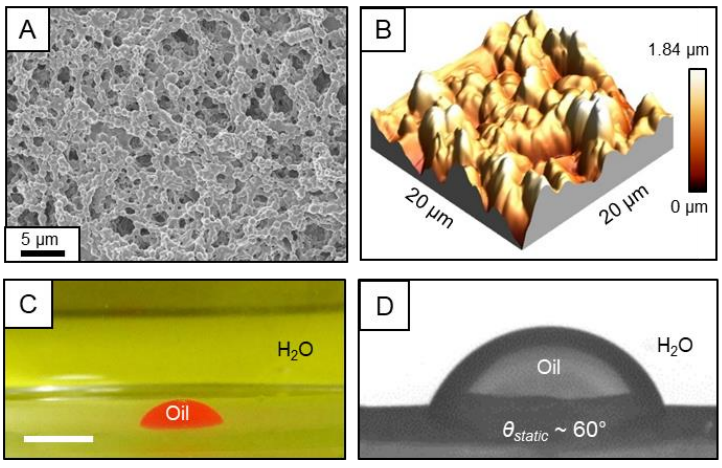

Figure 3.2. (A) Representative field emission scanning electron microscope (FESEM) and (B) atomic force microscopy (AFM) micrographs of 20 bilayer coatings. (C) Representative photograph and (D) contact angle goniometer image of the oil droplet (dicholorethane (DCE), red-dyed) on the unmodified multilayer coating underwater. Scale bar, 5 mm.

amine groups at ambient conditions. The unmodified multilayer coatings inherently displayed an underwater oleophilicity, indicated by the beading of a droplet of DCE (a model oil phase) on the coating with an OCA of ~ 60°, as shown in Figure 3.2C and D. First, the chemical modification of one of the types of residual groups was performed to explore their effect on the oleophobicity of the coating. When the acrylate groups were modified with primary amine-containing hydrophilic molecules (*e.g.*, DMAPA, β-alanine, or glucamine), the amine-functionalized coating exhibited an underwater superoleophobicity to beaded DCE droplets with an advancing OCA >165° and a CAH < 5°, as shown in Figure 3.3A. In contrast, when the amine groups of the coating were functionalized with CEA, the modified coating exhibited an oil-adhesive underwater superoleophobicity with an advancing OCA of ~161° and a CAH of ~ 30°. The modification of same coating using other acrylates, such as DMAEA and HEA, leading to a decrease in the OCA, as depicted in Figure 3.3A. This difference in the oil wettability of the coating functionalized with acrylates could be attributed to the different

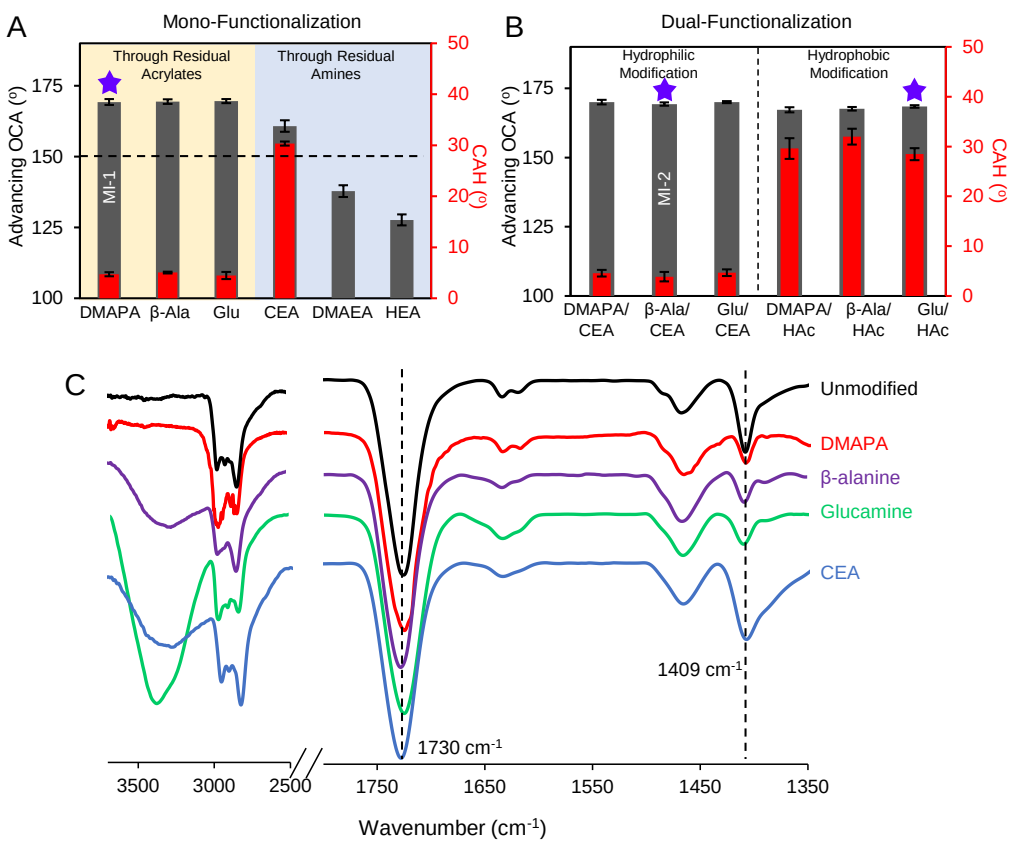

Figure 3.3. Effect of (A) mono-functionalization and (B) dual-functionalization on the advancing oil contact angle (OCA) and contact angle hysteresis (CAH) of beaded oil droplets on the multilayer coating. The purple star indicates the appropriate modifications for demonstrating the sensing performance. (C) Attenuated total reflection-Fourier transform infrared (ATR-FTIR) spectra of the multilayer coatings before and after chemical modifications with selected modifiers.

hydrophilic groups of the used acrylate molecules. The above independent modification of acrylate and amine groups was confirmed using Attenuated total reflection-Fourier transform infrared (ATR-FTIR) spectral analysis (Figure 3.3C). Specifically, the prominent existence of characteristic IR signatures for the C–H of vinyl and carbonyl stretching at 1409 cm^{-1} and 1730 cm^{-1}, respectively, confirmed the presence of residual acrylate groups in the coatings (Figure 3.3C (black)). The modification of the acrylate groups with primary amines caused a depletion of the characteristic C–H signal at 1409 cm^{-1} when compared to the carbonyl stretching at 1730 cm^{-1}; and the functionalization of amine groups with CEA generates a broad IR peak in the region between 3000 cm^{-1} and 3600 cm^{-1}, corresponding to the OH stretching of carboxylic acid groups. Overall, these results led us to conclude that the covalent functionalization of acrylate groups with hydrophilic amines can lead to a non-oil-adhesive superoleophobicity, whereas modification of amine groups with hydrophilic acrylates gave rise to an oil-adhesive superoleophobicity. It is noteworthy that after modifying a single type of residual group of the

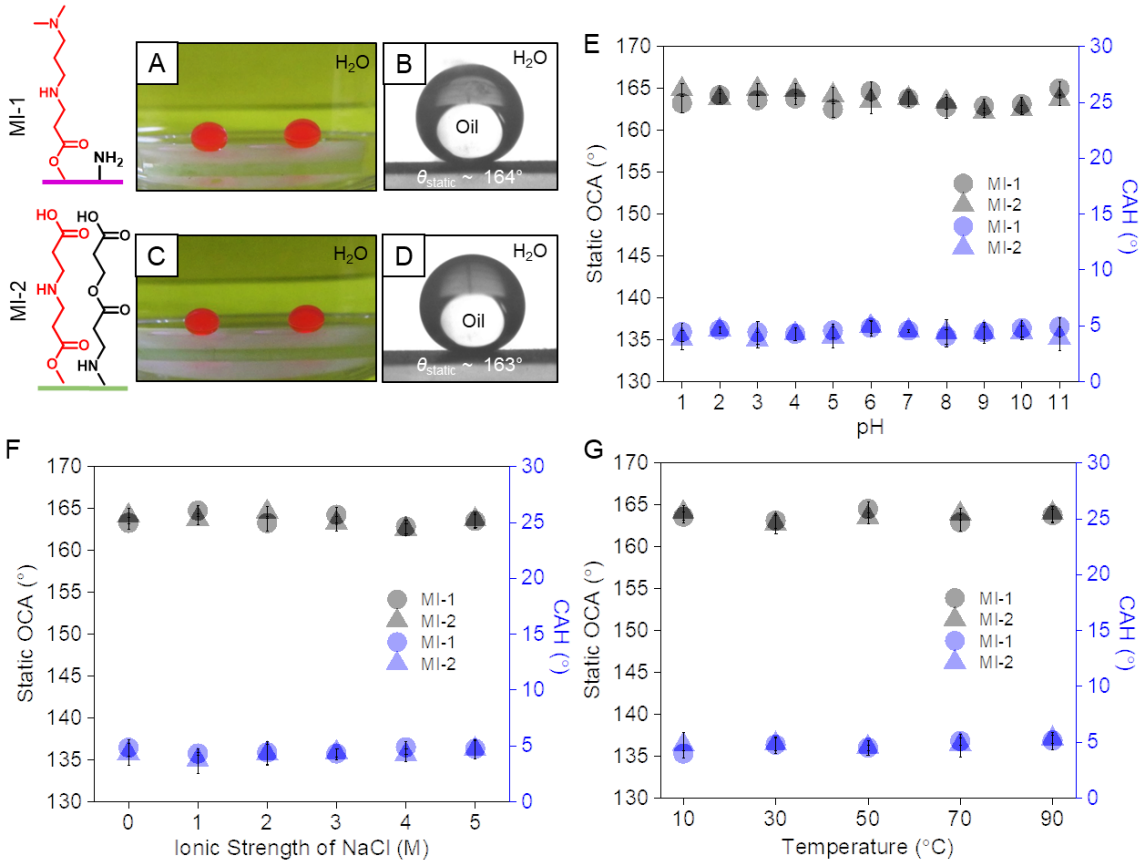

Figure 3.4. (A–D) Photographs (A, C) and contact angle goniometer images (B, D) of the beaded oil droplets on MI-1 (A–B) and MI-2 (C–D) multilayer coatings. (E–G) Static OCA and CAH of beaded oil droplets on MI-1 and MI-2 as a function of (E) pH, (F) NaCl concentration, and (G) temperature. Oil droplet volume was 5 μL.

coating, the multilayer coating possessed the other reactive residual that allowed subsequent functionalization.

Next, the effect of the functionalization of the other reactive residual on the underwater oil wettability of the coating was studied. First, a hydrophilic acrylate, CEA, was used to functionalize the residual amine groups of the mono-functionalized (DMAPA, β-alanine, or glucamine)-multilayer coatings, which initially exhibited a non-oil-adhesive superoleophobicity. After modification with CEA, the resultant dual-modified coatings retained their non-adhesive superoleophobicity, as shown in Figure 3.3B. Second, a hydrophobic hexyl acrylate (HAc) was used to functionalize the residual amine group of the mono-functionalized multilayer coatings. In contrast to the hydrophilic acrylate

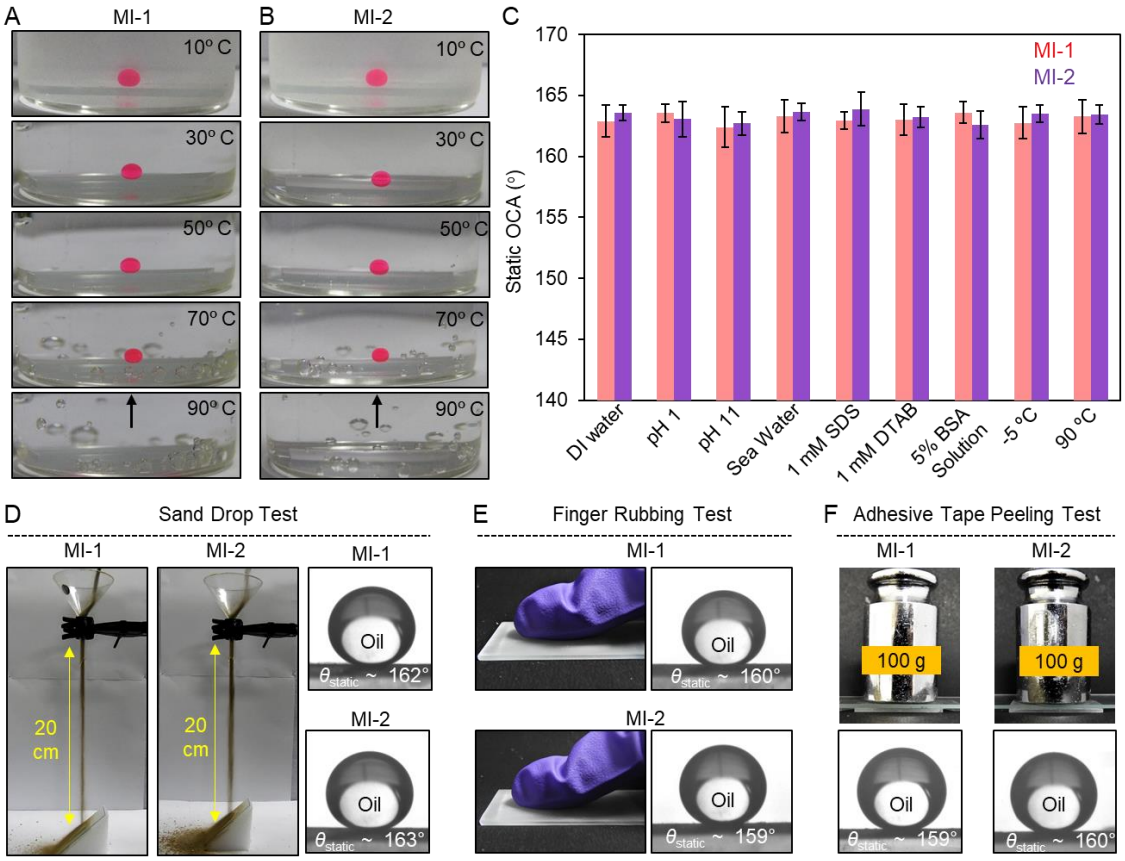

Figure 3.5. (A, B) Photographs of oil droplets on the underwater superoleophobic (A) MI-1 and (B) MI-2 at different temperatures. The oil (DCE) droplets remained spherical due to the extreme oil repellence of the underwater superoleophobic multilayers before the complete evaporation of the oil droplet at high temperatures. (C) Graph represents the static OCA on the MI-1 and MI-2 after exposing the coatings to various chemically contaminated aqueous phases and temperatures (-5°C and 90°C). (D−F) Digital images demonstrate sand drop test, finger rubbing test and adhesive tape test performed on MI-1 and MI-2, and sequential contact angle goniometer images show beaded oil droplets on MI-1 and MI-2 underwater, after carrying out the mentioned tests.

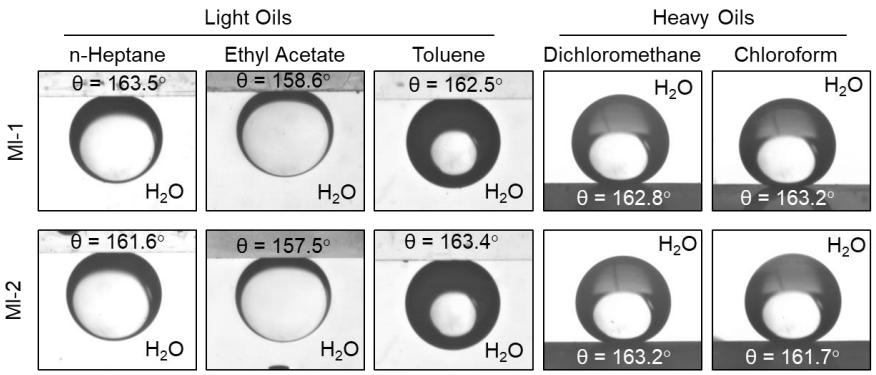

Figure 3.6. Beaded droplets of various water-immiscible organic phases remained extremely repellent on both the MI-1 and MI-2 surfaces.

functionalization, hexyl acrylate modification converted the mono-functionalized coatings from non-adhesive to oil adhesive (CAH > 28°) while the OCA remained above 160°, as shown in Figure 3.3B. This increase in the CAH after the hexyl acrylate functionalization may result from the enhanced contact between the beaded oil droplet and the coating caused by the hydrophobic tail of the hexyl acrylate. These results revealed that the orthogonal functionalization of the residual acrylate and amine groups provides a novel method to independently tune the OCA and CAH of the multilayer coating. The selection of other appropriate acrylate-based hydrophobic small molecules allowed for the controllable tuning of the underwater oil adhesion, which will be discussed in detail later.

3.3.3. Reversible Modification of Underwater Non-Adhesive Superoleophobic Coatings *via* Cooperative Assembly of Amphiphiles

In the next set of experiments, two different types of underwater superoleophobic coatings: (1) a mono-functionalized (modified with DMAPA) coating, denoted as modified interface-1 (MI-1, Figure 3.4A, B) and (2) a dual-functionalized coating (modified with both β-alanine and CEA), labeled as modified interface-2 (MI-2, Figure 3.4C, D), were rationally selected to reversibly switch between oil adhesive and non-adhesive behaviors through the cooperative assembly of surfactants on the modified interfaces. Both MI-1 and MI-2 exhibited non-adhesive underwater superoleophobicity, with a static OCA > 160° and a CAH < 5°, over a wide range of pH (from 1 to 11, Figure 3.4E), ionic strength (from 0 to 5 M NaCl, Figure 3.4F,), and temperature (from 10 °C to 90 °C, Figure 3.4G and 3.5A). Moreover, the coatings were exposed to various thermally/chemically harsh conditions for a prolonged duration (10 days, Figure 3.5C) and physical challenges, including sand drop test (Figure 3.5D), finger rubbing test (Figure 3.5E) and adhesive tape peeling test (Figure 3.5F); however, the underwater

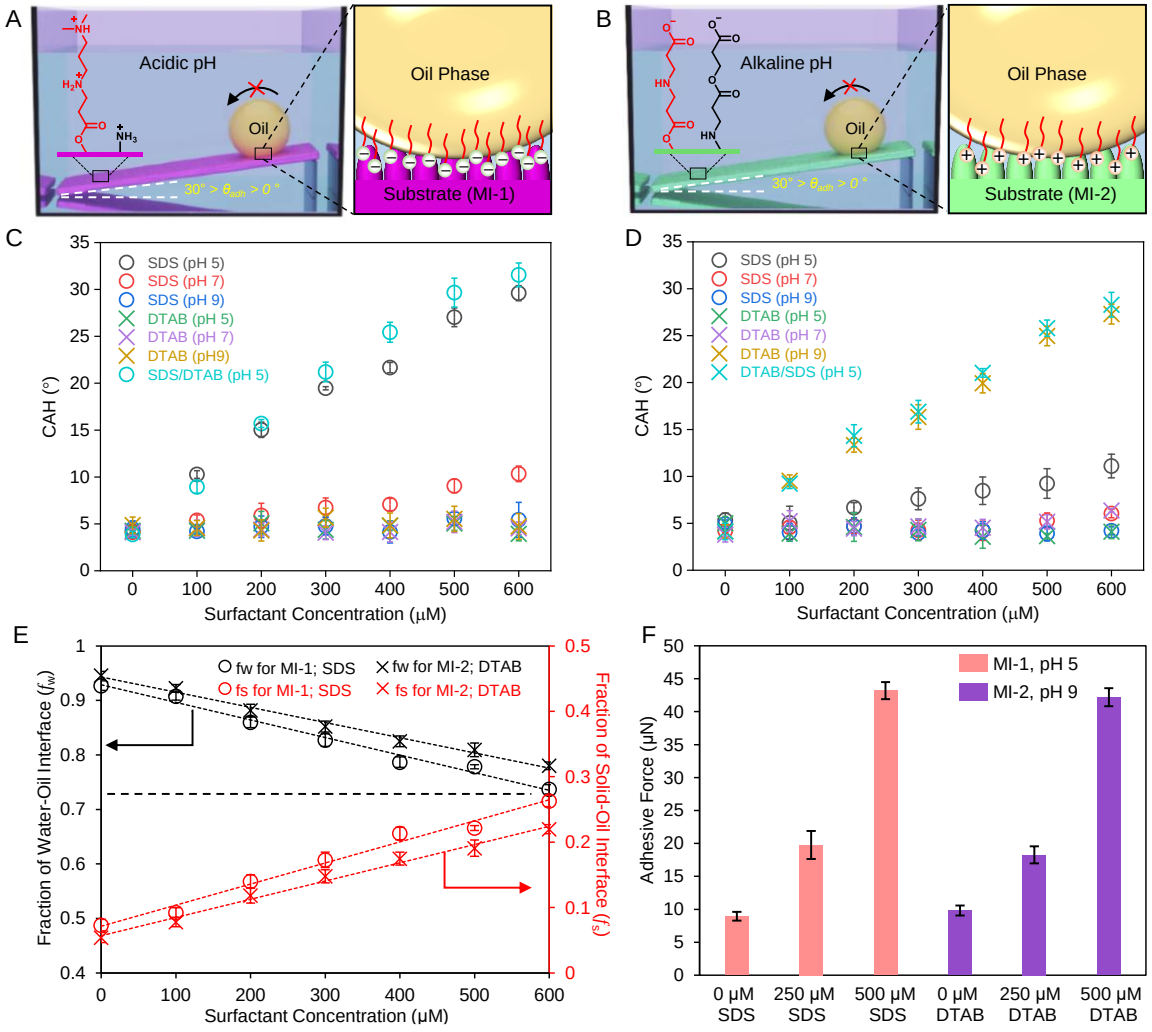

Figure 3.7. (A, B) Schematic illustration of the cooperative assembly of (A) anionic surfactants on MI-1 in acidic solution and (B) cationic surfactants on MI-2 in alkaline solution, resulting in an enhancement in the contact between the beaded oil droplet and the surfactant-decorated multilayer coating. (C, D) Effect of surfactant type and concentration on the CAH of oil droplets on (C) MI-1 and (D) MI-2 at different pH values. (E) Calculation of the fraction of contact area of the water-oil interface (f_w; black) and solid-oil interface (f_s; red) of the oil droplets on modified superoleophobic coatings as a function of surfactants (SDS: circle; DTAB: cross) concentration. (F) Underwater oil adhesive forces on modified superoleophobic coatings as a function of surfactant concentration. Oil droplet volume was 5 μL.

superoleophobic property remained unperturbed. Further, an extreme underwater oil-wettability with an OCA ~ 160° was noted for beaded droplets of other model oils—including *n*-heptane, ethyl acetate, toluene, dichloromethane, and chloroform, as shown in Figure 3.6.

Next, the ability for cooperative assembly of surfactants on the modified coatings at different pH was studied. Upon the addition of an anionic surfactant, SDS, to the aqueous solution, the MI-1 surface exhibited an oil adhesive superoleophobicity with an advancing OCA > 160° in

an acidic condition (pH = 5; Figure 3.7A), and the CAH of a beaded oil droplet (5 μL) adopted a linear increase from 4.2 ± 0.2° to 29.6 ± 0.8° with an increase in the concentration of SDS from 0 μM to 600 μM, as shown in Figure 3.7C (black circles). In contrast, in neutral and alkaline conditions (pH = 9), no measurable change in the CAH was observed over a wide range of SDS concentrations, as shown in Figure 3.7C. Therefore, this SDS concentration-dependent CAH at pH = 5 can be attributed to the electrostatic attraction between the anionic head groups of SDS and the protonated amine moieties of the MI-1 surface, which resulted in an enhancement of the physical contact between the beaded oil droplet and the exposed hydrocarbon tail of the assembled SDS on the MI-1 surface. In contrast, the addition of a cationic surfactant, DTAB, which possesses the same hydrocarbon tail but a cationic head group, did not alter the CAH of the MI-1 surface in acidic pH condition due to the electrostatic repulsion between DTAB and the amine moieties of the MI-1 surface and same trend was noted for other pH as well, as shown in Figure 3.7C.

To provide insight, the fraction of the contact area between the beaded oil droplet and the porous and modified multilayer coating was calculated using the following Cassie–Baxter equations:[1,31]

$$\cos\theta_{CB} = f_s \cos\theta - f_w \quad (1)$$

$$f_s + f_w = 1 \quad (2)$$

where θ_{CB} and θ are the static contact angles of a beaded oil droplet on the porous multilayer coating and a respective smooth coating (5 bilayers of BPEI/5Acl), respectively, both of which were modified with identical chemicals. f_s and f_w denote the fraction of contact area between the coating and the oil droplet, and the fraction of contact area between the coating and the aqueous phase trapped in the pores of the multilayer coating, respectively. In the absence of SDS, the f_s of MI-1 was estimated to be 0.073, which gives rise to an oil non-adhesive superoleophobicity. However, f_s increased (red circles in Figure 3.7E) with an increase in the concentration of SDS in acidic conditions and reached a value of 0.26 at an SDS concentration of 600 μM, as shown in Figure 3.7E. This calculation supports the hypothesis that hydrocarbon tails of the SDS adsorbed at the MI-1 surface promote the interaction between the MI-1 surface and the oil droplet, giving rise to an increase in the oil adhesion from 8.9 ± 0.7 μN to 43.1 ± 1.3 μN, a characteristic behavior of an underwater oil-adhesive superoleophobicity, as shown in Figure 3.7F (red bar).

Similarly, the dissociation of the carboxylic acid groups of the MI-2 surface in alkaline conditions can trigger a cooperative assembly of cationic surfactants at the surface, resulting in a change in the CAH of the surface (Figure 3.7B). In the absence of DTAB, or in an aqueous solution of DTAB in neutral and acidic pH conditions, the MI-2 surface retained its intrinsic non-adhesive underwater superoleophobicity with an advancing OCA > 165° and a CAH < 5°. In the presence of DTAB in alkaline conditions (pH = 9), the MI-2 surface adopted an oil-adhesive underwater superoleophobicity, where concentration of DTAB modulated CAH and adhesive force, as shown in Figure 3.7D. The f_s was calculated to increase with an increase in the concentration of DTAB (Figure 3.7E), and the oil-adhesion force of MI-2 increased from 9.8 ± 0.8 μN to 42.1 ± 1.4 μN (Figure 3.7F, purple bar)) in alkaline conditions. In contrast, SDS caused no measurable change to the oil adhesion behavior of MI-2, and the addition of an adequate amount of DTAB to an aqueous solution of SDS in alkaline conditions (pH of 9) allowed for control over the CAH in the underwater superoleophobic coating (Figure 3.7D). However, the addition of a non-ionic surfactant (Triton-X 114, 100 μM to 600 μM) that does not possess any ionic head groups failed to alter the CAH on both MI-1 and MI-2 irrespective of the pH of the aqueous phase (acidic, neutral, or alkaline), as shown in Figure 3.8. Furthermore, both MI-1 and MI-2 can be switched between non-adhesive and adhesive states by reversibly varying the pH of the aqueous solution consisting of the ionic surfactants, as shown in Figure 3.9A and B. These results elucidate the effect of a charged head group on the oil adhesion of the appropriately modified multilayer coatings. Notably, the critical association concentration (CAC) for the cooperative assembly of ionic surfactants at the surface of the multilayer coatings (100 μM for SDS and 80 μM for DTAB) are lower than the critical micelle concentration (CMC) of surfactants in a bulk aqueous phase (8.2 mM for SDS and 14 mM for DTAB).[32] It is well established that the micellization of ionic surfactants is mainly driven by

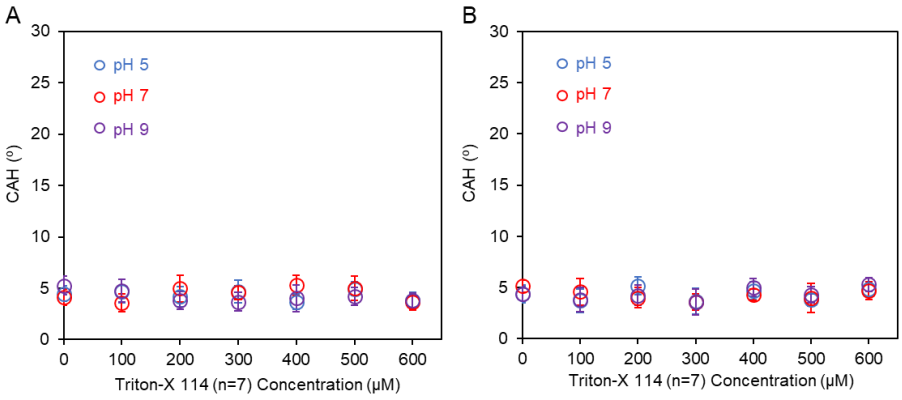

Figure 3.8. (A, B) Underwater CAH of the beaded oil droplets on (A) MI-1 and (B) MI-2 as a function of Triton-X 114 concentration at pH of 5, 7, and 9. Oil droplet volume was 5 μL.

the hydrophobic effect, which refers to the increase in the entropy of the water molecules surrounding the hydrocarbon chains of the surfactants. To provide fundamental insights into the driving mechanism of the cooperative assembly of surfactants at the multilayer reactive coatings, the change in the standard free energy accompanying the transfer of one SDS molecule from a singly-dispersed state in the bulk aqueous phase to the assembled state at the MI-1 surface at pH = 5 was calculated using the following equation:

$$\Delta G_1^{o} = k_B T \ln \text{CAC} \quad (3)$$

where k_B is the Boltzmann constant, T is the temperature, and CAC is the critical association concentration above which SDS assembles at the MI-1 surface. ΔG_1^{o} is calculated to be 13.23 $k_B T$. Furthermore, the effect of the hydrocarbon tail length of used surfactants on the oil-adhesion behaviour was investigated by using cationic surfactants with different tail lengths,

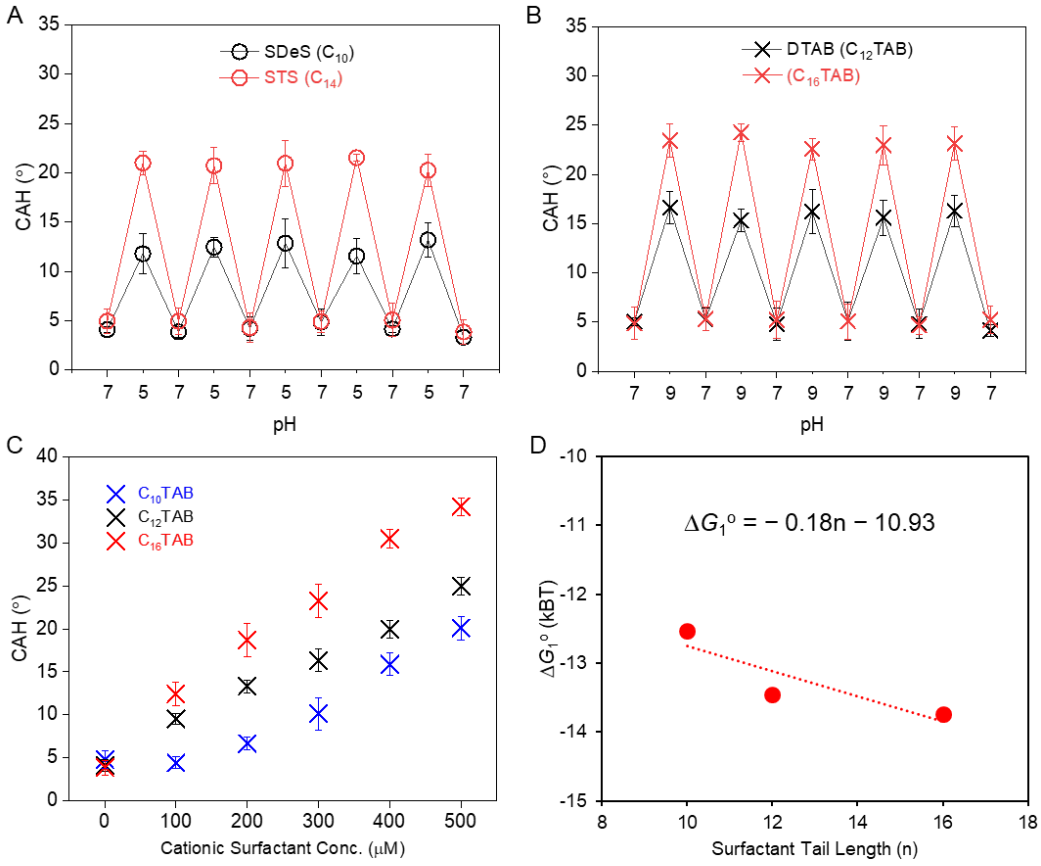

Figure 3.9. (A, B) Reversible manipulation of the CAH on (A) MI-1, and (B) MI-2 in aqueous solutions of surfactants by switching the pH. The concentration of surfactant was 300 μM. (C) Effect of the hydrocarbon tail length of cationic surfactants on the CAH of oil droplets on MI-2 at pH = 9. The volume of the oil droplets was 5 μL. (D) Plot showing standard free energy accompanying the transfer of one surfactant molecule from a singly-dispersed state in the bulk aqueous phase to the assembled state (ΔG_1^{o}) as a function of the hydrocarbon tail length (n) of the cationic surfactant molecules.

C_{10}TAB, DTAB/C_{12}TAB, and C_{16}TAB. In alkaline conditions (pH of 9), the CAH of MI-2 increases as the tail length of the cationic surfactant increases at a constant surfactant concentration, as shown in Figure 3.9C. Next the ΔG_1^{o} was calculated as a function of the cationic surfactant tail length using experimentally determined values of the CAC and was observed to exhibit a linear relationship. Specifically, the slope of the plot reveals that the driving forces for the cooperative assembly of the surfactant at the surface increased by 0.18 k_BT per methylene unit of the aliphatic tail (the contribution of the hydrophobic effect) (Figure 3.9D). The intercepts of the best-fit lines for the cationic surfactants with different tail lengths reveal that the electrostatic attraction between the head groups of the surfactants and the charged moieties of the coating is estimated to be −10.93 k_BT, which accounts for ~ 80% of the standard free energy of the cooperative self-association. These thermodynamic analyses reveal that the cooperative self- assembly of ionic surfactants on the coating is mainly driven by electrostatic interactions.

3.3.4. Patterned Underwater Superoleophobicity for Identifying the Ionic Type of Surfactants

Building on the above observations, it is believed that the mobility of oil droplets on the modified multilayer coatings can be used to determine the molecular structure of ionic surfactants in specific conditions (either acidic or alkaline). To test this hypothesis, a patterned superoleophobic surface was designed, where one half was modified with DMAPA (MI-1), and the other half was modified with β-alanine and CEA (MI-2) (Figure 3.10A), for the determination of the ionic type of surfactants with the naked eye. As expected, the two

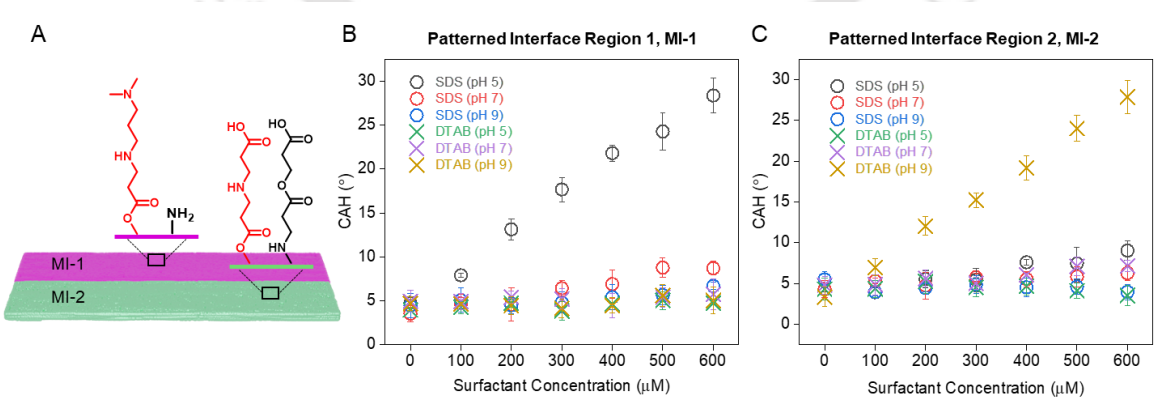

Figure 3.10. (A) Schematic illustration of a patterned superoleophobic coating with MI-1 (one half) and the MI-2 (another half). (B, C) CAH of oil droplets on the (B) MI-1 portion and (C) MI-2 portion of the patterned superoleophobic coating as a function of surfactant concentration at different pH values. Oil droplet volume was 5 μL.

distinctly modified portions of the patterned surface displayed a contrast in the underwater oil-adhesion depending on the ionic type (cationic or anionic) of the surfactants in acidic and alkaline conditions (Figure 3.10B and C).

As a proof of concept demonstration, the patterned surface was separately exposed to SDS in acidic conditions and DTAB in alkaline conditions with a tilting angle of 10°. Droplets (5 µL) of DCE were then placed on both parts of the patterned surface. First, in the presence of a 250

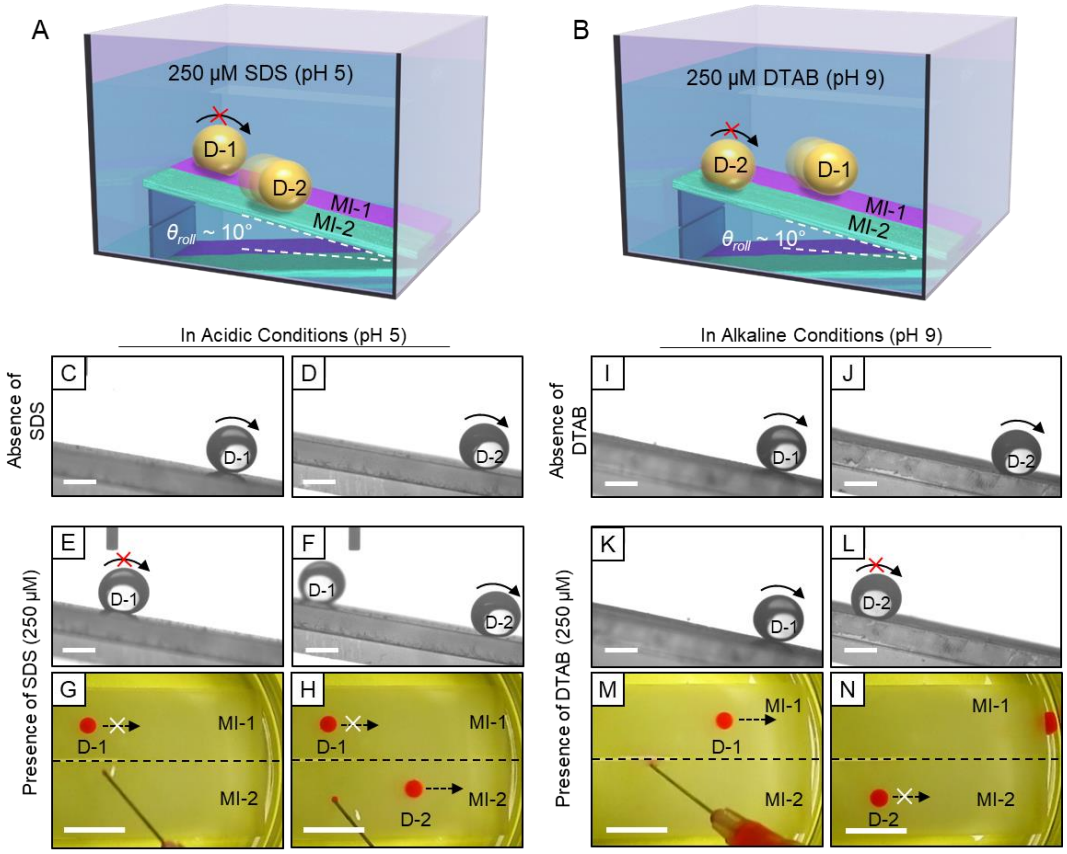

Figure 3.11. (A, B) Schematic illustration of oil droplet mobility on the patterned MI-1 and MI-2 superoleophobic coating, in presence of different surfactants at acidic and alkaline conditions. (C, D) Contact angle goniometer images showing the rolling of oil droplets on (C) MI-1 region and (D) MI-2 region of a tilted, patterned superoleophobic coating in an acidic solution (pH = 5) without surfactants. (E, F) Contact angle goniometer images and (G, H) photographs showing oil droplet mobility on MI-1 and MI-2 regions of a tilted, patterned superoleophobic coating in an acidic solution (pH = 5) of 250 µM SDS. (I, J) Contact angle goniometer images showing the rolling of oil droplets on (I) MI-1 and (J) MI-2 regions of a tilted, patterned superoleophobic coating in an alkaline solution (pH = 9) without surfactants. (K, L) Contact angle goniometer images and (M, N) photographs showing oil droplet mobility on MI-1 and MI-2 regions of a tilted, patterned superoleophobic coating in an alkaline solution (pH = 9) of 250 µM DTAB. The tilting angle of the surface was 10°. The volume of the oil droplets was 5 µL. Scale bars, 1 mm for C–F and I–L, and 1 cm for G–H and M–N.

μM SDS aqueous solution in acidic conditions (pH = 5), the beaded DCE droplet was pinned on the MI-1 part but instantly rolled off on the MI-2 part, as shown in Figure 3.11E−H. Second, in the presence of a 250 μM DTAB aqueous solution in alkaline conditions (pH of 9), the opposite behaviors of the beaded DCE droplets were observed on the same patterned interface; the DCE droplets rolled off on the MI-1 part and remained pinned on the MI-2 part, as shown in Figure 3.11K−N. In addition, when neither surfactant was present, the DCE droplets rolled off on both parts of the patterned surface in both acidic (Figure 3.11C and D) and alkaline (Figure 3.11I and J) conditions. These observations demonstrate that multilayer coatings with patterned superoleophobicities can enable the determination of ionic surfactants based on the ionic type-dependent oil droplet mobility in specific pH conditions. Considering the fact that both cationic and anionic surfactants have been widely used in various industrial applications, such as corrosion prevention and mineral flotation and as emulsifiers, antistatic agents, and dispersants,[33–35] and that cationic surfactants are widely considered to be harmful to human health and the environment,[36,37] these patterned surfaces may find use in the monitoring of industrial wastewater with the naked eye prior to discharge.

3.3.5. Design of Underwater Superoleophobic Coatings for Bile Acid Sensing

In the final set of experiments, I sought to explore the possibility of sensing biomolecules beyond synthetic surfactants. Bile acids, a class of physiologically important amphipathic metabolites and biomarkers, exist in a healthy human body in concentrations ranging from 4 μM to 10 μM in biological fluids.[38] An elevation in the concentration of bile acids by two- or threefold corresponds to the early diagnosis, monitoring, and treatment of liver and intestinal diseases.[38] Conventional detection techniques for bile acids include liquid chromatography-mass spectrometry (LC-MS), polarized light microscopy, enzyme-linked immunosorbent assays (ELISA), and nuclear magnetic resonance (NMR).[39–42] Recent studies have reported that interactions between bile acid and an ionic surfactant that has absorbed at an aqueous–liquid crystal interface trigger a transition of the orientational ordering of the liquid crystals within the microdroplet, resulting in an optical response that can be monitored using polarized light microscopy.[43–46] While promising, the above methods typically involve either the use of specialized equipment or complicated and long procedures, making them challenging to perform.

Here, the cooperative assembly of bile acid on an appropriately modified superoleophobic multilayer coating was explored to determine the bile acid concentration by monitoring the

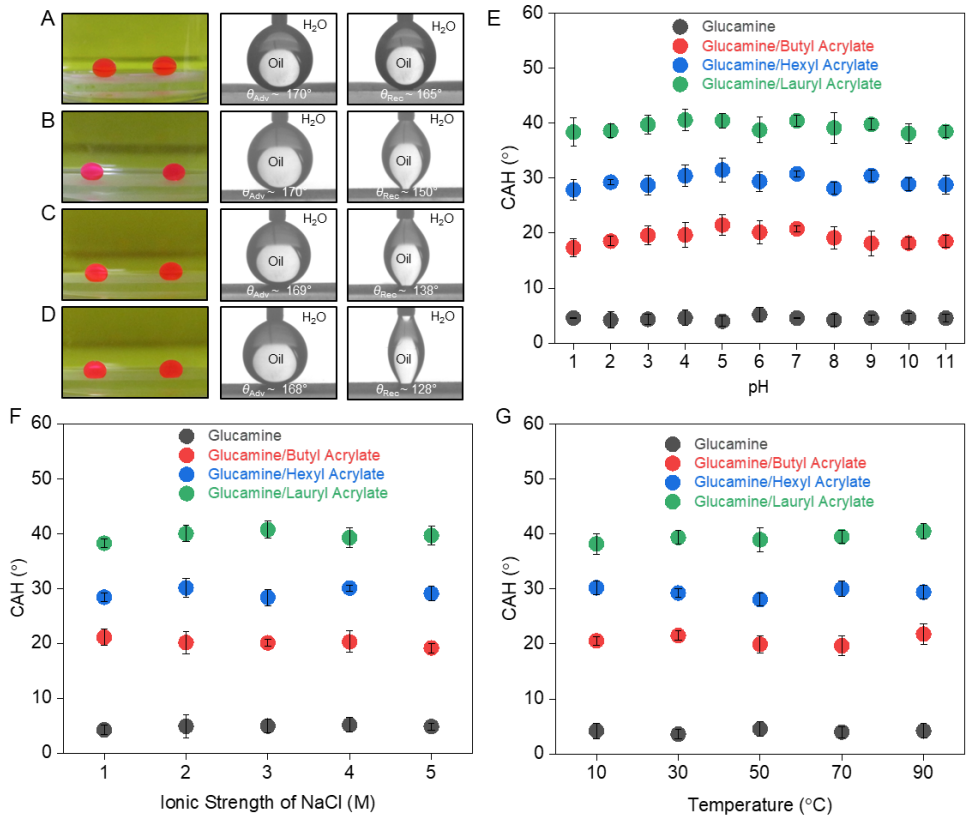

Figure 3.12. (A−D) Photographs, and advancing and receding OCA images of oil droplets on (A) glucamine, (B) glucamine/butyl acrylate, (C) glucamine/hexyl acrylate, and (D) glucamine/lauryl acrylate-modified surfaces. (E−G) Graphs detailing the independence of the CAH on the modified interfaces with respect to the (E) pH, (F) NaCl concentration, and (G) temperature. Oil droplet volume was 5 µL.

mobility of oil droplets on the surface. The multilayer coating was modified with non-ionic moieties (glucamine and alkyl acrylates) to minimize the impact of ionic interactions. The exposed hydrocarbon tail of the adhesive superoleophobic coatings was expected to interact efficiently with the hydrophobic region of the bile acid, resulting in a measurable change in the underwater oil adhesion state. To test this hypothesis, the dually reactive multilayer coating

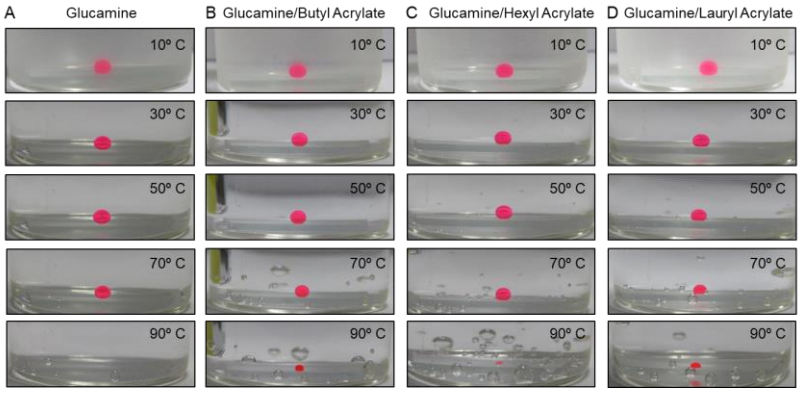

Figure 3.13. (A−D) Effect of the temperature on the oil wettability on the (A) glucamine, (B) glucamine/butyl acrylate, (C) glucamine/hexyl acrylate and (D) glucamine/lauryl acrylate-modified interfaces.

was covalently modified with non-ionic hydrophilic glucamine and hydrophobic alkyl acrylate to obtain oil-adhesive superoleophobic surfaces. The glucamine-modified coating exhibited a non-adhesive superoleophobicity with an advancing OCA of ~170° and CAH ~5° (Figure 3.12A), and the subsequent modification with hydrophobic alkyl acrylates transformed it into an adhesive underwater superoleophobicity with an increase in the CAH, as shown in Figure 3.12B−D. Specifically, the CAH of the glucamine/alkyl acrylate-modified coatings is ~20° for butyl acrylate, ~28° for hexyl acrylate, and ~40° for lauryl acrylate (Figure 3.12B−D). The CAH values for these modified surfaces remained constant over a wide range of pH (from 1 to

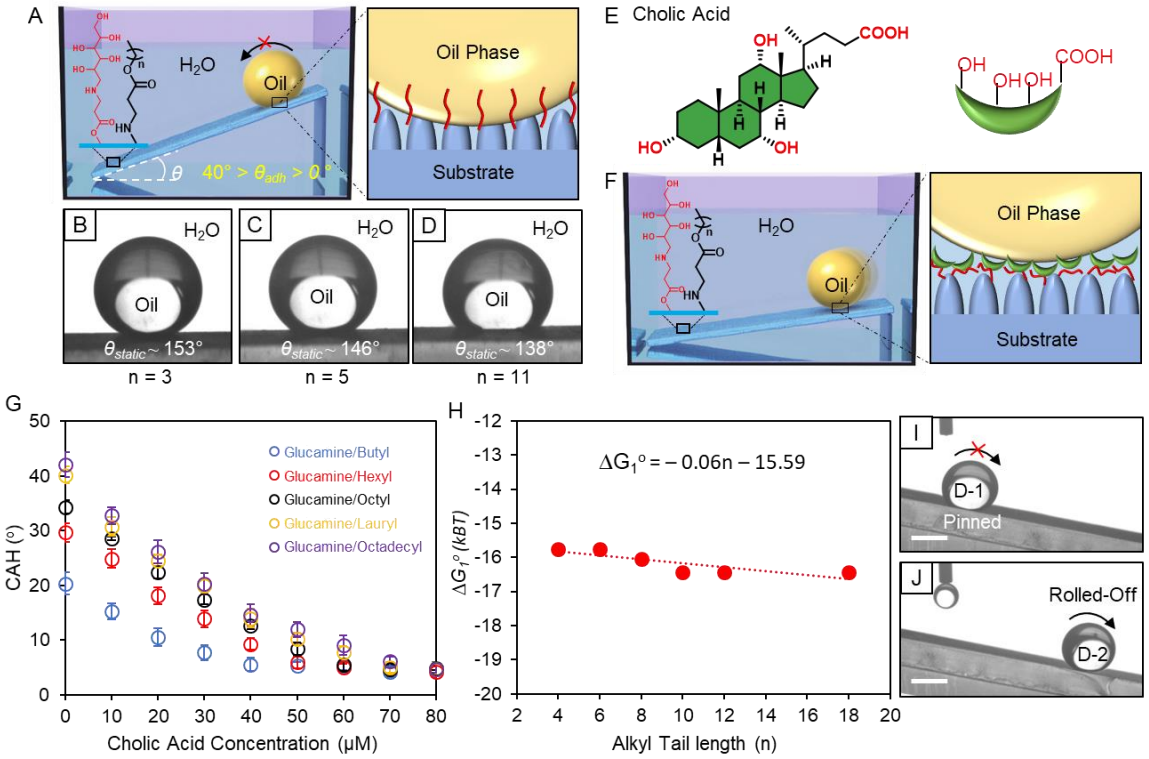

Figure 3.14. (A) Glucamine/alkyl acrylate-modified coatings exhibit underwater superoleophobicity with oil adhesion. (B–D) Micrographs showing the static OCA on the glucamine/alkyl acrylate-modified superoleophobic coatings with varying hydrocarbon tail lengths of the alkyl acrylate: (B) butyl acrylate, (C) hexyl acrylate, and (D) lauryl acrylate. (E) Molecular structure of cholic acid and (F) its cooperative assembly at the glucamine/alkyl acrylate-modified superoleophobic coating. (G) The effect of cholic acid concentration and the alkyl tail length of acrylates on the CAH of oil droplets on the glucamine/alkyl acrylate-modified superoleophobic coating. (H) Plot showing standard free energy accompanying the transfer of one cholic acid molecule from a singly-dispersed state in the bulk aqueous phase to the assembled state (ΔG_1^o) as a function of the alkyl tail length (n) of the glucamine/alkyl acrylate-modified coatings. (I, J) Contact angle goniometer images showing the oil droplet mobility in (I) pure water and (J) 50 μM cholic acid solution. The tilting of the surface was 10°. Oil droplet volume was 5 μL. Scale bars, 1 mm.

11; Figure 3.12E), ionic strength (from 0 M to 5 M NaCl; Figure 3.12F), and temperature (from 10° to 90°; Figure 3.12G and 3.13) conditions.

The association of different alkyl acrylate modifications, the static OCA of beaded oil droplets on the modified interfaces had altered, as shown in Figure 3.14B−D. Upon exposure to one of the primary bile acids, *i.e.*, cholic acid (Figure 3.14E), the glucamine/alkyl acrylate-modified superoleophobic coatings exhibited a cholic acid concentration-dependent oil adhesion, where the preferential interaction between the hydrocarbon tail of the coating and the cholic acid hide the hydrocarbon tail, rather the hydrophilic side of the cholic acid exposed to the oil droplet (Figure 3.14F). As shown in Figure 3.14G, the CAH of the beaded oil droplet on the superoleophobic coatings decreases with an increase in the concentration of cholic acid, and at high cholic acid concentrations, the glucamine/alkyl acrylate-modified surfaces switch to being

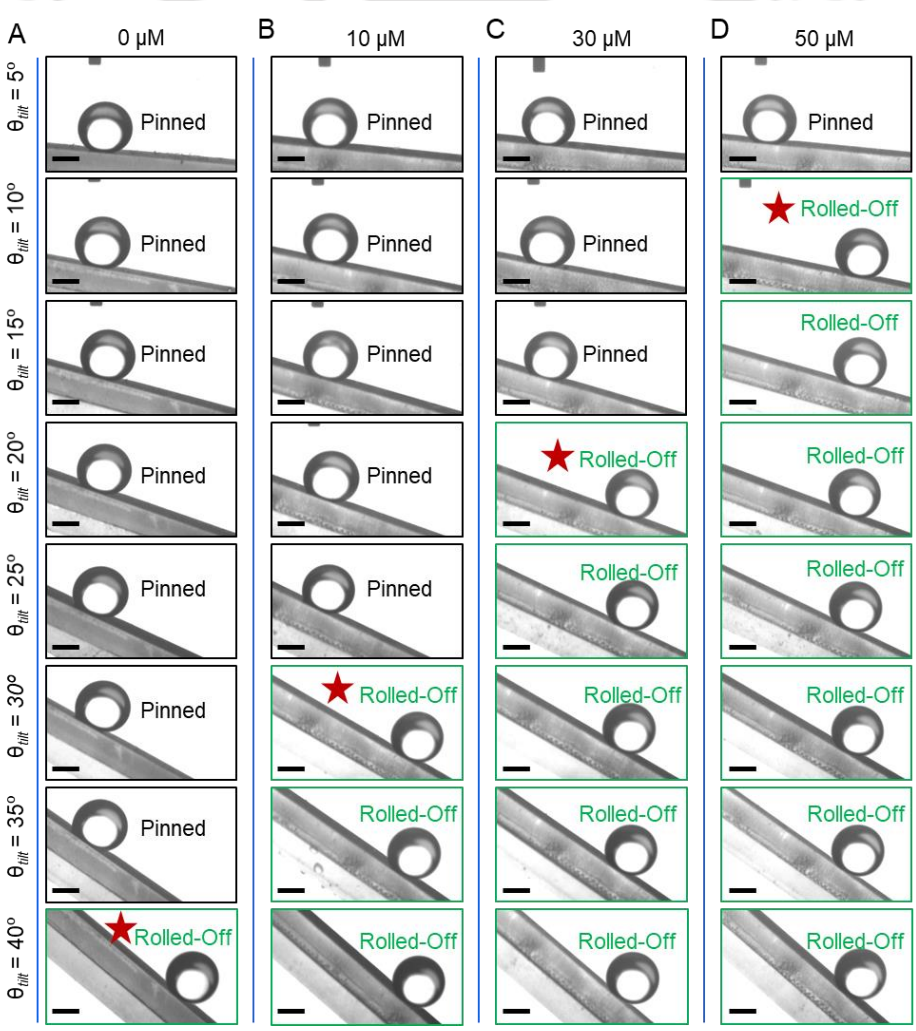

Figure 3.15. Photographs of the mobility of oil droplets on glucamine/lauryl acrylate−modified superoleophobic coatings as a function of cholic acid concentration. The red stars indicate the minimum tilting angle where the oil droplets started rolling off. Oil droplet volume was 5 μL. Scale bars, 1 mm.

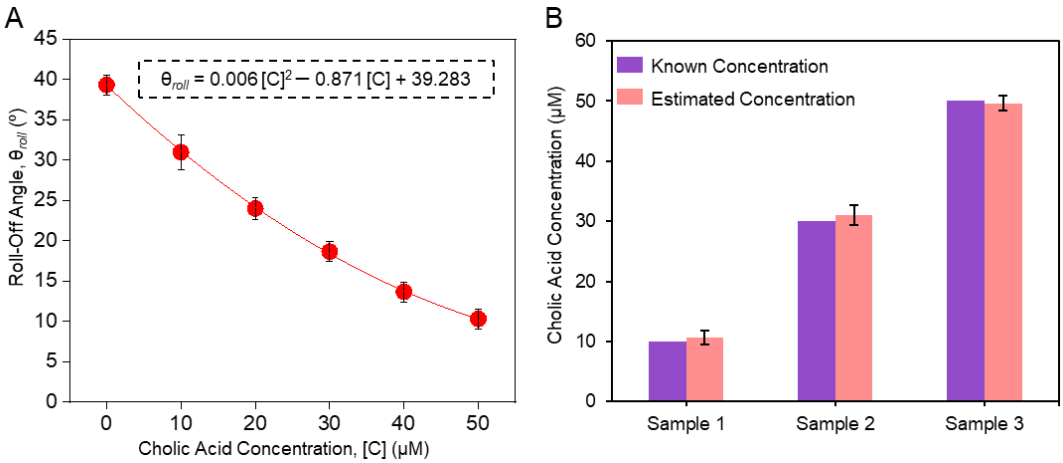

Figure 3.16. (A) Rolling-off angle (θ_{roll}) of oil droplets on glucamine/lauryl acrylate-modified superoleophobic coatings as a function of cholic acid concentration, [C]. The calibration curve is listed in the plot. (B) Estimation of the cholic acid concentration using the calibration curve in (A). Oil droplet volume was 5 μL.

non-adhesive and superoleophobic with a CAH < 5°. It is noteworthy that the CAC of cholic acid is almost independent of the tail length of the alkyl acrylates (the CAC lies between 4 μM and 8 μM for alkyl acrylates with tail lengths ranging from 4 to 18 carbons, corresponding to a driving force of ~ –16.15 k_BT per cholic acid molecule; Figure 3.14G), suggesting that four carbon lengths are sufficient to provide a strong hydrophobic effect to bind cholic acid on the glucamine/alkyl acrylate-modified superoleophobic coatings. Notably, only glucamine-modified coatings lack alkyl acrylate modification and exhibit an inherent independence on cholic acid concentration.

Interestingly, an increase in the length of the aliphatic tail of the alkyl acrylates increases the concentration window for cholic acid detection, *e.g.*, 8 μM to 30 μM for butyl acrylate and 4 μM to 70 μM for lauryl acrylate. However, no further improvement was noted beyond lauryl acrylate. The detection limit of cholic acid by glucamine/lauryl acrylate-modified superoleophobic surfaces (*i.e.*, 4 μM) would enable the monitoring of a concentration of bile acid similar to that found in a healthy human body, suggesting that these surfaces may provide a novel principle for the detection of bile acids with the naked eye for the early diagnosis of liver and intestinal diseases. To provide a proof of concept for the detection of cholic acid, the mobility of oil droplets on the glucamine/lauryl acrylate-modified surfaces in a cholic acid aqueous solution was monitored. In the absence of cholic acid, the beaded oil droplets were pinned on a 10° tilted surface (Figure 3.14I), whereas the presence of cholic acid (50 μM) caused the DCE droplet to roll off (Figure 3.14J). The corresponding relationship between the

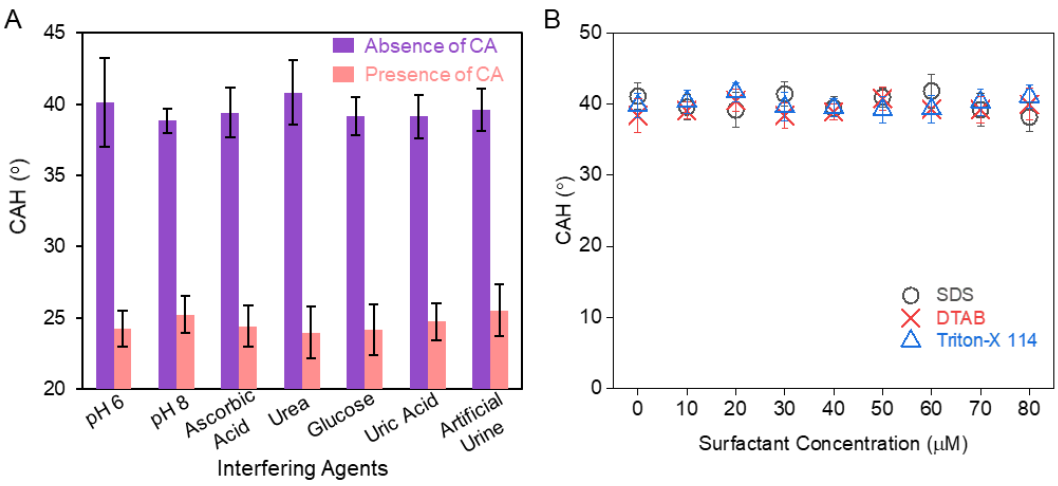

Figure 3.17. (A) Effect of pH and interfering agents on the CAH of oil droplets on the glucamine/lauryl acrylate-modified coatings. The concentration of cholic acid and interfering agents was 20 μM, and 500 μM, respectively. (B) CAH of oil droplets on the glucamine/lauryl acrylate-modified coating as a function of anionic (SDS), cationic (DTAB), and non−ionic (Triton−X 114) surfactant concentration at a neutral pH. Oil droplet volume was 5 μL.

roll-off angle (θ_{roll}) and the concentration of cholic acid ([C]) can be written as (Figure 3.15 and 3.16A):

$$\theta_{roll} = 0.006[C]^2 - 0.871[C] + 39.283 \quad (4)$$

According to equation (4), the cholic acid concentration of unknown samples can be successfully determined, as shown in Figure 3.16B. Interestingly, such glucamine/lauryl acrylate-modified superoleophobic coatings exhibited an ultraselectivity of cholic acid, and their oil adhesion behaviors (*i.e.*, CAH) are unaffected by the pH of the aqueous solution and

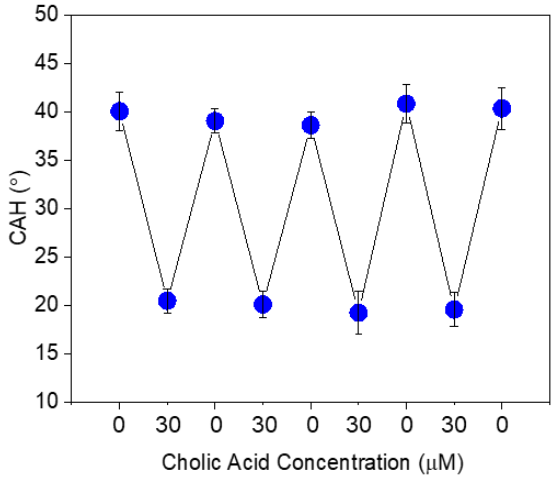

Figure 3.18. Reversible manipulation of the CAH on the glucamine/lauryl acrylate-modified superoleophobic coatings in aqueous solutions of cholic acid by switching its concentration between 0 and 30 μM. Oil droplet volume was 5 μL.

other relevant interfering agents, such as ascorbic acid, urea, glucose, and uric acid, which are present in a urine sample (Figure 3.17A). Moreover, the glucamine/lauryl acrylate-modified coating remains insensitive toward the presence of ionic or non-ionic surfactants (Figure 3.17B). Finally, it was observed that the change of the oil adhesion behavior of the glucamine/lauryl acrylate-modified coatings is completely reversible in nature (Figure 3.18), which promises a high level of reusability for the multilayer coatings for cholic acid sensing.

3.4. Conclusions

To conclude, this chapter demonstrates the design and synthesis of a novel class of multilayer coatings with dually reactive moieties that enable further orthogonal chemical functionalization to independently tune their underwater superoleophobicity and oil adhesion. Furthermore, the non-covalent, cooperative assembly of synthetic surfactants at the surface of these multilayer coatings is able to reversibly program the CAH of oil droplets at the surface, which revealed new principles by which the molecular self-assembly and oil droplet mobility can be coupled on the surfaces. It also hints at directions by which the concentration and ionic type of amphiphiles can be rapidly and efficiently sensed with the naked eye. Additionally, this design principle is general and has been demonstrated to be able to be applied to bio-relevant amphiphiles, *i.e.*, bile acids. Future efforts will seek to use oil adhesion behaviors at superoleophobic surfaces to monitor biological events, including protein–lipid interactions and enzymatic activity.

3.5. References

1 M. Liu, S. Wang, Z. Wei, Y. Song and L. Jiang, *Adv. Mater.*, 2009, **21**, 665.

2 B. Su, Y. Tian and L. Jiang, *J. Am. Chem. Soc.*, 2016, **138**, 1727.

3 J. Yong, F. Chen, Q. Yang, J. Huo and X. Hou, *Chem. Soc. Rev.*, 2017, **46**, 4168.

4 Y. Si, Z. Dong and L. Jiang, *ACS Cent. Sci.*, 2018, **4**, 1102.

5 X. Liu, J. Zhou, Z. Xue, J. Gao, J. Meng, S. Wang and L. Jiang, *Adv. Mater.*, 2012, **24**, 3401.

6 L. P. Xu, J. Zhao, B. Su, X. L. Liu, J. T. Peng, Y. B. Liu, H. L. Liu, G. Yang, L. Jiang, Y. Q. Wen, X. J. Zhang and S. T. Wang, *Adv. Mater.*, 2013, **25**, 606.

7 J. Yong, F. Chen, Q. Yang, U. Farooq and X. Hou, *J. Mater. Chem. A*, 2015, **3**, 10703.

8 Y. Cai, Q. Lu, X. Guo, S. Wang, J. Qiao and L. Jiang, *Adv. Mater.*, 2015, **27**, 4162.

9 K. Han, L. Heng and L. Jiang, *ACS Nano*, 2016, **10**, 11087.

10 D. Zang, H. Yi, Z. Gu, L. Chen, D. Han, X. Guo, S. Wang, M. Liu and L. Jiang, *Adv. Mater.*, 2017, **29**, 1602869.

11 X. Yuan, W.-C. Nie, C. Xu, X.-H. Wang, Q. Xiao, F. Song, X.-L. Wang and Y.-Z. Wang, *Adv. Funct. Mater.*, 2018, **2**, 1704956.

12 S. Zhang, G. Jiang, S. Gao, H. Jin, Y. Zhu, F. Zhang and J. Jin, *ACS Nano*, 2018, **12**, 795.

13 Z. Chu, Y. Feng and S. Seeger, *Angew. Chem., Int. Ed.*, 2015, **54**, 2328.

14 S. Wang, K. Liu, X. Yao and L. Jiang, *Chem. Rev.*, 2015, **115**, 8230.

15 K. Chen, S. Zhou and L. Wu, *ACS Nano*, 2016, **10**, 1386.

16 M. Ge, C. Cao, J. Huang, X. Zhang, Y. Tang, X. Zhou, K. Zhang, Z. Chen and Y. Lai, *Nanoscale Horiz.*, 2018, **3**, 235.

17 Y. Peng, Y. Ning, X. Ma, Y. Zhu, S. Yang, B. Su, K. Liu and L. Jiang, *Adv. Funct. Mater.*, 2018, **28**, 1800712.

18 Z. Lian, J. Xu, Z. Yu, P. Yu, W. Ren, Z. Wang and H. Yu, *ACS Appl. Mater. Interfaces*, 2020, **12**, 6573.

19 W. Chen, P. Zhang, R. Zang, J. Fan, S. Wang, B. Wang and J. Meng, *Adv. Mater.*, 2020, **32**, 1907413.

20 X. Huang, B. Li, L. Wang, X. Lai, H. Xue and J. Gao, *ACS Appl. Mater. Interfaces*, 2019, **11**, 24533.

21 Z. Lia and Z. Guo, *Nanoscale*, 2019, **11**, 22636.

22 J. Tan, J. Xu, D. Wang, J. Yang and S. Zhou, *J. Mater. Chem. A*, 2020, **8**, 24086.

23 Y. Cheng, Q. Yang, Y. Fang, J. Yong, F. Chen and X. Hou, *Adv. Mater. Interfaces*, 2019, **6**, 1900067.

24 H. Liu, X. Zhang, S. Wang and L. Jiang, *Small*, 2015, **11**, 3338.

25 L. Tie, Z. Guo and W. Liu, *ACS Appl. Mater. Interfaces*, 2015, **7**, 1064.

26 T. Du, S. Ma, X. Pei, S. Wang and F. Zhou, *Small*, 2017, **13**, 1602020.

27 B. Shang, M. Chen and L. Wu, *Small*, 2019, **15**, 1901888.

28 W. Liu, S. Xiang, X. Liu and B. Yang, *ACS Nano*, 2020, **14**, 9166.

29 D. Parbat and U. Manna, *Chem. Sci.*, 2017, **8**, 6092.

30 D. Parbat and U. Manna, *J. Mater. Chem. A*, 2018, **6**, 22027.

31 A. B. D. Cassie and S. Baxter, *Nature*, 1945, **155**, 21.

32 M. P. Rodríguez, G. Prieto, C. Rega, L. M. Varela, F. Sarmiento and V. Mosquera, *Langmuir*, 1998, **14**, 4422.

33 B. P. Singh, L. Besra, P. S. R. Reddy and D. K. Sengupta, *Fuel*, 1998, **77**, 1349.

34 S. Tcholakova, N. D. Denkov and A. Lips, *Phys. Chem. Chem. Phys.*, 2008, **10**, 1608.

35 E. Nyankson, O. Olasehinde, V. T. John and R. B. Gupta, *Ind. Eng. Chem. Res.*, 2015, **54**, 9328.

36 O. Kaczerewska, R. Martins, J. Figueiredo, S. Loureiro and J. Tedim, *J. Hazard. Mater.*, 2020, **392**, 1222992.

37 A. Colomer, A. Pinazo, M. T. García, M. Mitjans, M. P. Vinardell, M. R. Infante, V. Martínez and L. Perez, *Langmuir*, 2012, **28**, 5900.

38 K. Rani, P. Garg and C. S. Pundir, *Anal. Biochem.*, 2004, **332**, 32.

39 S. Reiter, A. Dunkel, A. Metwaly, J. Panes, A. Salas, D. Haller and T. Hofmann, *J. Agric. Food Chem.*, 2021, **69**, 5238.

40 X. Zhang, M. Zhu, B. Xu, Y. Cui, G. Tian, Z. Shi and M. Ding, *Biosens. Bioelectron.*, 2016, **85**, 563.

41 G. Tian, M. Ding, B. Xu, Y. He, W. Lyu, M. Jin and X. Zhang, *Biosens. Bioelectron.*, 2018, **118**, 31.

42 D. Sangaraju, Y. Shi, M. V. Parys, A. Ray, A. Walker, R. Caminiti, D. Milanowski, A. Jaochico, B. Dean and X. Liang, *J. Am. Soc. Mass Spectrom.*, 2021, **32**, 2033.

43 J. Deng, X. Lu, C. Constant, A. Dogariuc and J. Fang, *Chem. Commun.*, 2015, **51**, 8912.

44 J. Deng, W. Liang and J. Fang, *ACS Appl. Mater. Interfaces*, 2016, **8**, 3928.

45 H. Ma, Q. Kang, T. Wang, J. Xiao and L. Yu, *Colloids Surf. B*, 2019, **173**, 178.

46 X. Han, D. Han, J. Zeng, J. Deng, N. Hu and J. Yang, *Microchem. J.*, 2020, **157**, 105057.

Chemically Selective Underwater Raising and Rolling of Oil-Droplet Enabled Sensing of Toxic Chemicals*

A dual chemically reactive multilayer coating is rationally subjected to mono and dual-functionalization through a 1, 4-conjugate addition reaction at ambient conditions to depict the raising of the oil contact angle and rolling of a beaded oil-droplet underwater, respectively, only in the presence of targeted toxic chemicals (e.g., nitrite ion and hydrazine). The covalently embedded hydrophobic moiety in both mono and dual-functionalized coating can selectively transform into hydrophilic moiety in the presence of a specific toxic chemical. The conversion of the hydrophobic aromatic moiety into a hydrophilic moiety in the modified multilayer coatings via selected modified Griess reaction and Schiff base reaction contributed to the desired change in underwater oil wettability, reflected as i) raising in oil contact angle (for the mono-functionalized coating, and ii) rolling of beaded oil droplet (for the dual-functionalized coating). Eventually, this approach allowed equipment-free and naked-eye chemical sensing of toxins with high selectivity and sensitivity.

*A. Borbora, J. Das and U. Manna, *Chem. Commun.*, 2023, **59,** 7915.

4.1. Introduction

Sensing toxic chemicals is essential to manage pollution timely and efficiently.[1-4] In the past, various approaches—i.e., electrochemistry, surface-enhanced Raman spectroscopy (SERS), colorimetry, fluorometry, chromatography etc., were successfully introduced for sensing relevant toxic chemicals.[5-16] For example, nitrite ion (NO_2^-) and hydrazine are (N_2H_4) common, colourless, and water-soluble toxic chemicals that pollute fresh water—due to their unavoidable or excessive industrial utilizations.[17-32] Consumption of water polluted with nitrite ion and (or) hydrazine is known to affect our health severely. In the past, different strategies were introduced to sense and quantify these toxic chemicals with high sensitivity and selectivity—but most of these reported approaches are heavily dependent on the use of sophisticated equipments—including spectrophotometer, electrochemical workstation, Raman spectrometer, etc.[17-32] Ideally, sensing and quantifying such toxic chemicals with the naked eye without demanding any equipment would be an economic and user-friendly approach.

In a rare attempt, a liquid crystal (LC) infused porous surface is being recently introduced for sensing amphiphilic molecules with the naked eye by measuring the velocity of moving water droplets on the surface, where interdigitation of the hydrocarbon chain of ionic amphiphiles with LC phase slows down the sliding speed of the beaded water droplet.[33] But such an approach is inappropriate to sense other toxic chemicals—that lack hydrocarbon tail to exhibit interdigitation with the LC. In this current approach, a dual chemically reactive multilayer coating comprised of residual acrylate and amine groups is strategically customized for the proof of concept demonstration of separate sensing of nitrite ion and hydrazine with high selectivity and sensitivity with the naked eye—without using any equipment.

In this chapter, a dual chemically reactive multilayer coating (Figure 4.1A) was rationally modified with specifically selected hydrophobic and hydrophilic moieties to achieve mono and dual-functionalization through a 1, 4-conjugate addition reaction as shown in Figure 4.1B−D. The covalently embedded hydrophobic moiety in both mono and dual-functionalized coating can selectively convert into hydrophilic moiety in the presence of a specific toxic chemical, as shown in Figure 4.1C, D. Such converted hydrophilic moiety in mono and dual-functional coatings attributes to the raising in the oil contact angle (OCA, Figure 4.1C) and rolling of beaded oil droplets (Figure 4.1D) underwater, respectively, indicating the presence of a toxic chemical. For instance, to demonstrate the sensing of nitrite, the dual chemically reactive multilayer coating was first functionalized with hydrophobic phenyl of N-phenylethylenediamine (PEDA), then the hydrophobic phenyl moiety was converted into

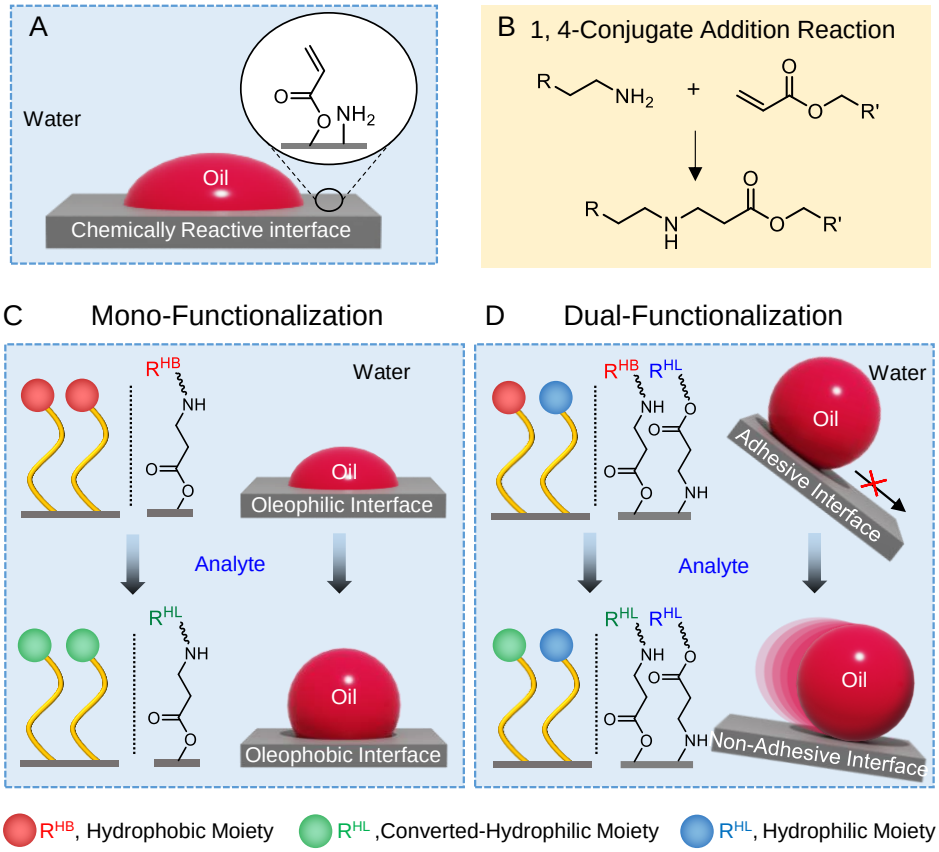

Figure 4.1. (A) Schematic depiction of a chemically reactive multilayer coating composed of residual acrylate and amine moieties, displaying underwater oleophilicity. (B) The 1, 4-conjugate addition reaction between amine and acrylate was explored to achieve mono and dual-functionalization of the chemically reactive multilayer coating. (C, D) Schematic representation of (C) mono and (D) dual-functionalization with hydrophobic and hydrophilic moieties, where the selected hydrophobic aromatic moiety converts into a hydrophilic moiety on exposure to selected analytes, resulting in the raising of the oil contact angle (OCA) and rolling of beaded oil droplets underwater, respectively.

hydrophilic sulfonamide moiety in the presence of nitrite ion, through a modified Griess reaction.[19,34] Furthermore, hydrazine sensing was achieved by terephthaldehyde (TPA) modification of the multilayer coating to associate hydrophobic moiety in the coating. The conversion of hydrophobic moiety into the hydrophilic group through Schiff base reaction[25,27,28] in the exposure to hydrazine provided a basis for chemical sensing just by monitoring the raising and rolling of oil droplets.

4.2. Experimental Section

4.2.1. Materials Required

N-Phenylethylenediamine (PEDA), pentyl amine (PA), sulphanilamide, p-terephthalaldehyde (TPA), 2-amino-2-methyl-1-propanol (AMP), hydrazine were purchased from Sigma-Aldrich,

India. Sodium nitrite ($NaNO_2$), sodium nitrate ($NaNO_3$), sodium bromide (NaBr), sodium sulphate (Na_2SO_4), sodium carbonate (Na_2CO_3), sodium phosphate (Na_3PO_4), and sodium chlorate ($NaClO_3$) were procured from Merck Specialities Pvt. Ltd, Mumbai, India. The details of all other materials and chemicals used in this work were discussed previously in Chapters 2 and 3.

4.2.2. Characterization

The instruments used in this chapter for the characterization of synthesized materials were the same as discussed previously in section 2.2.2 of Chapter 2.

4.2.3. Fabrication of Dual-Reactive Multilayer Coatings

The fabrication procedure for dual reactive multilayer (20-bilayer) coating was discussed in section 2.2.3 of Chapter 2.

4.2.4. Mono and Dual-Functionalization of Multilayer Coatings

To achieve the nitrite ion responsive interface, the residual acrylate of the dual reactive multilayer coating was post-modified with hydrophobic PEDA by exposing the multilayer coating in the PEDA solutions (25 µL mL^{-1} in ethanol) for 12 hours at ambient conditions. After PEDA modification, the multilayer was washed with ethanol and dried in air. For dual functionalization, mono (PEDA)-functionalized multilayers were further treated with an ethanol solution containing a hydrophilic acrylate, 2-carboxyethyl acrylate (CEA, 25 µL mL^{-1}), overnight at ambient conditions, and next washed with ethanol and air dried.

To achieve hydrazine-responsive mono-functionalized coating, the multilayer coating was treated with TPA (25 µL mL^{-1} in ethanol) for 6 hours at ambient conditions and then washed with ethanol and air dried. For dual-functionalization, the TPA-functionalized multilayer was subsequently treated with an ethanol solution of a hydrophilic amine, AMP (25 µL mL^{-1}), overnight at ambient conditions, and next washed with ethanol prior to air drying.

4.2.5. Nitrite Ion Sensing with Mono and Dual-Functionalized Multilayer Coating

For sensing experiments, a 1 mM stock solution of nitrite ions in deionized (DI) water was prepared, and subsequently, different solutions of varying concentrations of nitrite ions in DI water were prepared by diluting the stock solution. The solutions of nitrite ions were then mixed with 0.5% sulfanilamide solution (prepared in 0.1N HCl) in a 1:1 ratio. The mono (PEDA) and dual (PEDA/CEA)-functionalized multilayer coatings were treated separately

with the as-prepared solutions containing varying concentrations of nitrite ions for 15 minutes. After the successful Griess reaction, the modified coatings were washed thoroughly with DI water to remove the unreacted reactants and then air dried. Next, the contact angle goniometer instrument was used to characterize the increase in the underwater oil wettability in the mono-functionalized coating and the decrease in the underwater oil adhesion in the dual-functionalized coating.

4.2.6. Hydrazine Sensing with Mono and Dual-Functionalized Multilayer Coating

For hydrazine sensing experiments, different solutions containing different hydrazine concentrations were prepared in DI water by diluting a stock solution. The mono (TPA) and dual (TPA/AMP)-functionalized multilayer coatings were treated separately with the hydrazine solution for 30 minutes. After the conversion of the residual aldehydes on the mono and dual-functionalized coatings to hydrazones, the coatings were washed thoroughly with DI water to remove the unreacted hydrazines and then air dried. Next, the contact angle goniometer instrument was used to characterize the increase in the underwater oil wettability in the mono functionalized coating and the decrease in the underwater oil adhesion in the dual-functionalized coating. To demonstrate the reusability of the hydrazine-responsive coatings, the hydrazine (120 µM) modified coating was exposed to an acidic solution (pH 3) to hydrolyze the imine bonds in the coating. The coating was then post-modified with TPA and subsequently treated with hydrazine (120 µM) following the above-mentioned procedures. The hydrazine exposure resulted in an increase in the underwater OCA. This process was repeated for several cycles to demonstrate the reusability of the coating.

4.3. Results and Discussion

4.3.1. Mono and Dual-Functionalization of Dual Reactive Multilayer Coatings for Nitrite Sensing

In this chapter, the 1, 4-conjugate addition reaction between amine and acrylate at ambient conditions is applied to prepare a dual reactive multilayer coating of chemically reactive nanocomplex (CRNC), where the mixing of branched polyethyleneimine (BPEI) and dipentaerythritol pentaacrylate (5Acl) in ethanol resulted in a dispersion of CRNC (as described in chapter 2 and 3).[35-37] The prepared coating (with adhesion force 66 ± 4 KPa on the glass substrate) is strategically modified with functionalizable aromatic small molecules to unprecedentedly demonstrate both the raise and rolling of beaded oil-droplet, specifically in the presence of targeted toxic chemicals, where the choice of selected aromatic small molecules

and chemical pathways (e.g., Griess reaction[19,34] Schiff base type reaction[25,27,28]) ensures the selective change in oil-wettability underwater. For instance, here, I had rationally modified the dual chemically reactive multilayer coating with hydrophobic phenyl of PEDA and hydrophilic carboxylic acid of CEA to achieve mono and dual-functionalization in the coating, where the hydrophobic phenyl moiety is capable of conversion into hydrophilic sulfonamide moiety in the presence of nitrite ion, through a modified Griess reaction, as shown in Figure 4.2A.

The prepared coating was characterized with field emission scanning electron microscope (FESEM) and Attenuated total reflection-Fourier transform infrared (ATR-FTIR) analysis (Figure 4.2B−D), where the coating remained highly porous with granular domains (Figure 4.2B, C). Such topography is essential to confer high underwater oleophobicity through appropriate chemical modulation. On the other side, the existence of IR signatures at 1730 cm^{-1} for carbonyl stretching and 1409 cm^{-1} for vinylic C-H deformation in the ATR-FTIR spectra (Figure 4.2D, black spectrum) confirmed the presence of residual acrylate groups in the

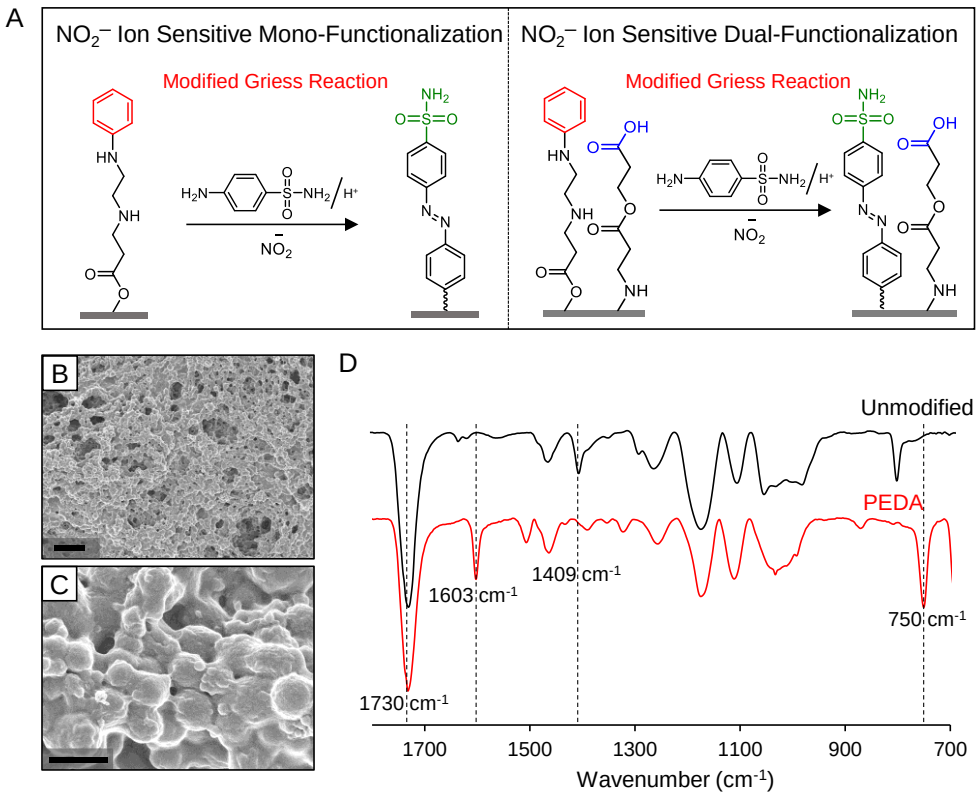

Figure 4.2. (A) Nitrite ion sensitive mono and dual-functionalization of multilayer coatings, where the hydrophobic phenyl moiety converts into a hydrophilic moiety in the presence of nitrite ions, following a modified Griess reaction. (B, C) Representative field emission scanning electron microscope (FESEM) micrographs of reactive multilayer coatings at (B) low and (C) high magnifications. Scale bars, 5 μm, and 1 μm. (D) Attenuated total reflection-Fourier transform infrared (ATR-FTIR) spectra of the multilayer coating before (black) and after chemical modifications with N-phenylethylenediamine (PEDA, red).

coating. This residual chemical reactivity enabled the covalent modification of the coating with PEDA—and such functionalization is essential for coupling phenyl moiety with diazonium cation derived from the reaction of sulfanilamide and nitrite ion under acidic conditions through a modified Griess reaction, as shown in Figure 4.2A. The PEDA-modification is further validated with ATR-FTIR analysis, where the characteristic IR peak for vinylic C-H deformation (1409 cm^{-1}) is significantly depleted with respect to the normalized IR signature for carbonyl stretching (1730 cm^{-1}), as shown in Figure 4.2D (red spectrum). Moreover, new IR peaks appeared at 1603 cm^{-1} and 750 cm^{-1} for aromatic C-C stretching (in-ring) and aromatic C-H bending (out of plane) (Figure 4.2D, red spectrum), independently reconfirmed the modification of multilayer coating with PEDA. Interestingly, during this post-covalent modification of the prepared coating with PEDA (referred as mono-functionalized coating), no change in underwater oleophobicity was observed (Figure 4.3A−C), the OCA of the beaded model oil (DCE) was found to be ~ 63º. However, the static water contact angle (WCA) was increased by ~ 10° with respect to the native multilayer coating (Figure 4.3E); this supports the

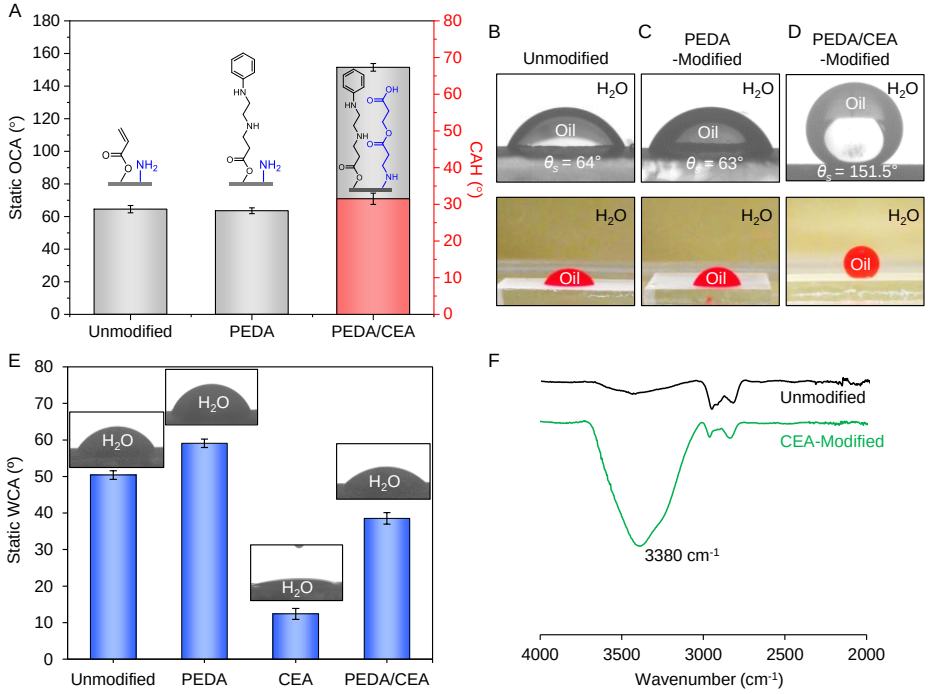

Figure 4.3. (A) Effect of mono (PEDA) and dual (PEDA/CEA)-functionalization on the underwater oil-wettability (*i.e.* static OCA and contact angle hysteresis (CAH)) of beaded oil droplets (5 µL) on the multilayer coating. (B−D) Contact angle goniometer and digital images showing underwater oil wettability (DCE, 5 µL (red dyed)) on unmodified, mono (PEDA) and dual (PEDA/CEA)-functionalized multilayer coating. (E) Effect of different mono and dual-functionalizations on the static water contact angle (WCA) of the modified coatings. (F) ATR-FTIR spectra showing the appearance of a broad OH stretching band in the multilayer coating after CEA-modification.

hypothesis of the association of hydrophobic aromatic moiety. Thereafter, the PEDA-modified multilayer coating was subsequently post-modified with CEA to achieve dual-functionalized multilayer coating. This post-covalent modification resulted in an adhesive underwater superoleophobicity with advancing OCA of ~ 164º and contact angle hysteresis (CAH) of ~ 31º, as shown in Figure 4.3A and D. The association of hydrophilic carboxylic acid groups led to decrease in the WCA (Figure 4.3E) and was verified with the appearance of a broad IR signature at 3380 cm^{-1} (Figure 4.3F). Thus, the strategic mono (PEDA) and dual (PEDA/CEA)-functionalized multilayer coatings exhibit underwater oleophilicity and adhesive-superoleophobicity, respectively (Figure 4.3C, D).

4.3.2. Modulation of Underwater Oil Wettability for Nitrite Sensing

In the next set of experiments, the mono (PEDA) and dual (PEDA/CEA)-functionalized multilayer coatings were individually utilized to demonstrate the sensing of nitrite ion following two distinct methods—i) raising of OCA and ii) rolling of beaded oil droplets, underwater. Firstly, mono (PEDA)-functionalized coating was exposed to a mixture of the sulfanilamide and nitrite ions at acidic conditions, which resulted in the elevation of underwater OCA depending on the concentration of nitrite ions in the aqueous phase, as shown in Figure 4.4A and B. The sulfanilamide and nitrite ions mutually reacted at acidic conditions to yield diazonium cations—which subsequently coupled with available phenyl moieties of PEDA-modified coating. The appearance of the characteristic IR signatures at 1520 cm^{-1} for N=N stretching and at 1328 cm^{-1} and 1150 cm^{-1} for asymmetric and symmetric stretching of S=O, respectively, revealed the successful coupling of diazonium cation with phenyl moiety through modified Griess reaction (Figure 4.4C). Such treatment resulted in a change in water wettability from ~ 63º to ~ 7º (Figure 4.4D and E) due to the conversion of hydrophobic phenyl moiety into hydrophilic sulfonamide derived from sulfanilamide. Eventually, a gradual rise in the underwater OCA was noticed with an increase in the concentration of nitrite ions—due to more conversion of hydrophobic phenyl groups to hydrophilic sulfonamide moiety, as depicted in Figures 4.4A. This approach remained highly sensitive as the underwater OCA raised by ~ 30° in the presence of nitrite ions at a concentration of just 5 μM—which is significantly lower than the permissible limit (65 μM, recommended by the World Health Organization (WHO)[14]. In a control experiment, the multilayer coating was modified with hydrophobic alkyl amine, PA, and then exposed to the mixture of the sulfanilamide and nitrite ions at acidic conditions, where no such change in underwater OCA was noticed, as the diazonium cation failed to couple

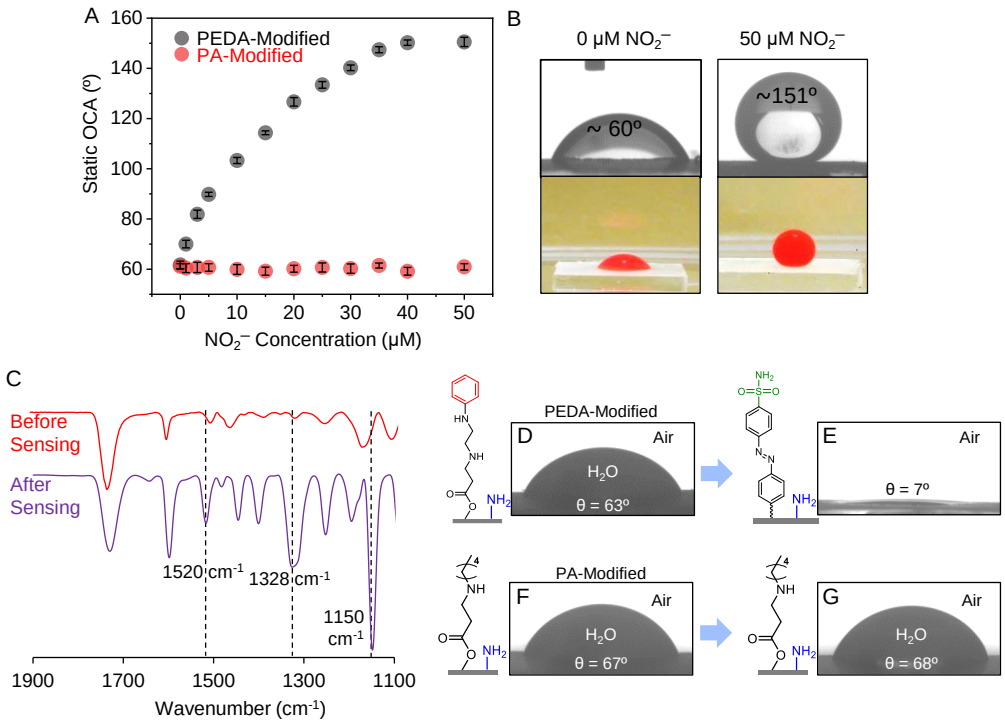

Figure 4.4. (A) The effect of the concentration of nitrite ions (during Griess reaction) on the static OCA of PEDA-modified and pentylamine (PA)-modified multilayer coatings. (B) Contact angle goniometer images and photographs show the raise in OCA on PEDA-modified multilayer coatings after Griess modification. (C) ATR-FTIR spectra accounting for the chemical conversion of the PEDA-modified coating through the Griess reaction. (D, E) Contact angle goniometer images show depletion of water contact angle after the Griess conversion of phenyl moiety into hydrophilic sulphonamide moiety (F, G) Chemical functionalities in the PA-modified coating that cannot show conversion through Griess reaction and the show unaltered water wettability. Oil/Water droplet volume was 5 μL.

and convert the hydrophobic hydrocarbon moiety into hydrophilic moiety (Figure 4.4A, red circle). As expected, no change in water wettability was noted in such chemical treatment (Figure 4.4F, G). Moreover, the raising in OCA of the PEDA-modified coating remained highly selective to only nitrite ions, and the OCA raised from ~ 63° to ~ 125 ° at a concentration of 20 μM (Figure 4.5). In the absence of nitrite ions, no rise in underwater OCA was noticed even if the PEDA-modified coating was exposed to the equivalent amount of other relevant interfering anions—including Br^-, Cl^-, NO_3^-, CO_3^{2-}, SO_4^{2-}, PO_4^{3-}, ClO_4^- and OH^- (Figure 4.5, grey bars). Moreover, such coating remained capable of sensing nitrite ions in the presence of the aforementioned interfering ions (Figure 4.5, red bars).

In the next set of experiments, the dual (PEDA/CEA)-functionalized coating that displayed adhesive underwater superoleophobicity was explored to demonstrate the sensing of nitrite ions just by observing the rolling of a beaded oil droplet at a certain tilting angle of the surface. The

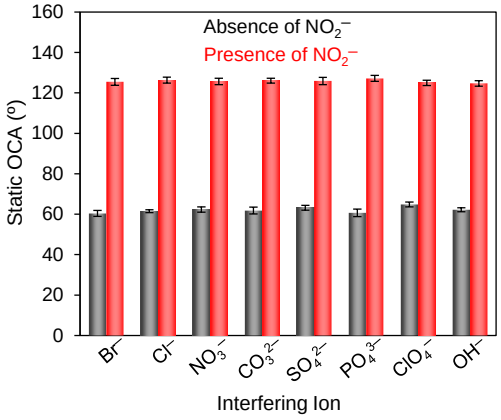

Figure 4.5. Effect of relevant interfering reagents on the static OCA on the PEDA-modified coating after exposure to acidic sulfanilamide solution in the presence of nitrite ions and individual interfering ions.

underwater oil adhesion property of the dual-functionalized coating was reduced on exposure of the coating to a mixture of the sulfanilamide and nitrite ion at acidic conditions. This can be attributed to the conversion of the hydrophobic phenyl moiety of the dual-functionalized coating into hydrophilic moiety through coupling with diazonium moiety derived from sulfanilamide via modified Griess reaction. The elevated concentration of nitrite ion reduced

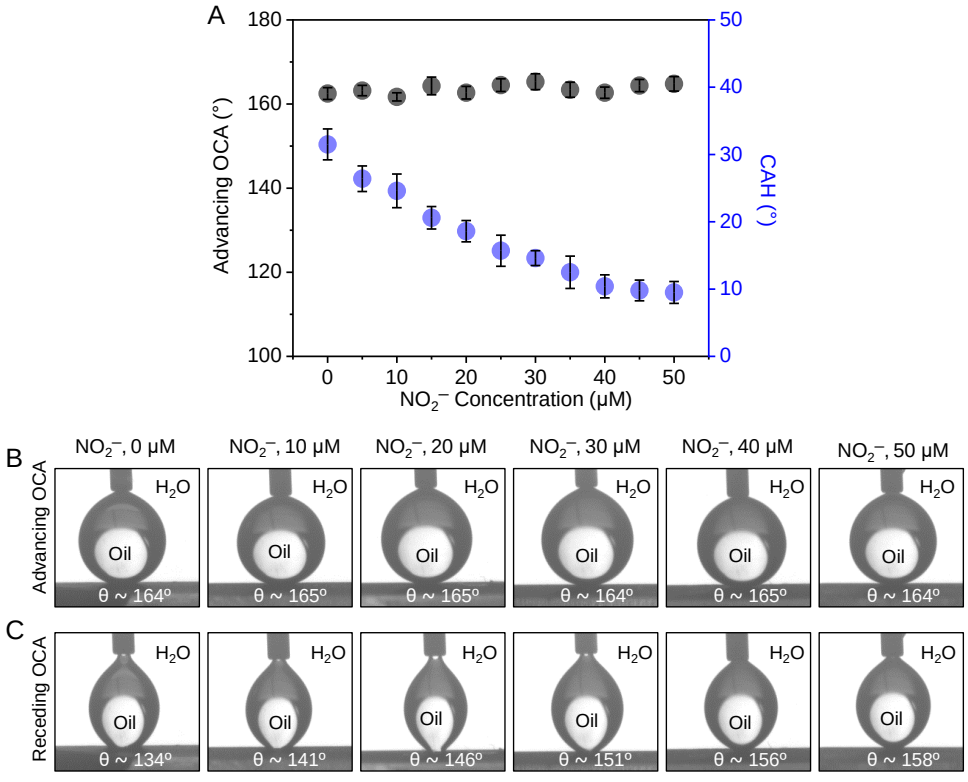

Figure 4.6. (A) Effect of concentration of nitrite ions (during modified Griess reaction) on the advancing OCA and CAH of oil droplets on PEA/CEA-modified coatings. (B) and (C) Contact angle goniometer images showing (B) advancing and (C) receding OCA on PEA/CEA-modified coating after modified Griess reaction in the presence of the specified nitrite ion concentration. Oil droplet volume was 5 μL.

the oil adhesion property as indicated by the decrease in the CAH and receding contact angle (Figure 4.6A and C), keeping the underwater extreme oil repellence (advancing OCA >160°, Figure 4.6A and B) intact. The dual-functionalized coating exhibits a tilting angle, i.e., the minimum angle allowed to roll the beaded oil droplet (denoted as roll-off angle, θ_R) approximately 32° for a beaded oil droplet (5 µL). While the beaded oil droplet (5 µL) adhered to the tilted (~ 31°) dual-functionalized coating, the treatment of acidic sulfanilamide in the presence of nitrite ions at a concentration of 10 µM enabled the rolling of the same oil droplet, even at a lower tilting angle, i.e., ~ 26°, as depicted in Figure 4.7A, B. A similar trend was observed at higher concentrations of nitrite ions. On increasing the nitrite concentration, θ_R was gradually decreased, and a minimum $\theta_R \sim 8°$ was observed for the nitrite ions at a concentration of 50 µM, as shown in Figure 4.7A, B. The relationship between the θ_R and the concentration of nitrite ion ([C]) can be represented as:

$$\theta_R = 0.0001\,[C]^3 - 0.005\,[C]^2 - 0.47\,[C] + 29.79 \quad (1)$$

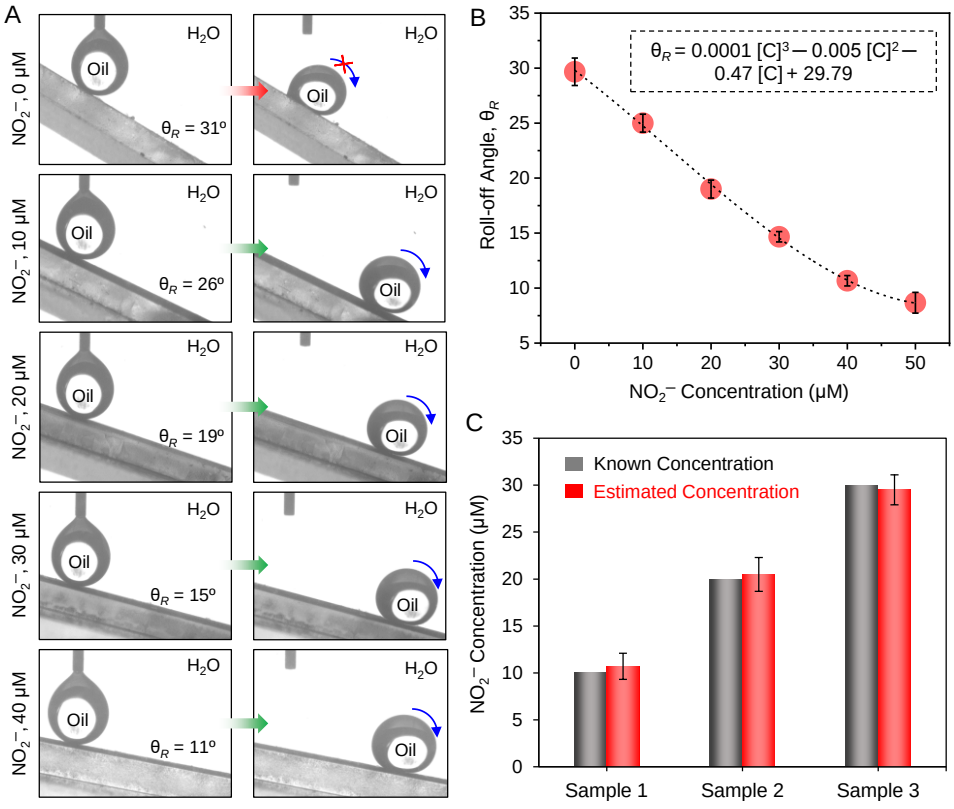

Figure 4.7. (A) Photographs of the mobility of oil droplets on PEDA/CEA-modified coating after Griess reaction as a function of nitrite ion concentration [C], at a minimum tilting angle where the oil droplets started rolling off. (B) Curve shows the roll-off angle (θ_R) of oil droplets as a function of nitrite ion concentration [C]. (C) Estimation of the nitrite ion concentration in contaminated samples using a calibration curve. Oil droplet volume was 5 µL.

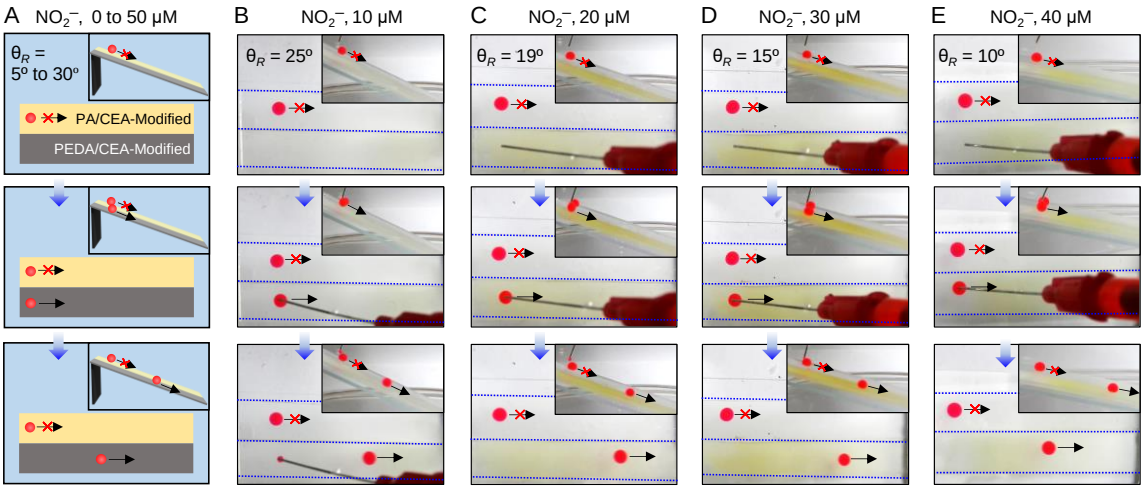

Figure 4.8. (A) Schematic illustration and (B−E) sequential photographs show the oil droplet mobility on PA/CEA and PEDA/CEA-modified interfaces placed alongside on a tilting surface after exposure to Griess reagents as a function of different nitrite ions concentrations, where beaded oil droplets adhere on the PA/CEA modified coatings irrespective of the tilting angle, whereas rolled-off on the PEDA/CEA modified coatings, at different tilting angles as a function of nitrite ion concentration. Oil droplet volume was 5 µL.

This relationship, presented in equation 1, allowed to estimate the concentration of unknown samples, as shown in Figure 4.7C. However, the rolling of the beaded oil droplets on a PA/CEA-modified coating was not observed as on the PEDA/CEA-modified coating. In this context, after similar exposure to acidic sulfanilamide solution in the presence of nitrite ions, a PA/CEA modified surface and a PEDA/CEA modified surface were placed side-by-side in a tilting surface, as depicted in Figure 4.8A. The beaded oil droplets remained pinned on the PA/CEA modified, irrespective of the tilting angle from 5º to 30º, whereas the beaded oil droplets rolled on the PEDA/CEA modified coating with decreasing the tilting angle while increasing the nitrite concentration (Figure 4.8B−E), This change in roll-off angle of beaded oil droplets follows the equation 1. Such alteration in the oil adhesion, reflected as the rolling of the oil droplets, only in the case of PEDA/CEA modified coating was noted due to the conversion of hydrophobic phenyl moiety into hydrophilic sulfonamide derived from sulfanilamide. Thus, this simple approach allows to detect the concentration of nitrite ions present in an aqueous solution just by monitoring the roll-off angle of the beaded oil droplet on the selected modified coating without using any equipment.

4.3.3. Modulation of Underwater Oil Wettability for Hydrazine Sensing

To illustrate the scope of this current design, completely different types of mono and dual-functionalization were adopted to sense another relevant toxic chemical, i.e., hydrazine (N_2H_4). Instead of using PEDA and CEA, TPA and AMP were strategically selected to develop another

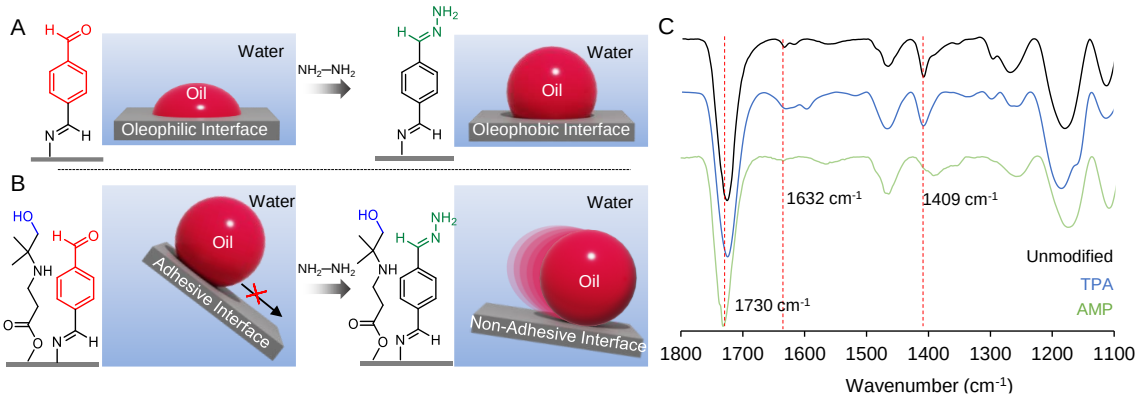

Figure 4.9. (A, B) Schematic depicting (A) mono (TPA)-functionalized multilayer coating exhibiting underwater oleophilicity and its conversion into oleophobicity, and (B) dual (TPA/AMP)-functionalized multilayer coating exhibiting underwater adhesive superoleophobicity and its conversion into non-adhesive superoleophobicity, after treatment with an aqueous solution of hydrazine. (C) ATR-FTIR spectra of the multilayer coatings before and after chemical modifications with TPA and AMP.

set of mono and dual-functionalized coatings, as depicted in Figure 4.9A and B. First, to achieve the mono-functionalized coating, the residual amines in the coating were modified with TPA via the Schiff base reaction. Next, the residual acrylates in the coating were subsequently modified with AMP via the 1, 4-conjugate addition reaction to obtain the dual-functionalized coating. The post-covalent modifications were characterized with ATR-FTIR spectral study (Figure 4.9C), where the appearances of the characteristic IR signatures at 1632 cm^{-1} for the

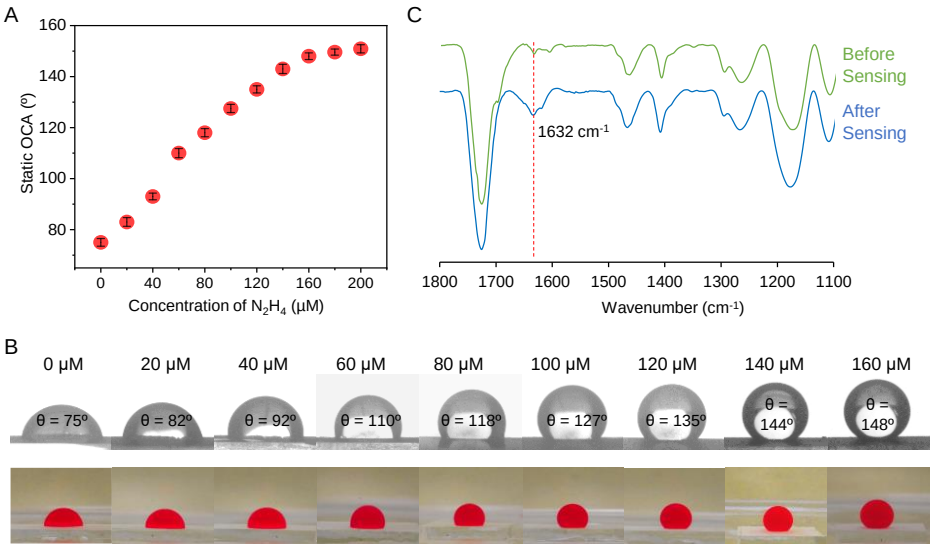

Figure 4.10. (A) The effect of hydrazine concentration on the alteration of static OCA on the TPA-modified coating. (B) Contact angle goniometer images and photographs show the effect of the concentration of hydrazine on the static OCA of oil droplets on TPA-modified multilayer coatings after the condensation reaction of the residual aldehydes on the coating with the hydrazine. (C) ATR-FTIR spectra representing TPA-modified coating before and after modifications with hydrazine.

imine (C=N) bond validated the covalent modification of the amines with the aldehyde of the TPA, and the depletion of IR peak corresponding to the vinylic C−H deformation (1409 cm^{-1}) with respect to the normalized IR signature for carbonyl stretching (1730 cm^{-1}), indicated the covalent post modification of the acrylates with AMP. In the case of the mono (TPA)-functionalized coating, the residual aldehyde group present in it allowed to demonstrate the raise in underwater OCA through Schiff base reaction with hydrazine, as shown in Figure 4.10A, B. The covalent modification with hydrazine is evident from ATR-FTIR analysis, where enhancement of the C=N peak (1632 cm^{-1}) was observed due to the covalent modification of the residual aldehydes with hydrazine (Figure 4.10C). A gradual elevation of underwater OCA was noticed with increasing the concentration of hydrazine (Figure 4.10 A, B). This method remained highly sensitive and OCA was raised by ~ 17° in the presence of 40 µM concentrated aqueous solution of hydrazine (Figure 4.10A).

On the other side, the dual (TPA/AMP)- functionalized coating displayed adhesive underwater superoleophobicity with advancing OCA of >160º and CAH of ~ 25º as shown in Figure 4.11A−C. Notably, a gradual depletion in the receding OCA and CAH with an increase in the exposed concentration of hydrazine, while maintaining the advancing OCA >160º (Figure 4.11A−C), which indicated the depletion in the oil adhesion property. As expected, the roll-off

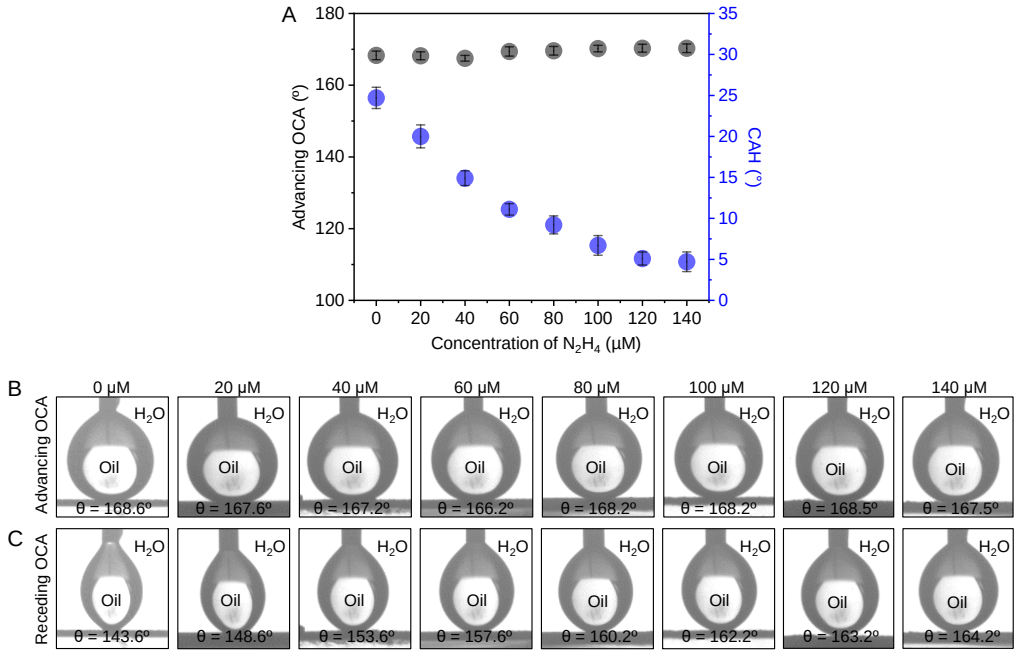

Figure 4.11. (A) Effect of concentration of hydrazine on the advancing OCA and CAH of oil droplets on TPA/AMP-modified coatings after treatment with an aqueous solution of hydrazine. (B) and (C) Contact angle goniometer images showing (B) advancing and (C) receding OCA on TPA/AMP-modified coating after modification with hydrazine. Oil droplet volume was 5 µL.

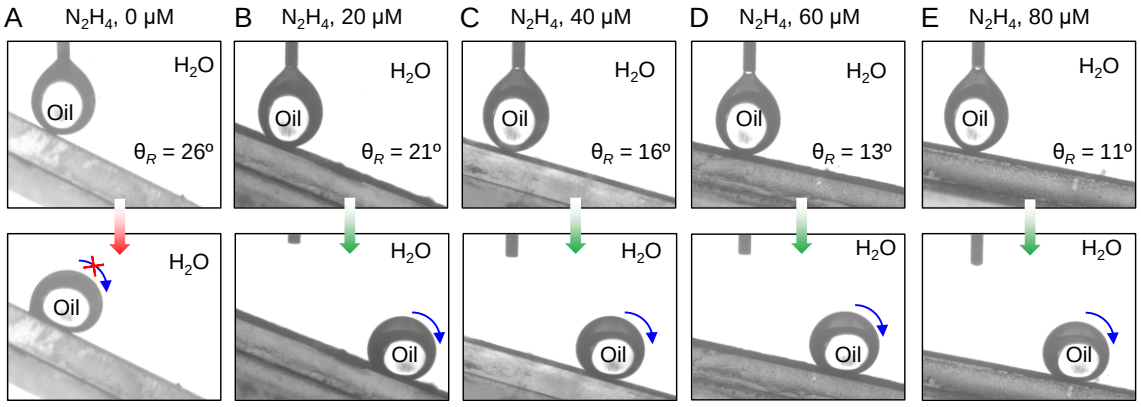

Figure 4.12. (A-E) Contact angle images showing the mobility of oil droplets on TPA/AMP-modified coating at a minimum tilting angle where the oil droplets started rolling-off, as a function of hydrazine concentration. Oil droplets volume was 5 µL.

angle of beaded oil droplets on the dual-modified coating was decreased on exposure to an aqueous solution of hydrazine, and its elevated concentration enabled the rolling of beaded oil droplets at a lower tilting angle, as shown in Figure 4.12. Thus, the rationally modified coatings allow to detect the concentration of hydrazine present in an aqueous solution just by monitoring the raise in OCA and roll-off angle of the beaded oil droplet on it without using any equipment.

Furthermore, I sought to demonstrate the reusability of the coatings after modifying with hydrazine several times to detect hydrazine. As the imine bonds get hydrolyzed at the acidic condition, the same mono and dual-functionalized coatings can be re-utilized for sensing hydrazine for multiple cycles—by acidic exposure in between, which allows to reset the coating for further sensing of hydrazine. As shown in Figure 4.13, a freshly mono (TPA)-

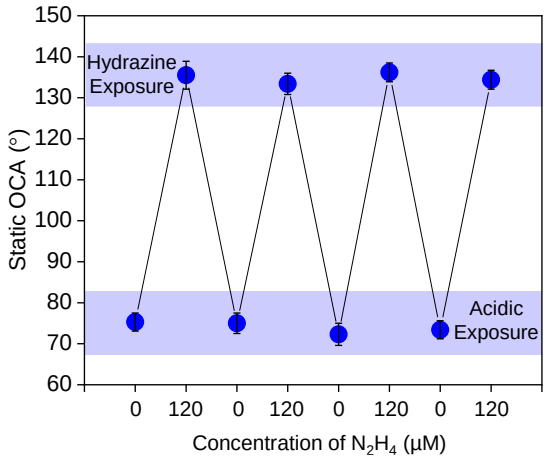

Figure 4.13. Reversible manipulation of the OCA on the TPA-modified coating after treatment with hydrazine, where the residual reactivity in the coating was re-installed by acidic solution treatment.

functionalized coating detects the concentration of hydrazine solution (120 μM) by altering its oil wettability from oleophobicity (OCA ~ 74º) to oleophobicity (OCA ~ 135º). Further, the acidic pH (pH 3) solution treatment facilitated the hydrolysis of the imine bonds and reinstalled the residual amines in the coating. Next, the treatment of the amines with the TPA and subsequent exposure to hydrazine exhibits a raise in the OCA (~ 135º) underwater (Figure 4.13). This process was repeated for multiple (4) cycles to demonstrate the reusability of the coating.

4.4. Conclusions

In this chapter, a simple and adequate mono and dual-functionalization of a dual reactive coating through a 1, 4-conjugate addition reaction at ambient conditions is introduced to depict raising of the OCA and rolling of a beaded oil-droplet underwater, respectively, only in the presence of targeted toxic chemicals (e.g., nitrite ion and hydrazine). The rational association of hydrophobic moiety through covalent bonds in the mono and dual-functionalized coatings and its conversion into a hydrophilic moiety following two independent reaction pathways in the presence of specific toxic chemicals, enabled the alteration in the oil wettability in the modified coatings. This toxic chemical responsive alteration in the oil wettability is reflected as i) raise in OCA (for mono-functionalized coating) and ii) rolling of beaded oil droplet (for dual functionalized coating) could be an economic and user-friendly methods for naked-eye and equipment-free sensing of relevant toxic agents (nitrite ions and hydrazine) present in water with high sensitivity and selectivity.

4.5. References

1 M. P. Ajith, S. Pardhiya and P. Rajamani, *Small*, 2022, **18**, 2105579.

2 H.-L. Hou, C. Anichini, P. Samorì, A. Criado and M. Prato, *Adv. Funct. Mater.*, 2022, **32**, 2207065.

3 C. Anichini, W. Czepa, D. Pakulski, A. Aliprandi, A. Ciesielski and P. Samorı, *Chem. Soc. Rev.*, 2018, **47**, 4860.

4 L. Zhang, Z. Li, J. Yang, J. Zhou, Y. Zhang, H. Zhang and Y. Li, *ACS Sens.*, 2022, **7**, 1183.

5 S. Tajik, H. Beitollahi, F. G. Nejad, I. Sheikhshoaie, A. S. Nugraha, H. W. Jang, Y. Yamauchi and M. Shokouhimehr, *J. Mater. Chem. A*, 2021, **9**, 8195.

6 T. Antón-Cánovas and F. Alonso, *Angew. Chem., Int. Ed.*, 2023, **62**, e202215916.

7 Z. Li, J. R. Askim and K. S. Suslick, *Chem. Rev.*, 2019, **119**, 231.

8 K. Xu, R. Zhou, K. Takei and M. Hong, *Adv. Sci.*, 2019, **6**, 1900925.

9 E. H. Koh, W.-C. Lee, Y.-J. Choi, J.-I. Moon, J. Jang, S.-G. Park, J. Choo, D.-H. Kim and H. S. Jung, *ACS Appl. Mater. Interfaces*, 2021, **13**, 3024.

10 F. Wang, L. Wang, X. Chen and J. Yoon, *Chem. Soc. Rev.*, 2014, **43**, 4312.

11 M. Lan, J. Wu, W. Liu, W. Zhang, J. Ge, H. Zhang, J. Sun, W. Zhao and P. Wang, *J. Am. Chem. Soc.*, 2012, **134**, 6685.

12 R. D. Crapnell and C. E. Banks, *Sens. Diagn.*, 2022, **1**, 71.

13 Z. Lu, W. Fan, X. Shi, Y. Lu and C. Fan, *Anal. Chem.*, 2017, **89**, 9918.

14 H. Yin, Y. Zhang, H. Dong, L. Liu, X. Wang, Y. Zhang, M. Xu and Y. Zhou, *ACS Appl. Nano Mater.*, 2022, **5**, 9737.

15 W. W. Yu and I. M. White, *Analyst*, 2013, **138**, 3679.

16 J. A. Kraai, A. X. Wang, G. L. Rorrer, *Adv. Mater. Interfaces*, 2020, **7**, 2000191.

17 M. Wang, H. Zhu, B. Liu, P. Hu, J. Pan and X. Niu, *ACS Appl. Mater. Interfaces*, 2022, **14**, 44762.

18 H. Wang, X. Wang and J. Cheng, *ACS Nano*, 2022, **16**, 14849.

19 U. Baruah and U. Manna, *Chem. Sci.*, 2021, **12**, 2097.

20 L. Singh and N. Ranjan, *J. Am. Chem. Soc.*, 2023, **145**, 2745.

21 Y. Ma, X. Song, X. Ge, H. Zhang, G. Wang, Y. Zhang and H. Zhao, *J. Mater. Chem. A*, 2017, **5**, 4726.

22 Z. Ma, J. Li, X. Hu, Z. Cai and X. Dou, *Adv. Sci.*, 2020, **7**, 2002991.

23 N. Vijay and S. Velmathi, *ACS Sustainable Chem. Eng.*, 2020, **8**, 4457.

24 X. Ma, K.-L. Tang, K. Lu, C. Zhang, W. Shi and W. Zhao, *ACS Appl. Mater. Interfaces*, 2021, **13**, 40942.

25 X. Gu and J. P. Camden, *Anal. Chem.*, 2015, **87**, 6460.

26 T. Liu, L. Yang, W. Feng, K. Liu, Q. Ran, W. Wang, Q. Liu and H. Peng, *ACS Appl. Mater. Interfaces*, 2020, **12**, 11084.

27 Y. Jung, I. G. Ju, Y. H. Choe, Y. Kim, S. Park, Y.-M. Hyun, M. S. Oh and D. Kim, *ACS Sens.*, 2019, **4**, 441.

28 A. Zhou, X. Chen, C. Li, W. Yang, J. He, T. Fang, W. Chen, Y. Xu, H. Ge, Z. Chen and X. Ning, *ACS Appl. Mater. Interfaces*, 2023, **15**, 2054.

29 N. Askari, A. Baghizadeh, A. Beheshti-Marnani, M. B. Askari and A. D. Bartolomeo, *Adv. Mater. Interfaces*, 2022, **9**, 2201180.

30 X. Liu, L. Tang, R. Niessner, Y. Ying and C. Haisch, *Anal. Chem.*, 2015, **87**, 499.

31 J. Lei, B. Wang, Y.-P. Li, W.-J. Ji, K. Wang, H. Qi, P.-T. Chou, M.-M. Zhang, H. Bian and Q.-G. Zhai, *ACS Appl. Mater. Interfaces*, 2021, **13**, 22457.

32 G. Bharath, A. Naldoni, K. H. Ramsait, A. Abdel-Wahab, R. Madhu, E. Alsharaeh and N. Ponpandian, *J. Mater. Chem. A*, 2016, **4**, 6385.

33 Y. Yao, R. K. A. Bennett, Y. Xu, A. M. Rather, S. Li, T. C. Cheung, A. Bhanji, M. J. Kreder, D. Daniel, S. Adera, J. Aizenberg and X. Wang, *Proc. Natl. Acad. Sci. U. S. A.*, 2022, **119**, e2211042119.

34 T. L. Mako, A. M. Levenson and M. Levine, *ACS Sens.*, 2020, **5**, 1207.

35 S. L. Bechler and D. M. Lynn, *Biomacromolecules*, 2012, **13**, 1523.

36 D. Parbat and U. Manna, *Chem. Sci.*, 2017, **8**, 6092.

37 J. Yanga, H. Wanga, Z. Taoa, X. Liua, Z. Wanga and R. Yuea, *Chem. Eng. J.*, 2019, **359**, 149.

Chemically Customizing Mechanical Properties and Optical Transparency in Underwater Superoleophobic Coating*

The inherent ability of bio-inspired underwater superoleophobicity to prevent oil/oily fouling underwater makes it appropriate for a wide range of applications related to environmental remediation, bio-adhesion, microfluidics, chemical sensing, etc.; however, the co-association of mechanical durability and optical transparency is essential for realistic performance. While the design of mechanically durable and absolutely optically transparent underwater superoleophobic coating remains challenging, here, a covalently cross-linked and chemically reactive sol-gel conversion process is introduced through 1, 4-conjugate addition reaction to achieve a substrate-independent and tolerant coating for orthogonally modulating the underwater oil wettability, optical transparency, and even mechanical properties of highly deformable porous and fibrous substrates. The post-modification of residual chemical reactivity in the prepared coating allows to embed underwater superoleophobicity, and the cross-linking chemistry improves the mechanical property of selected deformable substrates. Moreover, it displayed unperturbed performance even after prolonged (30 days) exposures in practically relevant chemically harsh aquatic conditions—including extremes of pH, artificial seawater, surfactant-contaminated water, etc. The approach is successfully applied to coat various substrates—including porous, fibrous, and planar objects, and it would be useful in protecting various relevant marine infrastructures from oil/oily fouling and various other potential applications.

*A. Borbora, M. Dhar, A. Shome, N. Barman, S. Roy and U. Manna, *Adv. Funct. Mater.*, 2023, **33**, 2302569**.**

5.1. Introduction

Marine infrastructures are extremely important for the mass transport of crude oil, trading of essential goods, communication, tourism, etc.[1-3] The accidental oil/oily spillages during the porting of crude oil/oily materials and maintenance of heavy machineries contaminate the marine environment and its infrastructures—including the platforms, subsea structures, pipelines, leisure vessels, seawalls, jetties, water tanks, and oceanographic sensors etc. and the subsequent microbial contaminations damage the infrastructures.[4-6] In this context, the design of a substrate-independent, durable, and optically transparent coating with the ability to 1) prevent oil/oily fouling and 2) transform a delicate and commercially available porous/fibrous substrate into mechanically hard and durable material is likely to provide remedies to the existing challenges at the marine environment. Inspired by the naturally existing underwater extreme oil-repellent property of biological creatures (e.g., nacre, fish scale, and seaweed), various research groups developed artificial underwater superoleophobicity to protect the interfaces from oil/oily fouling.[7-12] Such interfaces are with immense prospects for various relevant potential applications—including anti-biofouling, chemical sensing, developing efficient microfluidic devices, etc.[13-16] Moreover, the strategic association of such wettability with geometrically complex substrates (e.g., fibrous substrates) allowed to develop membranes for filtration-based oil/water and oil-in-water emulsions separation.[17-19] However, an adequate co-association of underwater superoleophobicity, durability (both mechanical and chemical), and optical transparency would be essential for its realistic applications in diverse and severe aquatic conditions. In the past, different approaches, such as deposition of metal oxides,[20-22] electrostatic multilayers,[23-24] polymeric hydrogels,[25-27] and other approaches[9,28-35] were introduced to achieve highly water absorbing interfaces decorated with hierarchical topography for conferring an artificial underwater superoleophobicity. However, the success of developing optically transparent and easily functionalizable bio-inspired coatings that survive various abrasive and challenging physical and chemical exposures is rare in the literature. More importantly, there has been no attempt to design an underwater superoleophobic coating that could transform highly deformable porous and fibrous substrates into non-deformable and mechanically robust materials that would perform in harsh aqueous conditions.

In some rare attempts in the past, mostly geometrically well-ordered structures[28-31,35] were introduced to attain mechanically durable underwater oil-repellent free-standing films and coatings on planar substrates. For example, Meng and co-workers introduced nacre-inspired biomineralized coating to achieve mechanically durable and optically transparent underwater

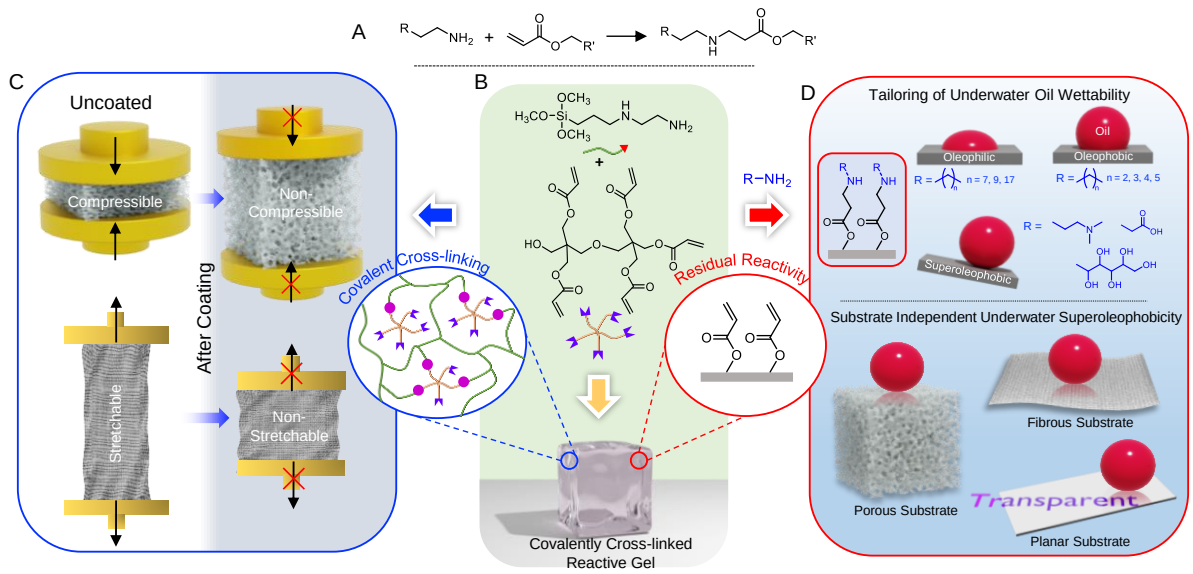

Figure 5.1. (A) 1, 4-Conjugate addition reaction between the amines and acrylates functionalities. (B) The mutual reaction between [3-(2-Aminoethylamino)propyl]trimethoxysilane (AEAPTMS) and dipentaerythritol penta-acrylate (5Acl) following the 1, 4-conjugate addition reaction yields a covalently cross-linked reactive gel comprising of residual acrylate moieties. (C) Schematic represents the customization of the mechanical properties (compressive and tensile) of the highly deformable porous and fibrous substrates after coating with the covalently cross-linked reactive gel. (D) Schematic depicting the tailoring of underwater oil wettability following the post modification of the residual acrylates on the coating with different amine-containing small molecules (top panel); and the development of substrate-independent and transparent underwater superoleophobicity on porous, fibrous and planar substrates (bottom panel).

superoleophobicity through the controlled association of single crystalline aragonite platelets. Although such nacre-inspired derivation of well-ordered crystalline structures provided promising results on planar substrates, the development of such well-ordered structures on geometrically complex (i.e., fibrous and porous) substrates would be challenging.[28-31,35] Moreover, the inherent instability of such earlier reported mechanically tough coating at relevant harsh settings (i.e., in acidic environment, presence of chelating agents, etc.)[28,30,35] would impact the uninterrupted performance of the embedded bio-inspired wettability at diverse aquatic conditions. Therefore, further design is essential to address the existing challenges related to substrate independence, uninterrupted performance in challenging marine environments, tailoring mechanical properties, and optical transparency—following a single and scalable fabrication process.

In this chapter, instead of designing another geometrically ordered structure, I have introduced a chemical approach (Figure 5.1A, B) for orthogonal tailoring of i) the mechanical property of highly deformable (compressive/tensile) porous/fibrous substrates (Figure 5.1C), and ii)

underwater oil-wettability (Figure 5.1D) through developing a covalently cross-linked and chemically reactive coating. In this design, the covalent cross-linking in the prepared coating tailored the mechanical property of selected porous/fibrous substrates, and the embedded residual reactivity of the coating enabled the modulation of underwater oil-wettability through the 1, 4-conjugate addition reaction[36-38] at ambient conditions. Moreover, the chemical composition of the selected reactants in the reaction mixture controls the optical transparency of the prepared coating. Thus, the single chemical approach allowed orthogonal modulation of underwater oil-wettability, optical transparency, and mechanical property of even porous and fibrous deformable substrates.

5.2. Experimental Section

5.2.1. Materials Required

3-(2-Aminoethylamino)propyl-trimethoxysilane (AEAPTMS), propylamine, butylamine, pentylamine, hexylamine, octylamine, decylamine and rhodamine-B were purchased from Sigma-Aldrich, India. Ethanol was purchased from Changshu Hongsheng Fine Chemical. Hexane was purchased from Alfa-Aesar. Polyurethane (PU) fabric, abrasive sandpaper, vegetable oil, and calibration weights were purchased from Amazon, India. Melamine formaldehyde (MF) sponge was procured from AR Acoustics LLP Maharashtra, India. Adhesive tape, aluminium foil, plastic, spectacles, petrol, diesel and kerosene were procured from local shops in Guwahati (Assam, India). Crude oil was obtained from Oil India Refinery, Assam. Vegetable oil and spray bottle was purchased from Amazon India. Bricks, granite, glass, tin plate, and PVC plastic were arranged from construction sites at IIT Guwahati, Assam, India. The details of all other materials and chemicals used in this work were discussed previously in Chapters 2 and 3.

5.2.2. Characterization

The mechanical strength of all the materials was determined using the ZwickRoell 5KN Electromechanical Universal Testing Machine (UTM). The compressive analysis of the sponges was performed using samples of dimensions 4 cm × 2.5 cm × 2 cm. The tensile analysis of the fabrics was performed using samples of dimensions 5 cm × 2 cm. Dynamic light scattering (DLS) measurements were conducted using a Zetasizer Nano ZS90 instrument (model no. ZEN3690). Stylus surface profilometer, Veeco (Dektak 150) was used to measure the thickness of the coating on glass substrate. To examine the optical transparency of prepared coating, the transmission spectra of the coatings on the planar substrate (glass) were recorded

underwater with the Perkin-Elmer UV Lambda 750 spectrometer in the wavelength range from 200 nm to 800 nm in double-beam mode. The other instruments used in this chapter for the characterization of synthesized materials were discussed previously in section 2.2.2 of Chapter 2.

5.2.3. Preparation of Chemically Reactive Coating on Deformable Porous and Fibrous Substrates

Different reaction mixtures were prepared by simply mixing AEAPTMS to the ethanolic solution of dipentaerythritol pentaacrylate (5Acl), keeping the same molar ratio of the two reactants 1:1. At first, 5Acl was dissolved in the desired amount for different reaction mixture compositions in ethanol. Then, the required amount of AEAPTMS was added to the previously prepared 5Acl solution and kept under mild agitation to get the chemically reactive solution. Table 5.1 provides specifics on reactant concentration for various reaction mixtures. Before depositing the different reaction mixtures as mentioned above in Table 5.1, the selected fabrics and sponges were thoroughly washed with acetone and methanol for several times and dried in oven. Pieces of MF sponge (5 cm × 2.5 cm × 2.5 cm) and PU fabric (13 cm × 12 cm) were dipped into these different reaction mixture solutions (50 ml) with mild agitation and taken out before the gelation started for that particular solution. Then, dip-coated substrates were dried in an oven at 70 °C for 1 h.

The obtained chemically reactive coated sponge and fabrics were further reacted with different amine-containing small molecules to embed tailorable underwater oil wettability. The oleophilic coating on selected substrates were post-covalently modified with 3-

Table 5.1. Accounting the compositions of selected reactants in different reaction mixtures.

Different Mixtures	Concentration of Reactants (5Acl and AEAPTMS) (M)	Molar Ratio of Reactants	Result
RM1	0.1	1:1	Turbid solution
RM2	0.2	1:1	Opaque Gel
RM3	0.4	1:1	Opaque Gel
RM4	0.6	1:1	Translucent Gel
RM5	0.8	1:1	Transparent Gel

(dimethylamino)-1-propylamine (DMAPA, 0.02 g ml^{-1} in ethanol) glucamine (3 mg ml^{-1} in water) and β-alanine (3 mg ml^{-1} in water) for 12 h to achieve underwater superoleophobicity. Further, to modulate the underwater oil wettability, the reactive coatings on fabric and sponge were post-modified with different amine-containing small molecules, propyl amine (0.02 mg ml^{-1} in ethanol), butylamine (0.02 g ml^{-1} in ethanol), pentylamine (0.02 g ml^{-1} in ethanol), hexylamine (0.02 g ml^{-1} in ethanol), octylamine (0.02 g ml^{-1} in ethanol), decylamine (2mg ml^{-1} in ethanol) and octadecylamine (3 mg ml^{-1} in ethanol).

5.2.4. Preparation of Optically Transparent and Underwater Superoleophobic Coating on Planar Substrates

To extend the concept of chemically reactive coating on planar substrates, water-in-oil type emulsion as prepared. Specifically, the reaction mixture (RM5) was prepared by dissolving 2.1 g of 5Acl in 5 mL of toluene, followed by adding 0.88 g of AEAPTMS to it. To this reaction mixture, different volumes of (0.5, 1, 2, 3, 4 and 5%) aqueous phase was added in the presence of a stabilizer, i.e., sodium dodecyl sulfate (SDS, 5 mM). The vortex mixing of the resultant deposition solution for the 30 s resulted in a water-in-oil type emulsion solution. The as-obtained reaction mixture containing water microdroplets was applied on different planar substrates, such as microscopic glass slide, large glass piece, plastic film, aluminium foil, granite slab, tin plate, and PVC plastic by adopting the doctor blade method, followed by oven drying at 70 °C for 1 h to evaporate the water droplets from the coating.

Next, to embed underwater superoleophobicity in the different substrates, the coated substrates with residual acrylates were subjected to post-modification with DMAPA (0.02 g ml^{-1} in ethanol) for 12 hours, followed by washing with ethanol and air drying.

5.2.5. Physical Abrasion on the Prepared Underwater Superoleophobic Materials

The durability of underwater oil wettability of DMAPA-modified coating on selected porous and fibrous substrates was tested using commonly adopted forms of physical abrasions and chemically contaminated aqueous phases. Details on the abrasion studies have been described in the section below.

a) Sand Paper Abrasion:

Underwater superoleophobic MF sponges (5 cm × 2.5 cm × 2.5 cm) were manually rubbed with abrasive sandpaper (400 grit) in a back-and-forth motion across a distance of approximately 300 cm with an applied load of 500 g. Underwater superoleophobic PU fabrics

(9 cm × 2.5 cm) were also subjected to sandpaper abrasion with an applied pressure of 25 kPa for a distance of about 3000 cm. The underwater oil wettability of the superoleophobic sponge and fabric was repeatedly tested using contact angle measurements and digital images.

b) Knife Scratch Test:

In the knife scratch test, coated PU fabrics and MF sponges were damaged manually with a sharp knife in random motion multiple times. Afterward, the underwater oil wettability of these damaged interfaces was examined through contact angle measurements and visual inspection by taking digital images.

c) Adhesive Tape Test:

In this test, an adhesive tape was attached to the surface of the coated fabrics and sponges with an applied load of 500 g to ensure proper contact between the coated substrate surface and adhesive tape. After 5 min, the tape was manually peeled from the surface. After every five cycles of the adhesive peeling test, a fresh adhesive surface was used, and the process was repeated 300 times. Finally, the underwater oil wettability was examined through contact angle measurements and visual inspection.

d) Sand Drop Test:

In a sand drop test, 150 g of sand was dropped from a height of 20 cm onto substrates that had been pre-tilted at a 45° angle. This test was conducted on both the underwater superoleophobic sponges and fabrics. Thereafter, the underwater oil wettability was investigated on both the underwater superoleophobic fabrics and sponges through contact angle measurements and digital images.

5.2.6. Chemical Durability of the Prepared Underwater Superoleophobic Coating

To examine the chemical durability, DMAPA-modified coating on fabrics, sponges, and glass substrates were subjected to various chemically contaminated aqueous phases for 30 days. The underwater static oil contact angle (OCA) and contact angle hysteresis (CAH) were measured at regular time intervals after exposing these materials to various chemically contaminated aqueous phases such as extremes of pH (pH1 and pH 12), surfactants contaminated water (SDS, 1M and dodecyltrimethylammonium bromide (DTAB, 1M)), river water and artificial seawater (solution of 0.226 g $MgCl_2$, 0.325 g $MgSO_4$, 2.673 g NaCl, and 0.112 g $CaCl_2$ in 100 mL of deionized (DI) water).

5.3. Results and Discussion

5.3.1. Development of Covalently Cross-linked Reactive Gel

In the past, β-amino-ester linkage was explored to improve the mechanical property of polymer networks.[39,40] Inspired by this inherent ability of β-amino-ester linkage, I have unprecedentedly applied the 1, 4-conjugate addition reaction between a self-polymerizable monomer, i.e., AEAPTMS and a cross-linker, i.e., 5Acl, at ambient conditions was adapted for developing a substrate-independent coating for orthogonally customizing mechanical property of selected deformable porous and fibrous substrates, underwater oil wettability, and the optical transparency of the prepared coating. In the past, the 1, 4-conjugate addition reaction was explored to construct a multilayer coating[38] of chemically reactive polymeric nanocomplex for modulating underwater superoleophobicity and oil adhesion, independently.[41,42] Such earlier laborious multi-step approach remained inappropriate to modulate the mechanical property of selected porous and fibrous substrates and the optical transparency of prepared coating. The mutual covalent reaction between AEAPTMS and 5Acl in ethanol yielded a covalently cross-linked, optically transparent, and chemically reactive gel within 10 min, as shown in Figure 5.2A, whereas the solutions of AEAPTMS and 5Acl in ethanol remained stable over time, as shown in Figure 5.2B and C. The concentration of two reactants in the reaction mixture significantly influenced both the gelation time and optical transparency of the yielded gel material, as shown in Figure 5.2D. In this context, five different reaction mixtures were prepared by varying the concentrations of 5Acl and AEAPTMS—keeping the molar ratio of

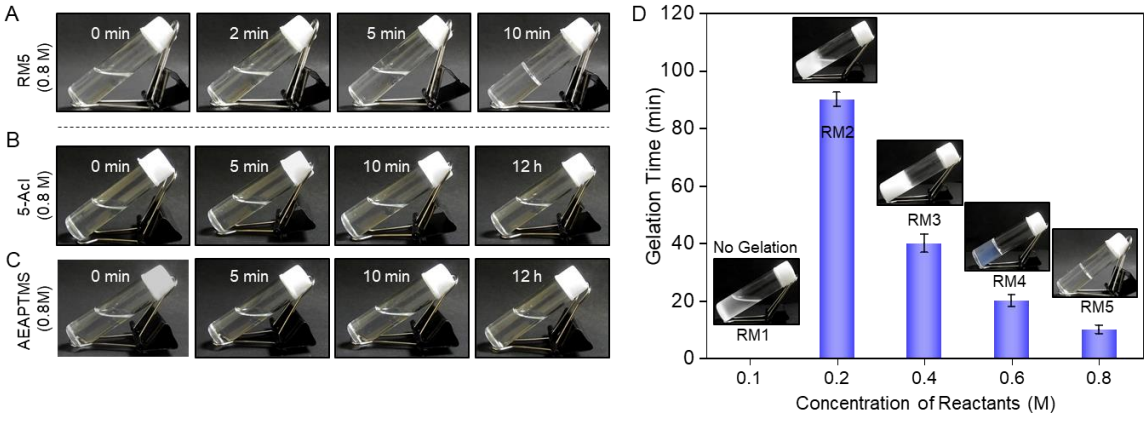

Figure 5.2. (A) The digital images depicting the progress of sol-gel conversion of the reaction mixture-5 (RM5, 0.8 M) that results in the formation of a transparent gel after 10 minutes. (B, C) Photographs representing the stability of (B) 5Acl and (C) AEAPTMS solutions over 12h in ethanol. (D) Time required for gel formation by the different reaction mixtures with the increased concentration of the reactants (AEAPTMS and 5Acl). Inset photographs are the resultant mixture after gel formation in the specified time.

selected reactants identical (1:1), as described in Table 5.1. Both the gelation time (from 90 to 10 min) and optical transparency were improved with increasing the molar concentration of reactants in the reaction mixture from 0.1 to 0.8 M, as shown in Figure 5.2D. The elevated concentration of the reaction mixture enhanced the access between two mutually reactive groups (amine and acrylate) in the solution—which contributed to the faster gelation through the 1, 4-conjugate addition reaction between the AEAPTMS and 5Acl at ambient conditions.

The progress of the reaction during gelation of the reaction mixture (having a concentration of 0.8 M for each reactant; labeled as RM5) of 5Acl and AEAPTMS, was monitored with attenuated total reflection-Fourier transform infrared (ATR-FTIR) spectral analysis, as shown in Figure 5.3A. During the 1, 4-conjugate addition reaction between amine and acrylate of AEAPTMS and 5Acl, respectively, a β-amino ester-type bond was formed through selective

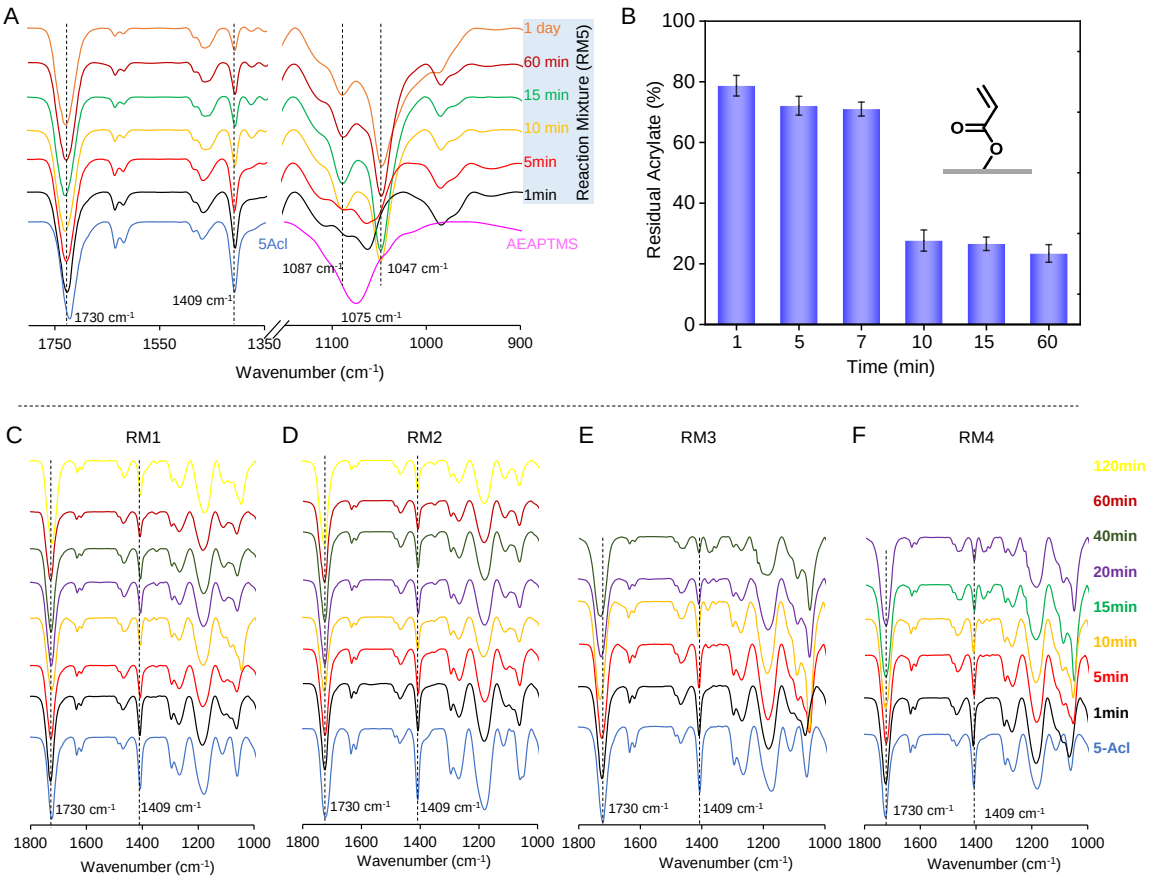

Figure 5.3. (A) Attenuated total reflection-Fourier transform infrared (ATR-FTIR) analysis of the reaction mixture, RM5, at different time intervals with respect to 5Acl (blue) and AEAPTMS (pink). (B) The percentage of residual acrylates in the reaction mixture, RM5, at different time intervals. (C−F) FTIR-ATR spectral analysis for the progression of reaction at different time intervals for different reaction mixtures (C) RM1, (D) RM2, (E) RM3, and (F) RM4, prepared in ethanol.

consumption of vinyl moiety of the acrylate functionality.[14,38,41] Hence, a gradual depletion of characteristic IR signature for symmetric deformation of the C─H bond of the vinyl group at 1409 cm^{-1} with respect to the IR peak for carbonyl stretching at 1730 cm^{-1} unambiguously validated the gradual consumption of acrylate moiety of the selected cross-linker toward the formation of β-amino ester-type cross-linking till the gelation of the entire reaction mixture. However, no significant depletion of the acrylate peak was noted further even after ageing the converted gel material for 1 day. The existence of this residual acrylate group in the prepared gel was estimated to be 23.4% (Figure 5.3B). Such depletion of acrylate signature was also noted for the diluted reaction mixtures (RM1, RM2, RM3, and RM4) (Figures 5.3C−F). The prepared optically transparent gel materials possessed residual acrylate groups (Figure 5.3B), which provided a facile and independent basis to post-modify the prepared material—through the 1, 4-conjugate addition reaction at ambient conditions, to tailor underwater oil wettability. The chemically modulated underwater oil wettability is separately accounted in the later section. On the other side, prominent and characteristic antisymmetric stretching vibrations of Si─O─Si at 1047 and 1087 cm^{-1} after 10 min for the RM5 suggested the self-polymerization of the silane moiety of AEAPTMS—after its cross-linking with the used cross-linker, i.e., 5Acl as shown in Figure 5.3A.

5.3.2. Customizing Mechanical Property of Deformable Porous and Fibrous Substrates

Next, taking advantage of such facile sol-gel conversion of the reaction mixture of the small molecule and cross-linker, two distinct (fibrous and porous) geometrically complex, and highly deformable (compressive and tensile) substrates were coated with the above-mentioned chemically reactive gel, following the dip-coating approach with the prepared reaction mixture. The stretchable PU fabric and compressible MF sponge were separately dipped into RM5, and selected substrates were isolated from the reaction mixture after 5 min of the chemical reaction and well before its gelation. After the complete gelation and oven drying, the mechanical property of the coated substrates was examined. The tensile and compressive modulus of the highly deformable substrates was significantly improved after the deposition of RM5 (Figure 5.4A), followed by its gelation. The coated fibrous substrate remained successful in withstanding an applied load of 2 kg with a nominal tensile strain of 10%, whereas 200% tensile deformation was noted for the uncoated fibrous substrate under an identical applied load (i.e., 2 kg), as shown in Figure 5.4C, D. In fact, the concentration of the reaction mixture controls tensile modulus of the coated fibrous substrate, as presented in Figure 5.4A. A similar impact of concentration of the deposited reaction mixtures was noted for the highly

compressible MF sponge as well, where the compressive modulus of the coated sponges was also gradually increased from 0.052 to 29.51 MPa (Figure 5.4A). The coated sponge derived from RM5 successfully tolerated an applied load of 5 kg—without any noticeable deformation of the coated substrate, whereas the uncoated sponge deformed significantly under the same applied load in the dry condition, as shown in Figure 5.4E, F. In a controlled study, two separate solutions (concentration of 0.8 m) of used reactants, i.e., 5Acl and AEAPTMS were independently deposited on the selected deformable substrates, which barely influenced the mechanical property of the coated substrates, as shown in Figure 5.4B. Thus, the mutual chemical reaction between 5Acl and AEAPTMS through the 1, 4-conjugate addition reaction resulted in cross-linkages—and attributed to the gradual improvement of both compressive and tensile modulus of the selected porous and fibrous substrates, as shown in the schematic

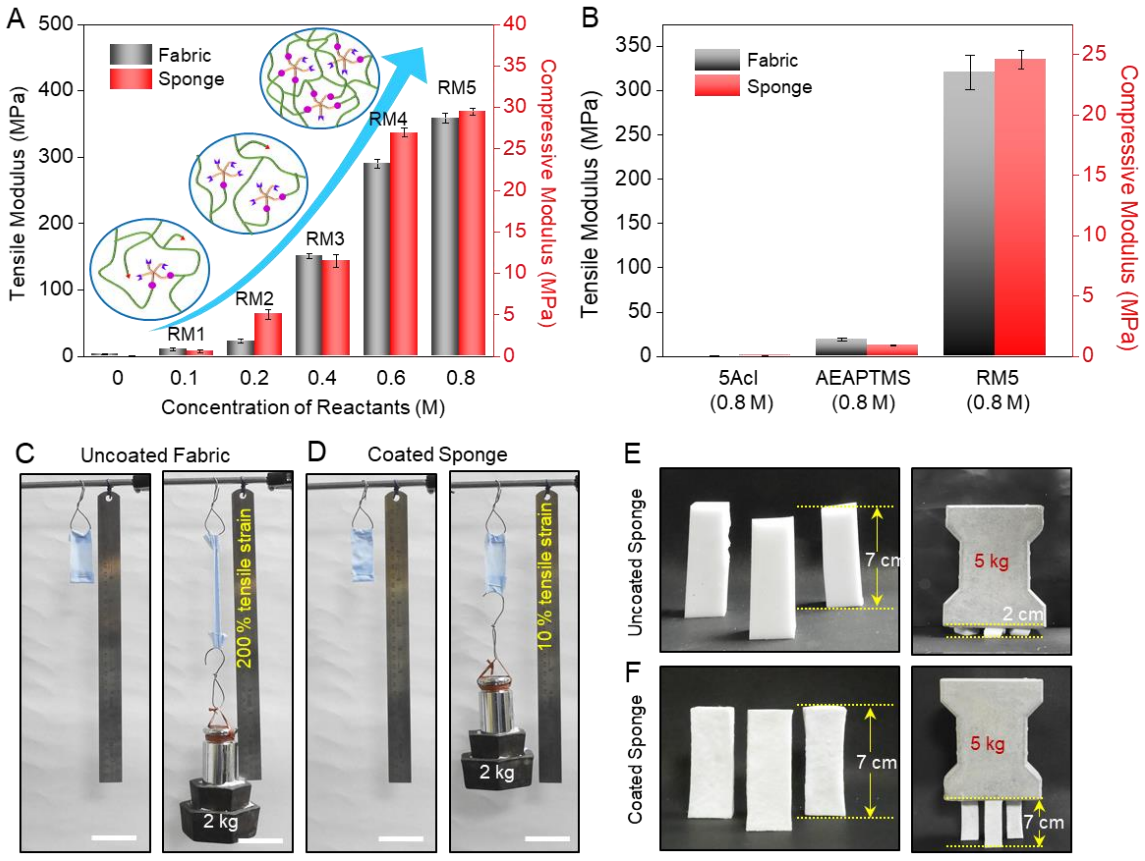

Figure 5.4. (A) Graph illustrates the impact of different reaction mixture coatings on the tensile modulus and compressive modulus of polyurethane (PU) fabric (grey) and melamine formaldehyde (MF) sponge (red), respectively. The inset schematic represents the increase of the cross-linking on the coating with the increment of the concentration of the reactants. (B) Comparison of tensile and compressive modulus of fabric and sponge coated with 5Acl, AEAPTMS and RM5 reaction mixture. (C, D) Digital images showing tensile deformation of (C) bare and (D) RM5-coated PU fabric under an applied load of 2 kg. Scale bars, 5 mm. (E, F) Photographs of compressive deformation of (E) bare and (F) RM5 coated MF sponge under an applied load of 5 kg.

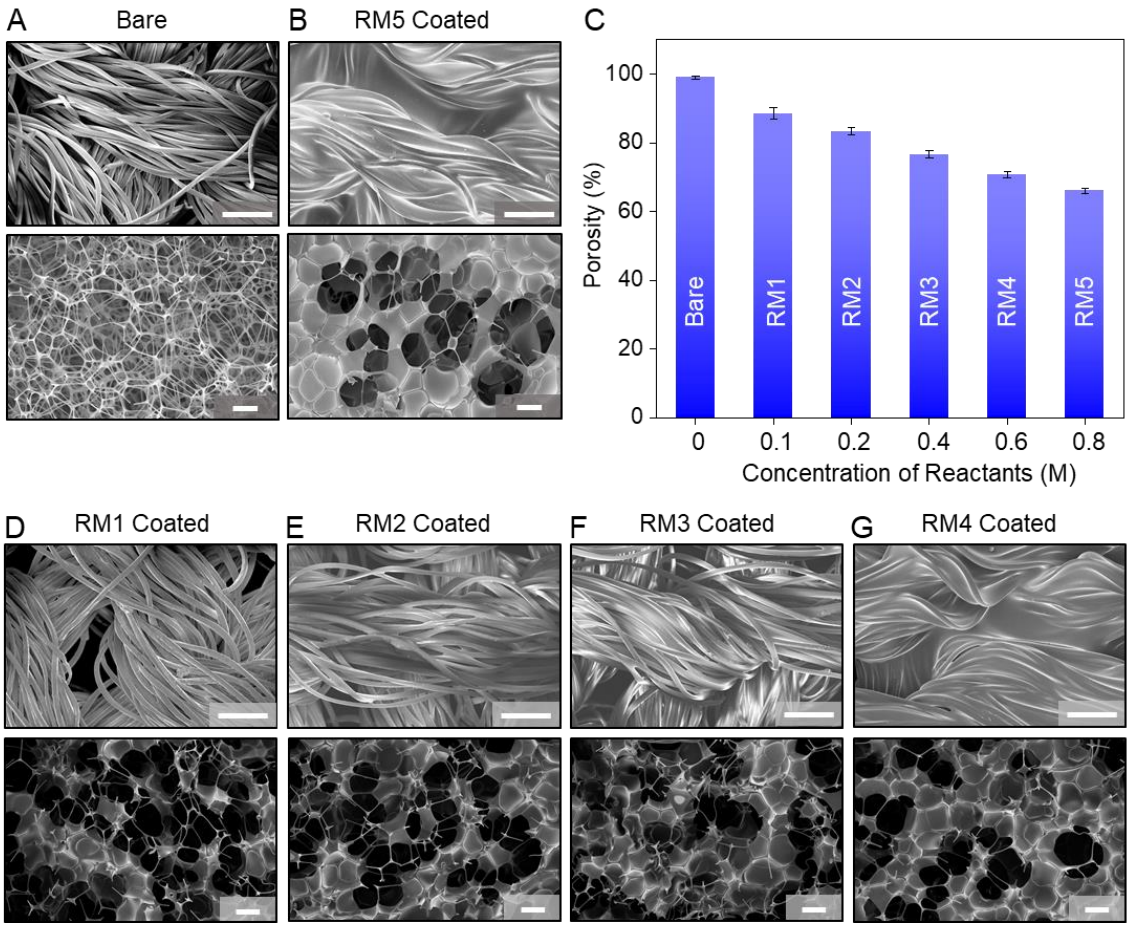

Figure 5.5. (A, B) Field emission scanning electron microscopy (FESEM) images of the (A) native and (B) coated PU fabric (top panel) and MF sponge (bottom panel), with reaction mixture RM5. (C) Porosity calculation for MF sponge after coating with different reaction mixtures. (D−G) FESEM images of PU fabric (top panel) and MF sponge (bottom panel) coated with different reaction mixtures- (D) RM1, (E) RM2, (F) RM3, and (G) RM4. Scale bars, 100 μm.

representation 5.4A (inset). Next, the field emission scanning electron microscopy (FESEM) imaging of the porous and fibrous substrates before and after the deposition of the reaction mixture (RM5) revealed the successful deposition of the coating, where the appearance of distinct morphology of the selected substrates, compare to their natives attributed to the sol-gel conversion of the reaction mixture on the respective and selective substrates, as shown in Figure 5.5A, B. Moreover, the deposition of the other reaction mixtures (RM1 to RM4) on the porous and fibrous substrates led to a similar change in its appearance under FESEM, as shown in Figure 5.5D−G. The pores of the selected porous substrates were covered with the deposited gel network, and eventually, the porosity of the coating also gradually decreased with increasing the concentration of reactants in the respective reaction mixture, as shown in Figure 5.5C.

5.3.3 Orthogonal Association of Underwater Oil Wettability

Thereafter, the residual chemical reactivity on the coating of the fabric and sponge was explored to achieve underwater superoleophobicity, following the post-modification through the 1, 4-conjugate addition reaction at ambient conditions. The ATR-FTIR analysis of the coating revealed the existence of residual acrylate groups on it (Figure 5.6A, black spectrum). The successful modification of the residual acrylate of the prepared coating with the selected amine-containing small molecule, DMAPA, through the 1 ,4-conjugate addition reaction at ambient condition is validated by the IR spectral analysis, where a significant depletion of the IR signature for residual acrylate groups at 1409 cm^{-1} is observed (Figure 5.6A, red spectrum) after the selected post-covalent modification. Such simple and appropriate chemical modification resulted in the extreme alteration in the underwater oil wettability (from

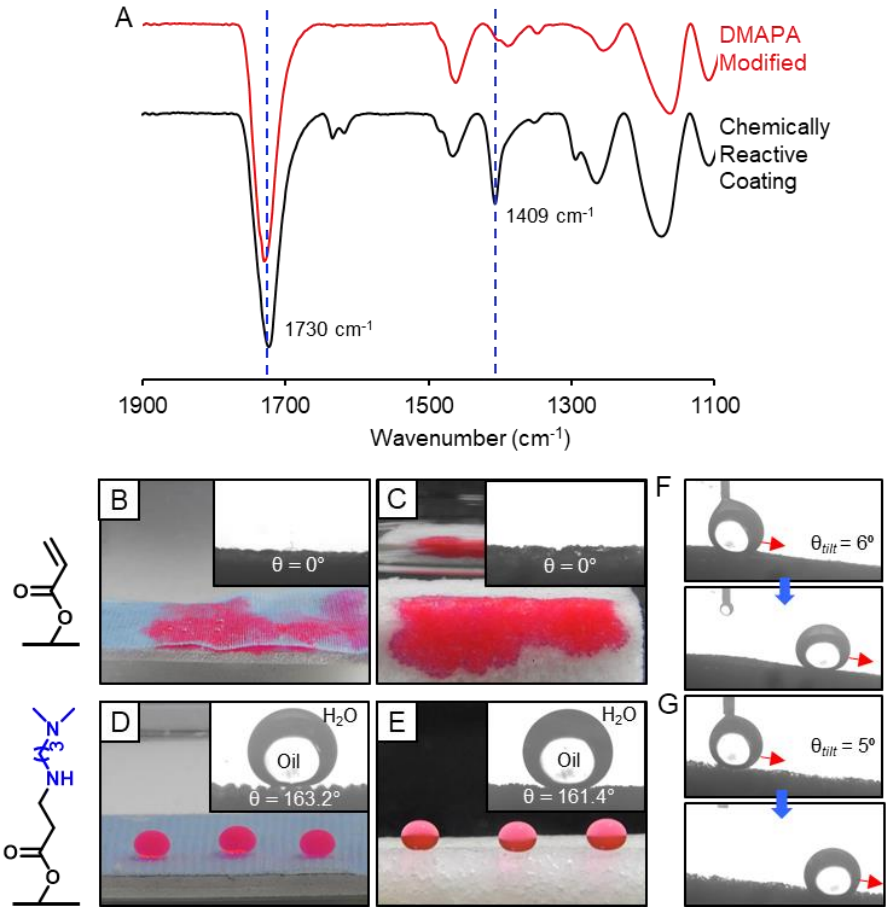

Figure 5.6. (A) ATR-FTIR spectra of the RM5 coating before (black) and after (red) post-modifications with N, N-dimethylaminopropylamine, DMAPA. (B−G) Photographs and contact angle goniometer images (inset) showing the underwater oil wettability of the RM5 coated (B, D) fabric and (C, E) sponge, (B, C) before and (D, E) after post-modification with DMAPA. (F, G) Contact angle goniometer images show the underwater rolling of beaded oil droplet (dichloroethane, DCE), on RM5 coated and DMAPA-modified (F) fabric and (G) sponge, at tilting angle of 6º and 5º, respectively.

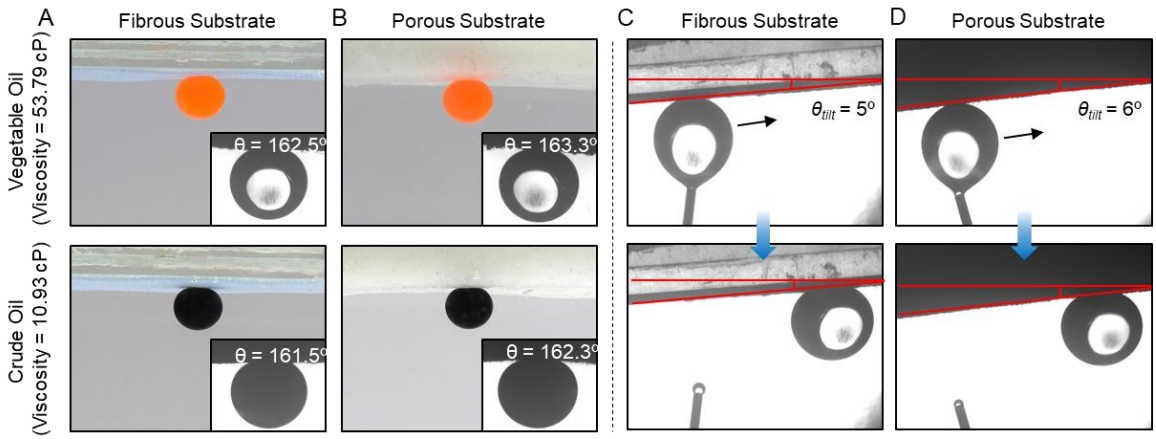

Figure 5.7. (A, B) Digital images and contact angle goniometer images (inset) showing the underwater vegetable oil (top panel) and crude oil (bottom panel) repellency of the RM5 coated (A) fabric and (B) sponge, after post-modification with DMAPA. (C, D) Contact angle goniometer images demonstrating roll-off angle for vegetable oil droplet beaded on modified (C) fabric and (D) sponge.

superoleophilicity to superoleophobicity) of the coated substrates, as shown in Figure 5.6B-E. As a consequence, droplets of model oil phase (dichloroethane (DCE); red colored aids visual inspection) beaded on the DMAPA-modified coated substrates with underwater OCA >160° (Figure 5.6D, E), whereas the same oil phase immediately soaked into the coated fibrous and porous substrates (Figure 5.6B, C). Thus, the underwater superoleophilic interfaces transformed into non-adhesive superoleophobic interfaces with a roll-off angle <10° (Figure 5.6F, G). Further, the underwater oil repellence property to higher viscous oils, e.g., crude oil (10.93 cP) and vegetable oil (53.79 cP) was examined, and the coated fibrous and porous substrates successfully exhibited non-adhesive underwater superoleophobicity with static OCA >160° (Figure 5.7A, B) and roll-off angle <10° (Figure 5.7C, D), after DMAPA modification. Thereafter, the self-cleaning ability of the prepared coating was demonstrated, where the selected viscous vegetable oil was placed on the prepared coating to contaminate the dry interface in air, prior to submerging into the water. The de-wetting of the spread and spilled oil phase, followed by the detachment of vegetable oil, was noticed immediately after transferring the oil-contaminated interface into the aqueous phase, as shown in Figure 5.8. Additionally, such a strategy of facile post-modification of the residual reactivity in the coating

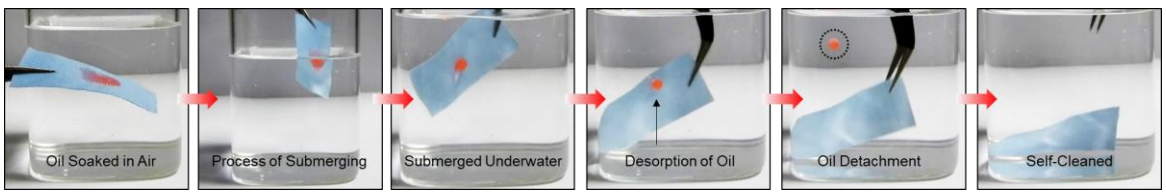

Figure 5.8. Snapshots showing the process of immersion of the vegetable oil fouled coated fabric into the water, its oil desorption, and self-cleaned performance underwater.

with primary amine-containing other hydrophilic small molecules, glucamine, β-alanine, etc., also yielded underwater non-adhesive superoleophobicity, as shown in Figure 5.9A. However, the selection of hydrophobic alkylamines as modifiers provided a facile basis to modulate other intermediate underwater oil-wettability. For instance, on increasing the length of hydrocarbon tails (from ─C_3H_7 to ─$C_{18}H_{37}$) in the selected alkylamines—propylamine (n = 2), butylamine (n = 3), pentylamine (n = 4), hexylamine (n = 5), octylamine (n = 7), decyamine (n = 9), and octadecylamine (n = 17)— the underwater OCA gradually decreased from 150° to 0°, as shown in Figure 5.9A. Furthermore, the successful post-covalent modifications of the coating with the modifiers mentioned above were characterized by ATR-FTIR analysis (Figure 5.9B. Thus, the existing residual acrylate groups allowed the customization of desired underwater oil-wettability through facile chemical modifications at ambient conditions.

In the next set of experiments, the mechanical property of the coated substrates, both in dry and wet conditions, was examined after the association of chemically modulated extreme underwater oil repellence. In this context, different reaction mixtures (from RM1 to RM5) were individually applied to dip coat a stretchable fibrous substrate prior to post-modification with DMAPA. All the coated and DMAPA-modified fibrous substrates displayed underwater superoleophobicity with OCA >160°, irrespective of the concentration of the reaction mixture, as shown in Figures 5.10A, C. Such post-modification of reactive coating on selected substrates barely affected the mechanical properties of the coated substrates. As expected, on increasing

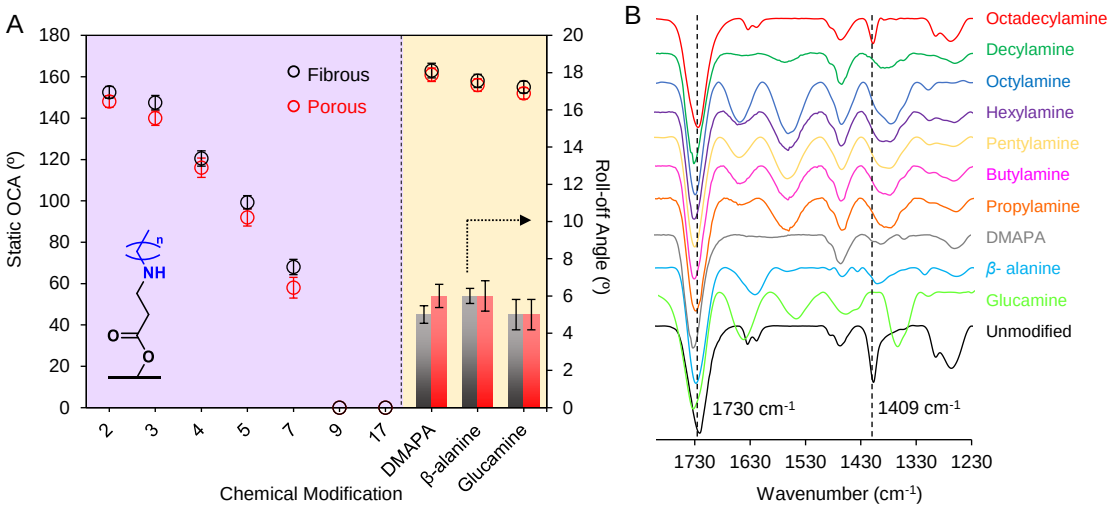

Figure 5.9. (A) Graph representing the impact of post-modification of the residual acrylates with different amine-containing small molecules (e.g., propylamine, butylamine, pentylamine, hexylamine, octylamine, decylamine, octadecylamine, DMAPA and β-alanine, and glucamine) on the underwater static oil contact angle (OCA) and roll-off angle of the RM5 coated fabric (black) and sponge (red). (B) FTIR-ATR spectra of RM5 coating after post-chemical modification with different amine-containing small molecules.

the concentration of the reaction mixture (with a constant molar ratio of reactants at 1:1), the mechanical property of the coated fibrous substrates displayed a gradual and significant improvement of tensile modulus—both at the dry and wet conditions (soaked with water) of the coated substrates, as shown in Figure 5.10A. In the wet condition, the tensile modulus of the coated (with RM5) fibrous substrate was observed to be 320.8 MPa, which is significantly higher (115 folds) in comparison to the native substrate. Similar results were obtained by substituting the stretchable fibrous substrate with the highly compressible sponge, as shown in Figure 5.10B, D. Although the coated fibrous substrate exhibited restrictions to tensile deformation, it remained highly flexible for repetitive bending, twisting, and rolling, as shown in Figure 5.10E. Thus, the facile 1, 4-conjugate addition reaction between a small molecule and a cross-linker provided an avenue to convert the highly deformable substrates to non-

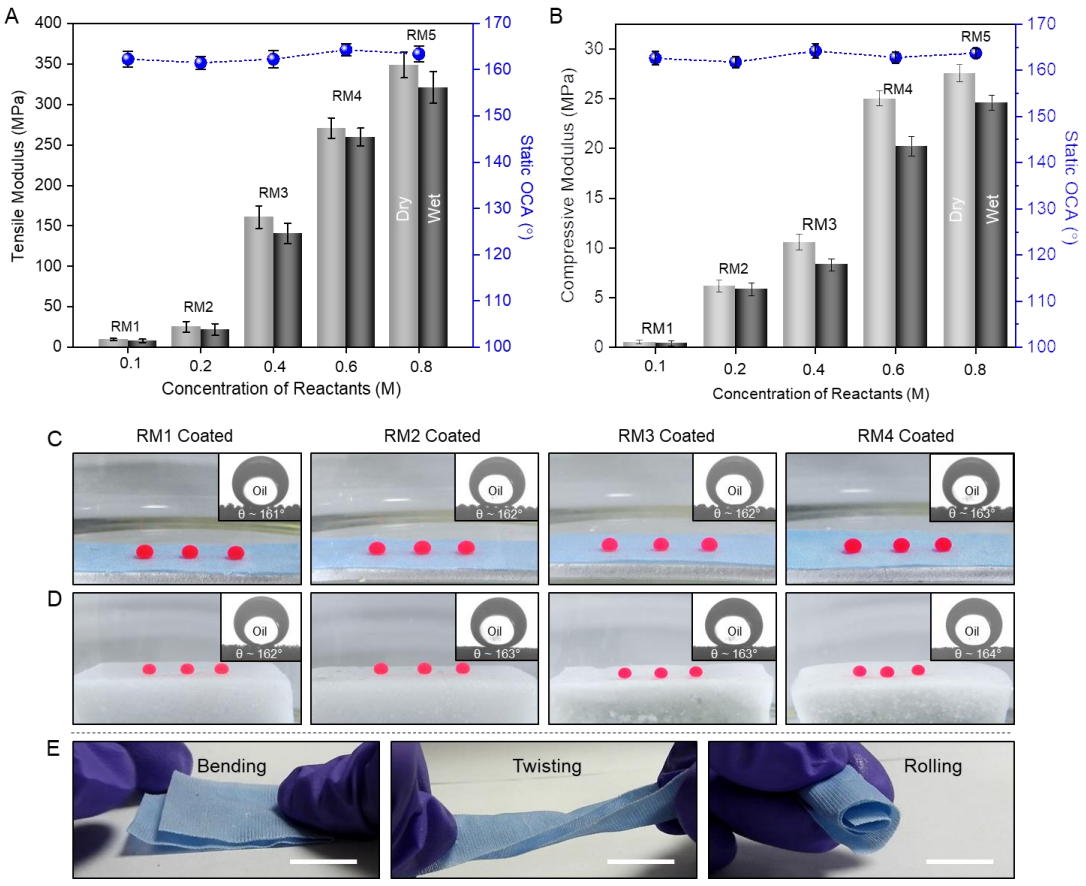

Figure 5.10. (A, B) Graph representing tensile/compressive modulus (dry (grey) and wet (black) conditions) and underwater static OCA (blue) of (A) PU fabrics and (B) MF sponges, after individually coating with different reaction mixtures (from RM1 to RM5) and sequentially post-modifying with DMAPA. (C, D) Photographs and contact angle goniometer images (inset) of beaded oil droplets underwater on RM1, RM2, RM3 and RM4 coated (C) fabrics and (D) sponges, after DMAPA modification. (E) Photographs demonstrating physical manipulation, such as bending, twisting, and rolling of RM5-coated fabric. Scale bars, 2 cm.

deformable materials with tailorable underwater oil wettability. Reports on such versatile coating having the ability to modulate orthogonally the mechanical property as well as underwater oil wettability on a highly deformable substrate are unprecedented.

5.3.4. Durability of Coated Substrates and Embedded Oil-wettability

The underwater superoleophobicity performs only in wet conditions, hence, the physical and chemical durability of the artificial underwater superoleophobic materials is essential for its prospective outdoor applications. In this section, we examined the various practically relevant and commonly adopted severe physical and chemical durability tests on the coated and sequentially DMAPA-modified substrates individually derived from both RM1 and RM5 for comparing the stability of both substrates and embedded underwater oil wettability. In this context, the respective coated fibrous substrates were separately abraded with sandpapers with

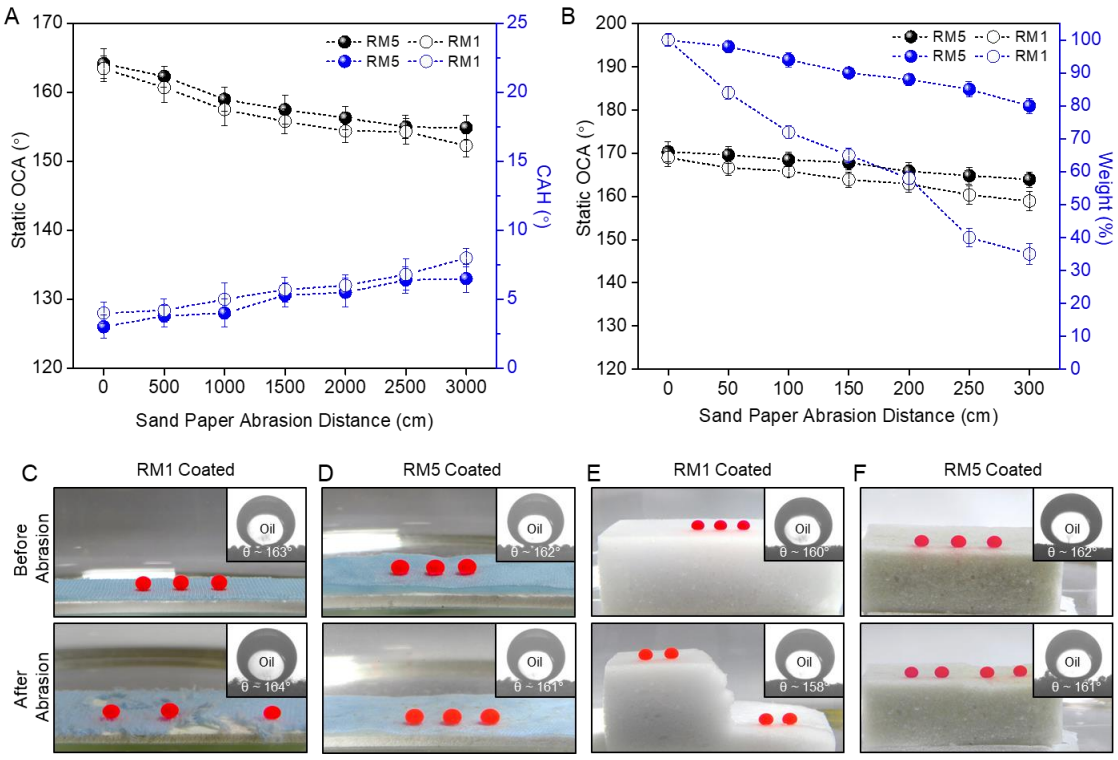

Figure 5.11. (A) Graph illustrating the effect of sandpaper abrasion over a distance of 3000 cm on underwater static OCA (black) and contact angle hysteresis (CAH, blue) of the RM1 and RM5 coated underwater superoleophobic fabric. (B) Graph illustrating the effect of sandpaper abrasion over a distance of 300 cm on underwater static OCA (black) and percentage weight loss (blue) of the RM1 and RM5 coated underwater superoleophobic sponges. (C, D) Photographs and contact angle goniometer images (inset) depict the oil repellence property of (C) RM1 and (D) RM5 coated fabrics before and after 3000 cm of sandpaper abrasion distance. Photographs and contact angle goniometer images (inset) showing the underwater superoleophobicity of (E) RM1 and (F) RM5 coated sponges before and after 300 cm of sandpaper abrasion distance.

an average speed of 35 cm s^{-1} under an applied external pressure of 25 KPa. Both underwater static OCA and CAH were measured at regular intervals of the sandpaper abrasion distance, as shown in Figure 5.11A. The embedded underwater non-adhesive superoleophobicity in both the coated substrates remained intact with OCA >150° and CAH <10°—even after the application of abrasive sandpaper for a 3000 cm distance (Figure 5.11A, C and D). However, the physical integrity of the coated fabric derived from RM1 was significantly damaged and started tearing apart after applying the sandpaper abrasion for just a 1000 cm distance (Figure 5.12A). In comparison, the other coated (RM5) fibrous substrate successfully survived the sandpaper abrasion distance of 3000 cm, as shown in Figure 5.12B, without any noticeable physical damage in the treated substrate. A similar result was noticed for a highly compressible porous substrate coated individually with RM1 and RM5—followed by DMAPA post-modification. The sandpaper abrasion process led to a gradual and significant physical erosion of the RM1 coated substrate and the 300 cm of abrasion distance resulted in a weight loss of ≈ 65%, as shown in Figures 5.11B, E and 5.12C. However, significantly less physical erosion (20% weight loss) was noted for the substrate coated with RM5 at the identical experimental

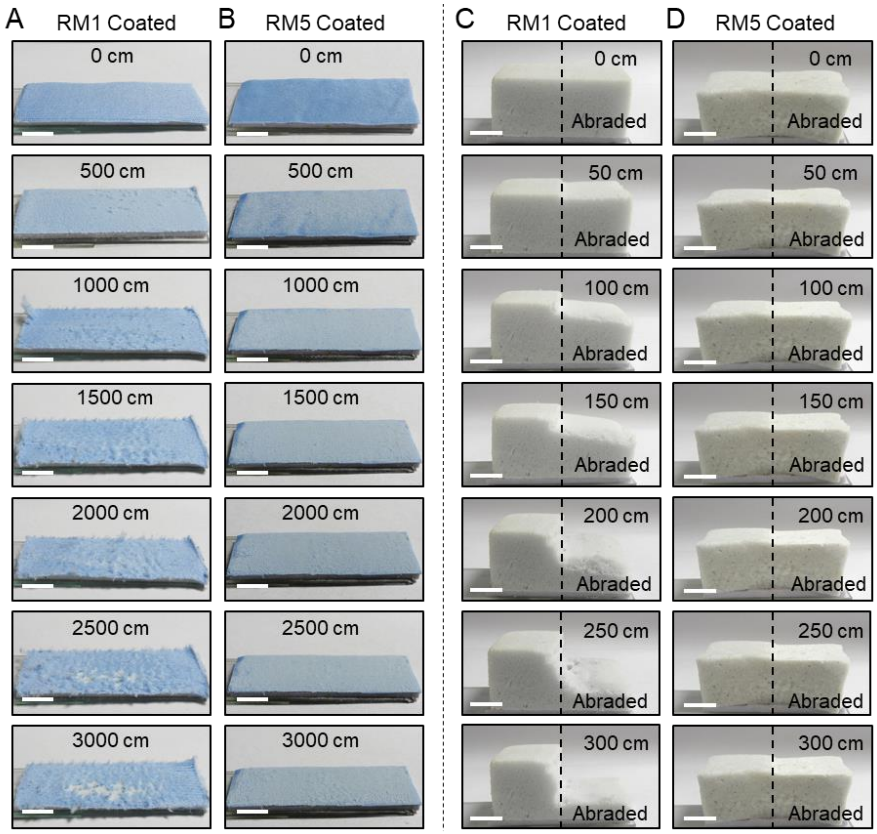

Figure 5.12. (A, B) Sequential photographs comparing the physical integrity of (A, B) fabrics and (C, D) sponges coated with two different reaction mixtures, (A, C) RM1 and (B, D) RM5, during sandpaper abrasions at different abrasion distances. Scale bar = 1cm.

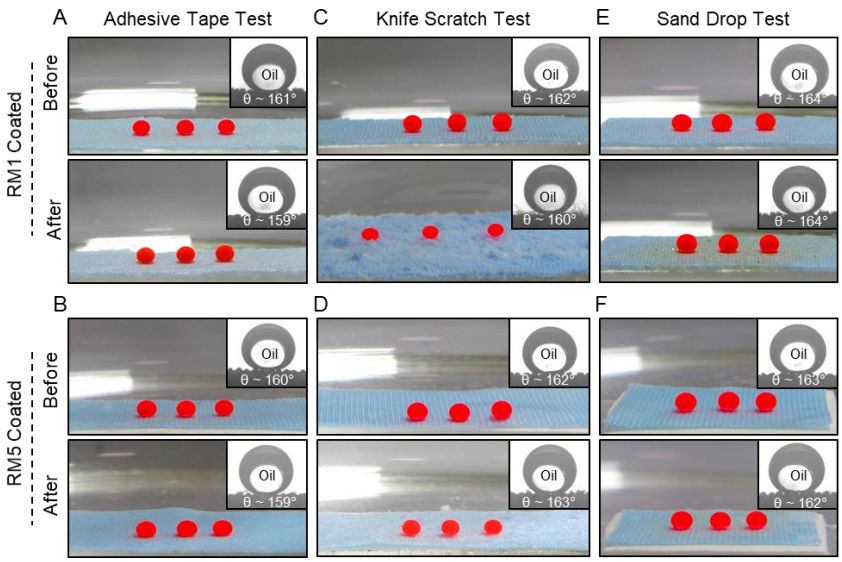

Figure 5.13. (A−F) Photographs and contact angle goniometer images (inset) of beaded oil droplets underwater on RM1 (A, C, E) and RM5 (B, D, F) coated fabrics before and after adhesive tape test (A, B), knife scratch test (C, D), and sand drop test (E, F).

set-up (Figure 5.11B, F and 5.12D). Irrespective of the physical erosion of the materials, the embedded underwater superoleophobicity remained intact with underwater OCA of >150° (Figure 5.11E, F). Thereafter, both the coated fibrous and porous substrates were subjected to other physical abrasion processes—including adhesive tape peeling test (with an applied load of 500 g), sand drop test (150 g from 20 cm height), knife scratch test, and both the underwater

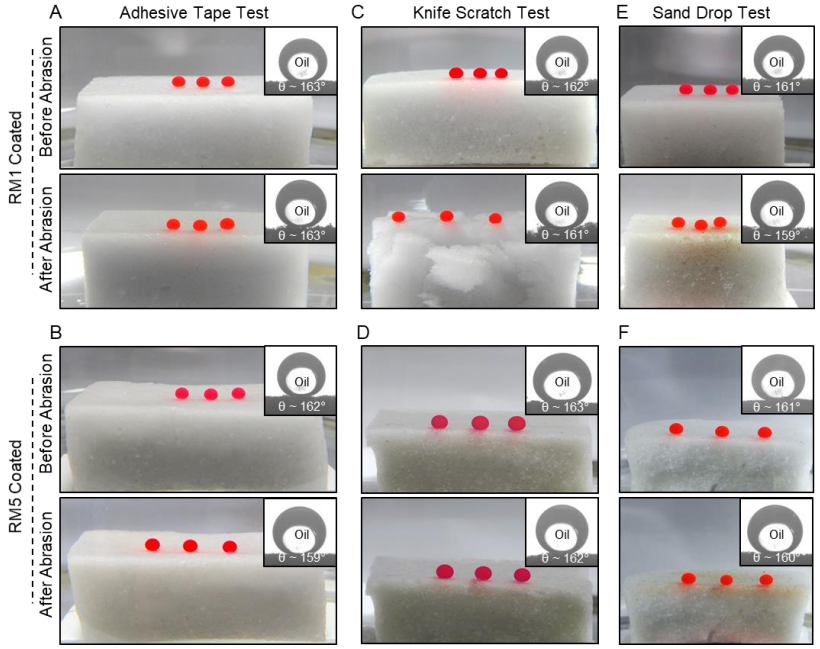

Figure 5.14. (A−F) Photographs and contact angle goniometer images of beaded oil droplets underwater on RM1 (A, C, E) and RM5 (B, D, F) coated sponges before and after adhesive tape test (A, B), knife scratch test (C, D,), and sand drop test (E, F).

superoleophobicity and physical integrity remained intact as shown in Figures 5.13 and 5.14. Thus, the design of bio-inspired coating displays an abrasion-tolerant underwater superoleophobicity—and importantly, the improved mechanical property protects the substrates from unwanted physical damage at severe abrasive conditions. Additionally, the prepared coating remained efficient in tolerating exposures to subzero (−18 °C) and elevated (70°) temperatures without compromising the embedded underwater superoleophobicity (Figure 5.15A, B). A separate experiment was performed to examine the tolerance of the coating underwater toward applied external pressure. During the adhesive force measurement, a suspended oil droplet placed on a metal holder was beaded and squeezed on the coated surface with a specific preload force, prior to detaching the same oil droplet from the surface. The change in force was measured by a highly sensitive microbalance. The underwater adhesive force for the oil droplet remains in the range between 0 to 4.1 ± 0.2 µN upon increasing the preload force from 0 to 80 µN. However, the adhesive force increased slightly to 9.3 ± 1.2 µN when the preload force was further increased to 100 µN, as shown in Figure 5.15C.

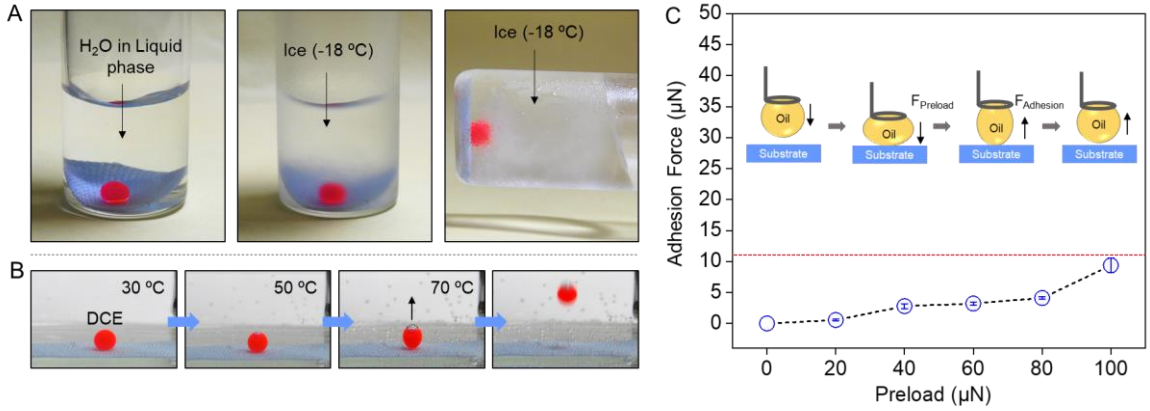

Figure 5.15. (A) Sequential digital images of beaded oil droplets (DCE) on coated fabric underwater, after freezing (-18 °C) the water phase and tilting the frozen water phase at 90°. (B) Illustrating the effect of the elevated temperature of the water phase on the oil-wetting property of the coated fabric, where the temperature was raised from 30 °C to 70 °C. During the process of elevating the temperature of water, vaporized gas bubble adhered to beaded oil droplet pushes upward direction, the beaded droplet left the coated fabric at 70 °C without leaving any oil residue. (C) Adhesion force versus preload force of oil droplet (DCE, 10 µL) underwater, demonstrating low adhesion until the preload force reaches to 100 µN.

This fish-scale inspired bio-inspired wettability specifically performed underwater conditions, hence the development of underwater superoleophobicity serving unperturbed extreme oil repellency at diverse and severe aquatic conditions is essential for its prospective application in “real-world” scenarios. In this context, some recently developed mechanically durable underwater superoleophobic coatings inherently remained inadequate to perform at either

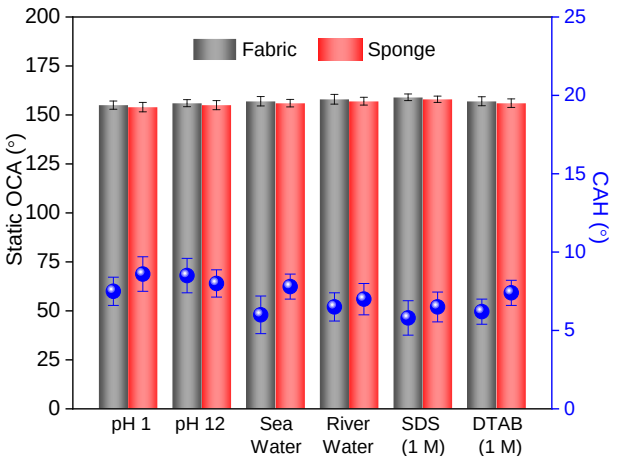

Figure 5.16. The underwater static OCA and CAH (blue) on the RM5 coated underwater superoleophobic fibrous (grey bar) and porous (red bar) substrates after continuously exposing the coatings to various chemically contaminated aqueous phases for 30 days.

acidic[28,35] or alkaline[27] conditions. However, further design is essential to achieve mechanically and chemically durable underwater superoleophobicity in diverse corrosive environments. Thus, the chemical stability of the fibrous and porous substrates coated with RM5 and post-modified with DMAPA was examined by exposing them to various harsh aquatic conditions—including extremes of pH (1 and 12), artificial seawater, and surfactant contaminations (cationic: DTAB and anionic: SDS; 1 M) for a prolonged duration, i.e., 30 days. Notably, irrespective of the nature of aquatic exposure, the coated substrates displayed an uninterrupted underwater superoleophobicity with underwater static OCA >150° and CAH <10°, as shown in Figure 5.16. Such chemical durability is attributed to the existence of β-amino ester-type cross-linking through the 1, 4-conjugate addition reaction.

5.3.5. Optically Transparent Underwater Superoleophobic Coating on Planar Substrates

Unlike fibrous and porous substrates, whose inherent topographies contribute to achieving underwater superoleophobicity, developing such oil-repellence property on featureless substrates is more challenging as it demands co-optimization of both essential topography and adequate surface chemistry. Thus, I sought to achieve such bio-inspired transparent coating on a featureless planar substrate following a simple doctor blade method—that requires much less deposition solution compared to the dip coating method. The deposition of the same reaction mixture—i.e., RM5 on a microscopic glass slide (model planar substrate) resulted in a transparent and chemically reactive coating, but unfortunately, it remained incapable of exhibiting underwater superoleophobicity—despite the DMAPA modification (as confirmed by IR spectral analysis, Figure 5.17C), instead, displayed underwater oleophobicity with an

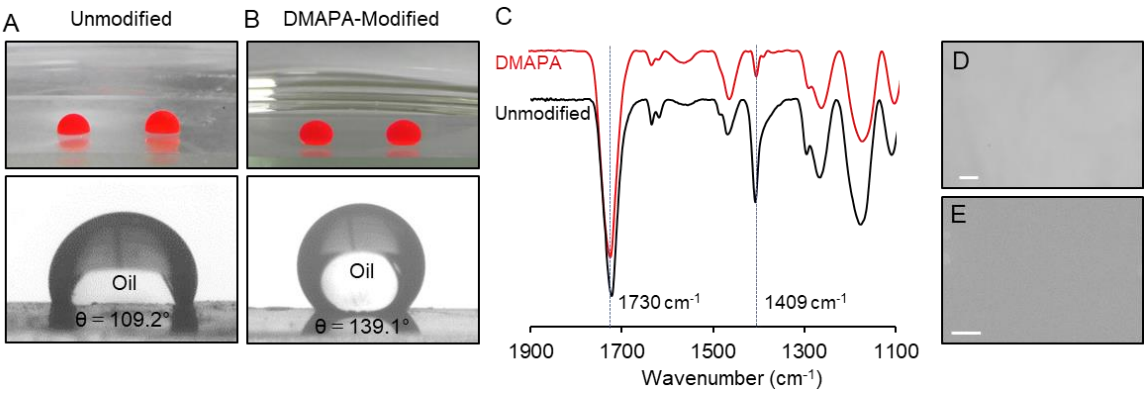

Figure 5.17. (A, B) Digital images and contact angle goniometer images of beaded oil droplet underwater on a glass slide coated with ethanolic solution of RM5 (A) before and (B) after DMAPA modification. (C) FTIR-ATR spectra of RM5 coating (black spectra) after post modification with DMAPA (red spectra). (D) Optical microscope and (E) FESEM images of a glass slide coated with ethanolic solution of RM5. Scale bars, 20 µm for D and 5 µm for E.

OCA of 138.6 ± 1.2° (Figure 5.17A, B). The FESEM images revealed the lack of essential hierarchical topography in the deposited coating on the glass substrate (Figure 5.17E). To generate adequate topography on a planar surface for conferring underwater superoleophobicity, another simple strategy was introduced, where micrometer-sized droplets of DI water were dispersed in the reaction mixture prior to coating the planar objects, which resulted in the generation of essential topography after solvent evaporation. In this context, AEAPTMS and 5Acl (RM5) were dissolved in a water-immiscible organic solvent, i.e., toluene instead of ethanol, and the inverse emulsion of DI water was generated by vortex mixing for 30 s in the presence of a stabilizer, i.e., SDS (5 mM), as shown in Figure 5.18A. Notably, on increasing the water content in the reaction mixture, the gelation time was reduced, but the prepared gel became optically opaque beyond the water content (v/v) of 2% (Figure 5.18D, E); therefore, the reaction mixture with 2% (v/v) DI water was selected to coat on a planar surface (thickness 294.3 ± 11.2 nm). The formation of microdroplets of water in the RM5 solution in toluene was characterized with DLS study, where the average size of the droplet was calculated to be 5.17 ± 0.4 µm (Figure 5.18F). Thereafter, the planar substrate was coated with the as-obtained reaction mixture and kept for gelation (for 20 min) prior to the removal of the dispersed water droplets by heating at 80 °C for 1 h (Figure 5.18B). The reaction mixture present in the continuous phase of toluene spontaneously transformed into a gel within 17 min (Figure 5.18E), and the evaporation of dispersed water droplets on elevated temperature left behind depleted hierarchical topography in the coating as confirmed by the optical microscopic and FESEM images in Figure 5.18G, H. As expected, the prepared coating comprised residual

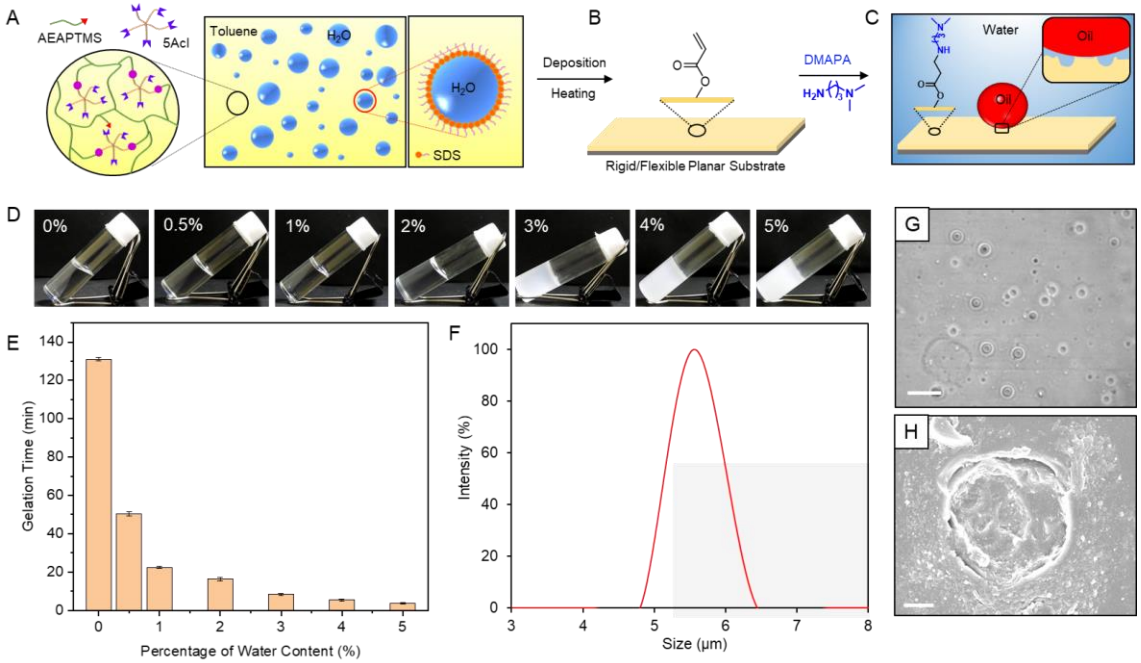

Figure 5.18. (A) Schematic depicting the dispersed micrometer-sized droplets of water (with SDS as a stabilizer) in the reaction mixture of AEAPTMS and 5Acl (RM5) in toluene. (B) The deposition of as prepared reaction mixture on a planar substrate and sequential heating gives covalently cross-linked coating with residual acrylates. (C) The post-modification of residual acrylates with DMAPA conferred underwater superoleophobicity. (D) Photographs of RM5 reaction mixture in toluene (containing different percentages of water) after gel formation. (E) Time required for gelation of RM5 in toluene with increasing the water content of water-in-toluene emulsion. (F) Size distribution curve of water microdroplets dispersed RM5 (in toluene, v/v, 2 %). Scale bars, 10μm. (G) Optical microscopic image of the coating on a glass surface. Scale bars, 10 μm. (H) FESEM image show coating on a glass substrate with depleted hemispherical domains. Scale bars, 2 μm.

acrylate groups, as confirmed by the appearance of two characteristic IR peaks at 1730 and 1409 cm^{-1} for carbonyl stretching and C─H deformation of β carbon of the vinyl group of acrylate moiety (Figure 5.19A). Such residual reactivity allowed the post-covalent modification of the coating with DMAPA—which resulted in the improvement of underwater oil-wettability from oleophobicity (OCA = 125.6 ± 1.6°) to superoleophobicity (OCA = 154.4 ± 1.6°), as shown in Figure 5.19B and C. It is worth noting that the underwater oil-wettability of the DMAPA-modified coatings was gradually improved on increment in the volume % of DI-Water in the reaction mixture, where the dispersed water droplet-driven topography contributes to the heterogeneous oil-wettability underwater. To prove this hypothesis, the fraction of contact area between the prepared coating and beaded oil droplet underwater was estimated on change in the content of dispersed aqueous phase in the reaction mixture following Cassie–Baxter equation:[14,42]

$$cos\theta_{CB} = f_s cos\theta - f_w \quad (1)$$

$$f_s + f_w = 1 \quad (2)$$

where θ_{CB} and θ are the static contact angles of the oil droplet on the coatings that were derived from RM5 in toluene with and without doping the micrometer-sized water droplets, respectively. The coatings were post-modified with DMAPA prior to measuring static OCA underwater. In both equations, f_s denotes the fraction of the contact area between the respective coating and the beaded oil droplet, and f_w denotes the fraction of the contact area between the entrapped aqueous phase and the beaded oil droplet in the prepared coating.

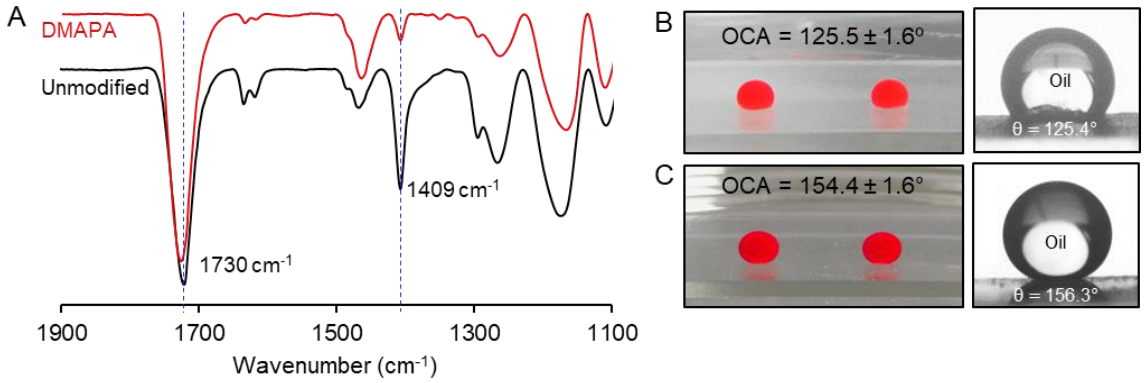

Figure 5.19. (A) FTIR-ATR spectra of RM5 coating developed in toluene (with water microdroplets) after DMAPA modification. (B, C) Digital images and contact angle goniometer images (inset) of underwater oil wettability of coating RM5 coating prepared in toluene (with water microdroplets) on a glass substrate (B) before and (C) after modification with DMAPA.

The fraction of contact area between the beaded oil droplet and prepared coatings underwater was gradually reduced from 0.99 ± 0.07 to 0.23 ± 0.03 on increasing the content of dispersed aqueous phase in the reaction mixture—due to the confinement of the external third phase (i.e., water) (Figure 5.20A). As a consequence, the fraction of area between the beaded oil droplet and the external third phase elevated (from 0.002 ± 0.07 to 0.76 ± 0.03) with increasing the content of dispersed aqueous phase in the depositing reaction mixture as the depleted hemispherical domains (Figure 5.20A) in the prepared coating facilitated the confinement of more external third phase underwater. To verify it, the prepared coating was submerged in the dyed (rhodamine-B) aqueous solution—and an intense, confined fluorescence signal appeared from the prepared coating as the depleted hemispheres accommodated the external third phase, i.e., dyed aqueous phase, as shown in Figure 5.20B. Although the increment of the dispersed aqueous phase in the depositing reaction mixture improved the static OCA from 139.3 ± 1.2° to 160.3 ± 1.4° after DMAPA modification, the optical transparency of the resultant coating on

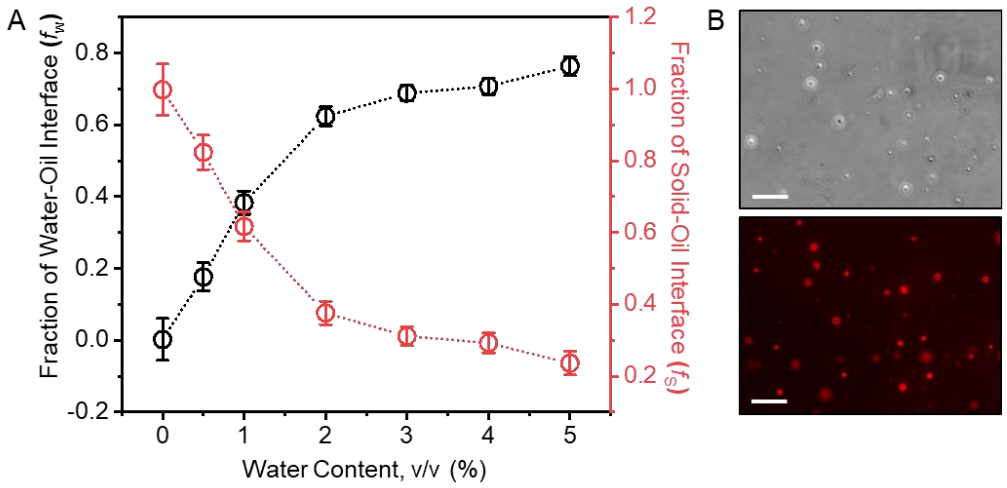

Figure 5.20. (A) Calculation of the fraction of contact area of the water-oil interface (f_w, black) and solid-oil interface (f_s, red) of the oil droplets on coatings with increasing content of dispersed water microdroplet in the reaction mixture (RM5). (B) Bright field and fluorescence microscopic images of glass coated with RM5 (in toluene, with 2% water droplets), after submerging in the dyed (rhodamine-B) aqueous solution. Scale bars, 10µm.

the glass substrate was significantly compromised once the aqueous content in the depositing reaction mixture increased beyond 2% (v/v), as shown in Figure 5.21A. The reaction mixture with 2% (v/v) of dispersed aqueous phase remained appropriate to display both extreme oil repellency under water and optical transparency, similar to bare microscopic glass, as shown in Figure 5.21B.

In addition, such coating remained successful in displaying extreme oil-wettability underwater with static OCA >150°, irrespective of surface tension of the water-immiscible organic solvents

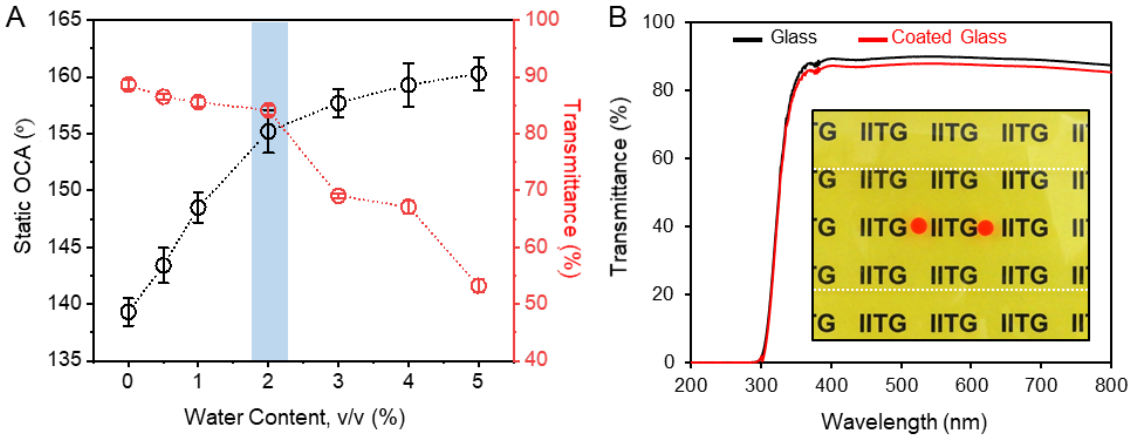

Figure 5.21. (A) Static OCA and percentage of optical transmission on microscopic glass substrate after coating with RM5 (in toluene) with increasing the water content in the reaction mixture and sequentially modifying with DMAPA. (B) Comparison of optical transparency of bare glass and coated glass. Inset image show beaded oil droplets on the transparent coated glass.

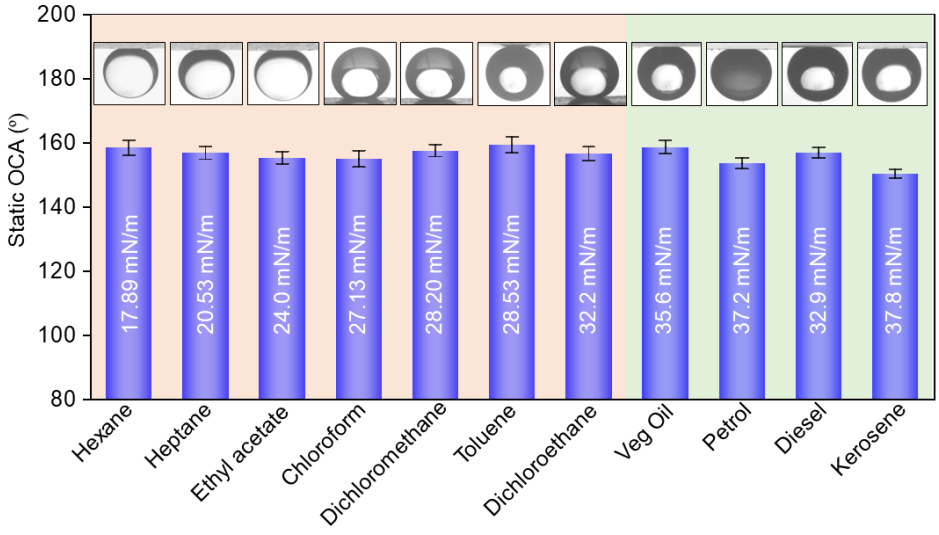

Figure 5.22. Static OCA of beaded droplets of various water-immiscible organic phases on the coated glass substrate.

and commercially available oils, as shown in Figure 5.22. Moreover, the prepared coating on the planar substrate sustained prolonged (30 days) exposures to various and severe chemically contaminated water phases—including extremes of pH (1 and 12), artificial seawater, river water (Brahmaputra river, Guwahati), and surfactants contaminated water (Figure 5.23). Thereafter, such coating was exposed to widely adopted various physically abrasive conditions—including tissue paper wiping test, finger rubbing test, sand drop test (150 g from 20 cm height), and repetitive (for 100 times) adhesive tape peeling test (under an applied load of 500 g). However, the embedded underwater superoleophobicity remained unperturbed, and the modified interfaces continued to display underwater extreme oil repellency with OCA >150° and CAH <10°, as shown in Figure 5.24. Such chemical and physical tolerance is

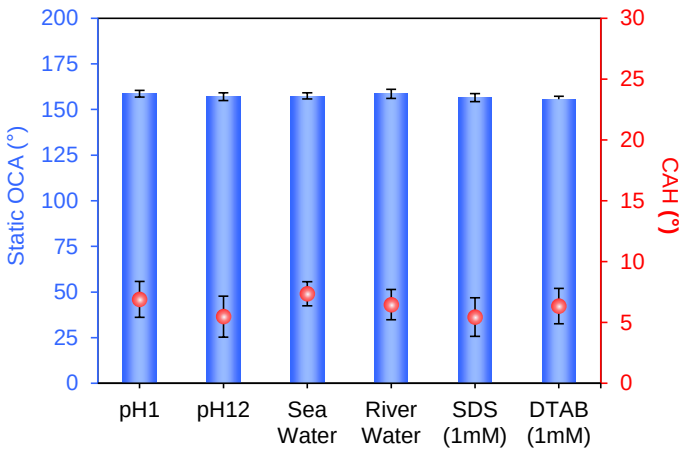

Figure 5.23. The underwater static OCA and CAH (blue) on the RM5 (in toluene with water microdroplets) coated underwater superoleophobic glass slide after continuously exposing the coatings to various chemically contaminated aqueous phases for 30 days.

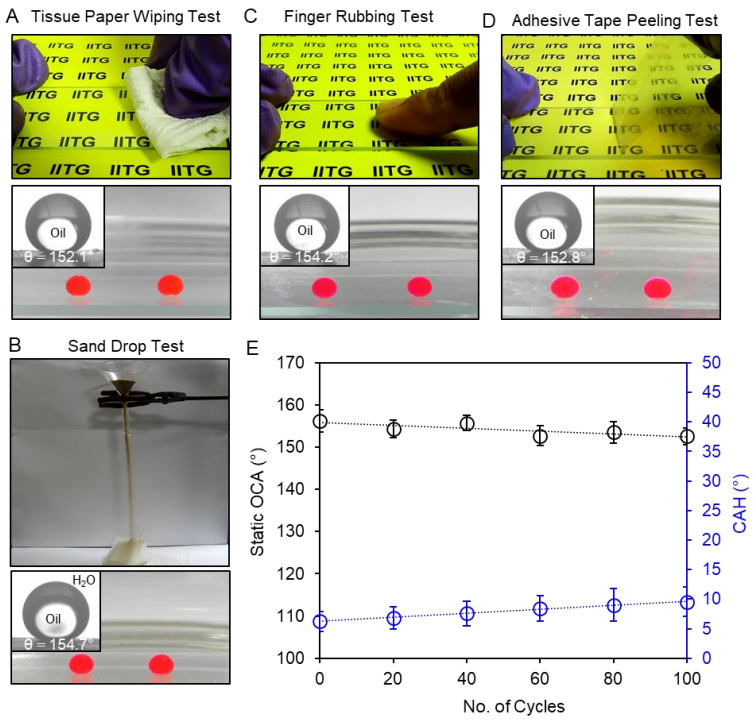

Figure 5.24. Photographs depicting the (A) tissue paper wiping test, (B) sand drop test, (C) finger rubbing test on DMAPA modified RM5 coated glass slide, and digital and contact angle goniometer images (inset) represents its impact on the underwater oil repellence property. (D) Photographs depicting the adhesive tape peeling test on DMAPA modified RM5 coated glass slide. Underwater photographs and contact angle goniometer images (inset) depict the underwater oil repellence property after the adhesive tape peeling test. C) Sustainability study of underwater oil-repellence of DMAPA modified RM5 coated glass slide towards repetitive adhesive tape peeling test.

attributed to the existence of covalently cross-linked sol-gel conversion of the reaction mixture through 1, 4-conjugate addition reaction at ambient conditions.

Taking advantage of the simplicity of the coating process, I further successfully applied this water microdroplet embedded reaction mixture to coat various objects, including large glass surface, flexible (plastic film, aluminium foil), and rigid planar (granite slab, tin plate, and PVC plastic) substrates. A uniform optically transparent and underwater non-adhesive (Figure 5.25B) superoleophobic coating was applied on a comparatively large glass object (25 cm × 25 cm), and the beaded droplets of model oil (dyed with Nile red for visual inspection) readily rolled-off on tilting such coated interface, whereas the beaded oil droplets adhered on a bare glass substrate and fouled the interface with oil/oily phase as shown in Figure 5.25A. Further, this coating was successfully deposited on a commercially available object, i.e., spectacle, to achieve optically transparent underwater superoleophobicity for protecting the interface from oil/oily contamination. The beaded oil droplets readily rolled off from the

portion of coated spectacle (left side) and adhered on the other half of the uncoated spectacle (right side) with OCA of 124.6 ± 1.7°—and failed to roll off, as shown in Figure 5.25C. Next, pieces of other planar objects, such as plastic film, aluminium foil, granite slab, tin plate, and PVC plastic, were also similarly modified to demonstrate the successful adaptation of underwater superoleophobicity, and as expected, the oil droplets beaded underwater on the coated substrates with static OCA of >155º, as shown in Figure 5.25D−H. The embedded underwater superoleophobicity on the plastic remained unaltered after exposure to various repetitive physical manipulations—including bending, twisting, and rolling, as confirmed by the visual inspection and contact angle measurements, as shown in Figure 5.25I, J. Thus, the

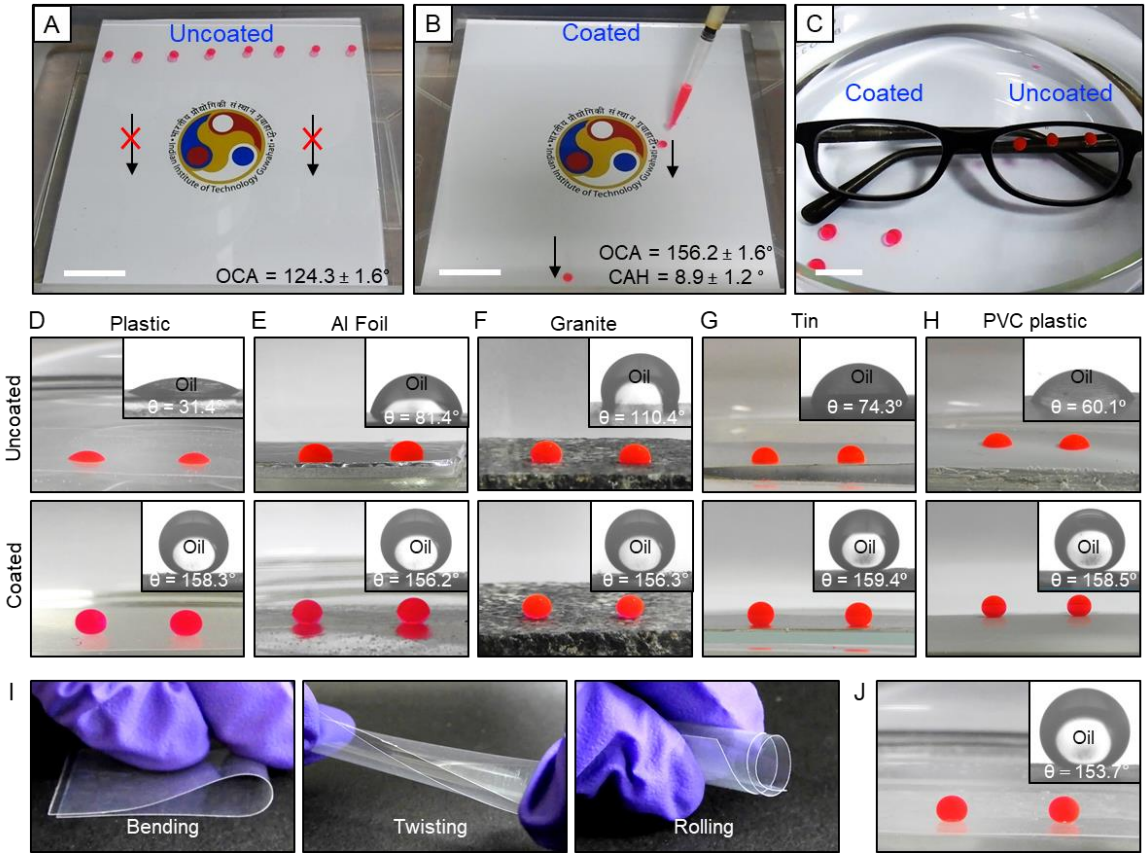

Figure 5.25. (A, B) Photographs showing the pinning and rolling of beaded oil droplets (dyed DCE, used as model oil) on a large glass substrate (A) before and (B) after applying DMAPA-modified coating, respectively. Digital images clearly show the transparency of the glass remains similar after the coating. Scale bars, 5 cm. (C) Digital image represents the rolling of beaded oil droplets on the coated side of a spectacle (left side) and adhering of beaded oil droplets on the uncoated side of the spectacle (right side). Scale bars, 2 cm. (D−H) Digital and contact angle goniometer images (inset) showing the underwater oil wetting behaviour on (D) plastic film, (E) Aluminium (Al) foil, (F) granite slab, (G) tin plate and (H) PVC plastic, before and after depositing DMAPA modified coating. (I, J) Photographs demonstrating successive physical manipulation, such as (I) bending, twisting, and rolling on coated plastic film; and (J) demonstration of unperturbed underwater oil repellence property.

current approach remains appropriate to coat a wide range of substrates, including porous, fibrous, planar, flexible, rigid, etc., with optically transparent underwater superoleophobicity.

In the final set of experiments, a highly deformable sponge was dip-coated with RM5 and followed by post-modification with DMAPA prior to examining the tolerance of such material against the impact of a 1 kg load that dropped from 1 m height, as shown in Figure 5.26A. The prepared material survived such an impact test; however, conventional structure material, i.e., clay brick (collected from the construction site of IITG), failed to sustain, rather broken pieces were found at the end (Figure 5.26B). Next, four pieces of coated MF sponge (height: ≈ 8 cm, width: ≈ 3.5 cm, thickness: ≈ 2.5 cm, weight: ≈ 8.4 g) were kept aligned vertically underwater with the help of double-sided adhesive tape as shown in Figure 5.26C. Such a simple set-up remained successful in holding an external load of 10 kg (i.e., ≈ 300-fold higher than the coated sponge's weight) without causing any noticeable deformation and physical damage to the coated MF sponge under water. However, the uncoated MF sponge failed to display such performance under identical exposure to same external load (Figure 5.26D). Furthermore, the altered mechanical property of highly stretchable substrates because of the dip-coating of RM5 is applied to demonstrate the ability to hold a significantly higher external load without causing noticeable physical deformation that too at wet conditions. In this context, an external load of 10 kg was placed on a lycra-based highly stretchable fibrous substrate (60 cm × 60 cm), and as

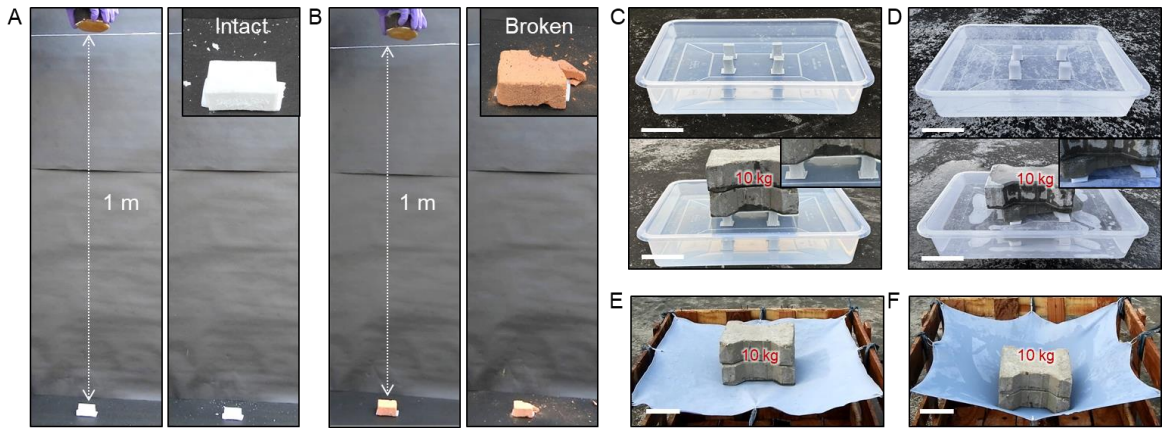

Figure 5.26. (A, B) Digital images accounting the impact of 1 kg load from a height of 1 m on (A) coated MF and (B) conventional structure material, i.e. clay brick of similar sizes. (C, D) Photographs depicting four separate pieces of (C) coated and (D) bare MF sponges vertically aligned underwater by fixing from the button with the help of double-sided adhesive tape, and sequential images show the coated sponges can withstand 10 kg of external load without any deformation, whereas the similar load caused deformation of bare sponges. Scale bars, 10 cm. (E, F) Digital images depict the impact of 10 kg of external load on large (E) coated and (F) bare fibrous lycra fabric after soaking with water. Scale bar = 10 cm.

expected, a significant deformation and depletion of the uncoated fibrous substrate was observed (Figure 5.26F). However, after dip-coating the same substrate with RM5, it became highly efficient in holding the same external load (10 kg) at even wet conditions without causing much deformation, as shown in Figure 5.26E. The design of such coating capable of improving the mechanical property and oil-wettability of deformable and porous substrates is likely to be useful as an efficient structure material for developing anti-oil-fouling marine infrastructures.

5.4. Conclusions

In conclusion, in this chapter a covalently cross-linked and chemically reactive sol-gel process is introduced to develop an optically transparent, chemically reactive and substrate-independent coating to orthogonally modulate the mechanical property of highly deformable fibrous and porous substrates and the underwater oil wettability. The covalent cross-linkage in the deposited coating through the 1, 4-conjugate addition reaction between amine and acrylate moieties attributed to an improved tensile (3.5 to 348.8 MPa) and compressive (0.052 to 29.51 MPa) modulus of the selected fibrous and porous substrates, respectively, whereas the residual reactivity of the coating allowed to independently customize underwater oil-wettability—including superoleophobicity with OCA >160° through 1, 4-conjugate addition reaction at ambient condition. The embedded extreme oil repellence property survived various challenging chemical and physical exposure, and the improved mechanical property due to the cross-linked coating protects the porous and fibrous substrates from severely abrasive physical exposures. Moreover, the deposition of the same reaction mixture loaded with micrometer-sized water droplets on planar substrates provided optically transparent underwater superoleophobicity, where the evaporation of micrometer-sized water droplets from the deposited coating created adequate topography to entrap aqueous phase for conferring underwater superoleophobicity. Such a facile and scalable chemical approach of developing optically transparent, substrate-independent, and physically/chemically tolerant underwater superoleophobicity would be useful in a wide range of relevant indoor and outdoor applications.

5.5. References

1 X. Feng, S. Hu, W. Gu, X. Jin and Y. Lu, *Transp. Res. E Logist. Transp. Rev.*, 2020, **142**, 102051.

2 M. L. Miller, *Ocean Coast Manag.*, 1993, **20**, 181.

3 M. Visbeck, *Nat. Commun.*, 2018, **9**, 690.

4 W. Cornwall, *Science*, 2015, **348**, 22.

5 I. Helle, J. Mäkinen, M. Nevalainen, M. Afenyo and J. Vanhatalo, *Environ. Sci. Technol.*, 2020, **54**, 2112.

6 C. P. D. Brussaard, L. Peperzak, S. Beggah, L. Y. Wick, B. Wuerz, J. Weber, J. Samuel Arey, B. van der Burg, A. Jonas, J. Huisman and J. R. van der Meer, *Nat. Commun.*, 2016, **7**, 11206.

7 Z. Bai, K. Jia, S. Zhang, G. Lin, Y. Huang and X. Liu, *Adv. Funct. Mater.*, 2022, **32**, 2204612.

8 Y. Mo, F. Zhang, H. Dong, X. Zhang, S. Gao, S. Zhang and J. Jin, *ACS Nano*, 2022, **16**, 20786.

9 W. Liu, S. Xiang, X. Liu and B. Yang, *ACS Nano*, 2020, **14**, 9166.

10 D. Yu, J. Huang, Z. Zhang, J. Weng, X. Xu, G. Zhang, J. Zhang, X. Wu, M. Johnson, J. Lyu, H. Yang and W. Wang, *Adv. Mater.*, 2022, **34**, 2106908.

11 Z. Liao, G. Wu, D. Lee and S. Yang, *ACS Appl. Mater. Interfaces*, 2019, **11**, 13642.

12 X. Wan, L. Jia, X. Liu, B. Dai, L. Jiang and S. Wang, *Adv. Mater.*, 2022, **34**, 2110408.

13 K. Chen, S. Zhou and L. Wu, *ACS Nano*, 2016, **10**, 1386.

14 K. Maji and U. Manna, *J. Mater. Chem. A*, 2018, **6**, 6642.

15 X. Huang, B. Li, L. Wang, X. Lai, H. Xue and J. Gao, *ACS Appl. Mater. Interfaces*, 2019, **11**, 24533.

16 Y. Cheng, Q. Yang, Y. Fang, J. Yong, F. Chen and X. Hou, *Adv. Mater. Interfaces*, 2019, **6**, 1900067.

17 A. Shome, A. M. Rather and U. Manna, *J. Mater. Chem. A*, 2018, **6**, 22465.

18 Q. Zhong, G. Shi, Q. Sun, P. Mu and J. Li, *J. Membr. Sci.*, 2021, **640**, 119836.

19 H. Li, P. Mu, J. Li and Q. Wang, *J. Mater. Chem. A*, 2021, **9**, 4167.

20 K. Han, L. Heng and L. Jiang, *ACS Nano*, 2016, **10**, 11087

21 J. Yong, F. Chen, Q. Yang, U. Farooq and X. Hou, *J. Mater. Chem. A*, 2015, **3**, 10703.

22 S. Zhang, G. Jiang, S. Gao, H. Jin, Y. Zhu, F. Zhang and J. Jin, *ACS Nano*, 2018, **12**, 795.

23 L.-P. Xu, J. Zhao, B. Su, X. Liu, J. Peng, Y. Liu, H. Liu, G. Yang, L. Jiang, Y. Wen, X. Zhang and S. Wang, *Adv. Mater.*, 2013, **25**, 606.

24 N. Han, C. Yang, Z. Zhang, W. Wang, W. Zhang, C. Han, Z. Cui, W. Li and X. Zhang, *ACS Appl. Mater. Interfaces*, 2019, **11**, 35479.

25 P. Zhang, C. Zhao, T. Zhao, M. Liu and L. Jiang, *Adv. Sci.*, 2019, **6**, 1900996.

26 S. Gao, J. Chen, Y. Zheng, A. Wang, D. Dong, Y. Zhu, Y. Zhang, W. Fang and J. Jin, *Adv. Funct. Mater.*, 2022, **32**, 2205990.

27 Z. Bai, K. Jia, C. Liu, L. Wang, G. Lin, Y. Huang, S. Liu and X. Liu, *Adv. Funct. Mater.*, 2021, **31**, 2104701.

28 W. Chen, P. Zhang, R. Zang, J. Fan, S. Wang, B. Wang and J. Meng, *Adv. Mater.*, 2020, **32**, 1907413.

29 X. Meng, M. Wang, L. Heng and L. Jiang, *Adv. Mater.*, 2018, **30**, 1706634.

30 M. Li, Y. Chen, L.-B. Mao, Y. Jiang, M.-F. Liu, Q. Huang, Z. Yu, S. Wang, S.-H. Yu, C. Lin, X. Y. Liu and H. Cölfen, *Langmuir*, 2018, **34**, 2942.

31 T. Guo, L. Heng, M. Wang, J. Wang and L. Jiang, *Adv. Mater.*, 2016, **28**, 8505.

32 L.-P. Xu, J. Peng, Y. Liu, Y. Wen, X. Zhang, L. Jiang and S. Wang, *ACS Nano*, 2013, **7**, 5077.

33 J. Yong, F. Chen, Q. Yang, D. Zhang, U. Farooq, G. Du and X. Hou, *J. Mater. Chem. A*, 2014, **2**, 8790.

34 T. Du, S. Ma, X. Pei, S. Wang and F. Zhou, *Small*, 2017, **13**, 1602020.

35 W. Chen, P. Zhang, S. Yu, R. Zang, L. Xu, S. Wang, B. Wang and J. Meng, *Nat. Protoc.*, 2022, **17**, 2647.

36 J. Ford, S. R. Marder and S. Yang, *Chem. Mater.*, 2009, **21**, 476.

37 S. L. Bechler and D. M. Lynn, *Biomacromolecules*, 2012, **13**, 1523.

38 A. M. Rather and U. Manna, *Chem. Mater.*, 2016, **28**, 8689.

39 D. M. Brey, I. Erickson and J. A. Burdick, *J. Biomed. Mater. Res. Part A*, 2008, **85A**, 731.

40 D. G. Anderson, C. A. Tweedie, N. Hossain, S. M. Navarro, D. M. Brey, K. J. V. Vliet, R. Langer and J. A. Burdick, *Adv. Mater.*, 2006, **18**, 2614.

41 D. Parbat and U. Manna, *Chem. Sci.*, 2017, **8**, 6092.

42 A. B. D. Cassie and S. Baxter, *Nature*, 1945, **155**, 21.

Conclusions and Future Directions

This chapter summarizes the various works discussed in the individual chapters. The thesis elaborates on the utilization of a facile 1, 4-conjugate addition reaction to design covalently crosslinked chemically reactive coatings loaded with residual chemical functionalities on various surfaces. While strategic post-covalent modification allowed to tailor oil wettability and oil adhesion underwater, the strategic covalent cross-linking chemistry modulated mechanical property.[1-4] In Chapter 1, I have provided a brief overview of the naturally existing creatures with extreme oil-repellence property underwater and the progression of the theoretical models introduced to understand liquid wettability on a solid surface. Moreover, I have outlined the various fabrication methods developed in the past to adopt anti-oil wettability artificially and the prospective applications of such underwater superoleophobic surfaces. Further, I have discussed the importance of the association of other essential properties, such as tailorable oil adhesion, transparency, and durability on underwater superoleophobic coatings, and existing challenges in the literature while attaining such properties. Thereafter, I have enlisted my motivation and objectives for this thesis work. In Chapter 2, I have introduced a simple chemical approach to fabricate a dual reactive multilayer coating following a 1, 4-conjugate addition reaction, and the post-covalent modification of the multilayer coating to achieve a patterned interface of adhesive super-LC-phobicity (underwater) with a hydrophobic background, where the highly sensitive bare micro-meter sized liquid crystal (μ-LC) droplets can be immobilized without affecting their sensitivity. Further, the triggered phase transition of immobilized μ-LC droplets provided a simple basis for unambiguous, rapid, and repetitive sensing of various relevant analytes with single, bare μ-LC droplet.[1] In Chapter 3, I have demonstrated the orthogonal chemical functionalization of the dual reactive multilayer coating to independently tune their underwater superoleophobicity and oil adhesion. Moreover, the non-covalent, cooperative assembly of amphiphilic molecules on the surface of these multilayer coatings enabled the reversible switching of contact angle hysteresis (CAH) of oil droplets at the surface, which revealed new principles for the detection and quantification of ionic amphiphiles with the naked eye. Additionally, this design principle was extended for the detection of synthetic surfactants with different charges and physiologically important metabolites (i.e., bile acids) with the naked eye.[2] In Chapter 4, the dual chemically reactive multilayer coating is rationally subjected to mono and dual-functionalization, where a hydrophobic moiety was covalently embedded in the functionalized coatings that can selectively transform into hydrophilic moiety in the presence of a specific toxic chemical. This

contributed to the desired change in underwater oil wettability, reflected as raising in OCA and rolling of beaded oil droplets, and eventually, this approach allowed equipment-free and naked-eye chemical sensing of toxins with high selectivity and sensitivity.[3] In Chapter 5, I designed a covalently cross-linked and chemically reactive sol-gel conversion process through 1, 4-conjugate addition reaction to achieve a substrate-independent and tolerant coating for orthogonally modulating the underwater oil wettability, optical transparency, and even mechanical properties of highly deformable porous and fibrous substrates. The embedded extreme oil repellence property survived various challenging chemical and physical exposures, and the improved mechanical property due to the cross-linked coating protects the porous and fibrous substrates from severely abrasive physical exposures. Moreover, the deposition of the same reaction mixture loaded with micrometer-sized water droplets on planar substrates provided optically transparent underwater superoleophobicity.[4]

In this research work, underwater superoleophobicity derived from dual reactive multilayer coatings is unprecedently utilized for the naked eye sensing of relevant toxic chemicals. In this context, such principles provide the basis for monitoring other toxic chemicals and biological events, such as protein-lipid interaction and enzymatic activity in underwater superoleophobic surfaces through modulation of oil wettability and oil adhesion, which will be explored in the future. Furthermore, past studies reported that underwater superoleophobicity has a significant role in exhibiting anti-platelet adhesion.[5,6] Biomedical devices and implanted materials easily absorb blood proteins and induce platelet activation and adhesion, which results in blood coagulation and, eventually, thrombosis. Notably, the wettability of the material surface has been found to significantly affect platelet activation/adhesion, and other properties of the surface, such as chemical composition, surface morphology, and charge, play crucial roles as well.[7,8] In this context, the chemically reactive coatings developed in this research work appeared as an ideal candidate for the investigations on platelet activation/adhesion, as it has the ability to tailor the surface topography and surface chemistry through desired chemical modifications. Thus, future efforts will seek a detailed investigation of the dual reactive multilayer coatings in anti-platelet adhesion, where the (i) surface morphology of the surface would be modulated by varying the deposition cycle during the layer-by-layer (LbL) process and the (ii) surface chemistry/charge would be tailored through appropriate post functionalization. The appropriate co-optimization of surface morphology and chemistry/charge can provide the coating with excellent anti-platelet adhesion property to apply in various biomedical devices.

Furthermore, the underwater superoleophobic surface is known for its inherent ability to inhibit air bubble adhesion on their surface after water immersion, which phenomenon is formally known as underwater superaerophobicity.[9-11] The underwater superaerophobic property has been used for various relevant underwater applications. In this context, the underwater superoleophobic coatings developed in the research work would efficiently perform underwater superaerophobic properties with tailored adhesion which will be explored in the field of controlled transport of gas bubbles, gas phase micro reactions, etc.[12-14] Moreover, the deposition of such underwater superaerophobic coating on electrochemical electrodes could enhance the efficiency of H_2 gas evolution in electrochemical hydrogen evolution reaction (HER).[15-17] In conventional HER, the efficiency of the H_2 gas evolution is reduced over time due to the adhesion of the produced H_2 gas bubbles on the electrode surface, thus blocking the active catalytic site. The creation of an underwater superaerophobic coating of the electrode surface minimizes the force of nucleated hydrogen gas-bubble adhesion to prevent blockage of electrocatalytic sites, and thus, such approaches would likely minimize the overpotential for the HER process. The simple chemical approaches developed in this research work possess potential for such energy-related applications.

6.1 References

1 A. Borbora and U. Manna, *Langmuir*, 2022, **38**, 9221.

2 A. Borbora, R. L. Dupont, Y. Xu, X. Wang and U. Manna, *Mater. Horiz*., 2022, **9**, 991.

3 A. Borbora, J. Das and U. Manna, *Chem. Commun*., 2023, **59**, 7915.

4 A. Borbora, M. Dhar, A. Shome, N. Barman, S. Roy and U. Manna, *Adv. Funct. Mater*., 2023, 2302569.

5 L. Chen, M. Liu, H. Bai, P. Chen, F. Xia, D. Han, and L. Jiang, *J. Am. Chem. Soc*., 2009, **131**, 10467.

6 D. Parbat, B. K. Bhunia, B. B. Mandal and U. Manna, *Chem. Asian J.*, 2021, **16**, 1081.

7 A. Ranella, M. Barberoglou, S. Bakogianni, C. Fotakis and E. Stratakis, *Acta Biomater*., 2010, **6**, 2711.

8 E. Stratakis, A. Ranella and C. Fotakis, *Biomicrofluidics*, 2011, **5**, 13411.

9 C. Yu, P. Zhang, J. Wang and L. Jiang, *Adv. Mater*., 2017, **29**, 1703053.

10 C. Huang and Z. Guo, *Nanoscale*, 2018, **10**, 19659.

11 R. Xu, X. Xu, M. He and B. Su, *Nanoscale*, 2018, **10**, 231.

12 S. Ben, Y. Ning, Z. Zhao, Q. Li, X. Zhang, L. Jiang and K. Liu, *Adv. Funct. Mater*., 2022, **32**, 2113374.

13 S. Kim, D. Yoo, S. Lee and J. Kim, *Adv. Mater. Interfaces*, 2022, **9**, 2200797.

14 C. Pei, Y. Peng, Y. Zhang, D. Tian, K. Liu and L. Jiang, *ACS Nano*, 2018, **12**, 5489.

15 Y. Li, H. Zhang, T. Xu, Z. Lu, X. Wu, P. Wan, X. Sun and L. Jiang, *Adv. Funct. Mater*., 2015, **25**, 1737.

16 Z. Lu, W. Zhu, X. Yu, H. Zhang, Y. Li, X. Sun, X. Wang, H. Wang, J. Wang, J. Luo, X. Lei and L. Jiang, *Adv. Mater*., 2014, **26**, 2683.

17 D. Jeon, J. Park, C. Shin, H. Kim, J.-W. Jang, D. W. Lee and J. Ryu, *Sci. Adv*., 2020, **6**, eaaz3944.

Journal Articles

Scientific Contributions (Included in the thesis)

1. **A. Borbora**, J. Das and U. Manna, *Chem. Commun*., 2023, **59**, 7915.
2. **A. Borbora**, M. Dhar, A. Shome, N. Barman, S. Roy and U. Manna, *Adv. Funct. Mater*. 2023, 2302569.
3. **A. Borbora** and U. Manna, *Langmuir*, 2022, **38**, 9221.
4. **A. Borbora**, R. L. Dupont, Y. Xu, X. Wang and U. Manna, *Mater. Horiz*., 2022, **9**, 991.

Scientific Contributions (Off the thesis)

1. **A. Borbora**, Y. Xu, S. Dey, X. Wang, Y. Yao, B. B. Mandal, X. Wang and U. Manna, *Adv. Mater*., 2023, 2302264.
2. A. Shome, A. Das, **A. Borbora**, M. Dhar and U. Manna, *Chem. Soc. Rev*., 2022, **51**, 5452.
3. A. M. Rather, Y. Xu, Y. Chang, R. L. Dupont, **A. Borbora**, U. I. Kara, J.-C. Fang, R. Mamtani, M. Zhang, Y. Yao, S. Adera, X. Bao, U. Manna and X. Wang, *Adv. Mater*., 2022, **34**, 2110085.
4. M. Dhar, A. Das, A. Shome, **A. Borbora** and U. Manna, *Mater. Horiz.*, 2021, **8**, 2717.
5. A. Shome, A. M. Rather, **A. Borbora**, P. Srikrishnarka, A. Baidya, T. Pradeep and U. Manna, *Chem Asian J*., 2021, **16**, 1.
6. **A. Borbora** and U. Manna, *Chem. Commun*., 2021, **57**, 2110.
7. **A. Borbora** and U. Manna, *Chem. Commun*., 2020, **56**, 7853.

Conferences/Workshops

1. *Oral Presentation in* North-East Research Conclave (NERC) Towards- Sustainable Science & Technology, Assam Biotech Conclave- 2022, organized by IIT Guwahati, Assam, India.

2. *Oral Presentation in* 7th International Conference on Advanced Nanomaterials and Nanotechnology (ICANN2021) organized by the Centre for Nanotechnology, IIT Guwahati, Assam, India.
3. *Poster Presentation in* Frontiers in Chemical Sciences- 2022, organized by IIT Guwahati, Assam, India
4. *Poster Presentation in* Chemical Research Society of India 28th National Symposium in Chemistry (CRSI NSC-28) organized by Chemical Research Society of India.
5. *Poster Presentation in* 20th National Conference on Surfactants, Emulsions and Biocolloids NATCOSEB XX organized by the Department of Chemistry, IIT Guwahati, Assam, India.
6. *Poster Presentation in* 57th Annual Convention of Chemists, 2020 & International Conference on "Recent Trends in Chemical Sciences (RTCS-2020)" organized by the Indian Chemical Society, Kolkata, India.
7. *Workshop attended* in "Theory and demonstration on thermal analysis (DSC and TG) of materials" organized by the Guwahati Regional Centre of Indian Institute of Chemical Engineers and the Department of Chemical Engineering in association with the Central Instruments facility, IIT Guwahati, Assam, India.